ESCUELA INTERNACIONAL DE DOCTORADO
Programa de Doctorado en Ciencias de la Salud

Diseño y caracterización de inhibidores de la fascina para el bloqueo de la invasión y la metástasis en cáncer colorrectal.

Autora:
Begoña Alburquerque González

Directores:
Dr. D. Pablo Conesa Zamora
Dra. Dª Silvia Montoro García

Murcia, Mayo de 2022

ESCUELA INTERNACIONAL DE DOCTORADO
Programa de Doctorado en Ciencias de la Salud

Diseño y caracterización de inhibidores de la fascina para el bloqueo de la invasión y la metástasis en cáncer colorrectal.

Autora:
Begoña Alburquerque González

Directores:
Dr. D. Pablo Conesa Zamora
Dra. Dª Silvia Montoro García

Murcia, Mayo de 2022

Los trabajos de investigación recogidos en la presente Memoria han sido financiados por los siguientes proyectos:

1. **Aproximación al abordaje farmacológico del adenocarcinoma serrado colorrectal: caracterización funcional de dianas terapéuticas y de sus inhibidores**. Instituto de Salud Carlos III. IP: Pablo Conesa Zamora. (Hospital Universitario Santa Lucía). 01/01/2016-31/12/2018. 86.515 €.

2. **Diseño y caracterización de inhibidores de fascina para el bloqueo de invasión y metástasis en cáncer colorrectal**. Instituto de Salud Carlos III. IP: Pablo Conesa Zamora. (Complejo Universitario Hospitalario de Cartagena). 01/01/2019- 31/12/2022. 93.000 €.

La firmante de esta Memoria ha disfrutado de un Contrato predoctoral del plan propio de la Universidad Católica de Murcia. Convocatoria 2017 (marzo 2018-julio 2022).

La presente Tesis adopta el formato de **COMPENDIO DE PUBLICACIONES**. En ella se recogen conceptos derivados de una revisión bibliográfica y ensayos *in vitro* e *in vivo*. El compendio consta de cuatro artículos ya publicados y uno pendiente de publicación. Los artículos que forman parte de esta Tesis son los siguientes:

ARTÍCULO 1:

Alburquerque-González, B., López-Calderón, F. F., López-Abellán, M. D., Esteban-Gil, Á., García-Solano, J., & Conesa-Zamora, P. (2020). **Biology and Therapeutic Targets of Colorectal Serrated Adenocarcinoma; Clues for a Histologically Based Treatment against an Aggressive Tumor.** *International Journal of Molecular Sciences*, *21*(6), 1991. https://doi.org/10.3390/ijms21061991

Factor de impacto 2020 (JCR): 5.924; Categoría (JCR): BIOCHEMISTRY & MOLECULAR BIOLOGY; Clasificación: 67/295 (Q1); Fecha de publicación: 2020.

ARTÍCULO 2:

Montoro-García, S., **Alburquerque-González, B.**, Bernabé-García, Á., Bernabé-García, M., Rodrigues, P. C., den-Haan, H., Luque, I., Nicolás, F. J., Pérez-Sánchez, H., Cayuela, M. L., Salo, T., & Conesa-Zamora, P. (2020). **Novel anti-invasive properties of a Fascin1 inhibitor on colorectal cancer cells.** *Journal of Molecular Medicine (Berlin, Germany)*, *98*(3), 383–394. https://doi.org/10.1007/s00109-020-01877-z

Factor de impacto 2020 (JCR): 4.599; Categoría (JCR): MEDICINE RESEARCH & EXPERIMENTAL SCIENCE; Clasificación: 48/176 (Q2, T1); Fecha de publicación: 2020.

ARTÍCULO 3:

Alburquerque-González, B., Bernabé-García, M., Montoro-García, S., Bernabé-García, Á., Rodrigues, P. C., Ruiz Sanz, J., López-Calderón, F. F., Luque, I., Nicolas, F. J., Cayuela, M. L., Salo, T., Pérez-Sánchez, H., & Conesa-Zamora, P. (2020). **New role of the antidepressant imipramine as a Fascin1 inhibitor in colorectal cancer cells.** *Experimental & Molecular Medicine*, *52*(2), 281–292. https://doi.org/10.1038/s12276-020-0389-x.

Factor de impacto 2020 (JCR): 8.718; Categoría (JCR): MEDICINE RESEARCH & EXPERIMENTAL SCIENCE; Clasificación: 34/295 (Q1); Fecha de publicación: 2020.

ARTÍCULO 4:

Alburquerque-González, B., Bernabé-García, Á., Bernabé-García, M., Ruiz-Sanz, J., López-Calderón, F. F., Gonnelli, L., Banci, L., Peña-García, J., Luque, I., Nicolás, F. J., Cayuela-Fuentes, M. L., Luchinat, E., Pérez-Sánchez, H., Montoro-García, S., & Conesa-Zamora, P. (2021). **The FDA-Approved Antiviral Raltegravir Inhibits Fascin1-Dependent Invasion of Colorectal Tumor Cells *In Vitro* and *In Vivo***. *Cancers*, *13*(4), 861. https://doi.org/10.3390/cancers13040861.

Factor de impacto 2020 (JCR): 6.639; Categoría (JCR): ONCOLOGY & SCIENCE; Clasificación: 51/242 (Q1); Fecha de publicación: 2020.

El artículo pendiente de publicación es el siguiente:

Alburquerque-González, B., Montoro-García, S., Bernabé-García, M., Bernabé-García, A., Campioni-Rodrigues, P., Luque-Fernández, I., Salo, T., Pérez-Sánchez, H., Cayuela-Fuentes, M.L., Luengo-Gil, G., Nicolás-Villaescusa, F.J., Conesa-Zamora, P. (2022). **Monastrol, a kinesin-Eg5 inhibitor, inhibits invasion and metastasis of human colorectal cancer cells by targeting fascin.** *Experimental & Molecular Medicine* (En revisión).

Además, el último capítulo de la Tesis recoge los resultados que aún están pendientes de ser recopilados en un manuscrito:

Alburquerque-González B, Montoro-García S, García-Bernal D, Bernabé-García M, Rodriguez-Arcas Mª J, Albaladejo- González A, Luengo-Gil G, García-Solano J, Cabezas-Herrera J, Conesa-Zamora P. **Testing the Potential Therapy with the fascin inhibitors Tofranil® and Issentress® in colorectal cancer mice models.** (En preparación).

UCAM

UNIVERSIDAD CATÓLICA
DE MURCIA

AUTORIZACIÓN DE LO/S DIRECTOR/ES DE LA TESIS
PARA SU PRESENTACIÓN

El Dr. D. Pablo Conesa Zamora y la Dra. Dª. Silvia Montoro García, como Directores de la Tesis Doctoral titulada "Diseño y caracterización de inhibidores de la fascina para el bloqueo de la invasión y la metástasis en cáncer colorrectal" realizada por Dña. Begoña Alburquerque González en el Departamento de Ciencias de la Salud, **autoriza su presentación a trámite** dado que reúne las condiciones necesarias para su defensa.

Lo que firmo, para dar cumplimiento al Real Decreto 99/2011, en Murcia a 25 de mayo de 2022.

Dr. D. Pablo Conesa Zamora

Dra. Dª. Silvia Montoro García

RESUMEN

TITULO: Diseño y caracterización de inhibidores de la fascina para el bloqueo de la invasión y la metástasis en cáncer colorrectal

Introducción: El adenocarcinoma serrado (ACS) es un subtipo histológico de cáncer colorrectal reconocido por la Organización Mundial de la Salud (OMS) y que representa alrededor del 9% de los carcinomas colorrectales. En comparación con el carcinoma convencional (CC), el ACS tiene peor pronóstico y supervivencia. Estas características son debidas a que el ACS presenta un débil desarrollo de la respuesta inmune, un frente invasor muy activo y no responde de manera eficiente a terapias dirigidas anti-EGFR debido a la alta frecuencia de mutaciones en *KRAS*/*BRAF*. No obstante, recientemente, se han identificado posibles dianas moleculares que podrían favorecer la búsqueda de nuevos tratamientos específicos para el ACS. En esta línea se ha identificado la fascina, una proteína que se encuentra sobre-expresada en este subtipo histológico de cáncer colorrectal y que es una proteína clave en el reordenamiento del citoesqueleto de actina ya que participa en la formación de filopodios y lamelipodios implicados en el movimiento celular. Debido al papel fundamental de la fascina en el empaquetamiento de haces de actina, esta proteína se convierte en una diana para el bloqueo de la invasión tumoral.

Objetivos: El principal objetivo de de la presente Tesis ha sido buscar nuevos inhibidores contra la fascina en cáncer colorrectal mediante cribado farmacológico. Posteriormente, hemos evaluado, mediante técnicas *in vitro*, el efecto de estos inhibidores en la proliferación, movilidad e invasión en líneas celulares de cáncer colorrectal con distintos niveles de expresión basal de la fascina. Igualmente, se analizó la capacidad anti-invasora y anti-metastásica de los inhibidores en modelos *in vivo* de pez cebra y murinos.

Resultados: Se realizó una búsqueda, mediante modelado molecular, de potenciales compuestos anti-fascina de una librería de 9591 compuestos (que incluían 2037 aprobados por la *Food and Drug Administration* (FDA). Fruto de

estudios *in silico*, identificamos varios compuestos como potenciales inhibidores de la fascina entre los que caben destacar: la imipramina (IMIP), el raltegravir (RAL) y el monastrol (MON). Previamente, el grupo del Dr. HY Huang descubrió el compuesto G2 mediante *screening* farmacológico y lo caracterizó como un inhibidor de la fascina capaz de bloquear la migración celular, la invasión y la metástasis en cáncer de mama. . Así pues, en esta Tesis, hemos testado las propiedades anti-fascina del compuesto G2, la IMIP, el RAL y el MON mediante ensayos *in vitro* e *in vivo* en los que se ha empleado la migrastatina (MGS) como fármaco control anti-fascina. En todos los casos, se observó un efecto anti-migratorio y anti-invasor al tratar líneas celulares de cáncer de colon como HCT-116 y DLD-1 con los compuestos anti-fascina en los ensayos *in vitro.* También se ha observado la capacidad anti-metastásica de los inhibidores *in vivo* (pez cebra) y hemos estudiado el efecto que tienen la IMIP y el RAL en un modelo murino de tumor primario.

Conclusiones: El cribado de fármacos juega un papel fundamental en la investigación traslacional. Hemos encontrado nuevas propiedades anti-migratorias y anti-invasoras de los compuestos G2, IMIP, RAL y MON en células de cáncer colorrectal. Además, existe un efecto dosis dependiente de estos compuestos que ha sido demostrado mediante un modelo *in vivo* de invasión y metástasis tumoral en pez cebra. Los resultados del modelo murino obtenidos en la presente Tesis son aún preliminares y no fueron significativos en comparación con los grupos control. Ello apunta a la necesidad de evaluar en el futuro, el efecto sinérgico de quimioterapéuticos junto con los inhibidores de la fascina descritos en este trabajo. Los presentes resultados abalan el reposicionamiento de fármacos en la investigación clínica, así como la utilidad terapéutica de estos fármacos para el tratamiento de las células tumorales metastásicas más agresivas, como las que se desarrollan en el ACS.

Palabras clave: Cáncer Colorrectal, Fascina, Actina, Inhibidores, G2, Imipramina, Raltegravir, Monastrol, Reposicionamiento, Migración, Invasión, Metástasis, *In vitro, In vivo,* Pez cebra, Ratón.

ABSTRACT

TITLE: Characterization and design of fascin inhibitors for blocking invasion and metastasis in colorectal cancer.

Introduction: Serrated adenocarcinoma (SAC) is a histological subtype of colorectal cancer recognized by the World Health Organization (WHO) and represents about 9% of colorectal carcinomas. Compared with conventional carcinoma (CC), SAC has a worse prognosis and survival. These features are the consequence that SAC present a weak development of the immune response, a very active invasive front, and also SAC doesn't respond efficiently to targeted therapies due to the high *KRAS*/*BRAF* frequency mutations. However, possible molecular targets have recently been identified, thus favoring the search for new specific treatments for SAC. In this line, the fascin protein arises which is over-expressed in SAC. Fascin is a key protein in the rearrangement of the actin cytoskeleton since it participates in the filopodia and lamellipodia formation that are necessary for the cell movement. Due to the fundamental role of fascin in the actin bundles formation, this protein becomes a target for blocking the tumoral invasion and migration.

Objectives: This Thesis aims to search for new fascin inhibitors in colorectal cancer through pharmacological screening. Subsequently, *in vitro* assays were performed to evaluate the effects of these inhibitors on the proliferation, motility and invasion in colorectal cancer cell lines with different levels of fascin expression. At the same time, the anti-metastatic capacities of the inhibitors were evaluated in zebrafish and mice models.

Results: *In silico screening* of 9591 compounds, including 2037 approved by the Food and Drug Administration (FDA) was performed, and selected compounds were analyzed for their fascin binding affinity. As a result of these studies, we have been identified several compounds as potential fascin inhibitors, including

imipramine (IMIP), raltegravir (RAL) and monastrol (MON). Additionally, G2 compound was previously discovered by drug screening and characterized, by Dr. XY Huang´s group as a fascin inhibitor blocking cell migration, invasion and metastasis in breast cancer cells. Thus, in this Thesis we have tested the anti-fascin properties of the following compounds: G2, IMIP, RAL and MON through *in vitro* and *in vivo* assays in which migrastatin (MGS) was used as a control of typical anti-fascin compound. In all cases an anti-migratory and anti-invasive effects are observed when the colorectal cancer cells, HCT-116 and DLD-1 cell lines, were treated with the anti-fascin compounds by *in vitro* assays. The anti-metastatic effect has also been observed in an *in vivo* zebrafish model.

Conclusions: *High Throughput Screening (HTS)* plays an important role in translational research. We have found new anti-migratory and anti-invasive properties of G2 compound, IMIP, RAL and MON in colorrectal cancer cells MGS. In addition, there is a dose-dependent effect of these compounds that has been demonstrated using a zebrafish model of tumor invasion and metastasis. The preliminary results of murine model were not significant in comparison with the control´s groups, thus led to investigate the synergic effect between fascin inhibitors and chemotherapeutic agents. These studies highlight the real utility of drug repurposing for clinical research. Finally, these findings could be of therapeutic interest for the treatment of metastatic tumor cells such as those found in SAC.

Keywords: Colorectal Cancer, Fascin, Actin, Inhibitors, G2, Imipramine, Raltegravir, Monastrol, Repurposing, Migration, Invasion, Metastasis, *In vitro*, *In vivo*.

A ti Jesús por ser el comienzo

A ti Clara por ser el camino

A ti Julia por ser la luz

AGRADECIMIENTOS

Creo que esta va a ser sin duda la parte más difícil de escribir que he tenido a lo largo de toda la Tesis puesto que no se trata de redactar aspectos científicos sino de agradeceros que hayáis formado parte de esta aventura.

En primer lugar me gustaría dar las gracias a las personas que han confiado en mí desde el principio y que han creído que yo era capaz de investigar y de hacer de la ciencia un modo de vida. Ellos son mis directores, Pablo y Silvia. Habéis hecho que crea en mis capacidades y que aprenda diariamente desde la mayor humildad e inteligencia que los dos desprendéis. Ambos sois únicos tanto profesional como personalmente y no podría haber tenido más suerte al encontraros. Me llevo muchas cosas de vosotros dos que no creo que pueda olvidar fácilmente. Pablo, gracias por ser la calma y la serenidad que he necesitado en muchas ocasiones y por enseñarme que todo se consigue con esfuerzo porque tú mismo eres un claro ejemplo de ello. Silvia, gracias por enseñarme a ser constante, a ponerle pasión al trabajo diario, a hacerme razonar y a demostrarme que hay que vivir al día. Gracias por implicarte siempre que lo he necesitado, eres un gran ejemplo a seguir.

A lo largo de estos años he conocido muchas personas que me han ayudado y a las que me gustaría dar las gracias por ello. Sois tantas que espero no dejarme a nadie por el camino.

Gracias al Servicio de Anatomía Patológica del Hospital Santa Lucia. Todos sois una gran familia que me ha hecho sentir como en casa. Gracias a todos los patólogos, en especial a Pepe por su sabiduría, sus consejos y su sencillez. Esta investigación no habría sido posible sin ti. A todos los técnicos del servicio, en especial a África, Nuria y Ana que me acogieron los primeros días que yo estaba perdida por el laboratorio. También a Mari Carmen por esas largas conversaciones y a Javi. De todos he aprendido y de todos me llevo algún recuerdo especial. Gracias a Javier Trujillo por contar conmigo para empezar a trabajar junto a Pablo y ver convertidos esos 5 meses en casi 6 años. Gracias a Edith por ser tan paciente y enseñarme tanto. Gracias a todos los residentes que he conocido y me han acompañado literalmente estos años: David, Alberto, Elena, Ana, Sara, Rubén y Loli.

No me olvido, ni mucho menos, de la familia fascinante que ha ido creciendo año tras año. Todos habéis hecho posible un trocito de esta Tesis: a Sasha por su alegría, a Patxi por acompañarme en los comienzos, a Dani por su compañerismo y sinceridad, a Rubén por su constancia y compañía, a Ruth por ser tan amable y a Vero por ser tan maravillosa en todo lo que hace. A las nuevas incorporaciones fascinantes que han hecho que este grupo sea mucho más completo y desprenda alegría y felicidad: Ana A, Ana H, Fátima y Ginés. Sois tan fascinantes que no concibo este trabajo sin vosotros. No dejáis de sorprenderme y estoy muy contenta de haberos conocido. Gracias y mil gracias más, todos sois increíbles. Vuestro apoyo tanto a nivel personal como profesional ha sido insaciable, no puedo dejar la fascina en mejores manos.

Gracias a mis compañeros y amigos con los que ha sido un placer trabajar estos años. Gracias por toda vuestra ayuda, por esos días de experimentos interminables y por esas horas en animalario. Gracias Ángel y gracias Manolo. Habéis sido sin lugar a duda uno de los mejores descubrimientos de estos años. Con vosotros llegaron Pepe, Isa, Almu y Alex, Inma y Miguel, y todos los peques. No podría estar más feliz de haberos conocido.

Gracias a todos los colaboradores que habéis participado de forma desinteresada y me habéis ayudado siempre que lo he necesitado. A Mª Luisa y su equipo, Elena N, Elena B, David, Miriam, Paqui y Jesús, recuerdo con una sonrisa el tiempo que estuve en vuestro laboratorio. A Franjo por tu implicación, dedicación y por tratarme siempre tan bien. Ha sido un placer trabajar contigo. Gracias Javi por estar siempre que lo he necesitado, eres genial. A Olga por enseñarme tanto de un mundo tan desconocido para mí y a todo el personal del animalario. A David García por su experiencia y amabilidad, a Juan por su gran ayuda y su paciencia después de tantas horas de IVIS durante la pandemia. A Horacio por tus consejos pre-depósito y por ofrecerte siempre a ayudarme. Gracias al grupo de Andrés Cervantes del INCLIVA en Valencia por acogerme, gracias a Pepa y Fede por transmitirme tanto, fue un placer estar con vosotros. Gracias a Irene Luque, Tuula, Priscila y Enrico.

Este trayecto, ha hecho que conozca a personas maravillosas que me han inculcado la pasión por la docencia. Gracias al departamento de Nutrición de la UCAM por confiar en mí y hacerme sentir una más de vosotros. Gracias Jose María, Carmen, Ana,Santiago, Isa, Estefanía y Jose por aguantarme todos estos años. Gracias a Jose y Gabi.

Como todo camino, este tiene un final y estos últimos tres meses he conocido a personas que han hecho más llevadero el día a día de la escritura. Gracias a los compañeros del HiTech: Ramiro, Cindy, Raúl, Noelia y Dennis por amenizar esta escritura. A Clara, Rubén Z y Rubén R por apoyarme. A Pepa,

Camilo e Iván por estos últimos y tediosos días en los que me habéis ayudado tanto.

Por último pero no por ello menos importante he dejado a mi familia. Realmente ellos son los que han estado siempre y en todo momento conmigo. A mi familia política, Loli, Rafa y Carmen por ser fundamentales para Jesús y las peques y por querernos tanto. A Mª del Mar y a mi tía Nuria por ser como hermanas mayores para mí.

A mis padres. Mamá, hasta que no me he convertido en madre no he sabido valorar todo lo que has hecho por mí, que ha sido muchísimo. Gracias por ser el apoyo incondicional de mi vida. Verme reflejada en ti en cada cosa que hago me hace muy feliz. Papá, gracias por transmitirme tu forma de ser de la que me siento muy orgullosa y enseñarme lo que es la constancia y la dedicación, sin ti y sin mamá nada de lo que he hecho en la vida tiene sentido. A Pablo por estar siempre ahí aunque estés lejos y a Marga por quererlo y cuidarlo tanto.

No me olvido de ti Jesús, mi razón de ser, el sentido de mi vida y mi compañero. Darte las gracias es insuficiente. Eres lo mejor que me ha pasado en la vida y haber formado una familia contigo es maravilloso. No me sueltes nunca. Gracias Clara porque revolucionaste mi vida hacia límites insospechados y gracias a mi pequeña bebé Julia porque me has terminado de completar. Por último A ti cacahuete que aunque nunca fuiste, nunca te olvidaré.

"No es la especie más fuerte la que sobrevive, ni la más inteligente, sino la que responde mejor al cambio".
Charles-Darwin (1809-1882).

ÍNDICE GENERAL

García, S., & Conesa-Zamora, P. (2021). **The FDA-Approved Antiviral Raltegravir Inhibits Fascin1-Dependent Invasion of Colorectal Tumor Cells *In Vitro* and *In Vivo***. *Cancers*, *13*(4), 861. https://doi.org/10.3390/cancers13040861.

Alburquerque-González, B., Montoro-García, S., Bernabé-García, M., Bernabé-García, A., Campioni-Rodrigues, P., Luque-Fernández, I., Salo, T., Pérez-Sánchez, H., Cayuela-Fuentes, M.L., Luengo-Gil, G., Nicolás-Villaescusa, F.J., Conesa-Zamora, P. (2022). **Monastrol, a kinesin-Eg5 inhibitor, inhibits invasion and metastasis of human colorectal cancer cells by targeting fascin.** *Experimental & Molecular Medicine* (En revisión).

Alburquerque-González B, Montoro-García S, García-Bernal D, Bernabé-García M, Rodriguez-Arcas Mª J, Albaladejo- González A, Luengo-Gil G, García-Solano J, Cabezas-Herrera J, Conesa-Zamora P. **Testing the Potential Therapy with the fascin inhibitors Tofranil® and Issentress® in colorectal cancer mice models.** (En preparación).

ÍNDICE DE FIGURAS

.

ÍNDICE DE TABLAS

ÍNDICE DE ANEXOS

SIGLAS Y ABREVIATURAS

ACS: Adenocarcinoma Serrado.
AM: Acoplamiento Molecular.
ARNm: Transcrito Primario del Ácido Ribonucleico.
CC: Carcinoma Convencional.
CCR: Carcinoma Colorrectal.
cfDNA: ADN circulante.
CIMP: Fenotipo Metilador de Islas CpG.
CIN: Inestabilidad Cromosómica.
CTLA-4: Antígeno 4 asociado a Linfocitos T Citotóxicos.
DM: Dinámica Molecular.
DXR: Doxorrubicina.
ECM: Matriz Extracelular.
EGF: Factor de Crecimiento Epidérmico.
EGFR: Receptor del Factor de Crecimiento Epidérmico.
EMA: *European Medicine Agency*.
FAK: Adhesiones Focales.
FDA: *Food and Drug Administration*.
FGFR: Receptor del Factor de Crecimiento de Fibroblastos.
FOLFIRI: Irinotecán, Fluorouracilo y Leucovorina.
FOLFOXIRI: Ácido Folínico, Fluorouracilo e Irinotecán y Oxiplatino.
GPCR: Receptores Acoplados a Proteína G.
hmMSI-H: Características Moleculares de Inestabilidad a Microsatélites.
HPP: Pólipos Hiperplásicos.
HTLV1: Virus Linfotrópico T Humano tipo 1.
IMIP: Imipramina.
MAPK: Proteína Quinasa Activada por Mitógenos.
mCCR: Cáncer Colorrectal Metastásico.
MEK: MAPK Regulada por Señales Extracelulares.
MET: Microscopía Electrónica de Transmisión.

MGS: Migrastatina.
MLC: Cadenas Ligeras de Miosina.
MON: Monastrol.
MSI: Inestabilidad de Microsatélites
MSI-H: Alta Inestabilidad de Microsatélites.
MSS: Microsatélite Estable.
MVD: Densidad Microvascular.
nFDA: No Aprobado por la FDA.
NHI: *National Institute of Health.*
OH: Órgano Habilitado
OMS: Organización Mundial de la Salud.
PCK: Proteína C Quinasa.
PDB: *protein data bank*.
PDGFR: Receptor del Factor de Crecimiento Derivado de Plaquetas.
PlGF: Factor de Crecimiento Placentario.
PRV: Virus Pseudorabia.
Ps: Pólipo Serrado.
qPCR: Reacción en Cadena de la Polimerasa Cuantitativa.
RAL:Raltegravir.
RMN. Resonancia Magnética Nuclear.
SSA: Adenoma Serrado Sésil.
TB: Gemación Tumoral o *tumor budding*.
TCA: Antidepresivo Tricíclico.
TEM: Transición Epitelio Mesénquima.
TGFR: Receptor del Factor de Crecimiento Transformante.
T_m: Temperatura de *Melting.*
TNBC: Cáncer de Mama Triple Negativo.
TNF: Factor de Necrosis Tumoral.
TSA: Adenoma Serrado Tradicional.
VEGF: Factor de Crecimiento del Endotelio Vascular.
VEGFR: Receptor del Factor de Crecimiento Endotelial Vascular tipo A.
VS: *virtual screening*.

I - INTRODUCCIÓN

I - INTRODUCCIÓN

1. CARCINOGENESIS COLORRECTAL

El carcinoma colorrectal (CCR) representa un problema sanitario de primer orden por su gran morbilidad y mortalidad asociada. El CCR es la tercera causa de muerte provocada por cáncer en todo el mundo y la segunda en nuestro país, por detrás del cáncer de pulmón en hombres y el de mama en mujeres (1). En el año 2020, la incidencia del CCR incrementó un 10%, posicionándose en tercer lugar tras el cáncer de mama y de pulmón con un aumento del 11,7% y 11,4% respectivamente (2). Sin embargo, este cáncer tiene una tasa de mortalidad a nivel mundial del 9,4%, por detrás del cáncer de pulmón con un porcentaje del 18%. Igualmente, el riesgo acumulado es mayor en Europa central (3.63%) que a nivel mundial (2,25%). Además, el pronóstico de los pacientes con CCR metastásico tiene una media de supervivencia a los 5 años de solo el 18,5% en los Estados Unidos y de un 27,7% en Europa (2). Por todo lo anterior, es comprensible que la detección, resección, tratamiento y cuidados paliativos del CCR generen elevados costes para la administración pública sanitaria.

Son muchos los factores de riesgo y las causas relacionadas con el CCR. Alrededor del 20% de los pacientes con este cáncer presenta algún tipo de agregación familiar. Aproximadamente, entre el 5-10% de los CCR se desarrollan en el contexto de síndromes de cáncer hereditarios definidos (3). Aunque otros muchos casos son esporádicos, por lo que la dieta, la genética y el exposoma son fundamentales.

El CCR es una enfermedad en cuya patogénesis intervienen varias rutas moleculares y que comprende varios subtipos anatomopatológicos, cada uno de ellos con unas características clínicas, patológicas y moleculares distintas; por tanto, se trata de una neoplasia heterogénea. El carcinoma polipósico o carcinoma convencional (CC) supone un 80% del total del CCR y se caracteriza porque su

progresión sigue la ruta adenoma-carcinoma. Esta ruta, la denominada como vía clásica, fue descrita por Vogelstein *et al.* (4) y se inicia con mutaciones del gen APC que producen inestabilidad cromosómica (CIN) para luego alterarse la ruta Wnt/beta-catenina y la de la proteína quinasa activada por mitógenos (MAPK), a través de la mutación en los oncogenes *KRAS* y *p53*. El CC tiene como lesiones precursoras los adenomas tubulares o vellosos (5).

La vía serrada de la carcinogénesis colorrectal es minoritaria y ocurre en un 10-20% de los cánceres colorrectales. En este caso, se desarrolla a partir de lesiones precursoras (pólipos hiperplásicos (HPP), adenomas serrados sésiles (SSA/Ps) o adenoma serrado tradicional (TSA)), siguiendo al menos dos rutas patológicas asociadas a las siguientes características genéticas: mutaciones en *BRAF*/*KRAS*, inestabilidad de microsatélites (MSI-H) y fenotipo metilador de islas CpG (CIMP) (6, 7).

Los tratamientos estándar para el CCR siempre han sido la cirugía, la quimioterapia y la radioterapia, que pueden utilizarse combinados o no. Sin embargo, estos tratamientos tienen muchos efectos secundarios debido a su falta de especificidad y elevada citotoxicidad hacia cualquier célula con capacidad proliferativa, incluyendo las células sanas. Además, muchos pacientes presentan recidivas incluso después de los tratamientos y es por ese motivo que se requiere de tratamientos alternativos y efectivos para este tipo de pacientes (8). Por ejemplo, la presencia de la mutación en *KRAS*, generalmente se asocia con una mayor agresividad clínica del cáncer y una menor supervivencia del paciente (9). Es por ello por lo que la determinación de las mutaciones en *KRAS* es un diagnóstico de rutina muy útil para predecir los pacientes que mejor van a responder a una terapia anti-receptor del factor de crecimiento epidérmico (EGFR) (10).

En los últimos años, el tratamiento contra el CCR se ha vuelto más eficaz gracias a esa búsqueda activa de tratamientos alternativos contra esta enfermedad. Además de un número mayor de fármacos citotóxicos como las fluoropirimidinas, el irinotecán, o el oxaliplatino, ahora disponemos también de anticuerpos monoclonales contra el factor de crecimiento del endotelio vascular (VEGF) o el EGF. Ambos tratamientos, han mejorado el pronóstico de los

pacientes con cáncer colorrectal metastásico de 24 a 30 meses en mediana de supervivencia (10).

1.1 ADENOCARCINOMA SERRADO

El adenocarcinoma serrado (ACS) ha sido reconocido en las últimas clasificaciones de tumores digestivos por parte de la Organización Mundial de la Salud (OMS) (11). El ACS representa entre el 7,5% y el 9,1% de todos los CCR y es diagnosticado según los criterios histológicos propuestos por Mäkinen *et al.* (12, 13). La apariencia serrada de las criptas glandulares epiteliales es la característica fundamental de este subtipo histológico de cáncer colorrectal (Figura 1). Existen tres series clínicas publicadas hasta ahora de ACS:

- Mäkinen con 45 casos, obtenida después de revisar 466 casos CCR.
- O´Brien con 9 casos, obtenida tras revisar 460 casos (14).
- La serie española de 120 casos, obtenida después de revisar 927 casos (13).

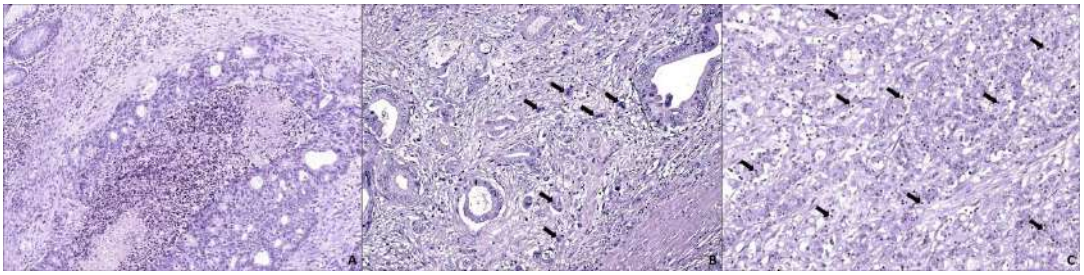

Figura 1. ***Diferentes características histológicas en los distintos tipos de cáncer colorrectal.*** ***(A)*** *Carcinoma convencional que muestra un patrón cribiforme con un citoplasma basofílico, con núcleos no estratificados, necrosis lobular sucia (centro) e infiltrados linfocíticos (esquina superior izquierda).* ***(B)*** *Adenocarcinoma serrado con el típico núcleo vesicular estratificado, citoplasma eosinofílico y lumen serrado (glándula izquierda) con débil infiltración linfocítaria, tumor budding (flechas negras) y estroma desmoplásico.* ***(C)*** *Carcinoma colorectal que presenta características histológicas y moleculares de inestabilidad de microsatélites caracterizado por un patrón sólido medular y abundante infiltración linfocitaria intraepitelial (flechas negras). Aumentos al 20X. Imagen obtenida de Alburquerque-González* et al. *(15).*

Las lesiones precursoras del ACS pueden ser HPP, SSA/Ps y TSA. Tanto SSA/Ps como TSA están relacionados con la displasia y favorecen la formación del carcinoma.

Como ya se ha comentado, la ruta serrada (Figura 2) se caracteriza por altos niveles de inestabilidad de microsatélites, elevada frecuencia en mutaciones en BRAF y el fenotipo CIMP. Estos parámetros parecen ser la causa del desarrollo de la carcinogénesis a pesar de que una gran proporción de adenocarcinomas serrados presentan mutaciones en *KRAS* y presentan estabilidad de microsatélites (16, 17). El ACS y el CCR que presenta características histológicas y moleculares del tipo MSI-H (hmMSI-H) (18) son considerados "puntos finales" de esta ruta patogénica (6, 7).

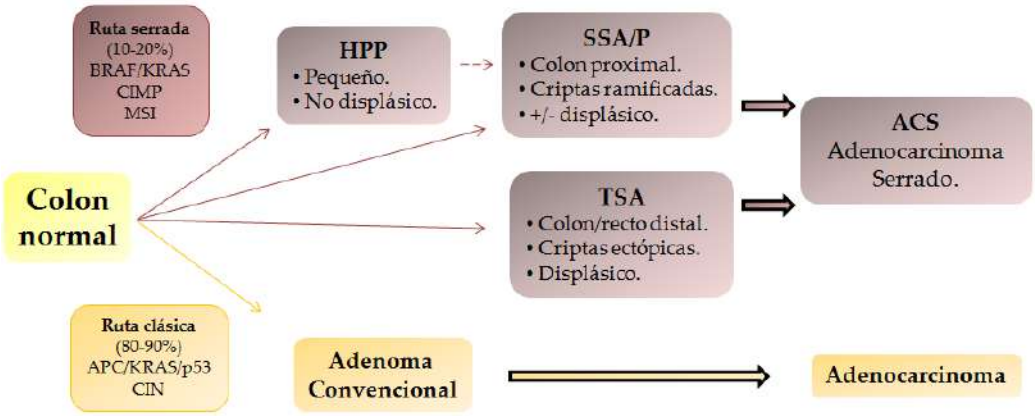

Figura 2. ***Diagrama esquemático de las vías clásica y serrada.*** *En la mitad superior (morado) aparece la vía serrada de la carcinogénesis colorrectal, asociada a diferentes características genéticas como mutaciones en los genes KRAS/BRAF, la inestabilidad de microsatélites y el fenotipo metilador de las islas CpG. En esta vía podemos observar las lesiones serradas que derivan en adenocarcinoma serrado. En la mitad inferior (anaranjado) se muestra la vía adenoma-carcinoma (clásica) mayoritaria en cánceres colorrectales. Imagen modificada de Baker AM* et al.*(19).*

Este patrón morfológico que presenta el ACS, se debe principalmente a la evasión apoptótica que fuerza al epitelio a proliferar lateralmente, adoptando un patrón de crecimiento serrado (12). De hecho, se ha encontrado que los genes

relacionados con la apoptosis están sobre-expresados en el ACS con respecto al CC. Además, se ha utilizado la expresión de hipocalcina (marcador antiapoptótico), como biomarcador pronóstico del ACS (20). El ACS se desarrolla mediante un proceso rápido a partir de adenomas serrados. Por esta razón podemos encontrar frecuentemente los ACS como CCR de "intervalo" que se relacionan con tumores colorrectales avanzados de tipo sincrónico y metacrónico (21).

El ACS tiene peor pronóstico que el CC (13) ya que presenta un frente invasor más prominente, caracterizado por factores histológicos adversos tales como la gemación tumoral ó *tumor budding* (TB), pseudofragmentos citoplasmáticos y un patrón tumoral infiltrativo (22). La pérdida de la expresión de E-cadherina y el incremento de marcadores mesenquimales son también más evidentes en el ACS que en el CC. Estas manifestaciones histológicas e inmunohistoquímicas de la actividad invasiva de las células tumorales del ACS están, además, asociadas con el reordenamiento del citoesqueleto y la actividad de pequeñas GTPasas (del inglés *small GTPases*) (20, 23). Curiosamente, la transición epitelio-mesénquima (TEM) en el ACS no parece implicar la ruta canónica Wnt/β-catenina, de hecho, la expresión de β-catenina es menor en el ACS que en el CC. La exclusión de β-catenina nuclear fue observada por Davies *et al*. en adenomas serrados de ratones transgénicos (Ptenfl/flKrasLSL/+) (24).

Este frente invasivo, histológicamente activo y a nivel molecular indicativo de la TEM, ha dado lugar a considerar al ACS como un CCR de tipo "mesenquimatoso" (25) o CMS4 según la clasificación molecular consenso de Guinney *et al.* (26), caracterizada por la estabilidad de microsatélites, baja respuesta inmune y mal pronóstico. Las tecnologías de alto rendimiento han arrojado hallazgos interesantes acerca de la biología y de los marcadores diagnósticos del ACS. Laiho *et al*. llevaron a cabo un análisis de enriquecimiento funcional para identificar las categorías de genes diferencialmente expresados en tumores con morfología serrada y no serrada. Cinco de las nueve categorías estaban relacionadas con la morfogénesis, organogénesis y genes asociados de membrana. Encontraron dos genes con menor expresión que estaban implicados en migración celular y morfogénesis (*EPHB2, PTCH*) mientras que un gen

relacionado con la angiogénesis se encontraba sobre-expresado en el ACS en comparación con el CC *(HIF1A)* (27). En esta línea, la angiogénesis y la señalización de VEGF (gen efector de la actividad HIF1-α) han sido descritas por otros autores como funciones asociadas al ACS (20, 23). Consecuentemente, la expresión inmunohistoquímica de HIF1-α, es más abundante en el ACS que en el CC (28). Nuestro grupo de investigación analizó en 2012 qué funciones genéticas se encontraban enriquecidas en el ACS en comparación con el CC, esto se comentará con más detalle más adelante (29). La ausencia de respuesta inmune es una de las características más importantes del ACS. De hecho, desde el punto de vista anatomopatológico, al observar el frente invasor hay una presencia significativamente menor de infiltrados linfocitarios peritumorales e intratumorales en el ACS en comparación con el CC (22).

Estudios independientes con pacientes de CCR procedentes de Finlandia y España, han demostrado la elevada combinación de tasa de mutación *KRAS*/*BRAF* en el ACS (78,6% s y 68,5% en la cohorte finlandesa y española respectivamente). Ello indica que la activación MAPK juega un papel fundamental en la ruta serrada. Estos porcentajes son mayores para el ACS que para el CC (40% y 33.1% en las poblaciones finlandesa y española, respectivamente). Esto justifica porqué los pacientes con ACS no se ven beneficiados por terapias anti-EGFR (16, 17).

Debido al comportamiento agresivo del ACS, su peor evolución y la mayor resistencia a las terapias anti-EGFR, en comparación con el CC, existe la necesidad de desarrollar terapias dirigidas específicamente para el ACS. En este sentido, la presencia de varias "dianas moleculares" asociadas a este tumor podría ser la base de un tratamiento adaptado a este subtipo histológico de CCR. Los principales enfoques terapéuticos del ACS se encuentran resumidos en la siguiente tabla **(Tabla 1).**

Tabla 1: Principales enfoques terapéuticos del ACS.

	Tratamiento potencial	Diana terapéutica	Aprobación FDA	Indicación actual del tratamiento	Justificación de la aplicación en cánceres serrados	Ref(s)
Terapia anti-angiogénica	Bevacizumab + quimioterapia	VEGF-A	Si	mCCR	El ACS presenta mayor expresión de HIF-1, VEGF y MVD en comparación con el CC.	(30)
	Aflibercept en combinación con FOLFIRI	VEGF-A, VEGF-B y PIGF	Si	mCCR		(30)
	Ramucirumab + FOLFIRI	VEGFR-2	Si	mCCR		(30)
	Regorafenib	VEGFR-1, VEGFR-2, VEGFR-3, Tie-2,cKIT, RET, BRAF PDGFR, y FGFR	Si	mCCR		(30, 31)
	Bevacizumab + FOLFOXIRI	VEGF-A	Si	mCCR*		(32)
Terapia para la evasión de la respuesta inmune	Anti-PD-L1 y Galunisertib	PD-L1 y TGFβR	Si	MSS-ACS	Posible utilidad en el ACS clásico basado en su estatus MSI-H.	(33)
	Atezolizumab y MEK inhibitors	PD-L1 y MEK	Si	MSS-ACS		(33)
	Ipilimumab y tremelimumab	CTLA-4	Si	MSIH ACS clásico		(34)
	MDX1105, durvalumab, avelumab y atezolizumab	PD-L1(CD274)	Si, MDX1105 estudio en fase 1	MSIH ACS clásico	Elevada expresión de PD-L1, ausencia de respuesta CD-8+.	(35)

	Nivolumab y pembrolizumab	PD-1(CD279)	Si	MSIH ACS clásico		(36, 37)
Posibles terapias dirigidas al frente invasor del ACS.	Migrastatina	Fascina	No	Ninguno	Sobre-expresión de fascina en el ACS. Fármaco sintético. Fármaco aprobado por la FDA.	(38)
	Compuesto G2	Fascina	No	Ninguno		(39)
	Imipramina	Fascina y GPCRs (proteína G acoplada a receptores)	Si	Antidepresivo		(40)

*CTLA-4: Ag-4 asociado a linfocitos T citotóxicos, MEK: MAPK/quinasa regulada por señales extracelular, mCCR; cáncer colorrectal metastásico, ACS: adenocarcinoma serrado, MSI-H: nivel alto de inestabilidad de microsatélites, MSS: microsatélite estable, MVD: densidad microvascular. FGFR: receptor del factor de crecimiento de fibroblastos, FOLFIRI: irinotecán, fluorouracilo y leucovorina. FOLFOXIRI: ácido folínico, fluorouracilo e irinotecán y oxaliplatino. GPCR: receptores acoplados a proteína G, PDGFR: receptor del factor de crecimiento derivado de plaquetas, PlGF: factor de crecimiento placentario, TGFR: receptor del factor de crecimiento transformante, VEGF: factor de crecimiento endotelial vascular tipo A, VEGFR: receptor de VEGF. *Opción razonable para pacientes con mCRC BRAFV600E mutado. Tabla modificada de Alburquerque* et al.*(15)*

1.1.1 Frente invasor: transición epitelio-mesénquima.

En comparación con el CC, el ACS exhibe más adversidades histológicas en el frente invasor. El frente invasor comprende un proceso dinámico de reprogramación celular de las células del carcinoma colorrectal conocido como TEM (41). La TEM es un proceso en el que las células epiteliales inmóviles y polarizadas, pierden la polaridad celular y la adhesión célula-célula provocado por la desregulación de la E-cadherina. En este proceso, las células se convierten en células mesenquimales capaces de migrar. La TEM origina cambios en el citoesqueleto de las células, siendo la pérdida de E-cadherina y la adquisición de N-cadherina respectivamente, sus principales características.

Se ha visto que, en la TEM, diversos factores de transcripción, como SNAIL y SLUG, inducen a las células a adquirir propiedades migratorias e invasivas. En condiciones no patológicas, la TEM participa en varios procesos fisiológicos, como la cicatrización de heridas y la embriogénesis (42). Sin embargo, en células cancerosas la TEM está asociada con el desarrollo de fenotipos más agresivos que presentan invasión, metástasis y resistencia a medicamentos (43, 44). La TEM, se puede identificar histológicamente por la presencia de TB, una característica que es específica de tumores que muestran un patrón de crecimiento infiltrativo (45). La incidencia del TB en CCR varía ampliamente en la literatura del 20% al 89%. Esto es debido al resultado de diferentes criterios de diagnóstico y métodos de cuantificación (23). García-Solano *et al.*, describieron que los ACS tienen mayor porcentaje de TB de alto grado que los CC (69,1-40,7% $p<0.0003$)(22), éste fenómeno está asociado a la baja expresión de E-cadherina que contrasta con una alta expresión de marcadores mesenquimales (46). La ruta de señalización Wnt inducida por el incremento en la expresión de β-catenina nuclear también está implicada en la formación de TB (45). Además de ser un factor de transcripción, la β-catenina, es un adaptador estructural que conecta cadherinas al citoesqueleto de actina, por lo tanto, participa en la adhesión célula-célula (47). En el 74,8% de los ACS no se observa expresión de β-catenina nuclear en comparación con el 39,6% en los CC, lo cual sugiere que este mecanismo no forma parte de la TEM en el ACS (23). Dada la heterogeneidad del CCR en términos de comportamiento clínico, se han llevado a cabo grandes esfuerzos con el objetivo de buscar

características que ayuden a caracterizar el CCR y, por tanto, pronosticar su agresividad. Una mejor caracterización del tipo de CCR ayudaría a seleccionar los pacientes para la monitorización terapéutica de los fármacos (48).

1.1.2 Citoesqueleto de actina.

Junto a la TEM, el reordenamiento del citoesqueleto de actina es indispensable para que las células tumorales adquieran un fenotipo invasor. Existen estudios sobre el papel de la actina y sus patrones de interacción. Éstos subrayan ciertas rutas de señalización clave, como por ejemplo, la vía de señalización Rho GTPasas, que a través del citoesqueleto facilitan la invasión, migración y metástasis de las células tumorales (49). Tres de las rutas más conocidas que estudian el reordenamiento del citoesqueleto de actina son la ruta de las Rho GTPasas de células eucariotas, Rho y Rac1. También encontramos la ruta de CDC42, que se encarga del reordenamiento del citoesqueleto de los microtúbulos (MT) (50). En términos generales Rho puede reclutar ROCK kinasas (proteínas kinasas asociadas a Rho) (51), las cuales regulan varias proteínas del citoesqueleto, induciendo estrés en la formación de fibras de actina y en la generación de fuerzas contráctiles (50). Por su parte, Rac1 reorganiza el citoesqueleto de actina para promover la formación de protuberancias citoplasmáticas, llamadas lamelipodios, que impulsan la motilidad celular en diferentes tipos celulares mientras que la señalización de CDC42 favorece la generación de "*micro-spikes*" ricos en actina que activan el movimiento celular.

Un principal efector aguas abajo de la familia Rho GTPasas, es la Rho kinasa que presenta un papel fundamental en la regulación de la remodelación de actina mediante la fosforilación de cofilina y cadenas ligeras de miosina (MLC). La evidencia científica parece mostrar que el ACS, a diferencia del CC, tiene un perfil característico en el reordenamiento del citoesqueleto. De hecho, la activación de rutas específicas relacionadas con pequeñas GTPasas y segundos mensajeros como son los fosfatidilinositoles, se encuentran aumentadas en el ACS (20, 23). Por lo tanto, el papel que desempeñan el fosfatidil-inositol-tirofosfato, pequeñas GTPasas, Rac1 y CDC42 en el ensamblaje de actina, es crucial en el reordenamiento de lamelipodios y filopodios, lo cual ocurre durante la migración de la célula tumoral (52).

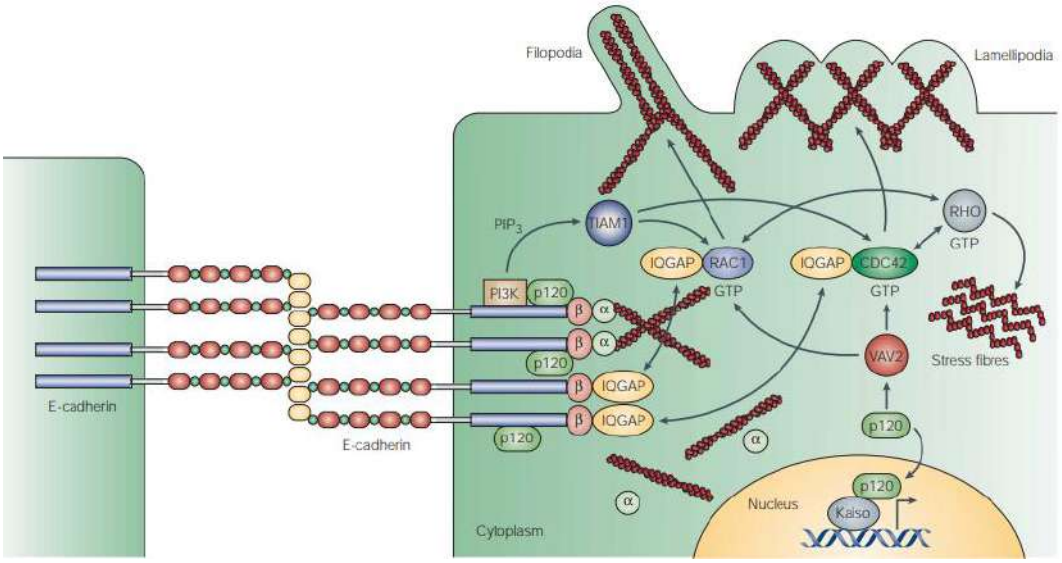

Figura 3. ***Rutas implicadas en la organización del citoesqueleto de actina.*** *Podemos observar como CDC42 activado, induce a la formación de filopodios, la activación de Rac1 da como resultado la formación de lamelipodios y la activación de Rho induce a la formación de fibras de estrés. Juntas, estas actividades afectan la organización del citoesqueleto de actina, y posiblemente el comportamiento migratorio de las células tumorales. Imagen obtenida de Cavallaro* et al.*(52).*

2. LA FASCINA

La fascina es una proteína encargada del empaquetamiento de filamentos de actina (actina-F). Se encuentra sobre-expresada en numerosos carcinomas humanos y juega un papel fundamental en la formación de protrusiones citoplasmáticas que la célula necesita para migrar. Además de promover la migración, favorece la invasión de células cancerígenas y contribuye a la metástasis en modelos murinos de xenoinjertos tumorales (53).

Las fascinas son proteínas globulares monoméricas de aproximadamente 55 KDa compuestas por 4 dominios en tándem, cada uno de los cuales corresponde estructuralmente a un pliegue de trébol β (54) (plegamiento proteico constituido

por seis horquillas beta, cada una formada por dos hebras beta y que en su conjunto componen una estructura tipo barril beta). Fueron aisladas originalmente del huevo de erizo de mar pero también se encuentran en *Drosophila melanogaster* (55), ciertos vertebrados (56) y en humanos (57). Se han descrito tres formas de la fascina en vertebrados. La fascina1 (fascina) forma parte de los filopodios de células neurales (58), dendríticas (59) y cancerígenas (60). La fascina2 se localiza en los foto-receptores de las células de la retina (61), mientras que la fascina3 se encuentra exclusivamente en testículos (62) (Figura 4).

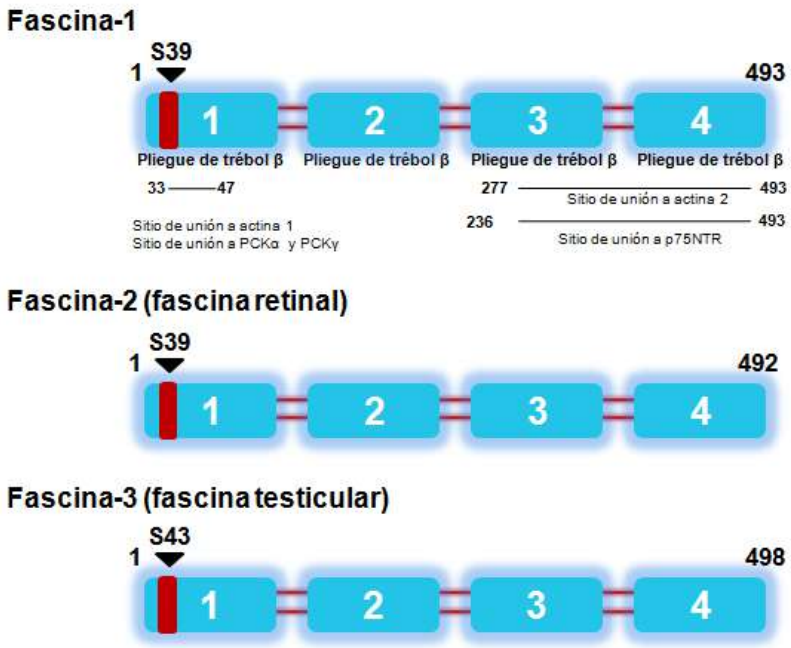

Figura 4. ***La familia de las fascinas.*** *Las fascinas se componen de 4 dominios trébol β. En granate se representan los sitios conservados de fosforilación de la proteína C quinasa. Para la fascina podemos observar los sitios de unión a actina. Imagen modificada de Hashimoto* et al. *(54).*

Como ya se ha comentado, el polipéptido de la fascina, se pliega en cuatro dominios trébol β. Los dominios 1-2 y 3-4 forman dos subunidades independientes conectadas por dos pliegues simétricos. La fascina tiene dos sitios de unión a actina ubicados dentro de los dominios trébol β 1 y 3 (63). Ono *et al.*, describieron que los sitios de unión a actina de la fascina, están regulados por la

fosforilación de una proteína quinasa C (PKC) (64). Esta fosforilación está regulada por los componentes estromales de la matriz extracelular, factores de crecimiento y citoquinas. Es por ello, que la inhibición de PKC está considerada como terapia para muchos tipos de carcinomas (65).

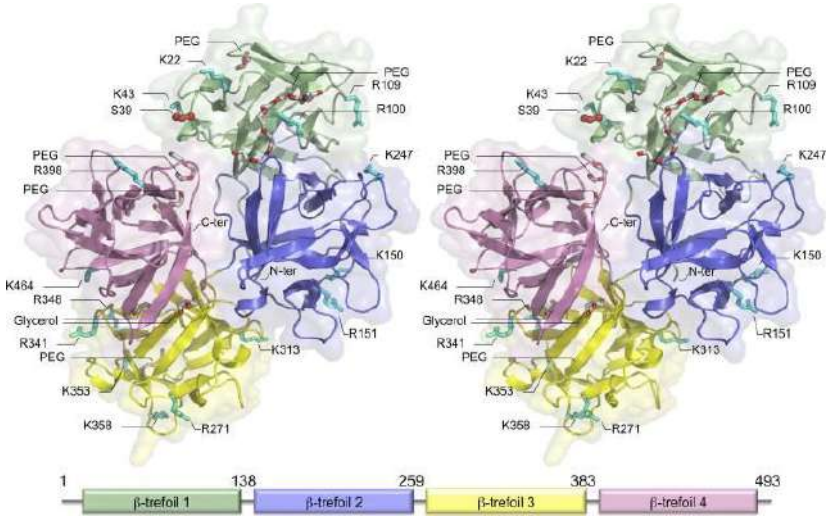

Figura 5. ***Estructura tridimensional de la fascina (PDB 3LLP).*** *Hay dos unidades de la fascina en la unidad asimétrica del cristal (A y B). En esta figura solamente se muestra la unidad A. Los cuatro dominios trébol β están marcados con diferentes colores tal y como se muestra en la leyenda inferior. En rojo, la Ser 39 que es fosforilada por la proteína C quinasa. Figura tomada del trabajo de Jansen S* et al.*(63).*

La mayoría de los residuos hidrofóbicos aminoacídicos de los dominios trébol β, están altamente conservados entre fascinas y contribuyen a la estabilidad estructural de la proteína y también a su unión a F-actina. De hecho, la unión de la F-actina a la fascina, puede inducir un cambio conformacional de la molécula que favorece la capacidad de empaquetamiento de haces de actina tanto *in vivo* como *in vitro* (66).

Así mismo, la proteína codificada por el gen de la fascina (UniProtKB_Q16658 (*FSCN1_HUMAN*), está descrita como esencial en la migración celular, la motilidad, la adhesión y las interacciones celulares. La expresión de este gen está regulada por varios microARN y su sobre-expresión puede desempeñar un papel en la metástasis en diferentes tipos de cáncer al

aumentar la motilidad celular. La expresión de este gen también es un marcador de las células Reed-Stenberg en el linfoma de Hodking. Un pseudogen de este gen se encuentra en el brazo largo del cromosoma 15 (67).

2.1 FUNCIONES DE LA FASCINA

La fascina promueve la motilidad, invasión y adhesión celular formando filopodios e invadopodios a través de su función canónica de empaquetamiento de haces de actina. Pero además de esta función, posee otras funciones no-canónicas en la célula que promueven la motilidad celular. Estas funciones no-canónicas, incluyen la regulación de la actividad de otras proteínas de unión a actina, unión y regulación de los MT. De hecho, Villari *et al*. demostraron que la fascina es esencial para el ensamblaje de las adhesiones focales de la célula para lo cual se requirió la unión fascina-MT (68). En este sentido, se ha determinado que hay una mayor dinámica de los MT a altas concentraciones de la fascina en células MDA-MB-231 y, por consiguiente, aumenta la metástasis. Este hecho ocurre independientemente de la unión fascina-actina, aunque sí depende de la concentración de la fascina (69). Otra función no-canónica de la fascina es la que confiere quimioresistencia a las células tumorales. Este efecto se observó en células de carcinoma hepático que adquirieron resistencia a doxorrubicina (DXR) tras disminuir la expresión de la fascina con la subsecuente inhibición de la TEM. De este modo, parece existir una relación entre la expresión de la fascina y la resistencia a agentes quimioterapéuticos (70). Las múltiples funciones de la fascina, deben regularse coordinadamente para controlar la migración celular (68).

2.1.1 Formación de protrusiones citoplasmáticas.

La fascina es la proteína principal encargada de llevar a cabo el empaquetamiento de filamentos de actina en haces paralelos en los filopodios y contiene dos sitios principales de unión a la actina, sitio de unión 1 y 2 (Figura 6). Por lo tanto, la fascina está implicada en la formación de diversas protrusiones celulares, como filopodios y lamelipodios, necesarias para la motilidad y migración celular (63, 71). Además, juega un papel fundamental en la formación

de *microspikes*, que se definen como invaginaciones de membrana y fibras de estrés (Figura 6). La proteína participa también en la formación del citoesqueleto de actina y el colapso del crecimiento de los axones en respuesta a proneurotrophin (proNGF) (72).

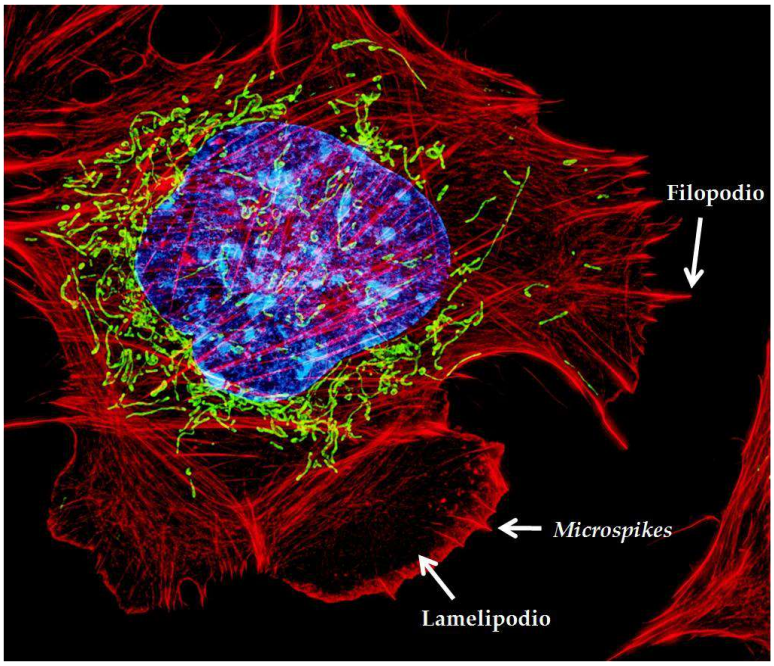

Figura 6. *Citoesqueleto de actina*. *En esta imagen podemos observar fibroblastos de ratón. Teñido en color azul se encuentra el núcleo, en verde las mitocondrias y en rojo el citoesqueleto de actina donde podemos visualizar las distintas protrusiones celulares: lamelipodios, filopodios y microspikes.Imagen modificada de Dylan Burnette y Jennifer Lippincott-Schwartz, Eunice Kennedy Shriver National Institute of Child Healthand Human Development, National Institutes of Health (73).*

Los haces de actina se encuentran organizados de forma paralela con una separación de 8 nm (74). Estos filamentos de actina, estructurados gracias a la fascina, son elementos importantes para el fortalecimiento del citoesqueleto ya que tienen que soportar la formación de protuberancias en el borde celular (Figura 7). En muchos tipos de células, las protrusiones toman una forma similar a la de un dedo (filopodios) y otras se asemejan más a zonas amplias de la membrana plasmática (lamelipodios) (75). Los filopodios tienen muchas

funciones en la migración celular, entre otras, funcionan como sensores del microambiente externo ya que pueden mediar la dirección de la migración. Además, estas extensiones de la membrana plasmática constituyen los contactos iniciales con la matriz extracelular (ECM) y permiten la generación de la tracción que origina el movimiento celular (65). Por su parte, los lamelipodios generan protuberancias sobre una superficie más amplia originando invadopodios y pseudopodios, ambas estructuras implicadas en la migración a lo largo de la ECM (76). En células normales mesenquimales, la fascina contribuye al ensamblaje de los haces de actina de ambas estructuras, tanto filopodios como lamelipodios, añadiendo rigidez. Además, L-plastina coopera con la fascina en este ensamblaje aportando flexibilidad a la estructura de los filopodios (77).

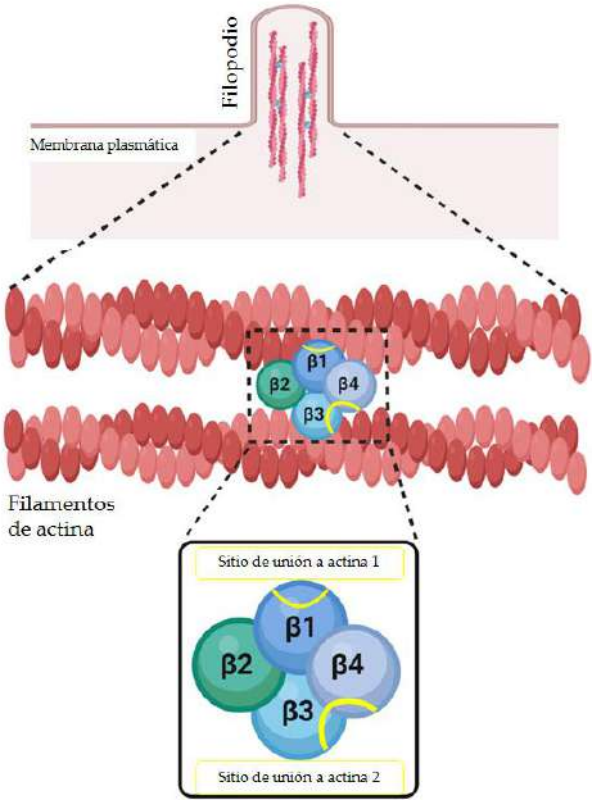

***Figura 7**. Mecanismo de formación de haces de actina mediado por la fascina y sitios de unión a actina. Podemos observar el empaquetamiento de haces de actina mediado por la fascina y un esquema de los dominios de unión a actina (amarillo) localizados en las subunidades trébol-β que componen la fascina (diferentes tonos de azul). Imagen modificada de Maureen* et al. *(68).*

2.1.2 Migración

La migración celular es un proceso cíclico que requiere una regulación coordinada de las protuberancias y adherencias en el borde de migración de la célula. La célula, en respuesta a un estímulo quimioatrayente, se polariza y extiende las protuberancias citoplasmáticas en la dirección de la señal (65). Las adherencias entre la EMC y la propia célula sirven como puntos de tracción para la migración e inician otras señales que regulan la dinámica de la adhesión y la contracción celular. Esta contracción es llevada a cabo por fibras de estrés de actomiosina que son las encargadas del movimiento de la célula hacia adelante. El ciclo de migración, termina cuando se liberan los anclajes con la EMC en la parte posterior de la célula, permitiendo así el movimiento hacia delante de la misma (78).

La migración, proporciona a las células tumorales la capacidad de abandonar el tumor primario (invasión local), entrar en los vasos sanguíneos, salir de la circulación e infiltrarse en los tejidos/órganos distantes (metástasis). Para que se produzca la migración y la invasión, el citoesqueleto de actina tiene que reorganizarse y originar los cambios dinámicos que necesita la célula para moverse (79). Existen numerosas evidencias de que la fascina, juega un papel principal en la regulación del borde de migración de la célula. Ensayos *in vivo* con células de la cresta neural, han demostrado que la fascina es necesaria en el proceso de migración (58). Además, la sobre-expresión de la fascina está relacionada con el aumento de la motilidad en ensayos con células epiteliales colónicas (80). Por otro lado, la ausencia de la fascina, provoca un retraso en la migración celular (81), y se ha observado que la célula metastásica expresa menos fascina cuando alcanza su destino, es decir cuando cesa la migración (82).

2.2 FASCINA Y CÁNCER

El papel de la fascina en cáncer ha sido ampliamente estudiado. En la mayoría de los epitelios normales, la fascina se encuentra ausente. La fascina se asociada ampliamente con un mayor riesgo de mortalidad en distintos tipos de carcinoma como son el de mama, colorrectal y esofágico y/o metástasis en cáncer colorrectal y gástrico (20, 83). La elevada expresión de la fascina, está relacionada

con formas de cáncer más agresivas como son el ACS y el cáncer de mama triple negativo (TNBC) (84, 85). Por consiguiente, la fascina está considerada como un marcador histológico de determinados cánceres agresivos. Además, su baja expresión en tejidos epiteliales no malignos, le confiere potencial como diana terapéutica (60). De hecho, varios estudios, incluyendo un meta-análisis, han demostrado que la expresión de la fascina está asociada con el aumento de los ganglios linfáticos, metástasis, progresión de la enfermedad y mortalidad en cáncer de colon y de mama (83, 86).

El principal mecanismo por el cual la fascina está implicada en la progresión del cáncer es porque se encuentra involucrada en los procesos de migración, invasión y metástasis (54, 60). En muchos estudios, las tinciones inmunohistoquímicas de la fascina son más positivas en tumores poco diferenciados o en estadios más avanzados. A menudo, esta tinción positiva para la fascina, se relaciona con una mayor probabilidad de metástasis en los ganglios linfáticos y con una baja expresión del marcador de proliferación KI67, lo cual parece indicativo de que la expresión de la fascina es específica de células altamente metastásicas (87-89).

Existen numerosos estudios *in vitro* e *in vivo* que avalan la relación directa entre la fascina y el cáncer. *In vitro*, la fascina aumenta la migración en células de carcinoma escamoso oral (90) y promueve la formación de filopodios en células de carcinoma de colon (91). La fascina, también está implicada en la regulación de la morfología y la migración en células de cáncer de mama (92). Curiosamente, la fascina también regula el inicio y la proliferación del cáncer, de hecho, el aumento de la expresión de la fascina en células de cáncer de colon, favoreció de forma positiva la formación del tumor en modelos murinos. Estos tumores progresaron más rápidamente y condujeron hacia la formación de adenocarcionomas más invasivos (93).

2.3 FASCINA COMO MARCADOR EN EL ACS.

Las técnicas de análisis masivo constituyen una interesante herramienta para la identificación de nuevas dianas moleculares susceptibles de tratamientos específicos en función del tipo tumoral (13). La fascina es un marcador inmunohistoquímico emergente de diagnóstico del ACS puesto que se encuentra

sobre-expresada, y está asociada al mal pronóstico en este subtipo de cáncer (13). Como ya se ha comentado, el ACS posee características inmunohistoquímicas únicas. Es por lo que nuestro grupo de investigación llevó a cabo un estudio para analizar y validar qué genes se encontraban diferencialmente expresados en el ACS en comparación con otros tipos de CC. Del análisis de los perfiles de expresión de ARNm, se identificaron 15 ARNm de entre los cuales 13 estaban sobre-expresados en ACS en comparación con CC. Entre los genes diferencialmente expresados, aparecieron *FSCN1* y *DAG1* (relacionados con funciones del citoesqueleto) y *HPCA* (relacionado con la unión a Ca^{2+}). Tras validar la expresión de los resultados del *microarray* por qPCR, se observó que la fascina y la hipocalcina estaban sobre-expresadas en el ACS, en comparación con el CC. Concretamente, la fascina apareció en un 88,6% de los ACS y en un 14,3 % de los CC estudiados (20).

La fascina está localizada en el núcleo central de los haces de actina y permite la formación de los filopodios en el borde migratorio de las células, favoreciendo así la migración de células cancerosas y no cancerosas (74, 89). Este hecho, podría explicar la incidencia de factores histológicos adversos en el frente invasor de ACS (22). En este sentido, Vingjevic *et al.* demostraron que el aumento de la expresión inducida de la fascina en líneas celulares de cáncer de colon producía una diseminación celular y metástasis (82). Taho *et al.*, observaron previamente que β-catenina se relacionada con la fascina en un complejo no-cadherina. De hecho, estos autores, determinaron que la fascina y la E-cadherina, utilizan un sitio de unión similar dentro de la β-catenina y que la fascina y la β-catenina co-localizan en los bordes dinámicos de la célula (94), lo cual explicaría por qué no encontramos β-catenina en el núcleo de las células en el ACS.

3. TÉCNICAS *IN SILICO*

Uno de los problemas científicos más importantes actualmente es el descubrimiento de nuevos compuestos bioactivos para problemas de relevancia biológica debido a que los compuestos conocidos previamente no son lo suficientemente efectivos. Tradicionalmente, ha sido la industria farmacéutica

quien se ha profundizado en el estudio de dichos problemas debido al gran coste económico que implica, además de sus dificultades técnicas. Sin embargo, existen otras metodologías que permiten acelerar dichos descubrimientos, y que pueden ser desarrolladas de manera eficiente en un entorno académico, y a un coste mucho menor (95). Debido a la gran cantidad de posibles fármacos candidatos que podemos encontrar mediante la metodología *in silico*, es necesario desarrollar una estrategia automática para encontrar los compuestos de interés. Actualmente, el enfoque que utiliza herramientas computacionales y que se está aplicando masivamente para predecir moléculas contra dianas concretas, recibe el nombre de Virtual *Screening* (VS) o cribado virtual (96).

Parte del método VS se basa en la búsqueda de interacciones entre dos compuestos químicos (típicamente una proteína, enzima o receptor, y una molécula pequeña o ligando), y se calcula utilizando funciones computacionales en varios puntos de unión ubicados sobre la superficie de la proteína, simulando así el proceso de interacción de cada ligando con la proteína de interés. Este proceso de interacción, recibe el nombre de *Docking* Molecular o método de acoplamiento molecular (AM) (97).

Con el objetivo de garantizar que la interacción molecular sea óptima, que la diana farmacológica sea específica y asegurar así, el objetivo biológico (desencadenar o bloquear una respuesta biológica), hay que tener en cuenta el conjunto de las características estéricas y electrónicas propias de la interacción mediante un modelado farmacofórico de dichas interacciones. Por ejemplo, para el análisis de reposicionamiento de fármacos, se realiza un modelado farmacofórico entre la diana de interés y una base de datos de fármacos entre los que figuran fármacos aprobados por la FDA y otros muchos en las últimas fases de ensayos clínicos (*Drugbank*) (98).

Finalmente, se aplica una metodología que permite predecir mediante simulación, la dinámica de la proteína para poder modelar su interacción de manera detallada con otras moléculas, como el acoplamiento a ligandos. Esta metodología se denomina Dinámica Molecular (DM) y es ampliamente utilizada en el proceso de diseño de fármacos (99). Recientemente, Montalbán *et al.* utilizaron la simulación mediante DM para dilucidar las interacciones farmacológicas entre la fibroína de la seda y determinadas drogas (100).

Por todo ello, la metodología *in silico* se utiliza cuando queremos buscar nuevos fármacos contra dianas bien definidas (101). Debido al papel que desempeña la fascina en la invasión y metástasis tumoral, es necesario realizar una búsqueda *in silico* para identificar nuevos compuestos químicos que bloqueen esta proteína. La metodología *in silico* ha sido utilizada en el descubrimiento de compuestos inhibidores de la fascina gracias a la capacidad de cómputo proporcionada por super-computadores. Para la identificación de nuevos fármacos, se emplean métodos de VS (102).

4. INHIBIDORES DE LA FASCINA

Debido al papel causal de la fascina en el fenotipo invasor de células tumorales y a que su sobre-expresión está relacionada con una peor supervivencia en numerosos tipos de cáncer, la búsqueda de nuevos inhibidores capaces de bloquear la fascina se convierte en una necesidad. Además, el ACS, puesto que muestra una elevada frecuencia en mutaciones *KRAS* y *BRAF*, en comparación con el CC, presenta mayor resistencia a terapias anti-EGFR. Esto apoya de nuevo la necesidad de buscar terapias alternativas (39).

Por lo tanto, los conocimientos actuales que se tienen sobre las características clinicopatológicas, histológicas, transcriptómicas y metilómicas del ACS, han permitido no sólo conocer la biología de este tumor sino identificar posibles dianas terapéuticas, que deben ser estudiadas desde el punto de vista funcional, así como el efecto de potenciales inhibidores (68).

Francis *et al.* diseñaron los complejos cristalinos de una serie de inhibidores (isoquinolonas y derivados de piridinas) con la fascina. Observaron la actividad anti-fascina que presentaban estos compuestos debido a su gran afinidad por esta proteína. Además, eran capaces de inhibir la agrupación de filamentos de actina mediada por la fascina. Por ello, estos compuestos, fueron considerados como punto de partida para terapias anti-metastásicas dirigidas a la fascina (103)

4.1 MIGRASTATINA

En el año 2000, Imoto *et al.* publicaron el descubrimiento de la migrastatina (MGS) como un producto natural secretado por la cepa *Streptomyces sp.* MK929-43F1 (104). Posteriormente, en 2004, se descifró la estructura definitiva de la MGS mediante análisis cristalográfico de rayos X (105).

La MGS es una macrolactona que contiene una cadena lateral alquil glutarimida, tal y como podemos observar en la Figura 8.

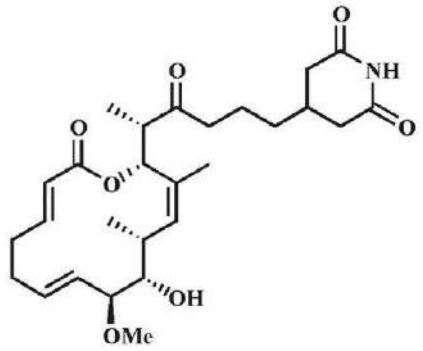

Figura 8. ***Estructura química de la migrastatina.***
Imagen obtenida de Chen et al.*(38)*

Imoto *et al.*, demostraron el poder antimigratorio de la MGS en células EC17 (células renales tumorales) así como en ratones con melanoma (104). La asociación de esta actividad con el efecto antimetastásico ha sido validada por numerosos métodos químicos y biológicos (105, 106). El descubrimiento de la MGS como agente antimigratorio y antitumoral ha estimulado el desarrollo de una amplia gama de análogos de la MGS, entre los cuales caben destacar las macrocetonas y las lactamas, con una gran capacidad para inhibir la migración celular tumoral tanto en modelos *in vivo* como *in vitro* (107).

Se ha demostrado que los análogos de la MGS, como las macrocetonas, son capaces de inhibir la migración, invasión y metástasis de células tumorales a través del bloqueo de la fascina, lo que sugiere un potencial papel específico para los análogos de MGS en el tratamiento del ACS. Sin embargo, la complejidad en

la síntesis de la macrocetona ha hecho que se prueben otros compuestos anti-fascina como indazol-furano-carboxamidas (38).

4.2 N-(1-(4-(TRIFLUOROMETIL)-BENCIL)-1H-INDAZOL-3IL) FURAN-2-CARBOXAMIDA: G2.

El compuesto G2 fue identificado por Huang *et al.* (85) como inhibidor de la fascina en un estudio *in vitro* con células MDA-MB-231, y además en ensayos *in vivo* con células 4T1, ambas de cáncer de mama siendo éstas últimas de TNBC. El compuesto G2 se une directamente a la fascina con un valor de K_d de 5 a 20 μM, inhibiendo la actividad de formación de haces de actina que posee la fascina, pero sin inhibir la L-plastina que también participa en la agrupación de los haces de actina (108). Para determinar la región de unión de G2 a la fascina, se generaron mutantes de la fascina. La función de la fascina se vio truncada al alterar tres residuos aminoacídicos: R149A, S39D y K358A (Figura 9). Las mutaciones R149A y S39D se localizan en los sitios de unión a actina de la fascina. Huang *et al*. demostraron así que el G2 interactúa directamente con la fascina y que se une a la región S39, inhibiendo la capacidad de la fascina de empaquetar correctamente los filamentos de actina (85).

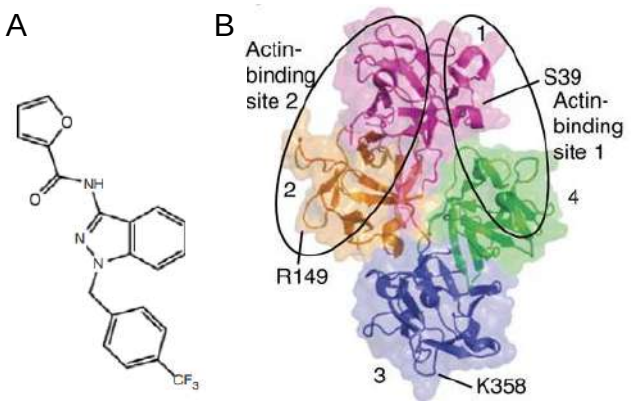

Figura 9. ***Estructura del compuesto G2*** *(A) y de la fascina que muestra los distintos mutantes (B) estudiados por Huang* et al. *Se encuentran marcados los cuatro dominios trébol β en diferentes colores y los dos sitios de unión a actina. Imagen obtenida de Huang* et al. *(85).*

Otros estudios han demostrado la capacidad inhibitoria del compuesto G2 en células de cáncer de cuello y cabeza, reduciendo la migración e invasión celular *in vitro* e inhibiendo la metástasis *in vivo* (109). También se han testado análogos del compuesto G2: NP-G2-011, NP-G2-044, NP-G2-113 y NP-G2-112, demostrando que NP-G2-011 y NP-G2-044 reducen la unión de fascina a actina. Para ello, se indujo la formación de filopodios en células 4T1 observando un efecto inhibitorio por parte de estos derivados de G2 (108). Sin embargo, no existen estudios actuales que indaguen en la utilidad anti-migratoria de este compuesto G2 en líneas celulares de cáncer de colon.

II - OBJETIVOS

II - OBJETIVOS

JUSTIFICACIÓN: El ACS es un subtipo de cáncer colorrectal caracterizado por su mal pronóstico y, además, no suele beneficiarse de las terapias moleculares más avanzadas como los tratamientos anti-EGFR o anti-PD1 debido a su perfil de mutaciones (*KRAS* o *BRAF* mutado y por presentar estabilidad para microsatélites). La fascina se encuentra sobre-expresada en el ACS. Por estas razones, es de suma importancia la identificación de nuevos inhibidores de la fascina que sean capaces de tratar el ACS, así como tumores agresivos que también se caracterizan por la sobre-expresión de la fascina.

HIPÓTESIS: El ACS se asocia a manifestaciones histológicas como el *tumor budding*, la inhibición de la E-cadherina y la sobre-expresión de la fascina, todas ellas relacionadas con la invasión tumoral. Nuestro estudio parte de la hipótesis de que la fascina desempeña un papel causal en la migración, invasión y metástasis de las células tumorales que la sobre-expresan. Por esta razón, la identificación y caracterización de inhibidores de la fascina pueden ser útiles para tratar tumores que, como el ACS, tengan una expresión elevada de la fascina.

Esta Tesis cuenta con tres objetivos principales:

1. Realizar un cribado farmacológico de alto rendimiento ("*High Throughput Screening*" *(HTS)),* usando como diana molecular la fascina, con el propósito de identificar nuevos compuestos químicos capaces de inhibir esta proteína.

2. Evaluar *in vitro,* mediante diferentes técnicas moleculares, el efecto de los nuevos inhibidores de la fascina en la proliferación, movilidad e invasión de distintos tipos de líneas celulares de CCR, para comprobar así su efecto antitumoral. Comparar siempre con el efecto de la MGS, como inhibidor

clásico de la fascina. Este presente objetivo se subdivide en los siguientes objetivos parciales:

2.1 Estudiar el efecto de los inhibidores de la fascina en la viabilidad celular de diversas líneas celulares de CCR.
2.2 Evaluar *in vitro* el efecto de los inhibidores de la fascina en la capacidad de empaquetar haces de actina.
2.3 Evaluar *in vitro* el efecto de los inhibidores de la fascina en la formación de estructuras citoplasmáticas, necesarias para el movimiento e invasión tumoral.
2.4 Evaluar *in vitro* el efecto de los inhibidores de la fascina sobre la migración e invasión de líneas celulares de CCR.

3. Evaluar *in vivo* la actividad invasora y metastásica de las células de CCR en un modelo de pez cebra y en un modelo murino. Observar el efecto de los inhibidores de la fascina en este proceso y compararlo con la MGS.

3.1 Analizar el posible reposicionamiento de estos fármacos para su uso en investigación clínica.

III – COMPENDIO DE ARTÍCULOS

III- COMPENDIO DE ARTÍCULOS

ARTÍCULO 1:

Alburquerque-González, B., López-Calderón, F. F., López-Abellán, M. D., Esteban-Gil, Á., García-Solano, J., & Conesa-Zamora, P. (2020). **Biology and Therapeutic Targets of Colorectal Serrated Adenocarcinoma; Clues for a Histologically Based Treatment against an Aggressive Tumor.** *International journal of molecular sciences*, *21*(6), 1991. https://doi.org/10.3390/ijms21061991

International Journal of
Molecular Sciences

MDPI

Review

Biology and Therapeutic Targets of Colorectal Serrated Adenocarcinoma; Clues for a Histologically Based Treatment against an Aggressive Tumor

Begoña Alburquerque-González [1,2], Fernando F. López-Calderón [1,2], María Dolores López-Abellán [3], Ángel Esteban-Gil [4], José García-Solano [1,2,5] and Pablo Conesa-Zamora [1,3,5,*]

1 Department of Histology and Pathology, Faculty of Life Sciences, Universidad Católica de Murcia (UCAM), 30107 Murcia, Spain; begoalbur@gmail.com (B.A.-G.); davolef@gmail.com (F.F.L.-C.); jgarcia652@ucam.edu (J.G.-S.)
2 Department of Pathology, Santa Lucía General University Hospital (HGUSL), Calle Mezquita sn, 30202 Cartagena, Spain
3 Department of Clinical Analysis, Santa Lucía General University Hospital (HGUSL), Calle Mezquita sn, 30202 Cartagena, Spain; mariadolores.lopezabellan@outlook.es
4 Biomedical Informatics & Bioinformatics Platform, Institute for Biomedical Research of Murcia (IMIB)/Foundation for Healthcare Training & Research of the Region of Murcia (FFIS), 30003 Murcia, Spain; angel.esteban@ffis.es
5 Research Group on Molecular Pathology and Pharmacogenetics, Institute for Biomedical Research of Murcia (IMIB), Calle Mezquita sn, 30202 Cartagena, Spain
* Correspondence: pablo.conesa@carm.es; Tel.: +34-968128600 (ext. 951615)

Received: 7 February 2020; Accepted: 9 March 2020; Published: 14 March 2020

Abstract: Serrated adenocarcinoma (SAC) is a tumor recognized by the WHO as a histological subtype accounting for around 9% of colorectal carcinomas. Compared to conventional carcinomas, SACs are characterized by a worse prognosis, weak development of the immune response, an active invasive front and a frequent resistance to targeted therapy due to a high occurrence of KRAS or BRAF mutation. Nonetheless, several high-throughput studies have recently been carried out unveiling the biology of this cancer and identifying potential molecular targets, favoring a future histologically based treatment. This review revises the current evidence, aiming to propose potential molecular targets and specific treatments for this aggressive tumor.

Keywords: colorectal cancer; serrated adenocarcinoma; angiogenesis; immune response; invasive front; molecular targets

1. Introduction

Colorectal carcinoma (CRC) accounts for the third–most frequent cause of cancer death worldwide [1]. This tumor develops from precursor lesions (polyps/adenomas) following at least two pathological routes; the most common one, the adenoma–carcinoma sequence, is typically characterized by chromosomal instability and microsatellite stability leading to the development of conventional carcinoma (CC). Less is known about the serrated pathway, in which a high level of microsatellite instability (MSI-H), high frequency of BRAF mutation and the CpG island methylation phenotype (CIMP) seem to be the leading carcinogenic causes, although significant proportions of SAC are KRAS-mutated and microsatellite-stable [2,3]. These alterations contribute to the development of serrated adenocarcinoma (SAC) and the CRC showing histological and molecular features of MSI-H (hmMSI-H) [4], which are considered as endpoints of this pathway [5,6]. MSI-H is a manifestation

of a deficiency in DNA mismatch repair mechanism which has been associated with histological features including the presence of signet-ring cells, mucine, tumor heterogeneity with a medullary component, poor differentiation, "pushing" type tumor growth pattern, peri- and intra-tumoral infiltrating lymphocytes, and "Crohn-like" inflammatory response [7]. SAC has been recognized in the latest WHO classifications of digestive tumors [8,9], accounts for 7.5%–9.1% of all CRCs and is diagnosed based on histological criteria put forward by Mäkinen [10,11], the serrated appearance of the epithelial glandular crypts being the most characteristic feature (Figure 1). This morphological pattern seems to be due to apoptotic evasion that causes the transformed epithelium to proliferate laterally, adopting a sawtooth growth pattern [8,10]. In fact, apoptosis-related genes were found to be enriched when comparing the expression signature of SAC with that of CC, and the immunohistochemical expression of hippocalcin, an anti-apoptotic protein, was proposed as a biomarker of SAC [12].

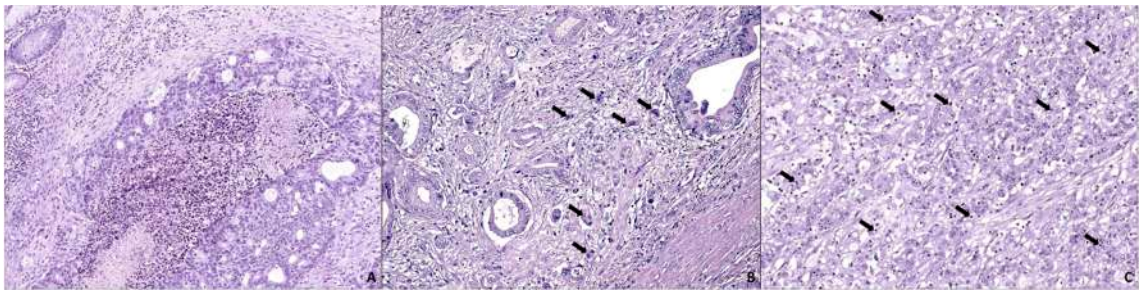

Figure 1. Differential histological features of histological subtypes of colorectal carcinoma. (**A**) Conventional carcinoma (CC) showing a cribriform gland pattern with basophilic cytoplasm, non-stratified nuclei, lobular dirty necrosis (centre) and lymphocytic infiltrates (upper-left corner). (**B**) Serrated adenocarcinoma (SAC) with typical vesicular stratified nuclei, eosinophilic cytoplasm and serrated lumen (left gland) with weak lymphocytic infiltration, tumor budding (black arrows) and desmoplastic stroma. (**C**) Colorectal carcinoma (CRC) with histological and molecular features of microsatellite instability (hmMSI-H) characterized by a medullar "solid" pattern and abundant intraepithelial tumor-infiltrating lymphocytes (black arrows) 20× original magnification. (Source: Authors).

SAC develops from serrated adenomas through a fast process. Therefore, it is not unexpected that SACs are frequently found as "interval" CRCs and are related with synchronous and metachronous advanced colorectal tumors [13]. In addition to this higher abundance of synchronous carcinoma compared to CC, distant polyps present in surgical resections containing SAC frequently show serrated morphology, thus suggesting a bystander effect or individual predisposition for serrated carcinogenesis [11]. At this point it, is noteworthy that smoking and alcohol abuse have been associated with the development of the serrated carcinogenesis pathway [14–16], as well as the presence of *Fusobacterium nucleatum* in the patient's feces [17].

Not surprisingly, SAC has a worse prognosis than CC [11], and in-depth studies have revealed that, compared to CC, SAC shows a more prominent invasive front, which is characterized by abundant histologically adverse prognostic factors such as tumor budding, cytoplasmic pseudofragments and an invasive tumor infiltrating pattern [18]. Consequently, the loss of E-cadherin expression and the increase in mesenchymal markers are more evident in SAC than in CC [19]. These histological and immunohistochemical manifestations of the invasive activity of SAC tumor cells were further confirmed by analyzing the molecular signatures of SAC compared to CC, where functions associated with cytoskeleton rearrangement and small GTPases' activity were frequently enriched in SAC [12,20]. Intriguingly, the epithelial mesenchymal transition (EMT) in SAC does not seem to involve the canonical Wnt/β-catenin, as the nuclear expression of β-catenin was lower in SAC than in CC. In fact, the same β-catenin nuclear exclusion was observed by Davies et al. in serrated adenomas spontaneously developed in transgenic mice ($Pten^{fl/fl}Kras^{LSL/+}$) [21]. Other mouse serrated models that abolish atypical

protein kinase C (aPKC) (*Prkci*$^{fl/fl}$ *Prkcz*$^{fl/fl}$ *Villin-cre*) drive serrated intestinal cancer, also showing a lack of nuclear staining of β-catenin [22].

This histologically active invasive front and molecularly manifest epithelial-mesenchymal transition have led SAC to be considered as belonging to the so-called "mesenchymal" or type 4 comprehensive consensus molecular subtype (CMS4) of CRC [23], which is characterized by microsatellite stability, weak immune response and worse prognosis. Histological and molecular classifications of CRC do not perfectly overlap, since another subtype of SAC, termed "classical serrated CRC", has been proposed that belongs to the CMS1 subtype and is characterized by BRAF mutation, CIMP, microsatellite instability (MSI), higher immune response and better prognosis than the "mesenchymal" SAC type [23].

High-throughput technologies have yielded interesting findings about SAC biology and potential diagnostic markers for SAC. Laiho et al. performed functional enrichment analysis to identify categories with significant enrichment based on the genes differentially expressed in tumors with serrated and non-serrated morphology. Five out of nine categories were linked to morphogenesis, organogenesis and membrane-associated genes. Two genes (*EPHB2*, *PTCH*) involved in cell migration and morphogenesis were found to be downregulated, whereas one gene (*HIF1A*) related to angiogenesis was upregulated in SAC compared to CC [24]. In this line, angiogenesis and signalling of VEGF (an effector gene of HIF-1α transcriptional activity) have been found by other authors to be characteristic enriched functions associated with SAC's molecular signature [12,20]. Consequently, the immunohistochemical expression of HIF-1α and the presence of microvascular density were significantly more abundant in SAC than in CC [25]. It is noteworthy that other enriched functions associated with SAC in molecular profiling studies are labelled as neural-related and, more remarkably, as related to immune response against either autoantigens or pathogens [12,20]. Freely accessible data from our research group have been retrieved from the ColPortal repository [26] and reanalyzed for function enrichment compared to CC (Figure 2). Common enriched functions found in SAC and CC compared to normal adjacent mucosa are presented as Figure S1. The lack of immune response is another important feature of SAC that has a histological manifestation when looking at this tumor invasive front where, compared to CC, there is a significantly lower presence of peritumoral and intratumoral lymphocytic infiltrates [18]. This poorer immune response of SAC is even more dramatic when compared to hmMSI-H, and therefore, transcriptome, micro-transcriptome and methylome studies have supported this histological observation [6,27,28]. These facts, added to the fact that most SACs are microsatellite-stable [2,3], do not make SAC a good candidate for biological therapy targeting the immune-checkpoint.

Independently studies on Finnish and Spanish CRC patients have shown that a high combined mutation rate of KRAS and BRAF in SAC (78.6% for the Finnish and 68.5% for the Spanish cohorts) indicates that mitogen-activated protein kinase (MAPK) activation plays a key role in the serrated pathway. These percentages in SAC are higher than those found in matched CC (40% in the Finnish and 33.1% in the Spanish patients), thus implying that most SACs will not benefit from anti-EGFR treatment, the major recent breakthrough in targeted therapy for metastatic CRC (mCRC) [2,3].

Given the aggressive behavior of SAC, its poorer outcome and the higher resistance to anti-EGFR compared to CC, there is an urgent necessity to develop targeted therapies for SAC. This review summarizes the current evidence about potential molecular targets that could be a basis for a treatment tailored to this histological subtype of CRC. Main potential therapeutic approaches against SAC histology or SAC-associated biomarkers are summarized in Table 1.

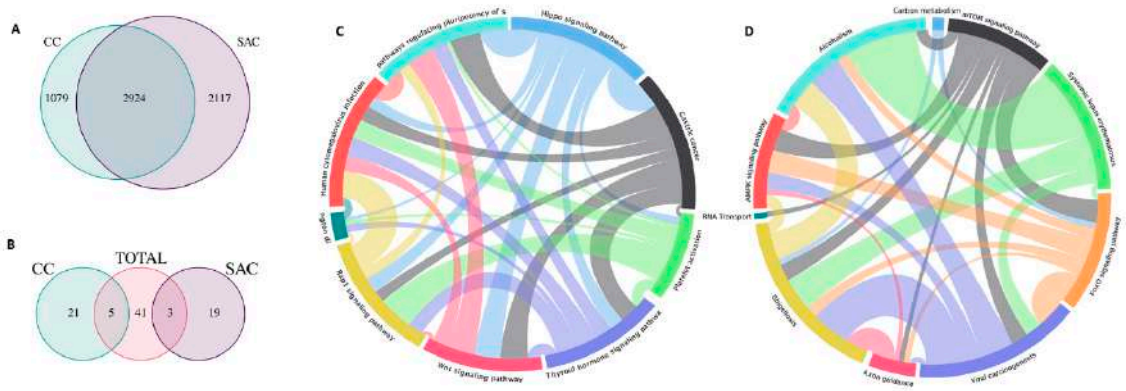

Figure 2. Differentially enriched functions in the SAC and CC transcriptomes. (**A**) Venn diagram displaying the number of common genes up- or down-regulated in SAC and CC compared to normal adjacent mucosa. Differential expression analysis has been performed on normalized data with the Linear Models for Microarray Data (Limma) package by Bioconductor [29]. Using Limma, two comparisons were made between 5 normal and 12 CC samples and the same 5 normal and 13 SAC samples. (**B**) The Kegga method from Limma was used to perform this analysis, which obtained 49 pathways significantly enriched for shared differentially expressed genes in both groups: 26 pathways for CC (5 of them shared) and 22 pathways for SAC (3 of them shared). As expected, there were no shared pathways between the different genes of the groups CC and SAC. For the false discovery rate (FDR), the Benjamini and Hochberg method was used to get corrected *p*-values [30]. Differentially enriched functions in CC (**C**), including Wnt-signalling and in SAC (**D**), including those lifestyle-, neural-, immune-hypoxia-related (**D**) are shown. The VEGF signalling pathway was close to significance in SAC, with 7 differentially expressed genes (MAPKAPK3, VEGFA, PIK3R2, RAF1, PLA2G4C, PPP3CB and PRKCB) and some related hypoxia-associated pathways (AMPK and mTOR signalling). FSCN1 is differentially expressed in the comparison Normal vs. SAC, but it is not in Normal vs. CC.

Table 1. Potential therapeutic approaches to treat tumors with SAC histology or SAC-associated biomarkers.

	Potential Treatment	Target(s)	FDA Approved	Treatment Current Indication	Rationale for Indication in Serrated Cancers	Reference(s)
Anti-angiogenic therapy	Bevacizumab + chemotherapy	VEGF-A	Yes	mCRC	SAC presents higher expression HIF-1, VEGF and MVD compared to CC	[31]
	Ramucirumab + FOLFIRI	VEGFR-2	Yes	mCRC		[31]
	Aflibercept in combination with FOLFIRI	VEGF-A, VEGF-B and PlGF	Yes	mCRC		[31]
	Bevacizumab + FOLFOXIRI	VEGF-A	Yes	mCRC*		[32]
	Regorafenib	VEGFR-1, VEGFR-2, VEGFR-3, Tie-2,cKIT, RET, BRAF PDGFR, and FGFR	Yes	mCRC		[31,33]
Therapy for avoiding immune response	Anti-PD-L1 and Galunisertib	PD-L1 and TGFβR	Yes	MSS-SAC	High PD-L1 expression, lack of CD-8+ response	[22]
	Atezolizumab and MEK inhibitors	PD-L1 and MEK	Yes	MSS-SAC		[22]
	Ipilimumab and tremelimumab	CTLA-4	Yes	MSIH classical SACs	Possible utility in classical SAC based on MSI-H status	[34]
	MDX1105, durvalumab, avelumab and atezolizumab	PD-L1(CD274)	Yes, MDX1105 in phase I study	MSIH classical SACs		[35]
	Nivolumab and pembrolizumab	PD-1(CD279)	Yes	MSIH classical SACs		[36,37]
Possible therapies targeting SAC invasive front	Migrastatin	Fascin1	No	None	Fascin1 overexpression in SAC Synthetic drug FDA approved drug	[38]
	G2	Fascin1	No	None		[39]
	Imipramine	Fascin1and GPCRs (G protein coupled receptors)	Yes	Antidepressant		[40–42]

CTLA-4: cytotoxic T lymphocyte-associated Ag-4, MEK: MAPK/extracellular signal-regulated kinase, mCRC; metastatic colorectal cancer, SAC: serrated adenocarcinoma, MSI-H: high level of microsatellite instability, MSS: microsatellite stable, MVD: microvascular density. FGFR: fibroblast growth factor receptor, FOLFIRI: irinotecan, fluorouracil and leucovorin. FOLFOXIRI: folinic acid, fluorouracil and irinotecan and oxaliplatin. GPCRs: G protein coupled receptors, PDGFR: platelet-derived growth factor receptor, PlGF: placental growth factor, TGFβR: transforming growth factor receptor β, VEGF: vascular endothelial growth factor type A, VEGFR: VEGF receptor. *Reasonable option for mCRC $BRAF^{V600E}$ mutated patients.

2. SAC Shows an Upregulation of Angiogenesis Markers

Clinically, antiangiogenic (anti-VEGF) therapy for mCRC has become the standard therapy in combination with several cytotoxic drugs [43]. Given the significant role of angiogenesis in SAC, as demonstrated by the overexpression of Hypoxia-inducible Factor 1α (HIF-1α) and VEGF and high microvessel density in serrated adenocarcinoma compared to conventional colorectal adenocarcinoma, these molecular biomarkers could be the key to new anti-angiogenic therapies specific to SAC.

Due to the characteristics of the tumor vascular network, tumor vessels exhibit immaturity and excessive permeability, leading to poor perfusion and increased hypoxia in the tumor microenvironment [44]. Under hypoxic conditions, HIF-1 is able to escape degradation and increases the transcription of genes involved angiogenesis, survival, cell proliferation, cell migration and glucose metabolism [45,46]. The angiogenic growth factors induced by inadequate local perfusion and chronic hypoxia in tumor tissue can also result in reduced leukocyte recruitment and resistance to both chemotherapy and radiotherapy [47]. This lack of immune activation is also characteristic of SAC and is discussed below.

HIF-1 expression can also be upregulated by oxygen-independent mechanisms triggered by oncogenes (e.g., EGFR, RAS and BRAF) or growth factors that stimulate MAPK, mTOR and PI-3K/Akt pathways, and by a lack of tumor suppressors such as VHL and PTEN [48,49].

Angiogenesis in CRC is induced by the HIF-1α subunit through the activation of expression of the HIF-1 target gene vascular endothelial growth factor (VEGF), as shown in a number of studies using immunohistochemistry in CRC tissue specimens [50].

Previous results on HIF-1α expression in normal colonic mucosa have shown its presence in cells in the upper part of the crypts and cells of the proliferative component in normal colorectal mucosa [51]. HIF-1α mRNA and/or protein is detected in both adenomas and CRCs, being more commonly expressed in adenocarcinomas than in adenomas, as a number of immunohistochemical studies indicate [52,53]. Thus, HIF-1α expression is also frequently correlated with the disease stage [50]. Rigopoulos et al. have also demonstrated significant association between VEGF and HIF-1α immunohistochemical expression, as well as deregulation of the EGFR/VEGF/HIF-1α signalling pathway in colon adenocarcinoma [54].

Importantly, in a meta-analysis by Chen et al., the results indicated a significant association of HIF overexpression with increased mortality risk, in terms of overall and disease-free survival, and proved an association of overexpressed HIF-1α with disease progression and unfavorable prognosis in Asian CRC patients [55]. Equally, VEGF mRNA and protein expression levels correlate with vascularity, tumor progression and poor prognosis in CRC [43,50].

Two independent studies on microarray mRNA profiling have revealed that, compared to conventional colon carcinoma (CC), SAC displays a higher representation of hypoxia-related functions and the VEGF pathway and an overexpression and stabilization of HIF-1α [12,24]. HIF-1α stands as one of the most discriminant immunohistochemical biomarkers between SAC and CC, with a positivity of 62.2% and 21.7%, respectively.

Unsurprisingly, in a study aiming to evaluate the functions enriched when comparing differentially methylated genes in SAC versus CC, differentially methylated activities related to VEGF signalling were found, amongst others, to be typically associated with SAC [20].

In the first and only study assessing hypoxia and angiogenesis markers in SAC, Tuomisto et al. revealed that HIF-1α and VEGF expressions and high microvascular density (MVD) were more frequent in SACs than in CCs, thus confirming prior gene expression profiling studies [25]. Specifically, immunohistochemistry analysis of HIF-1α and VEGF in colorectal polyps and colorectal cancers showed that both HIF-1α and VEGF were expressed in most (78–93%) of serrated precursors. In serrated adenocarcinoma, HIF-1α protein was also present in 77.8% of cases, while only 20.3% of CCs were HIF-1α–proficient. VEGF expression significantly correlated with HIF-1α expression in SACs and showed a trend towards a positive association in CCs.

MVD was significantly higher in SACs, and, surprisingly, serrated morphology was the only significant predictor of MVD in CRC after multivariate analysis. Finally, regarding the mechanism

of HIF-1α stabilization, HIF-1α expression was characteristic of well-vascularized tumor in SACs, suggesting a hypoxia-independent mechanism. Besides, in this study, neither BRAF nor KRAS mutation status was associated with HIF-1α and VEGF expressions, nor with HIF-1α stabilization in CC or SACs. Even more, the great majority of SACs carrying wild-type alleles for KRAS and BRAF (81%) were HIF-1α proficient, pointing out to other mechanisms for HIF-1α stabilization in SACs [25]. Figure 3 shows the abundance of SAC-associated MVD using fascin1 immunohistochemistry.

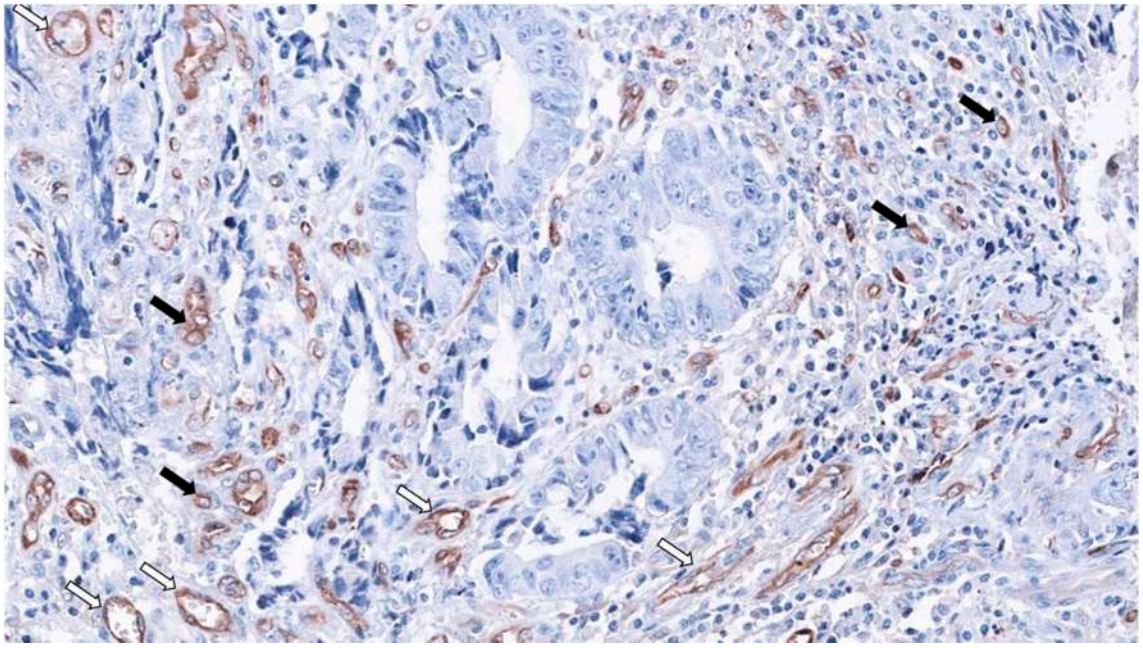

Figure 3. Fascin1 expression in SAC-staining tumor-budding cells (black arrows) and abundant surrounding microvessels (white arrows) 20× original magnification. (Source: Authors).

Therapeutic Opportunities Against Angiogenesis in SAC

Anti-angiogenic therapies aim to improve chemotherapy and radiotherapy treatments by combining with the latter. This improvement is probably due to a maturation effect on blood vessels, a process known as "vascular normalization" [44].

Recently, a number of antineoplastic therapies, such as blocking antibodies of VEGF, inhibitors of low–molecular weight VEGFR, and soluble VEGF constructs (VEGF-Trap), have been developed to neutralize VEGF [56,57]. Indeed, antiangiogenic (anti-VEGF) therapy for mCRC has become the standard therapy [43].

Bevacizumab, a humanized monoclonal antibody binding and neutralizing all human VEGF-A, was the first antiangiogenic drug approved by the US FDA for mCRC treatment in 2004, in combination with chemotherapy in both the first- and second-line setting. Another approach is targeting the receptor instead of the soluble growth factor. In this line, aflibercept is a recombinant fusion protein acting as a soluble decoy receptor binding with high-affinity VEGF-A, VEGF-B, and PIGF, thus inhibiting downstream signalling, and it has been registered as a second-line treatment in combination with FOLFIRI (irinotecan, fluorouracil and leucovorin). Likewise, ramucirumab, a fully humanized monoclonal antibody, selectively binds to VEGFR-2, the main VEGF family receptor involved in angiogenesis, and it received FDA approval in 2015 for the second-line treatment of mCRC (reviewed in [31]).

Regorafenib is a novel oral multikinase inhibitor against the activity of several protein kinases, such as VEGFR-1, VEGFR-2, VEGFR-3, the angiopoietin receptor Tie-2, as well as cKIT, RET, BRAF PDGFR, and FGFR [31]. It was approved by the FDA in 2012 for the treatment of mCRC progressing after failure to available standard treatments. VXM01 is an oral anti-angiogenic vaccine applied as

live attenuated *Salmonella* bacteria containing an expression plasmid encoding VEGFR-2, which is currently being tested in a phase I clinical trial in mCRC patients [58]. In a preclinical setting, it has also been described that miR-497 can inhibit CRC metastasis in vitro and in vivo by targeting the VEGF-A/ERK/MMP-9 signalling pathway [59].

At present, other novel anti-angiogenic drugs with various mechanism of action distinct from VEGF(R) inhibition are under clinical investigation, being the first results expected soon [60]. Angiopoietins may also be a valid target for anti-angiogenic drugs. AMG-386 (trebananib) is a peptide-Fc fusion protein that blocks angiogenesis by interfering Ang1 and Ang2 binding to Tie2 receptor. In preclinical studies, trebananib showed anti-tumor activity against colorectal tumor xenografts in mouse [61].

In another line of thought, the introduction of HIF-1α inhibitors in the treatment of CRC patients may be very useful clinically. Cinobufagin suppresses tumor neovascularization by altering the endothelial mTOR/HIF-1α pathway to trigger vascular endothelial cell apoptosis mediated by ROS, and it is emerging as a promising natural anti angiogenic agent [62]. Moreover, there is evidence that the antitumoral effects of the EGFR-blocking antibody cetuximab may be mediated through inhibition of the PI3K pathway, which in turn leads to downregulation of HIF-1α synthesis and activity [50]. Another study suggested that, by targeting the C-terminus of HSP90, it is possible to exploit the prolyl hydroxylase and proteasome pathway to induce HIF-1α degradation in hypoxic tumors [63].

Although there is much evidence reported in this field, resistance to antiangiogenic therapy is still a problem to solve, and many patients do not benefit from anti-angiogenic therapies or develop resistance in the course of treatment, for instance, through the activation and/or upregulation of different pro-angiogenic signals (such as FGF, PDGF, and Ang-1) by anti-angiogenic inhibitors [31]. Predictive biomarkers are needed to identify which patients will develop resistance mechanisms during treatment.

Despite this anti-angiogenic armamentarium and the consistent use of anti-VEGF in metastatic CRC, no studies so far have specifically analyzed whether SAC responds better or worse to anti-angiogenic therapies. Future studies are necessary with the aim of unveiling whether serrated histology could be a predictive marker of anti-angiogenesis response. Nonetheless, despite this lack of knowledge, molecular insights on SAC could give some clues. The most typical molecular alterations associated with the serrated neoplasia pathway could be the mutation in BRAF proto-oncogene [64] and the high level of CpG island methylation phenotype (CIMP-H) [65].

Cytotoxic and anti-angiogenic monoclonal antibody combinations have been tested in *BRAF*^{V600E}-mutated patients. FOLFOXIRI (folinic acid, fluorouracil and irinotecan plus folinic acid, fluorouracil, and oxaliplatin) plus bevacizumab is currently considered a potential first-line treatment option for patients with *BRAF*^{V600E}–mutated metastatic CRC, given the limitations of standard cytotoxic combinations [32]. Moreover, regorafenib, due to its broad-spectrum kinase inhibitory property, offers benefits in survival in all patient subgroups, including those carrying major oncogene mutations (e.g., RAS and BRAF), as shown in clinical trials [33]. Nowadays, these two molecular therapies in combination with chemotherapy might be the best option for SAC treatment targeting angiogenesis.

On the other hand, CIMP-H arises as a potential predictive biomarker of antiangiogenic treatment efficacy [66]. In 2015, an international consortium developed the Consensus Molecular Subtypes (CMS), classifying CRC into four distinct subgroups [67]. Among these, CMS1 (microsatellite instability immune) tumors are associated with poorer prognosis, high tumor mutational load, MSI, CIMP, BRAF mutation, female gender and right-sided location [67]. Notably, Lenz et al. recently reported that the CMS1 molecular subtype might be a predictive biomarker of response to bevacizumab [68]. This group determined the predictive and prognostic value of the CMS classification of CRC in patients previously enrolled in CALGB/SWOG 80405, a phase III trial that compared the addition of bevacizumab or cetuximab to fluorouracil, leucovorin and oxaliplatin or fluorouracil, leucovorin and irinotecan as the first-line treatment of advanced CRC in a heterogeneous cohort of patients [69]. Analyzing these patients' outcomes according to their tumor CMS profiles, CMS1 treated with bevacizumab showed

better results than treatment with cetuximab. Contrastingly, opposite results were observed for CMS2 (canonical) tumors. These evidences suggest that the CMS classification can be not only prognostic but also predictive of anti-angiogenic treatment efficacy, though further investigations are needed to standardize CIMP status's definition [31].

3. SAC is Especially Capable of Avoiding the Immune Response

The immune response in the serrated pathway plays a critical role in its development, growth and possible treatment response [23,70]. SACs are typically characterized by a weak peritumoral lymphocytic infiltration compared to CC and hmMSI-H tumors [18]. The significance of the relationship between a tumor's cells and its microenvironment has grown in the last few years through several studies [71]. Among the different components, two of them arise as the major drivers, namely the tumor-associated macrophages (TAMs) and the infiltrating T cells (TILs) [72], while others, such as neutrophils, natural killer cells and dendritic cells, play a supportive role [73,74]. Although the main roles of both TAMs and TILs remain elusive, or even contradictory [75], some discoveries have been made that shed some light on this scenario. On the one hand, in most tumors, TAMs display M2 differentiation, which favors tumor progression and metastases [76] and is correlated with poor prognosis [77] over the M1 differentiation, which, in contrast, leads to an inflammatory response. On the other hand, T cells show a plethora of functions, depending on their type. The T cell response is represented by CD8+ cytotoxic T lymphocytes, the CD4+ T-helper lymphocytes and the Treg cells. While the first have an important antitumoral effect through the release of perforin and granzyme B, the other two types vary in their function, from antitumoral activities to the control of excessive immune response [78].

The gastrointestinal tract continuously interacts with pathogens, developing a well-established immune cohort that contributes to the development and maintenance of the tissue [79]. In colorectal cancer (CRC), this status quo has been driven away, and multiple studies have shown the altered role of the tumor-infiltrating cells, like macrophages, lymphocytes and natural killer cells [71]. Apart from the type of cell, other parameters such as density, location and genetic mutations are key to properly predicting prognosis, patient survival and treatment response [80,81]. Furthermore, immune infiltration tends to improve survival in CRC [82,83], whereas other studies suggest that the interaction between the immune system and the tumor is crucial for the development of distal metastases, the main cause of related colorectal cancer deaths [84]. Here, TAMs arise as driving factors for the development of metastasis, paired with the epithelial-mesenchymal transition (EMT), migration and invasion [72]. These M2 polarized TAMs display a molecular signature that favors positive feedback on tumor cells through the release of anti-inflammatory cytokines [85].

Most SACs are found to be microsatellite-stable tumors [2,3] and thus generate few neoantigens [86]. However, over 10% of SACs are classified as MSI. These tumors bear an important neo-antigen load, which correlates with high immune infiltration [87,88]. Dendritic cells capture these neoantigens and present them on their surface, in MHC-II proteins in lymph nodes, where they activate CD4+ T helper cells, which trigger the activation of CD8+ cytotoxic T cells [89]. Due to this fact, MSI tumors have higher densities of Th1 cells and higher IFN-γ levels than MSS tumors. With this in mind, the so-called immunoscore has been developed in order to categorize the immune infiltration [90]. This is made by quantifying the presence of CD3+ and CD8+ lymphocyte populations in the tumor. This score can have a predictive role in prognosis, e.g., MSI tumors do not benefit from 5-fluorouracyl treatment, display a higher immunoscore and usually have a better prognosis, while some MSSs with good prognosis also have a high immunoscore [91]. However, it is still to be unveiled to what extent microsatellite-unstable SACs are clinically similar to those CRCs without serrated features that show both histological and molecular features of MSI-H, as the diagnostic score for identifying the latter (MSpath score) does not seem valid for the former [92]. These findings show that there is still no good method to predict an accurate prognosis, at least in SAC. Regarding this concern, microarray and methylome analysis comparing CC and SAC has revealed that there are differences between them in

terms of immune response. SACs show functional enrichment in phagocytosis, B-cell response and a down-representation of IL-12 pathways [12]. The increase of the B cell response can lead to an inhibition of the anti-tumor immunity [93], while the inhibition of IL-12 shifts the immune environment towards anti-inflammatory behavior [94]. This is also demonstrated by the fact that HIF-1α, whose expression is higher in SAC than in CC [24,25], has been associated with the development of an immunosuppressive microenvironment in the tumors [95]. The actin-bundling protein fascin1, which is also overexpressed in SAC [92], could be implicated as well in the regulation of the immune response, via suppressing RIG-I signalling and IFN-β production, and therefore preventing immune-related cell death [96]. In addition to this, the study of methylation of SAC compared to hm-MSI-H has shown differences in methylation and in the expression of some immune-related genes, such as CD14, TLR4 and HLA-DOA. CD14 and HLA-DOA tend to be more methylated in hmMSI-H than in SAC. These genes, along with CXCL14, are upregulated in SAC compared to hmMSI-H, although the cell of origin for this overexpression is elusive, as these genes are normally expressed in myeloid cells, which are not as abundant in SAC as they are in CC or hmMSI-H [27]. ICAM1, however, is more expressed in hmMSI-H than in SAC, which typically favors antigen presentation, is associated with less risk of metastases and is related with a good prognosis due to its association with leukocyte extravasation and improved immune response in the tumor microenvironment [6]. The study of the microtranscriptome has shown a difference in the expression of miR-181-a2, which is lower in SAC than in hmMSI-H. The lower levels of this mircroRNA regulate the immune response by enhancing the expression of IL-2, IL-22 and IL-17a in the serrated lesions, which then might favor an immunosuppressive phenotype [28,97]. These differences confirm the importance of understanding the immune environment in SAC. Along these lines, a new classification of SAC has recently been proposed. The "classical" serrated CRC shows MSI-H and strong immune infiltration, thus making this subtype a good candidate for immuno-checkpoint inhibition therapy (ICI). In contrast, the DKOIEC mouse model, which recapitulates the human "mesenchymal" serrated, displays immunosuppressive behavior, high levels of PD-L1 expression and exclusion of CD8+ cells from the tumor [22]. The future understanding of serrated lesions and their microenvironment would provide better tools for diagnosis and treatment.

Therapeutic Approaches for Avoiding Immune Evasion in SAC

In the last few years, the rise of immunotherapies based on the modulation of the immune response has opened a new horizon in tumor treatment therapeutics. These therapies' objective is to enhance T cell activation, targeting three main surface proteins: CTLA4, PD-1 and PDL-1. Despite the fact that immunotherapies against CRC have not rendered results as good as in other cancers like melanoma, considerable progress has been made in that field. As commented previously, the majority of SACs are MSS, this feature normally implying a low response to immune checkpoint treatments. Thus, in theory, only MSI-H "classical" SACs would be suitable for antibody therapies at the moment. CTLA4 (Cytotoxic T-lymphocyte antigen 4) is a membrane glycoprotein that inhibits T cell response and is key to the phenomenon of immune tolerance. Its blockade with monoclonal antibodies such as ipilimumab and tremelimumab induces T cell proliferation and increases IL-2 production and depletion of T regulatory lymphocytes in the tumor microenvironment [34].

PD-1 (Programmed Death-1 receptor) or CD279 is an inhibitory co-receptor that is expressed on the surface of CD8+ CTLs, NK cells and tumor-infiltrating lymphocytes [35]. Nivolumab and pembrolizumab are currently the available monoclonal antibodies approved by the FDA. The PD-1 blockade restores the CD8+ lymphocytes' infiltration and triggers the reduction of the tumor's size. In the case of pembrolizumab, the efficacy of these treatments has led to their rapid approval for patients with no alternative treatment options. Some studies have shown the high expression of PD-1 in MSI-H tumors, thus providing the evidence for including its immunohistochemical expression as a predictive marker [36,37].

PD-L1 (Programmed Death Ligand-1 receptor) or CD274 is expressed on the surface of certain activated immune components, such as B cells, T cells and NK cells CD14+-TAMs, and on the surface of

cancer cells [98,99]. The interaction between PD-1 and PD-L1 leads to the inhibition of T cell activation and reduces pro-inflammatory cytokine secretion (INF-γ, TNF-α and IL-2). Normally, this expression is necessary to avoid autoimmunity, but in certain types of cancer, it results in tumor growth and lack of adaptive immune response due to the fact that CTLs cannot properly attack cancer cells. At the moment, the available monoclonal antibodies are MDX1105, durvalumab, avelumab and atezolizumab. MDX 1105 is still in phase I study, while the rest have been approved by the FDA [35]. MDX1105 has been demonstrated to be unsuitable for CRC treatment, while the response rate of atezolizumab in CRC is still low. Despite the failure of monotherapies, preclinical and phase I clinical studies consisting of the co-administration of anti-PD-L1 with inhibitors of the TGFβ receptor (galunisertib) or MEK inhibitors and atezolizumab offer promising therapeutic approaches [22].

4. SAC Displays an Active Invasive Front

Compared to CC, SAC exhibits a higher occurrence of adverse histological and molecular features at the invasive front, including high-grade tumor budding (HG-TB), cytoplasmic pseudofragments and an infiltrating growth pattern [18]. The invasive front comprises a dynamic process of reprograming of colorectal carcinoma cells known as epithelial mesenchymal transition (EMT) [100]. EMT is a process in which epithelial cells lose cell polarity and cell–cell adhesion favored by downregulation of the epithelial cell adhesion molecule E-cadherin. EMT is triggered by several transcription factors, such as SNAIL and SLUG which induced cells to acquire migratory and invasive properties. In normal cells, EMT contributes to several physiological processes, such as wound healing and embryogenesis [101]. However, in cancer cells, EMT is associated with the development of tumor phenotypes, including invasion, metastasis and drug resistance [102,103]. EMT can be identified histologically by the presence of tumor budding (TB), a manifestation that is specific to tumors showing an infiltrating growth pattern [104]. The reported incidence of TB in CRC varies widely in the literature from 20% to 89%, being this wide range possibly as a result of different diagnostic criteria and quantification methods [20]. In this line, García-Solano et al. described that SACs had more high-grade TB than CCs (69.1–40.7%, $p = 0.0003$) [18], this phenomenon being associated with lower E-cadherin expression and higher of mesenchymal markers [19]. It is known that the implication of the Wnt signalling pathway in the main process of TB formation is usually induced by increased expression of nuclear β-catenin [105]. Apart from being a transcription factor, β-catenin is a structural adaptor that links cadherins to cytoskeletal actin, thus participating in cell–cell adhesion [106]. Nuclear β-catenin expression was absent in 78.4% of SACs, and this percentage was significantly higher than that observed in CCs (39.6%) ($p < 0.0001$), thus suggesting a lack of involvement of this mechanism in the EMT in SAC [20].

Given the heterogeneity of CRC in terms of clinical behavior, great efforts have been made to identify histological features that may help forecast the aggressiveness of a given CRC and hence select patients for closer monitoring and/or more aggressive treatment [104]. Cytoskeleton rearrangements are necessary for tumor cells to acquire an invasive phenotype. Studies on the role of actin and its interacting partners have underlined key signalling pathways, such as the Rho GTPases, and effector proteins that, through the cytoskeleton, facilitate tumor cell migration, invasion and metastasis [107]. The three most widely studied Rho GTPases in eukaryotic cells, Rho, Rac and Cdc42, control the assembly of the actin cytoskeleton, and Cdc42 that of the microtubule cytoskeleton [108]. In general terms, Rho can recruit the ROCK (Rho-associated coiled-coil forming protein kinase, or Rho kinase) family of kinases [109], which regulates various cytoskeletal proteins, inducing actin stress fibre formation and the generation of contractile forces [108]; Rac rearranges the actin cytoskeleton to promote formation of membrane protrusions, called lamellipodia, which drive motility in different cell types; and Cdc42 signalling favors the generation of actin-rich microspikes to sense extracellular chemotactic gradients and trigger directed cell movement. A main downstream effector of the Rho GTPase family is Rho kinase, which plays a crucial role in the regulation of actin remodelling via phosphorylation of cofilin and myosin light chain (MLC).

Evidences on differentially enriched functions and genes seem to demonstrate that SAC, unlike CC, has a characteristic profile of cytoskeletal rearrangement, which could account for particular cell adhesion and invasive properties. In fact, specific activation of pathways related to small GTPases and second messengers such as phosphatidylinositols are frequently found as enriched functions in SAC [12,20]. In this line, the roles of phosphatidylinositol trisphosphate and the small GTPases RAC and CDC42 in actin assembly are important for lamellipodia and filopodia rearrangement [110].

Fascin1 emerged as an immunohistochemical marker for SAC diagnosis, as the positive expression of fascin1 was observed in 88.6% of SACs and in 14.3% of CCs (88.6% sensitivity, 85.7% specificity) [12]. Intriguingly, Tao et al. had previously observed that β-catenin is associated with the actin-bundling protein fascin in a non-cadherin complex. In fact, these authors observed that fascin1 and E-cadherin use a similar binding site within beta-catenin and that fascin and beta-catenin co-localize at cell–cell boundaries and dynamic cell-leading edges of epithelial and endothelial cells [111], thus giving an explanation of why β-catenin was not observed in the nuclear location in SACs. Fascin1 protein localizes to the core actin bundles forming spikes and filopodia at the leading edge of migratory cells, increasing migration in several cell types [112] and therefore, it has been associated with adverse prognosis in CRC [113]. These facts can partly explain the higher incidence of adverse prognostic histologic factors at the invasive front of SAC (HG-TB and weak peritumoral lymphocytic infiltration (PLI)) and the worse outcomes observed in SACs [18]. Additionally, fascin1 expression is associated with shorter survival, as has been reported previously in CRC [114], thus supporting earlier observations showing that SAC fares worse than CC [113]. Induced expression of fascin1 in colorectal cancer cells increased migration and invasion in cell cultures and caused cell dissemination and metastasis [115]. Figure 3 shows the expression of fascin1 in both blood vessels and SAC cells at the invasive front, creating tumor budding.

Possible Therapies Targeting SAC Invasive Front

Migrastatin analogues, such as macroketone, have been shown to inhibit metastatic tumor cell migration, invasion via fascin1 blockade [38], thereby suggesting a possible role for migrastatin analogues in SAC treatment [12]. However, the complex structure of the macroketone hinders its synthesis, and other anti-fascin1 compounds derived from indazol-furan-carboxamides have been tested [38]. Huang et al. showed that G2 compound inhibits the actin-bundling function of fascin1 and blocks tumor cell migration, invasion and metastasis in breast tumor cells [116]. In this line, Montoro and Alburquerque et al. prove the in vitro and in vivo anti-tumoral activity of G2 compound on colorectal cancer cells and guide to design improved G2-based fascin1 inhibitors [39]. On the search for new anti-fascin1 drugs, this same group performed an in silico screening of 9591 compounds, including 2037 approved by the FDA, for the purpose of analyzing their fascin1 binding affinity. The screening results yielded the FDA-approved antidepressant imipramine as the most evident potential fascin1 blocker. This tricyclic antidepressant (TCA) has an anti-invasive and anti-metastatic activity in a dose-dependent manner more evident in fascin1-overexpressing colorectal cell lines, in both constitutive and induced fascin1 expression [40]. A previous study by Jahchan et al. also demonstrated the antitumoral effects of imipramine in human small-cell lung cancer and other neuroendocrine tumors implanted in mice [117]. In a clinical setting, Sauer and Jansen reported unexpected survival associated with imipramine treatment in a patient with metastatic lung cancer [41], and the epidemiological study by Walker et al., which included 31,953 cancer cases from different locations and 61,591 matched controls, concluded that tricyclic antidepressants like imipramine may have the potential to prevent both colorectal cancer and glioma in a dose- and time-dependent fashion [42]. All this evidence paves the way for a potential molecular targeted therapy for SAC and other fascin1-overexpressing tumors.

5. Concluding Remarks

This molecular classification of CRC provides a better understanding of the insights on the biology of different tumor subtypes, with the aim of forecasting the clinical behaviour and possible therapeutic

targets for a given tumor. However, this approach is far from the routine practice, as most CRCs are diagnosed based on histological grounds. With this in mind, the association of molecular features with each histological subtype is crucial for the proper clinical management of CRC patients. SAC is defined by a series of morphological criteria and associated with histologically adverse factors present at the tumor's invasive front. At the molecular level, the activation of the MAPK pathway (either by KRAS or BRAF mutation), the prominent EMT (not involving nuclear β-catenin expression) and the frequent CIMP-H status are characteristic of the tumor itself, whereas the abundance of microvascular density and the weak immune response are common features of the surrounding tumor microenvironment. All these findings give us clues about possible ways to treat this aggressive tumor, yet future studies, including preclinical trials using available serrated mouse models, clinical trials testing FDA-approved drugs against SAC targets or simply retrospective analysis based on histological features associated to the response to specific treatments, are needed.

Supplementary Materials: Supplementary materials can be found at http://www.mdpi.com/1422-0067/21/6/1991/s1. Figure S1. Plot showing the 10 significant pathways with the most affected genes after the enrichment analysis of the 2924 genes shared by CC and SAC. The pathways in cancer are the most represented, with 79 affected genes. In this chart, we can observe that these 79 genes are also affected by other pathways related to other types of cancer, the cell cycle and some metabolic processes. Other interesting pathways were also over-represented, such as RNA degradation and the p53 signalling pathway.

Author Contributions: P.C.Z. conceived of the presented idea and supervised this work; P.C.Z., B.A.-G., F.F.L.-C. and M.D.L.-A. wrote the review manuscript; P.C.-Z., B.A.-G., J.G.-S. and Á.E.-G. designed the images. All authors contributed to the final review version. All authors have read and agreed to the published version of the manuscript.

Funding: B.A.-G. and F.F.L.-C. belong to the Programa de Doctorado en Ciencias de la Salud from the Catholic University of Murcia (UCAM). B.A.-G. holds a predoctoral grant from UCAM (FPI05-UCAM/17). F.F.L.-C. was supported by the Junta Provincial Murcia Predoctoral Asociación Española Contra el Cáncer (AECC) (ref: PRDMU19002) grant. This work has been funded by Instituto de Salud Carlos III (Spanish Ministry of Health) and FEDER funds (refs: PI15/00626 and PI18/00144).

Conflicts of Interest: The authors declare no conflict of interest.

References

1. Bray, F.; Ferlay, J.; Soerjomataram, I.; Siegel, R.L.; Torre, L.A.; Jemal, A. Global cancer statistics 2018: GLOBOCAN estimates of incidence and mortality worldwide for 36 cancers in 185 countries. *CA Cancer J. Clin.* **2018**, *68*, 394–424. [CrossRef]
2. Stefanius, K.; Ylitalo, L.; Tuomisto, A.; Kuivila, R.; Kantola, T.; Sirniö, P.; Karttunen, T.J.; Mäkinen, M.J. Frequent mutations of KRAS in addition to BRAF in colorectal serrated adenocarcinoma. *Histopathology* **2011**, *58*, 679–692. [CrossRef] [PubMed]
3. García-Solano, J.; Conesa-Zamora, P.; Carbonell, P.; Trujillo-Santos, J.; Torres-Moreno, D.D.; Pagán-Gómez, I.; Rodríguez-Braun, E.; Pérez-Guillermo, M. Colorectal serrated adenocarcinoma shows a different profile of oncogene mutations, MSI status and DNA repair protein expression compared to conventional and sporadic MSI-H carcinomas. *Int. J. Cancer* **2012**, *131*, 1790–1799. [CrossRef] [PubMed]
4. Bettington, M.; Walker, N.; Clouston, A.; Brown, I.; Leggett, B.; Whitehall, V. The serrated pathway to colorectal carcinoma: Current concepts and challenges. *Histopathology* **2013**, *62*, 367–386. [CrossRef] [PubMed]
5. Snover, D.C.; Jass, J.R.; Fenoglio-Preiser, C.; Batts, K.P. Serrated polyps of the large intestine: A morphologic and molecular review of an evolving concept. *Am. J. Clin. Pathol.* **2005**, *124*, 380–391. [CrossRef]
6. García-Solano, J.; Turpin-Sevilla, M.; García-García, F.; Carbonell-Muñoz, R.; Torres-Moreno, D.; Conesa, A.; Conesa-Zamora, P. Differences in gene expression profiling and biomarkers between histological colorectal carcinoma subsets from the serrated pathway. *Histopathology* **2019**, *75*, 496–507. [CrossRef]
7. Bellizzi, A.M.; Frankel, W.L. Colorectal cancer due to deficiency in DNA mismatch repair function: A review. *Adv. Anat. Pathol.* **2009**, *16*, 405–417. [CrossRef]
8. Bosman, F.T.; Carneiro, F.; Hruban, R.H.; Theise, N.D. Carcinoma of the colon and rectum. In *WHO Classification of Tumors of the Digestive System*, 4th ed.; IARC: Lyon, France, 2010; pp. 134–146.

9. Nagtegaal, I.; Odze, R.; Klimstra, D.; Paradis, V.; Rugge, M.; Schirmacher, P.; Washington, K.M.; Carneiro, F.; Cree, I.A. WHO Classification of Tumours Editorial Board. The 2019 WHO classification of tumours of the digestive system. *Histopathology* **2020**, *76*, 182–188. [CrossRef]
10. Makinen, M.J. Colorectal serrated adenocarcinoma. *Histopathology* **2007**, *50*, 131–150. [CrossRef]
11. García-Solano, J.; Pérez-Guillermo, M.; Conesa-Zamora, P.; Acosta-Ortega, J.; Trujillo-Santos, J.; Cerezuela-Fuentes, P.; Mäkinen, M.J. Clinicopathologic study of 85 colorectal serrated adenocarcinomas: Further insights into the full recognition of a new subset of colorectal carcinoma. *Hum. Pathol.* **2010**, *41*, 1359–1368. [CrossRef]
12. Conesa-Zamora, P.; García-Solano, J.; García-García, F.; Turpin, M.; Trujillo-Santos, J.; Torres-Moreno, D.; Pérez-Guillermo, M. Expression profiling shows differential molecular pathways and provides potential new diagnostic biomarkers for colorectal serrated adenocarcinoma. *Int. J. Cancer* **2013**, *132*, 297–307. [CrossRef] [PubMed]
13. Kahi, C.J. Screening Relevance of Sessile Serrated Polyps. *Clin. Endosc.* **2019**, *52*, 235–238. [CrossRef] [PubMed]
14. Bailie, L.; Loughrey, M.B.; Coleman, H.G. Lifestyle Risk Factors for Serrated Colorectal Polyps: A Systematic Review and Meta-analysis. Gastroenterology. *Gastroenterology* **2017**, *152*, 92–104. [CrossRef] [PubMed]
15. Crockett, S.D.; Nagtegaal, I.D. Terminology, Molecular Features, Epidemiology, and Management of Serrated Colorectal Neoplasia. *Gastroenterology* **2019**, *157*, 949–966. [CrossRef]
16. Anderson, J.C.; Alpern, Z.A. Smoking and the Increased Risk for Serrated Polyps: Implications for Screening and Surveillance. *J. Clin. Gastroenterol.* **2019**, *53*, 319–321. [CrossRef]
17. Yu, J.; Chen, Y.; Fu, X.; Zhou, X.; Peng, Y.; Shi, L.; Wu, Y. Invasive Fusobacterium Nucleatum May Play a Role in the Carcinogenesis of Proximal Colon Cancer Through the Serrated Neoplasia Pathway. *Int. J. cancer* **2016**, *139*, 1318–1326. [CrossRef]
18. García-Solano, J.; Conesa-Zamora, P.; Trujillo-Santos, J.; Mäkinen, M.J.; Pérez-Guillermo, M. Tumour budding and other prognostic pathological features at invasive margins in serrated colorectal adenocarcinoma: A comparative study with conventional carcinoma. *Histopathology* **2011**, *59*, 1046–1056. [CrossRef]
19. García-Solano, J.; Conesa-Zamora, P.; Trujillo-Santos, J.; Torres-Moreno, D.; Mäkinen, M.J.; Pérez-Guillermo, M. Immunohistochemical expression profile of β-catenin, E-cadherin, P-cadherin, laminin-5γ2 chain, and SMAD4 in colorectal serrated adenocarcinoma. *Hum. Pathol.* **2012**, *43*, 1094–1102. [CrossRef]
20. Conesa-zamora, P.; García-solano, J.; Turpin, C.; Sebastián-león, P.; Torres-moreno, D.; Estrada, E.; Tuomisto, A.; Wilce, J.; Mäkinen, M.J.; Pérez-Guillermo, M.; et al. Methylome profiling reveals functions and genes which are differentially methylated in serrated compared to conventional colorectal carcinoma. *Clin. Epigenet.* **2015**, *7*, 101. [CrossRef]
21. Davies, E.J.; Marsh Durban, V.; Meniel, V.; Williams, G.T.; Clarke, A.R. PTEN loss and KRAS activation leads to the formation of serrated adenomas and metastatic carcinoma in the mouse intestine. *J. Pathol.* **2014**, *233*, 27–38. [CrossRef]
22. Nakanishi, Y.; Duran, A.; L'Hermitte, A.; Shelton, P.M.; Nakanishi, N.; Reina-Campos, M.; Moscat, J. Simultaneous Loss of Both Atypical Protein Kinase C Genes in the Intestinal Epithelium Drives Serrated Intestinal Cancer by Impairing Immunosurveillance. *Immunity* **2018**, *49*, 1132–1147. [CrossRef] [PubMed]
23. Nakanishi, Y.; Diaz-meco, M.T.; Moscat, J. Serrated Colorectal Cancer: The Road Less Travelled? *Trends Cancer* **2019**. [CrossRef] [PubMed]
24. Laiho, P.; Kokko, A.; Vanharanta, S.; Salovaara, R.; Sammalkorpi, H.; Tuppurainen, K.; Davalos, V.; Schwartz, S., Jr.; Arango, D. Serrated carcinomas form a subclass of colorectal cancer with distinct molecular basis. *Oncogene* **2007**, *26*, 312–320. [CrossRef] [PubMed]
25. Tuomisto, A.; García-solano, J.; Sirniö, P.; Väyrynen, J. HIF-1 α expression and high microvessel density are characteristic features in serrated colorectal cancer. *Virchows Arch. Int. J. Pathol.* **2016**, *469*, 395–404. [CrossRef] [PubMed]
26. Esteban-Gil, A.; Pérez-Sanz, F.; García-Solano, J.; Alburquerque-González, B.; Parreño-González, M.A.; Legaz-García, M.C.; Fernández-Breis, J.T.; Rodriguez-Braun, E.; Pimentel, P.; Tuomisto, A.; et al. ColPortal, an integrative multiomic platform for analysing epigenetic interactions in colorectal cancer. *Sci. Data* **2019**, *6*, 255. [CrossRef]

27. García-Solano, J.; Turpin, M.; Torres-Moreno, D.; Huertas-López, F.; Tuomisto, A.; Mäkinen, M.J.; Conesa, A.; Conesa-Zamora, P. Two histologically colorectal carcinomas subsets from the serrated pathway show different methylome signatures and diagnostic biomarkers. *Clin. Epigenet.* **2018**, *10*, 141. [CrossRef]
28. Kondelova, A.; Alburquerque-González, B.; Vychytilova-Faltejskova, P.; García-Solano, J.; Prochazka, V.; Kala, Z.; Pérez, F.; Slaby, O.; Conesa-Zamora, P. miR-181a-2* expression is different amongst carcinomas from the colorectal serrated route. *Mutagenesis* **2019**, *30*. [CrossRef]
29. Ritchie, M.E.; Phipson, B.; Wu, D.; Hu, Y.; Law, C.W.; Shi, W.; Smyth, G.K. Limma powers differential expression analyses for RNA-sequencing and microarray studies. *Nucleic Acids Res.* **2015**, *43*, e47. [CrossRef]
30. Benjamini, Y.; Hochberg, Y. Controlling the false discovery rate: A practical and powerful approach to multiple testing. *J. R. Stat. Soc. B* **1995**, *57*, 289–300. [CrossRef]
31. Battaglin, F.; Puccini, A.; Intini, R.; Schirripa, M.; Ferro, A.; Bergamo, F.; Lonardi, S.; Zagonel, V.; Lenz, H.; Loupakis, F.; et al. The role of tumor angiogenesis as a therapeutic target in colorectal cancer. *Expert Rev. Anticancer Ther.* **2018**, *18*, 251–266. [CrossRef]
32. Loupakis, F.; Cremolini, C.; Salvatore, L.; Masi, G.; Sensi, E.; Schirripa, M.; Michelucci, A.; Pfanner, E.; Brunetti, I.; Lupi, C.; et al. FOLFOXIRI plus bevacizumab as first-line treatment in BRAF mutant metastatic colorectal cancer. *Eur. J. Cancer* **2014**, *50*, 57–63. [CrossRef] [PubMed]
33. Arai, H.; Battaglin, F.; Wang, J.; Lo, J.H.; Soni, S.; Zhang, W. Molecular insight of regorafenib treatment for colorectal cancer. *Cancer Treat. Rev.* **2019**, *81*, 101912. [CrossRef] [PubMed]
34. Pardoll, D.M. The blockade of immune checkpoints in cancer immunotherapy. *Nat. Rev. Cancer* **2012**, *12*, 242–264. [CrossRef] [PubMed]
35. Postow, M.A.; Callahan, M.K.; Wolchok, J.D. Immune Checkpoint Blockade in Cancer Therapy. *J. Clin. Oncol.* **2015**, *33*, 1974–1982. [CrossRef]
36. Gatalica, Z.; Snyder, C.; Maney, T.; Ghazalpour, A.; Holterman, D.A.; Xiao, N.; Hamid, O. Programmed cell death 1 (PD-1) and its ligand (PD-L1) in common cancers and their correlation with molecular cancer type. *Cancer Epidemiol. Biomark. Prev.* **2014**, *23*, 2965–2970. [CrossRef]
37. Llosa, N.J.; Cruise, M.; Tam, A.; Wicks, E.C.; Hechenbleikner, E.M.; Taube, J.M.; Housseau, F. The vigorous immune microenvironment of microsatellite instable colon cancer is balanced by multiple counter-inhibitory checkpoints. *Cancer Discov.* **2015**, *5*, 43–51. [CrossRef]
38. Chen, L.; Yang, S.; Jakoncic, J.; Zhang, J.J.; Huang, X. Migrastatin analogues target fascin to block tumour metastasis. *Nature* **2010**, *464*, 1062–1066. [CrossRef]
39. Montoro-García, S.; Alburquerque-González, B.; Bernabé-García, A.; Rodrigues, P.C.; den-Haan, H.; Luque, I.; Nicolás, F.J.; Pérez-Sánchez, H.; Cayuela, M.L.; Salo, T.; et al. Novel anti-invasive properties of a fascin inhibitor on colorectal cancer cells. *J. Mol. Med.* **2020**, in press.
40. Alburquerque-González, B.; Bernabé-García, M.; Montoro-García, S.; Bernabé-García, Á.; Rodrigues, P.C.; Ruiz Sanz, J.; López-Calderón, F.F.; Luque, I.; Nicolas, F.J.; Cayuela, M.L.; et al. New role of antidepressant imipramine as a fascin1 inhibitor in colorectal cancer cells. *Exp. Mol. Med.* **2020**, *52*, 281–292. [CrossRef]
41. Sauer, T.; Lang, U.E. Is Imipramine Helpful in the Treatment of Cancer? A Case Presentation and Discussion of Possible Clinical Implications. *Biomed. J. Sci. Tech. Res.* **2018**, *4*, 4194–4195. [CrossRef]
42. Walker, A.J.; Card, T.; Bates, T.E.; Muir, K. Tricyclic antidepressants and the incidence of certain cancers: A study using the GPRD. *Br. J. Cancer* **2011**, *104*, 193–197. [CrossRef] [PubMed]
43. Chen, W.; Jiang, J.; Yu, X.; Xia, W.; Yu, P.; Wang, K.; Zhao, Z.; Chen, Z.; Chen, O.W.; Jiang, J.; et al. Endothelial cells in colorectal cancer. *World J. Gastrointest Oncol.* **2019**, *11*, 946–956. [CrossRef] [PubMed]
44. Viallard, C.; Larrive, B. Tumor angiogenesis and vascular normalization: Alternative therapeutic targets. *Angiogenesis* **2017**, *20*, 409–426. [CrossRef]
45. Moreno-sánchez, R. HIF-1 modulates energy metabolism in cancer cells by inducing over- expression of specific glycolytic isoforms HIF-1α modulates energy metabolism in cancer cells by modifying the status of glycolytic enzymes. *Mini Rev. Med. Chem.* **2009**, *9*, 1084–1101. [CrossRef]
46. Semenza, G.L. HIF-1 mediates metabolic responses to intratumoral hypoxia and oncogenic mutations. *J. Clin. Investig.* **2013**, *123*, 3664–3671. [CrossRef] [PubMed]
47. Klein, D. The Tumor Vascular Endothelium as Decision Maker in Cancer Therapy. *Front. Oncol.* **2018**, *8*, 367. [CrossRef]
48. Keith, B.; Johnson, R.S.; Simon, M.C. HIF1-α and HIF2-α: Sibling rivalry in hypoxic tumor growth and progression. *Nat. Rev. Cancer* **2012**, *12*, 9–22. [CrossRef]

49. Semenza, G.L. Hypoxia-inducible factors: Mediators of cancer progression and targets for cancer therapy. *Trends Pharmacol. Sci.* **2012**, *33*, 207–214. [CrossRef]
50. Ioannou, M.; Paraskeva, E.; Baxevanidou, K.; Simos, G.; Papacharalambous, C.; Samara, M.; Koukoulis, G. HIF-1α in colorectal carcinoma: Review of the literature. *J. Balk. Union Oncol.* **2015**, *20*, 680–689.
51. Morimoto, T.; Mitomi, H.; Saito, T. Distinct profile of HIF1α, PTCH, EphB2, or DNA Repair Protein Expression and BRAF Mutation in Colorectal Serrated Adenoma. *J. Gastroenterol. Hepatol.* **2014**, *29*, 1192–1199. [CrossRef]
52. Jiang, Y.; Fan, L.; Jiang, C.; Zhang, Y.; Luo, H.; Tang, Z.; Xia, D.; Wang, M. Expression and significance of PTEN, hypoxia-inducible factor-1 alpha in colorectal adenoma and adenocarcinoma. *World J. Gastroenterol.* **2003**, *9*, 491–494. [CrossRef] [PubMed]
53. Simiantonaki, N.; Taxeidis, M.; Jayasinghe, C.; Kurzik-dumke, U.; Kirkpatrick, C.J. Hypoxia-inducible factor 1 alpha expression increases during colorectal carcinogenesis and tumor progression. *BMC Cancer* **2008**, *8*. [CrossRef] [PubMed]
54. Rigopoulos, D.N.; Tsiambas, E.; Lazaris, A.C. Deregulation of EGFR/VEGF/HIF-1a Signaling Pathway in Colon Adenocarcinoma Based on Tissue Microarrays Analysis. *J. Balk. Union Oncol.* **2010**, *15*, 107–115.
55. Chen, Z.; He, X.; Xia, W.; Huang, Q.; Zhang, Z.; Ye, J.; Ni, C. Prognostic value and clinicopathological differences of HIFs in colorectal cancer: Evidence from meta-analysis. *PLoS ONE* **2013**, *8*, e80337. [CrossRef] [PubMed]
56. Urbich, C.; Dimmeler, S. Endothelial progenitor cells: Characterization and role in vascular biology. *Circ. Res.* **2004**, *95*, 343–353. [CrossRef]
57. Manzoni, M.; Comolli, G.; Torchio, M.; Mazzini, G.; Danova, M. Circulating Endothelial Cells and Their Subpopulations: Role as Predictive Biomarkers in Antiangiogenic Therapy for Colorectal Cancer. *Clin. Colorectal Cancer* **2015**, *14*, 11–17. [CrossRef]
58. Schmitz-Winnenthal, F.H.; Hohmann, N.; Niethammer, A.G.; Friedrich, T.; Lubenau, H.; Ulrich, A.; Buechler, M.W.; Pianka, F.; Springer, M.; Breiner, K.M.; et al. Anti-angiogenic activity of VXM01, an oral T-cell vaccine against VEGF receptor 2, in patients with advanced pancreatic cancer: A randomized, placebo-controlled, phase 1 trial. *Oncoimmunology* **2015**, *4*, e1001217. [CrossRef]
59. Qiu, Y.; Yu, H.; Shi, X.; Xu, K.; Tang, Q.; Liang, B.; Hu, S.; Bao, Y. microRNA-497 inhibits invasion and metastasis of colorectal cancer cells by targeting vascular endothelial growth factor-A. *Cell Prolif.* **2016**, *49*, 69–78. [CrossRef]
60. Seeber, A.; Gunsilius, E.; Gastl, G.; Pircher, A. Anti-angiogenics: Their value in colorectal cancer therapy. *Oncol. Res. Treat.* **2018**, *41*, 188–193. [CrossRef]
61. Coxon, A.; Bready, J.; Min, H.; Kaufman, S.; Leal, J.; Yu, D.; Lee, T.A.; Sun, J.; Estrada, J.; Bolon, B. Context-dependent role of angiopoietin-1 inhibition in the suppression of angiogenesis and tumor growth: Implications for AMG 386, an angiopoietin-1/2-neutralizing peptibody. *Mol. Cancer Ther.* **2010**, *9*, 2641–2651. [CrossRef]
62. Li, X.; Chen, C.; Dai, Y.; Huang, C.; Han, Q.; Jing, L.; Ma, Y.; Xu, Y.; Liu, Y.; Zhao, L.; et al. Cinobufagin suppresses colorectal cancer angiogenesis by disrupting the endothelial mammalian target of rapamycin/inducible factor 1-α axis. *Cancer Sci.* **2019**, *110*, 1724–1734. [CrossRef] [PubMed]
63. Kataria, N.; Martinez, C.A.; Kerr, B.; Zaiter, S.S.; Morgan, M.; McAlpine, S.R.; Cook, K.M. C-terminal HSP90 inhibitors block the HIF-1 hypoxic response by degrading HIF-1α through the oxygen-dependent degradation pathway. *Cell. Physiol. Biochem. Int. J. Exp. Cell. Physiol.* **2019**, *53*, 480–495. [CrossRef]
64. Chen, D.; Huang, J.; Liu, K.; Zhang, L.; Yang, Z.; Chuai, Z.; Wang, Y.; Shi, D.; Huang, Q.; Fu, W. BRAF V600E mutation and its association with clinicopathological features of colorectal cancer: A systematic review and meta-analysis. *PLoS ONE* **2014**, *9*, e90607. [CrossRef]
65. Park, S.; Rashid, A.; Lee, J.; Kim, S.G.; Hamilton, S.R. Frequent CpG island methylation in serrated adenomas of the colorectum. *Am. J. Pathol.* **2003**, *162*, 815–822. [CrossRef]
66. Morris, V.K. Systemic therapy in BRAF V600E-mutant metastatic colorectal cancer: Recent advances and future strategies. *Curr. Colorectal Cancer Rep.* **2019**, *15*, 53–60. [CrossRef] [PubMed]
67. Guinney, J.; Dienstmann, R.; Wang, X.; Reyniès, A.; Schlicker, A.; Soneson, C.; Marisa, L.; Roepman, P.; Nyamundanda, G.; Angelino, P.; et al. The consensus molecular subtypes of colorectal cancer. *Nat. Med.* **2015**, *21*, 1350–1356. [CrossRef]

68. Lenz, H.-J.; Ou, F.; Venook, A.P.; Hochster, H.S.; Niedzwiecki, D. Impact of Consensus Molecular Subtype on survival in patients with metastatic colorectal cancer: Results from CALGB/SWOG 80405. *J. Clin. Oncol.* **2019**, *37*, 1876–1885. [CrossRef]
69. Venook, A.P.; Niedzwiecki, D.; Lenz, H.; Innocenti, F. CALGB/SWOG 80405: Phase III trial of irinotecan/5-FU/leucovorin (FOLFIRI) or oxaliplatin/5-FU/leucovorin (mFOLFOX6) with bevacizumab (BV) or cetuximab (CET) for patients (pts) with KRAS wild-type (wt) untreated metastatic adenocarcinoma of the colon or re. *J. Clin. Oncol.* **2014**. [CrossRef]
70. Gutting, T.; Weber, C.A.; Weidner, P.; Herweck, F.; Henn, S.; Friedrich, T.; Yin, S.; Kzhyshkowska, J.; Gaiser, T.; Janssen, K.P.; et al. PPARγ-activation increases intestinal M1 macrophages and mitigates formation of serrated adenomas in mutant KRAS mice. *Oncoimmunology* **2018**, *7*, e1423168. [CrossRef]
71. Deschoolmeester, V.; Baay, M.; Lardon, F.; Pauwels, P.; Peeters, M. Immune Cells in Colorectal Cancer: Prognostic Relevance and Role of MSI. *Cancer Microenviron. J. Int. Cancer Microenviron. Soc.* **2011**, *4*, 377–392. [CrossRef]
72. Wei, C.; Yang, C.; Wang, S.; Shi, D.; Zhang, C.; Lin, X. Crosstalk between cancer cells and tumor associated macrophages is required for mesenchymal circulating tumor cell-mediated colorectal cancer metastasis. *Mol. Cancer* **2019**, *18*, 64. [CrossRef] [PubMed]
73. Hansen, M.; Andersen, M.H. The role of dendritic cells in cancer. *Semin. Immunopathol.* **2017**, *39*, 307–316. [CrossRef] [PubMed]
74. Chiossone, L.; Dumas, P.Y.; Vienne, M.; Vivier, E. Natural killer cells and other innate lymphoid cells in cancer. *Nat. Rev. Immunol.* **2018**, *18*, 671–688. [CrossRef] [PubMed]
75. Erreni, M.; Mantovani, A.; Allavena, P. Tumor-associated Macrophages (TAM) and Inflammation in Colorectal Cancer. *Cancer Microenviron.* **2011**, *4*, 141–154. [CrossRef] [PubMed]
76. Martínez, V.G.; Rubio, C.; Martínez-Fernández, M.; Segovia, C.; López-Calderón, F.; Garín, M.I.; Dueñas, M. BMP4 Induces M2 Macrophage Polarization and Favors Tumor Progression in Bladder Cancer. *Clin. Cancer Res.* **2017**, *23*, 7388–7399. [CrossRef] [PubMed]
77. Bingle, L.; Brown, N.J.; Lewis, C.E. The role of tumour-associated macrophages in tumour progression: Implications for new anticancer therapies. *J. Pathol.* **2002**, *196*, 254–265. [CrossRef]
78. Shunyakov, L.; Ryan, C.K.; Sahasrabudhe, D.M.; Khorana, A.A. The influence of host response on colorectal cancer prognosis. *Clin. Colorectal Cancer* **2004**, *4*, 38–45. [CrossRef]
79. Shi, N.; Li, N.; Duan, X.; Niu, H. Interaction between the gut microbiome and mucosal immune system. *Mil. Med. Res.* **2017**, *4*. [CrossRef]
80. Galon, J.; Costes, A.; Sanchez-Cabo, F.; Kirilovsky, A.; Mlecnik, B.; Lagorce-Pagès, C.; Pagès, F. Type, density, and location of immune cells within human colorectal tumors predict clinical outcome. *Science* **2006**, *313*, 1960–1964. [CrossRef]
81. Kocián, P.; Šedivcová, M.; Drgáč, J.; Cerná, K.; Hoch, J.; Kodet, R.; Fialová, A. Tumor-infiltrating lymphocytes and dendritic cells in human colorectal cancer: Their relationship to KRAS mutational status and disease recurrence. *Hum. Immunol.* **2011**, *72*, 1022–1028. [CrossRef]
82. Roxburgh, C.S.; McMillan, D.C. The role of the in situ local inflammatory response in predicting recurrence and survival in patients with primary operable colorectal cancer. *Cancer Treat. Rev.* **2012**, *38*, 451–466. [CrossRef] [PubMed]
83. Väyrynen, J.P.; Kantola, T.; Väyrynen, S.A.; Klintrup, K.; Bloigu, R.; Karhu, T.; Mäkinen, M.J. The relationships between serum cytokine levels and tumor infiltrating immune cells and their clinical significance in colorectal cancer. *Int. J. Cancer* **2016**, *139*, 112–121. [CrossRef] [PubMed]
84. Dillekås, H.; Rogers, M.S.; Straume, O. Are 90% of deaths from cancer caused by metastases? *Cancer Med.* **2019**, *8*, 5574–5576. [CrossRef]
85. Engström, A.; Erlandsson, A.; Delbro, D.; Wijkander, J. Conditioned media from macrophages of M1, but not M2 phenotype, inhibit the proliferation of the colon cancer cell lines HT-29 and CACO-2. *Int. J. Oncol.* **2014**, *44*, 385–392. [CrossRef] [PubMed]
86. Alexandrov, L.B.; Nik-Zainal, S.; Wedge, D.C.; Aparicio, S.A.; Behjati, S.; Biankin, A.V.; Stratton, M.R. Signatures of mutational processes in human cancer. *Nature* **2013**, *500*, 415–421. [CrossRef] [PubMed]
87. Schumacher, T.N.; Schreiber, R.D. Neoantigens in cancer immunotherapy. *Science* **2015**, *348*, 69–74. [CrossRef]
88. Thorsson, V.; Gibbs, D.L.; Brown, S.D.; Wolf, D.; Bortone, D.S.; Ou Yang, T.H.; Shmulevich, I. The Immune Landscape of Cancer. *Immunity* **2018**, *48*, 812–830. [CrossRef]

89. Catalano, I.; Grassi, E.; Bertotti, A.; Trusolino, L. Immunogenomics of Colorectal Tumors: Facts and Hypotheses on an Evolving Saga. *Trends Cancer* **2019**, *5*, 779–788. [CrossRef]
90. Pagès, F.; Mlecnik, B.; Marliot, F.; Bindea, G.; Ou, F.S.; Bifulco, C.; Galon, J. International validation of the consensus Immunoscore for the classification of colon cancer: A prognostic and accuracy study. *Lancet* **2018**, *391*, 2128–2139. [CrossRef]
91. Mlecnik, B.; Bindea, G.; Angell, H.K.; Maby, P.; Angelova, M.; Tougeron, D.; Galon, J. Integrative analyses of colorectal cancer show Immunoscore is a stronger predictor of patient survival than microsatellite instability. *Immunity* **2016**, *44*, 698–711. [CrossRef]
92. García-Solano, J.; Conesa-Zamora, P.; Carbonell, P.; Trujillo-Santos, J.; Torres-Moreno, D.; Rodriguez-Braun, E.; Vicente-Ortega, V.; Pérez-Guillermo, M. Microsatellite pathologic score does not efficiently identify high microsatellite instability in colorectal serrated adenocarcinoma. *Hum. Pathol.* **2013**, *44*, 759–765. [CrossRef] [PubMed]
93. Sarvaria, A.; Madrigal, J.A.; Saudemont, A. B cell regulation in cancer and anti-tumor immunity. *Cell Mol. Immunol.* **2017**, *14*, 662–674. [CrossRef]
94. Yan, J.; Smyth, M.J.; Teng, M. Interleukin (IL)-12 and IL-23 and Their Conflicting Roles in Cancer. *Cold Spring Harb. Perspect. Biol.* **2018**, *10*, a028530. [CrossRef] [PubMed]
95. Cubillos-Zapata, C.; Hernández-Jiménez, E.; Avendaño-Ortiz, J.; Toledano, V.; Varela-Serrano, A.; Fernández-Navarro, I.; López-Collazo, E. Obstructive Sleep Apnea Monocytes Exhibit High Levels of Vascular Endothelial Growth Factor Secretion, Augmenting Tumor Progression. *Mediat. Inflamm.* **2018**, 7373921. [CrossRef]
96. Matsumura, T.; Hida, S.; Kitazawa, M.; Fujii, C.; Kobayashi, A.; Takeoka, M.; Taniguchi, S.; Miyagawa, S. Fascin1 suppresses RIG-I–like receptor signaling and interferon-β production by associating with IκB kinase ϵ (IKKϵ) in colon cancer. *J. Biol. Chem.* **2018**, *293*, 6326–6336. [CrossRef]
97. Blake, S.J.; Teng, M.W. Role of IL-17 and IL-22 in autoimmunity and cancer. *Actas Dermosifiliogr.* **2014**, *105*, 41–50. [CrossRef]
98. Wang, X.; Teng, F.; Kong, L.; Yu, J. PD-L1 expression in human cancers and its association with clinical outcomes. *Onco Targets Ther.* **2016**, *9*, 5023–5039. [CrossRef] [PubMed]
99. Cantero-Cid, R.; Casas-Martín, J.; Hernández-Jiménez, E.; Cubillos-zapata, C.; Varela-serrano, A.; Avendaño-ortiz, J.; Casarrubios, M.; Montalbán-Hernández, K.; Villacañas-Gil, I.; Guerra-Ppastrián, L.; et al. PD-L1/PD-1 crosstalk in colorectal cancer: Are we targeting the right cells? *BMC Cancer* **2018**, *18*, 945. [CrossRef] [PubMed]
100. Natalwala, A.; Spychal, R.; Tselepis, C. Epithelial-mesenchymal transition mediated tumourigenesis in the gastrointestinal tract. *World J. Gastroenterol.* **2008**, *14*, 3792–3797. [CrossRef] [PubMed]
101. Kato, Y.; Kondo, S.; Itakura, T.; Tokunaga, M.; Hatayama, S.; Katayama, K.; Sugimoto, Y. SNAIL- and SLUG-induced side population phenotype of HCT116 human colorectal cancer cells and its regulation by BET inhibitors. *Biochem. Biophys. Res. Commun.* **2020**, *521*, 152–157. [CrossRef]
102. Dongre, A.; Weinberg, R.A. New insights into the mechanisms of epithelial–mesenchymal transition and implications for cancer. *Nat. Rev. Mol. Cell Biol.* **2019**, *20*. [CrossRef] [PubMed]
103. Kalluri, R.; Weinberg, R.A.; Kalluri, R.; Weinberg, R.A. The basics of epithelial-mesenchymal transition Find the latest version: Review series The basics of epithelial-mesenchymal transition. *Clin. Investig.* **2010**, *119*, 1420–1428. [CrossRef] [PubMed]
104. Prall, F. Tumour budding in colorectal carcinoma. *Histopathology* **2007**, *50*, 151–162. [CrossRef] [PubMed]
105. Brabletz, S.; Schmalhofer, O.; Brabletz, T. Gastrointestinal stem cells in development and cancer. *J. Pathol.* **2009**, *217*, 307–317. [CrossRef]
106. Conacci-sorrell, M.; Simcha, I.; Ben-yedidia, T.; Blechman, J.; Savagner, P.; Ben-ze, A. Autoregulation of E-cadherin expression by cadherin–Cadherin interactions: The roles. *J. Cell Biol.* **2003**, *163*, 847–857. [CrossRef]
107. Fife, C.M.; McCarroll, J.A.; Kavallaris, M. Movers and shakers: Cell cytoskeleton in cancer. *Br. J. Pharmacol.* **2014**, *171*, 5507–5523. [CrossRef]
108. Hall, A. Rho family GTPases. *Biochem. Soc. Trans.* **2012**, *40*, 1378–1382. [CrossRef]
109. Alexander, S.P.H.; Benson, H.E.; Faccenda, E.; Pawson, A.J.; Sharman, J.L.; Spedding, M.; Peters, J.A.; Harmar, A.J. The concise guide to pharmacology 2013/14: G protein-coupled receptors. *Br. J. Pharmacol.* **2013**, *170*, 1459–1581. [CrossRef]

110. Cavallaro, U.; Christofori, G. Cell adhesion and signalling by cadherins and Ig-CAMs in cancer. *Nat. Rev. Cancer* **2004**, *4*, 118–132. [CrossRef]
111. Tao, Y.S.; Edwards, R.A.; Tubb, B.; Wang, S.; Bryan, J.; Mccrea, P.D. b-Catenin Associates with the Actin-bundling Protein Fascin in a Noncadherin Complex. *Cell Biol.* **1996**, *134*, 1271–1281. [CrossRef]
112. Kureishy, N.; Sapountzi, V.; Prag, S.; Anilkumar, N.; Adams, J.C. Fascins, and their roles in cell structure and function. *Bioessays* **2002**, *24*, 350–361. [CrossRef] [PubMed]
113. Hashimoto, Y.; Skacel, M.; Lavery, I.C.; Mukherjee, A.L.; Casey, G.; Adams, J.C. Prognostic significance of fascin expression in advanced colorectal cancer: An immunohistochemical study of colorectal adenomas and adenocarcinomas. *BMC Cancer* **2006**, *11*, 1–11. [CrossRef]
114. Tan, V.Y.; Lewis, S.J.; Adams, J.C.; Martin, R.M. Association of fascin-1 with mortality, disease progression and metastasis in carcinomas: A systematic review and meta-analysis. *BMC Med.* **2013**, *11*, 52. [CrossRef] [PubMed]
115. Vignjevic, D.; Schoumacher, M.; Gavert, N.; Janssen, K.; Jih, G.; Lae, M.; Louvard, D.; Ben-ze, A.; Robine, S. Fascin, a novel target of b-Catenin-TCF signaling, is expressed at the invasive front of human colon cancer. *Cancer Res.* **2007**, 6844–6854. [CrossRef]
116. Huang, F.K.; Han, S.; Xing, B.; Huang, J.; Liu, B.; Bordeleau, F.; Reinhart-King, C.A.; Zhang, J.J.; Huang, X.Y. Targeted inhibition of fascin function blocks tumour invasion and metastatic colonization. *Nat. Commun.* **2015**, *6*, 7465. [CrossRef] [PubMed]
117. Jahchan, N.S.; Dudley, J.T.; Mazur, P.K.; Flores, N.; Yang, D.; Palmerton, A.; Sage, J. A drug repositioning approach identifies tricyclic antidepressants as inhibitors of small cell lung cancer and other neuroendocrine tumors. *Cancer Discov.* **2013**, *3*, 1364–1377. [CrossRef] [PubMed]

ARTÍCULO 2:

Montoro-García, S., **Alburquerque-González, B.**, Bernabé-García, Á., Bernabé-García, M., Rodrigues, P. C., den-Haan, H., Luque, I., Nicolás, F. J., Pérez-Sánchez, H., Cayuela, M. L., Salo, T., & Conesa-Zamora, P. (2020). **Novel anti-invasive properties of a Fascin1 inhibitor on colorectal cancer cells.** *Journal of molecular medicine (Berlin, Germany)*, *98*(3), 383–394. https://doi.org/10.1007/s00109-020-01877-z

Factor de impacto 2020 (JCR): 4.599; Categoría (JCR): MEDICINE RESEARCH & EXPERIMENTAL SCIENCE; Clasificación: 48/176 (Q2, T1); Fecha de publicación: 2020.

Journal of Molecular Medicine
https://doi.org/10.1007/s00109-020-01877-z

JMolMed

ORIGINAL ARTICLE

Novel anti-invasive properties of a Fascin1 inhibitor on colorectal cancer cells

Silvia Montoro-García[1] · Begoña Alburquerque-González[2] · Ángel Bernabé-García[3] · Manuel Bernabé-García[4] · Priscila Campioni Rodrigues[5,6] · Helena den-Haan[7] · Irene Luque[8] · Francisco José Nicolás[3] · Horacio Pérez-Sánchez[9] · María Luisa Cayuela[4] · Tuula Salo[5,6,10,11] · Pablo Conesa-Zamora[2,12]

Received: 22 January 2019 / Revised: 5 December 2019 / Accepted: 15 January 2020

Abstract

Tumor invasion and metastasis involve processes in which actin cytoskeleton rearrangement induced by Fascin1 plays a crucial role. Indeed, Fascin1 has been found overexpressed in tumors with worse prognosis. Migrastatin and its analogues target Fascin1 and inhibit its activity. However, there is need for novel and smaller Fascin1 inhibitors. The aim of this study was to assess the effect of compound G2 in colorectal cancer cell lines and compare it to migrastatin in in vitro and in vivo assays. Molecular modeling, actin-bundling, cell viability, inmunofluorescence, migration, and invasion assays were carried out in order to test anti-migratory and anti-invasive properties of compound G2. In addition, the in vivo effect of compound G2 was evaluated in a zebrafish model of invasion. HCT-116 cells exhibited the highest Fascin1 expression from eight tested colorectal cancer cell lines. Compound G2 showed important inhibitory effects on actin bundling, filopodia formation, migration, and invasion in different cell lines. Moreover, compound G2 treatment resulted in significant reduction of invasion of DLD-1 overexpressing Fascin1 and HCT-116 in zebrafish larvae xenografts; this effect being less evident in Fascin1 known-down HCT-116 cells. This study proves, for the first time, the in vitro and in vivo anti-tumoral activity of compound G2 on colorectal cancer cells and guides to design improved compound G2-based Fascin1 inhibitors.

Key messages

- Fascin is crucial for tumor invasion and metastasis and is overexpressed in bad prognostic tumors.
- Several adverse tumors overexpress Fascin1 and lack targeted therapy.
- Anti-fascin G2 is for the first time evaluated in colorectal carcinoma and compared with migrastatin.
- Filopodia formation, migration activity, and invasion *in vitro* and *in vivo* assays were performed.
- G2 blocks actin structures, migration, and invasion of colorectal cancer cells as fascin-dependent.

Keywords Fascin1 · Migrastatin · Invasion · Migration · Zebrafish xenograft · Colorectal cancer

Introduction

Tumor metastasis remains the leading cause of cancer mortality [1]. Acquisition of invading capacity is a prerequisite for carcinoma cells to get access to vessels and thus spread throughout the body. This process involves actin cytoskeleton rearrangement allowing the tumor cells to develop cellular protrusions, such as filopodia and lamellipodium, which contribute to cancer cell migration, invasion, and metastasis [2]. Fascin1 (FSCN1: ENSG00000075618) is a key protein in membrane protrusion, as it possesses actin-binding and actin-bundling activity by cross-linking filamentous actin into tightly packed parallel bundles. Fascin1 expression is often elevated in malignant tumors

Silvia Montoro-García and Begoña Alburquerque-González contributed equally to this work.

Electronic supplementary material The online version of this article (https://doi.org/10.1007/s00109-020-01877-z) contains supplementary material, which is available to authorized users.

✉ Silvia Montoro-García
smontoro@ucam.edu

✉ Pablo Conesa-Zamora
pablo.conesa@carm.es

Priscila Campioni Rodrigues
Priscila.CampioniRodrigues@oulu.fi

Extended author information available on the last page of the article

Published online: 29 January 2020

while its expression is low or absent in most normal adult epithelia [3]. Fascin1 has emerged as an important biomarker and therapeutic target due to its overexpression in several carcinomas and its association with mortality and metastasis [3, 4]. In fact, several studies including a meta-analysis have demonstrated that Fascin1 expression is associated with increased lymph node- and distant-metastasis, disease progression, and mortality in both colorectal and breast cancer [5, 6].

In a recent study, our group identified Fascin1 as overexpressed in serrated adenocarcinoma (SAC) [7], a histological subtype of colorectal carcinoma. SAC, in contrast to conventional colorectal carcinoma [8], has worse prognosis [9] and it is characterized by a more active invasive front evidenced by higher occurrence of tumor budding, cytoplasmic pseudofragments, infiltrative tumor growth pattern [10], and E-cadherin loss. Moreover, SACs show a higher frequency of KRAS and BRAF mutations than conventional carcinoma which make most of them resistant to anti-EGFR therapy [11, 12].

Given the causative role of Fascin1 in the invading phenotype of tumor cells together with the association of its overexpression to worse survival of a wide variety of cancer types [13–18], it would be desirable to find efficient Fascin1-activity blockers. In this line, migrastatin and its macroketone analogues are considered typical Fascin1 inhibitors [1]. Unfortunately, they are difficult to synthesize due to their complex structure [19].

In this study, we performed a search of patented potential Fascin1 inhibitors, such as those derived from indazol-furancarboxamides [20]. Among them, we found the leading compound G2 and showed an inhibitory effect on Fascin1 activity by using several in vitro and in vivo assays on well-characterized colorectal cell lines.

Material and methods

Compounds and molecular modeling

Compound G2 (N-(1-(4-(trifluoromethyl) benzyl)-1H-indazol-3-yl) furan-2-carboxamide; C20H15F3N3O2; PM 386.13) is covered by the patents WO 2014/031732 A2 and WO 2015/127125A1 and was synthesized as previously described [20]. Migrastatin was synthesized by AnalytiCon Discovery (NP-006108) and provided by MolPort (Riga, Latvia). The geometry of compound G2 was built with Autodock Tools [21], where partial charges were assigned using Gasteiger model [22]. The structural model for Fascin1 was extracted from the crystal structure of protein data bank (PDB) with code 6B0T [23] and converted to PDBQT format using default parameters. Molecular docking calculations based on the Blind Docking (BD) technique [24] were carried out using Blind Docking server (BDS, available at http://bio-hpc.ucam.edu/achilles) with Autodock 4 [21] as docking engine with default parameters. Graphical representations of the docking results as PyMOL (http://www.pymol.org) sessions were downloaded from BDS with default options as specified on the website.

All the protocols comply with the recommendation, the approval of which was obtained from the participant institutions and in accordance with the ethical standards laid down in the 1964 Declaration of Helsinki and its later amendments.

Cell culture

Distinct human colorectal adenocarcinoma cell lines HCT-116, DLD-1, SW480, HCT-15, HT-29, LS174T, SW620, and LoVo were obtained from the American Type Culture Collection (ATCC, Rockville, MD, USA). Cell lines were cultivated using standard high glucose Dulbecco's Modified Eagle's Medium (DMEM) supplemented with 10% heat-inactivated fetal bovine serum (FBS), 50 U/mL penicillin, and 50 μg/mL streptomycin (all from Sigma-Aldrich Chemical Co., USA) at 37 °C and 5% CO_2 and 95% humidified atmosphere. Subculturing was performed when cells reached 90% confluence. Cell RNA extraction and qPCR for Fascin1 expression quantification is described in Supplementary Material S1. The human colorectal carcinoma cells were genetically overexpressed (DLD-1) and knocked-down (HCT-116) for Fascin-1 (Supplementary Material S1).

Cell viability assay

Exponentially growing cells were plated in flat-bottomed 96-well plates (Nunc, Roskilde, Denmark) in triplicate (1500 cells/well). Cells were treated with a series of concentrations from 500 nM to 100 μM of either migrastatin or compound G2 up to 3 days (24, 48, and 72 h) in a 5% CO_2–humidified atmosphere. Control cells were treated with drug carrier (0.1% dimethyl sulfoxide (DMSO)). Cells were assayed for viability as follows. Briefly, Dulbecco's phosphate-buffered saline (DPBS) supplemented with 1.9 mg/mL tetrazolium (MTT) pH 7.2 was added to the cells (30 μL/well). After incubation at 37 °C for 4 h, the medium was carefully aspirated. The formazan crystals were dissolved in 200 μL DMSO for 30 min and the absorbance was read in a microtiter plate reader at 570 nm and 620 nm as reference. Results were calculated as cell viability (%) = average optical density (O.D.) of wells/average O.D. of control wells.

Cell migration assay

Cell migration was studied using HCT-116 and DLD-1 cell lines by performing a scratch wound healing assay in standard medium supplemented with 5% FBS. Typically, 50,000 cells were plated in low 35-mm-dishes with culture inserts following manufacturer instructions (Ibidi, Martinsried, Germany). After appropriate cell attachment and monolayer formation

(around 24 h), inserts were removed with sterile forceps to create a wound field of approximately 500 μm. Detached cells were gently removed with DPBS before the addition of drugs. Confluent cells were incubated in one of the following treatments: control (0.1% DMSO), 100 μM migrastatin, 5, 10, and 20 μM compound G2. Cells were then placed in a cell culture incubator and they were allowed to migrate. At 0, 4, and 7 h (linear growth phase), 10 fields of the injury area were photographed with an inverted phase contrast microscope using × 10 magnification. For each time point, the area uncovered by cells was determined by Image J software (National Institute of Health, Bethesda, MD, USA). Each treatment was performed in triplicate.

The migration speed of the wound closure was given as the percentage of the recovered area at each time point, relative to the initially covered area (t_0). The velocity of wound closure (%/h) was calculated according to the formula:

$$\text{Slope}\ (\%/\text{h}) = \frac{(\%\text{covered area}\ t_x) - (\%\text{covered area}\ t_o)}{(t_x - t_o)}$$

Slopes are expressed as percentages relative to control conditions.

Transwell invasion assay

The invasive capacity of HCT-116 cells was determined using Cytoselect TM 24 Well Cell Invasion Assay (Basement Membrane Colorimetric Format) with Matrigel^{R}-coated Transwell chambers (8 μm pore size) (Cell Biolabs Inc., CA, USA). Briefly, cells (9.5×10^4) were resuspended in serum-free medium with corresponding inhibitors (100 μM migrastatin and 20 μM compound G2) and seeded into the upper chamber. Additionally, 500 μL of standard medium were added to the well. After 30 h of incubation, cells that remained on the upper chamber were scraped away with a cotton swab, and the cells that had migrated through the matrigel and reached the bottom of the chamber were stained with the cell stain solution provided in the kit. Invasiveness was quantified by counting cells on the lower surface of the filter using Image J software (National Institute of Health, Bethesda, MD, USA). In addition, invasive cells at the bottom side of the filter were eluted and quantified at an absorbance of 560 nm.

Myoma organotypic invasion model

Tumoral cell invasion was assessed in the myoma organotypic cultures and performed according to the previously published myoma model protocol [25, 26]. Briefly, uterine leiomyoma tissues were obtained from routine surgery after informed consent of the donors and their use approved by The Ethics Committee of the Oulu University Hospital. The myoma tissue was sliced into 5 mm and disks were made with an 8-mm biopsy punch (Kai Industries Co., Gifu, Japan). Myoma disks were preincubated in either 0.1% DMSO, 100 μM migrastatin or 10 μM and 20 μM compound G2 at 4 °C for 48 h. The myoma disks were placed into Transwell inserts (diameter 6.5 mm; Corning Incorporated, Corning, NY) and 700,000 cells in 50 μL of media were added on top of each myoma disk. Cells were allowed to attach overnight and the myoma disks, transferred onto uncoated nylon disks and be treated with the compounds for 14 days, while changing the treatment media every 3 days. Subsequently, the myoma discs were fixed with 4% neutral-buffered formalin for 24 h and 6 μm sections were cut and stained with cytokeratin AE1/AE3 (M3515, Dako). Sections were documented at × 10 magnifications, using the Leica DMRB microscope DFC 480 camera with the Leica application suite v3.8 (Leica Microsystems, Wetzlar, Germany). Image J software (National Institute of Health, Bethesda, MD, USA) was used to measure invasion areas and depths. Each treatment was performed in triplicate.

Zebrafish invasion assays and treatments

The colonization of zebrafish (ZF) (*Danio rerio*) embryos by human cancer colorectal cell lines was performed as previously described [27]. The experiments performed comply with the Guidelines of the European Union Council (Directive 2010/63/EU) and the Spanish RD 53/2013. Experiments and procedures were performed as approved by the Bioethical Committee of the Murcia University (Spain). Briefly, human cell lines were trypsinized, washed, and stained with fluorescent CM-Dil (Vibrant, Invitrogen) following manufacturer's instructions. Fifty to 100 labeled cells were injected into the yolk sac of dechorionated ZF embryos and transferred into 24-well plates. Fish with fluorescently labeled cells appearing outside the implantation area at 2 h post-injection (dpi) were excluded from further analysis. All other fishes were treated, by bath immersion, with E3 medium (5 mM NaCl, 0.33 mM KCl, 0.33 mM $CaCl_2$, 0.33 mM $MgSO_4$, 0.1% methylene blue) (all from Sigma-Aldrich, St Louis, MO, USA) supplemented with either 100 μM migrastatin or 5–10 μM compound G2 for 96 h at 35 °C. Treatment was renewed every 24 h. Larvae analyzed with a M205-FA stereomicroscope equipped with a DFC365FX camera (Leica). The evaluation criteria for embryos being colonized by human cancer cells was the presence of more than three cells outside of the yolk sac and, with this criterion, ZF percentage of invasion was calculated.

With the aim of finding out whether the pro-metastatic activity of Fascin1-induced expression was affected by chemical compounds, a metastasis assay was carried out. Zebrafish embryos xenografted with Fascin1-transfected DLD-1 cells were incubated up to 144 h. The day of invasion screening (fourth day post-xenograft), freshly prepared E3 medium was supplemented with 100 μM migrastatin or 10 μM compound G2 together with 375 rotifers/mL (*Brachionus plicatilis* (L-

type); ReefNutrition, Campbell, CA, USA). The number of small colonies generated from individual invading cells was counted on the sixth day post-xenograft (6 dpi). This was considered as the number of ZF larvae with metastasis.

Data analysis

Data are expressed as mean ± standard deviation (SD). Data were analyzed for statistical differences by the Student's *t* test for paired and unpaired data after testing for normal distribution of the data. For in vitro experiments, one-way analysis of variance (ANOVA) was performed followed by a Tukey post hoc test to compare each group. Differences were considered significant at an error probability of $p < 0.05$. SPSS 18.0 software was used for the rest of statistical analyses (SPSS, Inc., Chicago, IL, USA). For myoma assay, OriginPro 2016 software was used for statistical calculations. One-way ANOVA (analysis of variance) with post hoc comparisons based on the Tukey's multiple comparisons test were applied. The level of significance considered was 5% ($p \leq 0.05$).

Results

Molecular modeling

Figure 1 shows the main resulting pose of compound G2 after blind docking calculations against whole Fascin1 protein surface. Most relevant intermolecular interactions established are related to hydrogen bonds (GLU215), pi-pi (TRP101), and hydrophobic interactions (LEU16, PHE14, LEU48, ILE93, VAL134, GLU215, PHE216). It must be noticed that these residues participate in the actin-binding site 2, located within the pocket formed by β-trefoil 1 and 2 from the Fascin1 structure, and that blind docking calculations were able to predict this interaction spot with no previous assumption about binding site. In addition, this prediction coincides rather well with crystallographic pose of ligand compound G2-029 (PDB: 6B0T), which is to be expected due to the small difference between compound G2 and G2-029 molecules, just a methyl group.

Compound G2 prevents in vitro Fascin1-induced F-actin bundling

In order to assess the effect of compound G2 on Fascin1, we performed an F-actin-bundling assay under transmission electron microscopy (TEM) (Supplementary Material S1). As shown in Fig. 2, only F-actin incubated in the presence of untreated Fascin1 formed filament bundles (12.00 [9.00–19.75]). Fascin1 preincubated with 100 μM migrastatin or compound G2 (up to 20 μM) lead to the disorganization of the bundles, resulting in fewer filaments than in control conditions (Kruskal-Wallis test, $p < 0.001$). No statistically changes were found between the different drug treatments (Kruskal-Wallis test, $p = 0.370$).

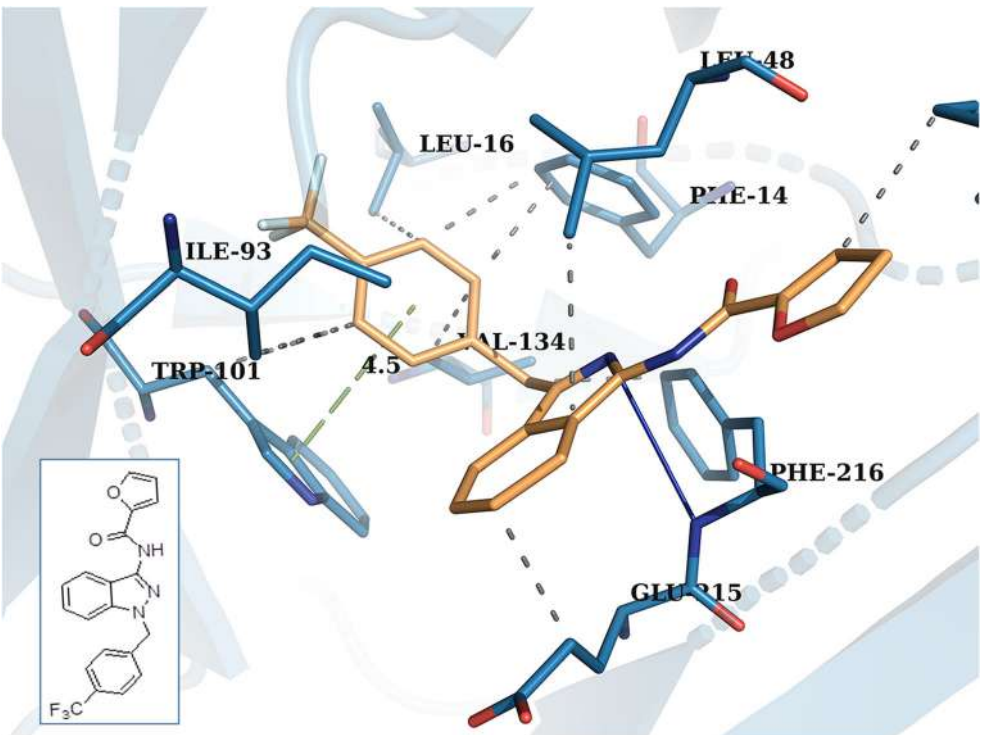

Fig. 1 Main interactions obtained after blind docking of compound G2 against Fascin1. Blue solid line represents hydrogen bond, green dashed line aromatic interactions, and dashed gray lines hydrophobic interactions. Inset: compound G2 chemical structure

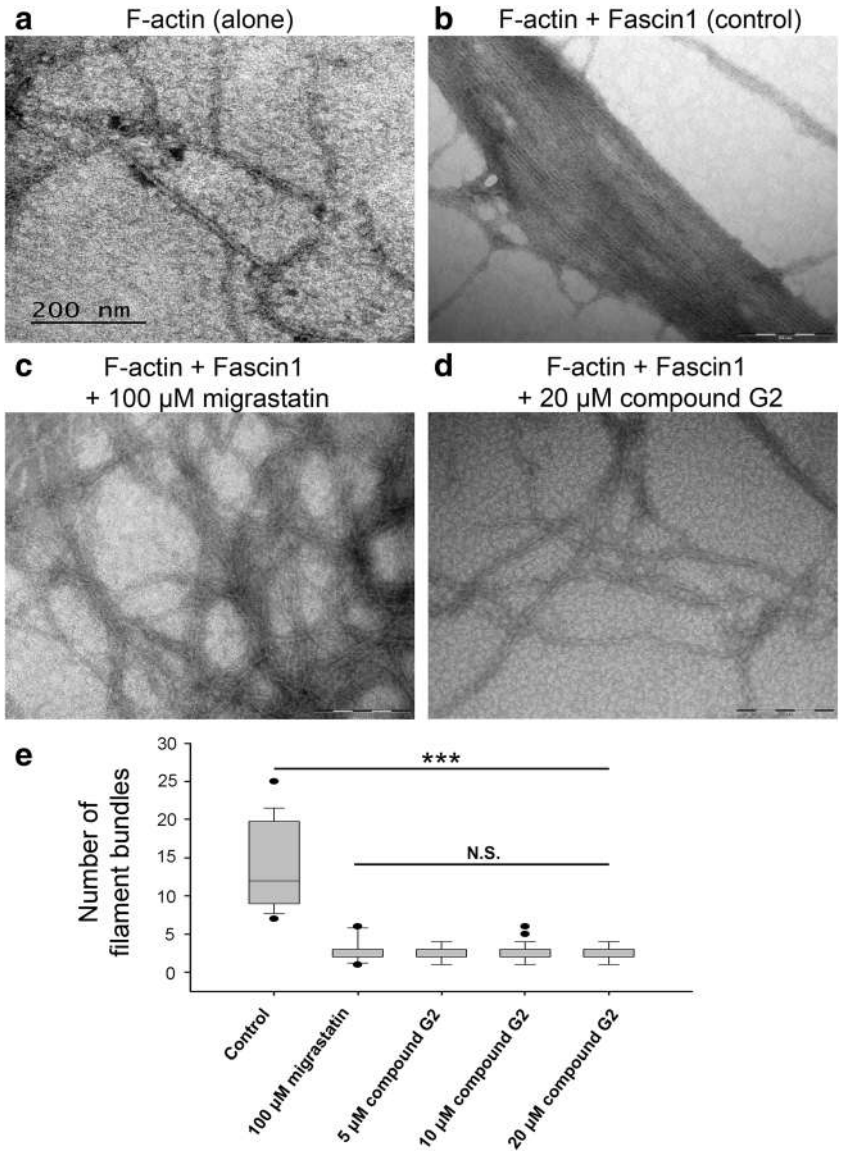

Fig. 2 Transmission electronic microscopy visualization of actin-binding and bundling activities of Fascin1 treated or not with inhibitors (negative staining). **a** Stained F-actin filaments alone. **b** F-actin-bundling assay with filamentous F-actin and untreated Fascin1 (1:1 molecular ratio) (control condition). **c** F-actin-bundling assay with filamentous F-actin and Fascin1 previously incubated with 100 μM migrastatin (1:1 molecular ratio). **d** F-actin-bundling assay with filamentous F-actin and Fascin1 previously incubated with 20 μM compound G2. Magnification: **a** × 120,000 and **b** to **d** × 93,000. **e** Quantitative analysis of the numbers of actin filaments bundles in the stated conditions (***$p < 0.001$ compared to control condition), non-significant (N.S.) between treatments (Kruskal-Wallis test)

Compound G2 affects cytoskeleton formation and Fascin1 localization at the lamellipodium

In order to choose colorectal cell lines with highest and lowest endogenous Fascin1 expression, a RT-qPCR was performed upon RNA extracted from eight cell lines. As shown in Supplementary Material 2, HCT-116 and SW480 exhibited the highest Fascin1 expression while LoVo, DLD-1, and HT-29 had the lowest. Given the ease for cell culture and the differences in endogenous Fascin1 expression, we selected DLD-1 (low Fascin1 expression) and HCT-116 (high Fascin1 expression) cell lines in subsequent assays.

To assess the Fascin1 inhibition activity of the compound G2 on cell viability, we tested different concentration of migrastatin and compound G2 on different colorectal cancer cells. As shown Supplementary Material S3, migrastatin was generally better tolerated than compound G2 by the DLD-1 and HCT-116 cell lines. Thus, the working concentrations for migrastatin and compound G2 were set up for subsequent in vitro studies at 100 μM and up to 20 μM, respectively.

The effect of compound G2 on Fascin1 localization and the reorganization of the actin cytoskeleton as well as on the protrusion of lamellipodium at the cell front was assessed by immunofluorescence. For that purpose, we used HCT-116, the colorectal cell line with maximum expression levels of Fascin1 together with Fascin1 silenced HCT-116 cells. As shown in Fig. 3, prominent lamellipodium formation was observed in control conditions and for EGF-treated cells (non-significant differences between each other were found). However, these cytoskeleton structures were absent in cells treated with migrastatin and compound G2, similarly to what it was observed with PD98059, an inhibitor targeting the MEK pathway. Lamellipodium protrusion

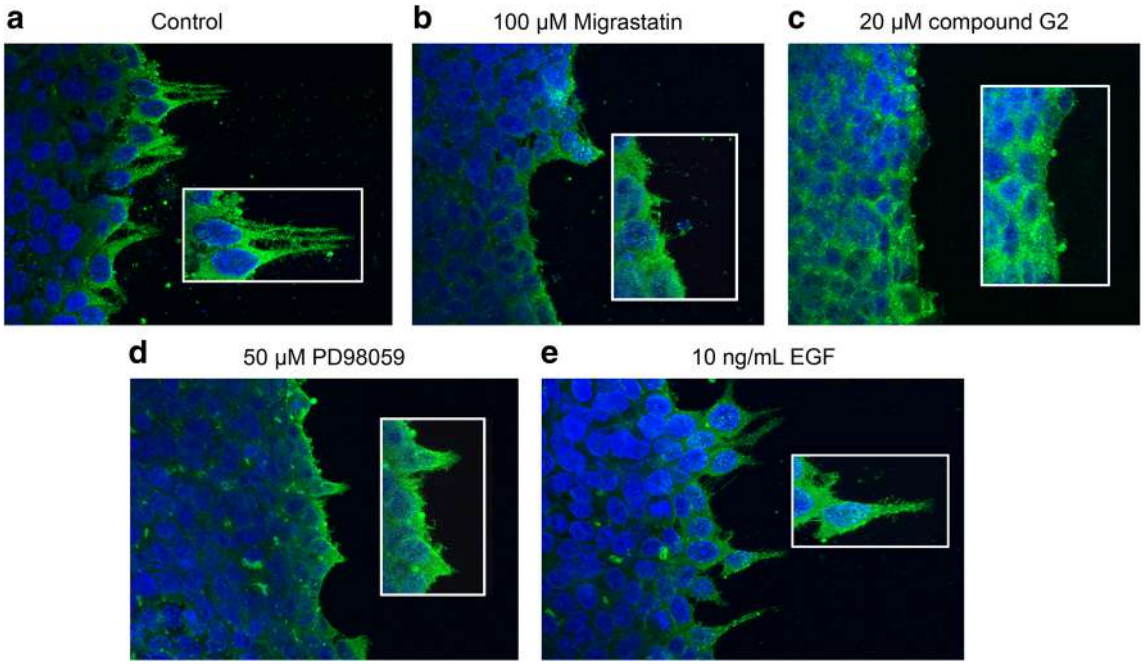

Fig. 3 Migrastatin and compound G2 affect lamellipodium formation and morphology of HCT-116. Representative images of immunofluorescence assays for Fascin1 (lower inset in detail) are shown. **a** Control condition; **b** 100 µM migrastatin; **c** 20 µM compound G2; **d** 50 µM PD98059 (Mek inhibitor); **e** 10 ng/mL epidermal growth factor (EGF, migration stimulator). Cells were fixed and stained with anti-Fascin1 antibody (1/250). Images were captured with a LSM 510 META confocal fluorescence microscope with × 63 oil objective. Fascin1 location is show in green in these structures. Co-staining with Hoechst-33258 was used to show the cell nuclei. Both migrastatin and compound G2 inhibited lamellipodium protrusion and Fascin1 localization in a similar way to the migration Mek inhibitor

numbers calculated at different conditions were significantly lower upon both migrastatin and compound G2 treatments when compared to control conditions (Table 1). Supplementary Material S4 showed that the treatments also abolished the actin bundles in lamellipodium. Similar results were observed with an extra cell line expressing Fascin1 (HaCat) as DLD1 morphology was not suitable for assessing lamellipodium formation (data not shown). Transcriptional Fascin1 silencing of HCT-116 abolished the Fascin1 accumulation at lamellipodium sites and produced an alteration of F-actin microfilament assembly in silenced cells (Supplemental S5D).

Compound G2 diminishes migration and inhibits Matrigel cell invasion of colorectal cancer cells

In order to correlate the observed effect of Fascin1 inhibitors on lamellipodium protrusion to an effect on cell migration, migrastatin- and compound G2–treated cells were investigated for their migration activity using an in vitro wound healing scratch assay. As shown in Fig. 4, compound G2 produces a remarkable inhibition of migration in HCT-116 and DLD-1 cell lines ($p < 0.01$). Compound G2 effect at 20 µM was more pronounced than migrastatin in DLD-1 cells, while in HCT-116 the effect of compound G2 on migration was lower.

Tumor cell invasion not only involves the acquisition of migration properties but also the ability to degrade the basement membrane and tumor stoma matrices, three-dimensional substrates [28]. For that reason, we performed a Transwell assay on Matrigel^{R} which resembles the basement membrane extracellular matrix composition. As shown in Supplementary Material S6, both compound G2 and migrastatin inhibit tumor cell invasion of HCT-116, the effect of the latter being slightly more evident.

To further confirm the inhibitory effect of compound G2 on the Fascin1 activity, we used Fascin1 silenced HCT116 and fascin1 overexpressed DLD-1 cells and

Table 1 Lamellipodium protrusion numbers in the different conditions in HCT-116 cells

	Control	100 µM migrastatin	20 µM compound G2	10 ng/mL EGF	50 µM PD98059
Lamellipodium numbers	9 ± 1.5	2 ± 2	5.8 ± 1.1	10.4 ± 1.5	1 ± 1
p value*		0.000139	0.002936	0.140178	5.9241E^{-06}

*Student *T* test compared to control condition

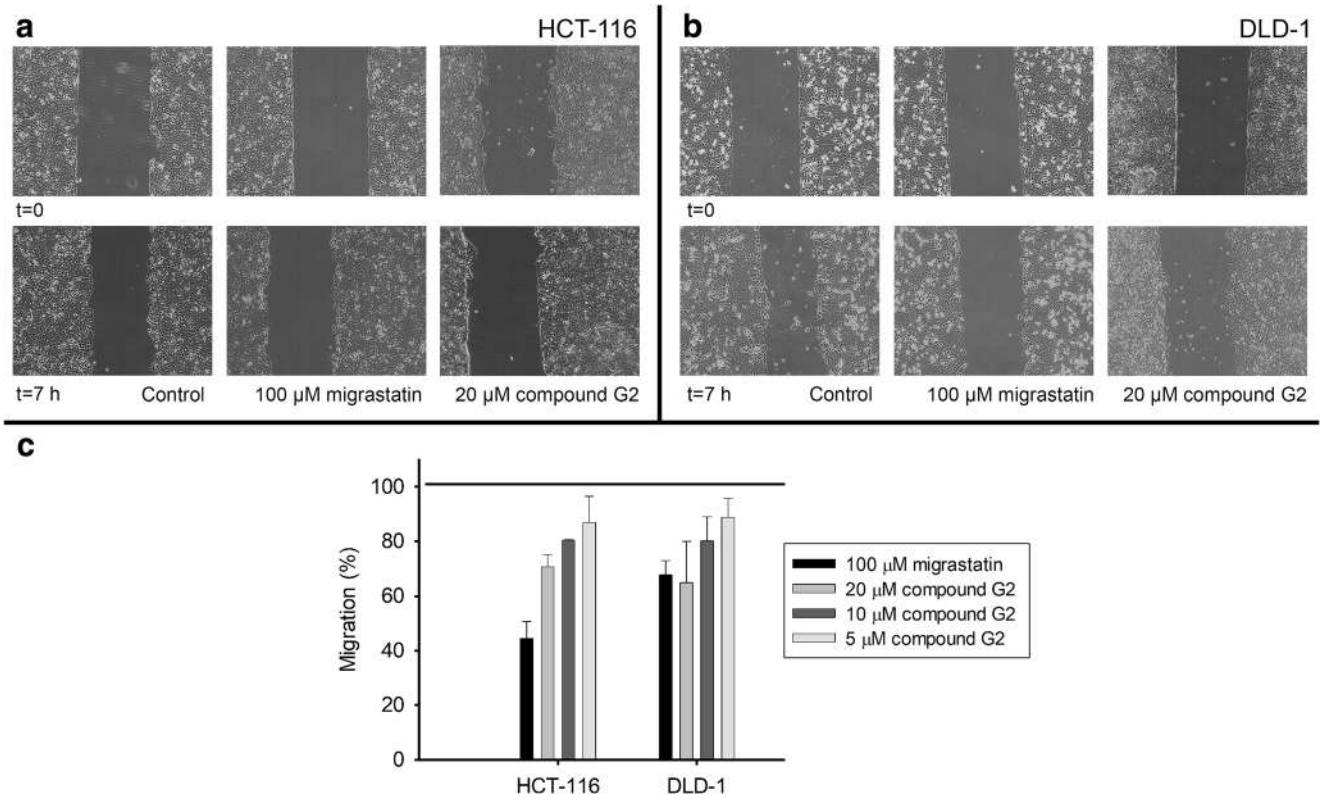

Fig. 4 Migrastatin and compound G2 prevent cell migration on HCT-116 and DLD-1 colorectal cancer cells. **a** Effect of 100 μM migrastatin and 20 μM compound G2 on HCT-116 and **b** DLD-1 cells. **c** Percentage of migration for 100 μM migrastatin and compound G2 (5, 10, 20 μM) treatments. Migration was calculated with respect to the control conditions (100%) for a slope between 4 and 7 h (lineal phase). $^{**}p < 0.01$

tested their migration and invasion properties. Fascin1 silencing produces a slight decrease of migration and invasion compared to MOCK HCT-116 cells ($p < 0.05$), whereas double inhibition (genetic and pharmacological) only produced a significant decrease in migration (Supplemental material S7A-B). Accordingly, 10 μM compound G2 strongly diminished migration and invasion in Fascin1 overexpressed DLD-1 cells ($p < 0.01$) (Supplemental material S7C-D).

Compound G2 diminishes HCT-116 colon cancer cell invasion in a human benign leiomyoma tissue in vitro 3D model

In order to find out whether the anti-invasive properties of compound G2 on cancer cell invasion could be translated into a 3D human model, a myoma disc organotypic model was used. As shown in Fig. 5, compound G2 (5 μM) significantly reduced the invasion depth and invasion area of HCT-116 cells into the discs when compared to untreated cells ($p < 0.01$). Similar results were obtained when cells were treated with 10 and 20 μM compound G2 (Supplementary Material S8).

Compound G2 inhibits the invasive capacity of HCT-116 tumor cells in an in vivo assay of zebrafish model

In order to find out whether the anti-invasive properties of compound G2 could be extrapolated to a living animal, a xenograft assay was carried by using the well-established zebrafish (ZF)-larvae invasion model. To test viability, groups of thirty larvae were treated with either 100 μM migrastatin or 5, 10, and 20 μM compound G2. The majority of larvae were viable after 30 days treatment with either 5 or 10 μM. However, 20 μM compound G2 treatment caused larvae death at the third day of treatment (Supplementary Material S9A). Therefore, concentrations chosen for ZF assays were 5 and 10 μM compound G2. Later on, detached and labeled colorectal cancer cells were injected into the yolk sac and colonization was followed up to 6 days. The percentage of invasion was studied for four colorectal cancer cell lines (Fig. 6a, b) that exhibited different Fascin1 expression levels (Supplementary Material S2). HCT-116 and DLD-1 were selected for being the cell lines with the highest and lower Fascin1 expression, respectively. Good correlation was observed between Fascin1 expression and cell invasion for all cell lines assayed except HCT-15 whose invasion was lower than expected (Fig. 6b) possibly due to other fascin1 independent factors

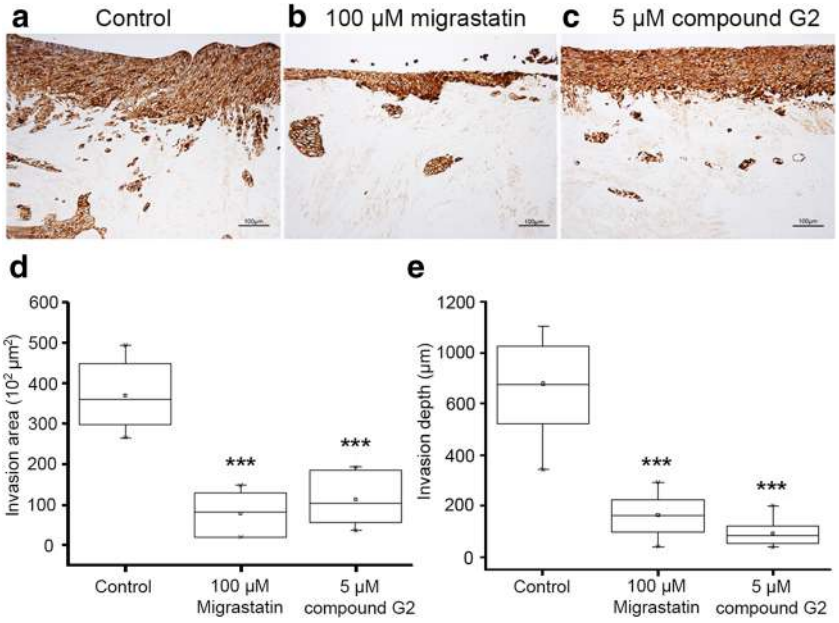

Fig. 5 Myoma organotypic invasion model in HCT-116 cell line. **a** Invasion of the cells within myoma discs after treatment in control conditions, **b** 100 μM migrastatin, and **c** 5 μM compound G2. Pictures were taken under a phase contrast microscope with × 100 magnification and 100 μm scale bars. **d** The invasion area and **e** invasion depth of cytokeratin positive cells were quantified with image J. Data is shown as mean ± SD compared with the control. ***$p < 0.001$

affecting invasion [29]. Therefore, and because of good correlation, HCT-116 was selected for being the cell line with the highest and DLD-1 for its lower Fascin1 expression and cell invasion. To further test the in vivo involvement of Fascin1 in this phenomenon, we performed exogenous silencing of Fascin1 in HCT-116 cells (Fig. 7a). Either genetic reduction of Fascin1 or its pharmacological inhibition by compound G2 decreased the invasion in HCT-116 cells (Fig. 7b, c). Conversely, we induced the overexpression of Fascin1 by means of plasmid transfection into DLD-1 cells (Fig. 7d), thus correlating with a higher invasion capacity (Fig. 7e). Compound G2 kept inhibiting invasion in both MOCK and transfected Fascin1-overexpressing cells (Fig. 7f). Consequently, in vivo invasion correlated with Fascin1 expression and compound G2 inhibited it in transfected cells (Fig. 7e, f). Furthermore, a clear increase of the number of ZF larvae with metastasis was observed with Fascin1-overexpressing DLD-1 cells although 10 μM compound G2 treatment had a similar effect on ZF groups subjected to either Fascin1 transfected or wild-type DLD-1 cells (Supplementary Material S10).

Discussion

Colorectal serrated adenocarcinoma and triple negative breast carcinoma are characterized by their bad prognosis, overexpression of Fascin1, and the absence of targeted molecular therapy [7, 8, 12, 30–35]. Han et al. demonstrated an

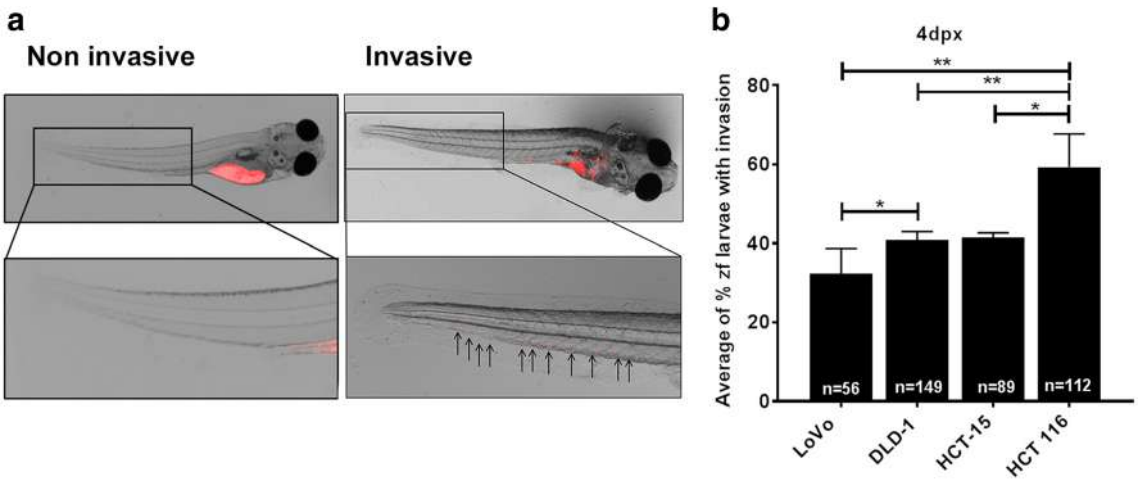

Fig. 6 Zebrafish invasion assays. **a** Zebrafish invasion model. Representative images of a zebrafish embryo with no invasion where the labeled cells remained in the yolk and never invaded the embryo and an embryo with invasion where the cells were able to migrate outside of the yolk. Magnification of the tail region of an embryo with invasion is shown at the right. **b** Invasiveness of each cell line in this model. Data is shown as mean ± SD; compared with the control. *p = 0.049–0.01; **p = 0.001–0.009

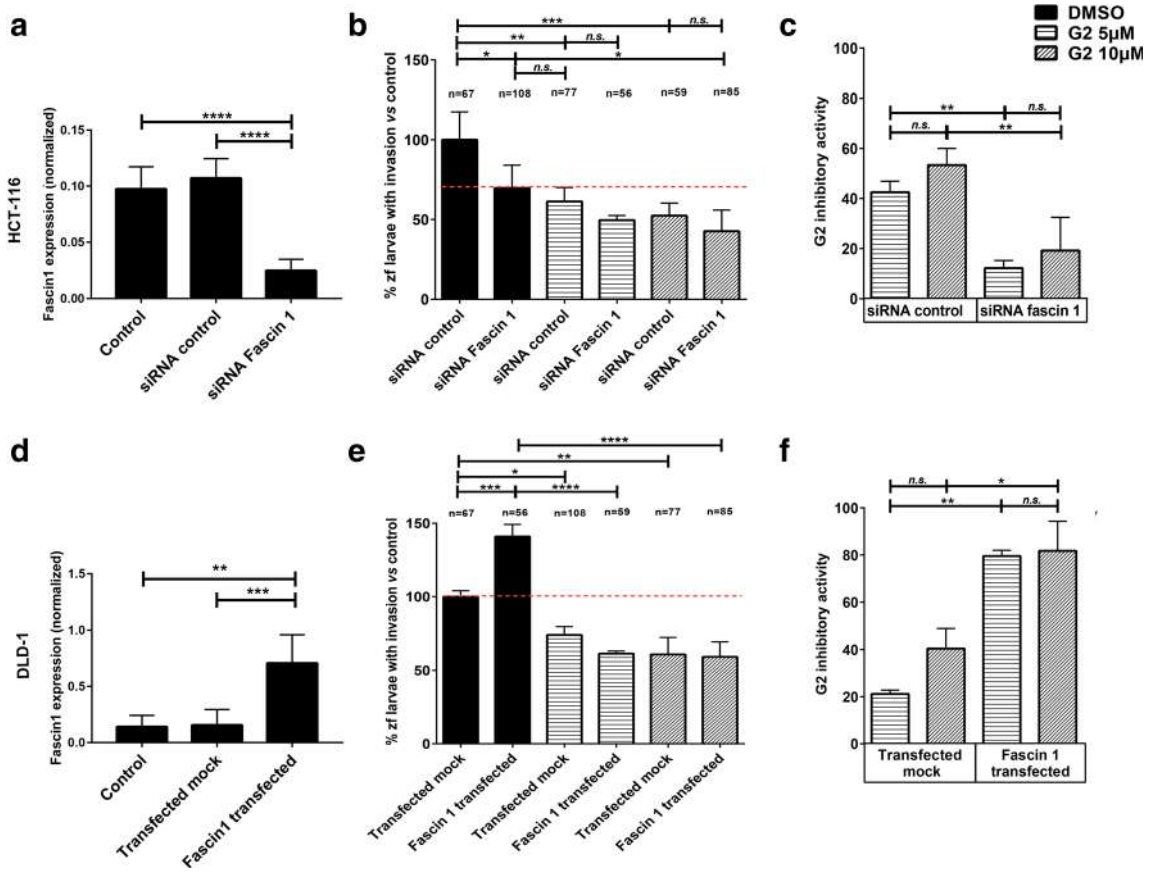

Fig. 7 Treatment effects on cancer cell invasion with different grades of Fascin1 expression. **a** Inhibition of Fascin1 gene expression upon siRNA-Fascin1 transfection in HCT-116 cells. **b** Effect of 5 and 10 μM compound G2 on HCT-116 invasion with endogenous and silenced Fascin1 expression. **c** Compound G2 inhibitory activity on control and siRNA Fascin1-transfected HCT-116 cells. First two columns represent the difference between percentage of invasion in control (MOCK) and percentage of invasion in treated cells. Second two columns represent the difference between percentage of invasion in siRNA Fascin1-transfected HCT-116 and percentage of invasion in compound G2-treated siRNA Fascin1-transfected HCT-116 cells. Note that the effect of compound G2 decreased when Fascin1 was silenced. **d** Overexpression of Fascin1 gene upon Fascin1 transfection in DLD-1. **e** Effect of 5 and 10 μM compound G2 on DLD-1 invasion with endogenous and exogenous Fascin1 expression. **f** Compound G2 inhibitory activity on control and Fascin1-transfected DLD-1 cells. First two columns represent the difference between percentage of invasion in control (MOCK) and percentage of invasion in treated cells. Second two columns represent the difference between percentage of invasion in Fascin1-transfected DLD-1 and percentage of invasion in compound G2–treated Fascin1-transfected DLD-1. Note that the effect of compound G2 increased when Fascin1 was overexpressed by transfection. Data is shown as mean ± SD; compared with the control, $*p = 0.049–0.01$. $**p = 0.001–0.009$. $***p = 0.0001–0.0009$. $****p < 0.0001$

inhibitory effect of compound G2 and its derivates on Fascin1-driven actin bundling. Moreover, they showed an anti-migratory and anti-invasive effect of compound G2 on breast cancer cells [20]. In the present report, we include a molecular model, which provided an improved understanding regarding atomic details of the interactions between compound G2 chemical class and Fascin1 inhibition and will guide the future identification of more potent anti-metastatic drugs. Using blind docking calculations, the model identified a region in Fascin1 possibly involved in compound G2 binding. Some prior evidences support this finding as this region is part of the actin-binding site 1, as described by Han et al. [20]. In accordance, preincubation of Fascin1 with migrastatin and compound G2 disrupted the F-actin bundle formation in vitro. Herein, among the different colorectal cell lines used in this study, HCT-116 expressed the highest Fascin1 levels and its migration capacity was clearly reduced after treatment with compound G2, even at lower concentrations than migrastatin and in a dose-dependent manner. Invasion and confocal studies were further performed with HCT-116 cells because of its morphological features and higher Fascin1 expression levels. We showed that both inhibitors, migrastatin and compound G2, strongly abolished the protrusion of lamellipodium, as confirmed by rescue experiments in Fascin1-silenced cells. Furthermore, we observed similar inhibitory effects of migrastatin and compound G2 on the Matrigel invasion assays with naïve and transfected HCT-116 and DLD-1 cells. Myoma discs represent a superior 3D model for cancer cell invasion studies compared to the other, non-human tissue–based, organotypic models [36]. In myoma assay, both migrastatin and compound G2 were similarly able to significantly decrease both the invasion depth and invasion area of HCT-

116 cells. It is important to notice that cell death caused by long-time incubation with the compound G2 was avoided in the migration and invasion in vitro assays, since viability did not seem to be compromised after 30 h. Of note, no previous studies have analyzed the effect of migrastatin or compound G2 on human solid, hypoxic, myoma disc organotypic invasion assay.

Moreover, in vivo assays using a model of ZF where Fascin1 expression was modified in colorectal cells showed that compound G2 effects on colorectal cancer cells invasion capacities showed a Fascin1 dependency. This compound inhibits the invasion of two cell lines of colorectal cancer with high expression of Fascin1, both constitutive and induced, without affecting the ZF viability and with a more pronounced effect than migrastatin. This activity also had an effect on colony formation from individual invading cells thus suggesting an inhibition of both invasion and metastasis of Fascin1-tranfected tumor cells. It is worth of mentioning that this validated model was capable of testing a very high number of individuals per assay. However and despite these evidences, additional off-target anti-tumoral effects of G2 apart from Fascin1 are also possible.

In conclusion, this study reports a Fascin1 inhibitor with anti-migratory and anti-invasive properties in colorectal cancer cells at lower concentrations than migrastatin, the typical Fascin1 inhibitor. Using this strategy, we have here confirmed a novel class of compounds for the study of therapeutic approaches for invasive and metastatic tumoral cells, such as SAC, providing the first rationale for a tailored therapy in this type of cancer.

Acknowledgments This research was partially supported by the e-infrastructure program of the Research Council of Norway, and the supercomputer center of UiT, the Arctic University of Norway, and by the supercomputing infrastructure of Poznan Supercomputing Center.

Funding information This project received grants from Instituto de Salud Carlos III (Spanish Ministry of Health) and FEDER funds (ref: PI12/1232 and PI15/00626), Spanish Ministry of Economy and Competitiveness MINECO (CTQ2017-87974-R), and by the Fundación Séneca del Centro de Coordinación de la Investigación de la Región de Murcia under Projects 18946/JLI/13 and 20646/JLI/18. BAG belongs to the "Programa de Doctorado en Ciencias de la Salud, Universidad Católica de Murcia (UCAM)" and holds a grant of the UCAM. PCR was supported by Finnish Cultural Foundation Grant (2017-2018).

Compliance with ethical standards

Conflict of interest The authors declare that there are no conflicts of interest.

References

1. Chen L, Yang S, Jakoncic J, Zhang JJ, Huang XY (2010) Migrastatin analogues target fascin to block tumour metastasis. Nature 464(7291):1062–1066
2. Machesky LM, Li A (2010) Fascin: Invasive filopodia promoting metastasis. Commun Integr Biol 3(3):263–270
3. Hashimoto Y, Kim DJ, Adams JC (2011) The roles of fascins in health and disease. J Pathol 224(3):289–300
4. Hashimoto Y, Skacel M, Adams JC (2005) Roles of fascin in human carcinoma motility and signaling: prospects for a novel biomarker? Int J Biochem Cell Biol 37(9):1787–1804
5. Omran OM, Al Sheeha M (2015) Cytoskeletal focal adhesion proteins Fascin-1 and Paxillin are predictors of malignant progression and poor prognosis in human breast cancer. J Environ Pathol Toxicol Oncol 34(3):201–212
6. Tan VY, Lewis SJ, Adams JC, Martin RM (2013) Association of fascin-1 with mortality, disease progression and metastasis in carcinomas: a systematic review and meta-analysis. BMC Med 11:52
7. Conesa-Zamora P, García-Solano J, García-García F, Turpin Mdel C, Trujillo-Santos J, Torres-Moreno D, Pérez-Guillermo M (2013) Expression profiling shows differential molecular pathways and provides potential new diagnostic biomarkers for colorectal serrated adenocarcinoma. Int J Cancer 132(2):297–307
8. García-Solano J, Conesa-Zamora P, Carbonell P, Trujillo-Santos J, Torres-Moreno DD, Pagán-Gómez I, Rodríguez-Braun E, Pérez-Guillermo M (2012a) Colorectal serrated adenocarcinoma shows a different profile of oncogene mutations, MSI status and DNA repair protein expression compared to conventional and sporadic MSI-H carcinomas. Int J Cancer 131(8):1790–1799
9. García-Solano J, Pérez-Guillermo M, Conesa-Zamora P, Acosta-Ortega J, Trujillo-Santos J, Cerezuela-Fuentes P, Mäkinen MJ (2010) Clinicopathologic study of 85 colorectal serrated adenocarcinomas: further insights into the full recognition of a new subset of colorectal carcinoma. Hum Pathol 41(10):1359–1368
10. García-Solano J, Conesa-Zamora P, Trujillo-Santos J, Mäkinen MJ, Pérez-Guillermo M (2011) Tumour budding and other prognostic pathological features at invasive margins in serrated colorectal adenocarcinoma: a comparative study with conventional carcinoma. Histopathology 59(6):1046–1056
11. García-Solano J, Conesa-Zamora P, Trujillo-Santos J, Torres-Moreno D, Mäkinen MJ, Pérez-Guillermo M (2012b) Immunohistochemical expression profile of β-catenin, E-cadherin, P-cadherin, laminin-5γ2 chain, and SMAD4 in colorectal serrated adenocarcinoma. Hum Pathol 43(7):1094–1102
12. Stefanius K, Ylitalo L, Tuomisto A, Kuivila R, Kantola T, Sirniö P, Karttunen TJ, Mäkinen MJ (2011) Frequent mutations of KRAS in addition to BRAF in colorectal serrated adenocarcinoma. Histopathology 58(5):679–692
13. Cao HH, Zheng CP, Wang SH, Wu JY, Shen JH, Xu XE, Fu JH, Wu ZY, Li EM, Xu LY (2014) A molecular prognostic model predicts esophageal squamous cell carcinoma prognosis. PLoS One 9(8): e106007
14. Jones RP, Bird NT, Smith RA, Palmer DH, Fenwick SW, Poston GJ, Malik HZ (2015) Prognostic molecular markers in resected extrahepatic biliary tract cancers; a systematic review and meta-analysis of immunohistochemically detected biomarkers. Biomark Med 9(8):763–775
15. Li A, Morton JP, Ma Y, Karim SA, Zhou Y, Faller WJ, Woodham EF, Morris HT, Stevenson RP, Juin A et al (2014) Fascin is regulated by slug, promotes progression of pancreatic cancer in mice, and is associated with patient outcomes. Gastroenterology 146(5): 1386–1396.e1381-1317
16. Rodrigues PC, Sawazaki-Calone I, Ervolino de Oliveira C, Soares Macedo CC, Dourado MR, Cervigne NK, Miguel MC, Ferreira do Carmo A, Lambert DW, Graner E (2017) Fascin promotes migration and invasion and is a prognostic marker for oral squamous cell carcinoma. Oncotarget 8(43):74736–74754
17. Stewart CJ, Crook ML (2015) Fascin expression in undifferentiated and dedifferentiated endometrial carcinoma. Hum Pathol 46(10): 1514–1520

18. Zhao W, Gao J, Wu J, Liu QH, Wang ZG, Li HL, Xing LH (2015) Expression of Fascin-1 on human lung cancer and paracarcinoma tissue and its relation to clinicopathological characteristics in patients with lung cancer. Onco Targets Ther 8:2571–2576
19. Gaul C, Njardarson JT, Shan D, Dorn DC, Wu KD, Tong WP, Huang XY, Moore MA, Danishefsky SJ (2004) The migrastatin family: discovery of potent cell migration inhibitors by chemical synthesis. J Am Chem Soc 126(36):11326–11337
20. Han S, Huang J, Liu B, Xing B, Bordeleau F, Reinhart-King CA et al (2016) Improving fascin inhibitors to block tumor cell migration and metastasis. Mol Oncol 10(7):966–980
21. Morris GM, Huey R, Lindstrom W, Sanner MF, Belew RK, Goodsell DS, Olson AJ (2009) AutoDock4 and AutoDockTools4: automated docking with selective receptor flexibility. J Comput Chem 30(16):2785–2791
22. Gasteiger J, Marsili M (1980) Iterative partial equalization of orbital electronegativity—a rapid access to atomic charges Y1 - 1980 Y2 - 1980. *Tetrahedron 36*(22):3219–3228 M1 - Generic
23. Huang J, Dey R, Wang Y, Jakoncic J, Kurinov I, Huang XY (2018) Structural insights into the induced-fit inhibition of Fascin by a small-molecule inhibitor. J Mol Biol 430(9):1324–1335
24. Sánchez-Linares I, Pérez-Sánchez H, Cecilia JM, García JM (2012) High-throughput parallel blind virtual screening using BINDSURF. BMC Bioinformatics 13(Suppl 14):S13
25. Nurmenniemi S, Sinikumpu T, Alahuhta I, Salo S, Sutinen M, Santala M, Risteli J, Nyberg P, Salo T (2009) A novel organotypic model mimics the tumor microenvironment. Am J Pathol 175(3): 1281–1291
26. Åström P, Heljasvaara R, Nyberg P, Al-Samadi A, Salo T (2018) Human tumor tissue-based 3D in vitro invasion assays. Methods Mol Biol 1731:213–221
27. Jelassi B, Chantôme A, Alcaraz-Pérez F, Baroja-Mazo A, Cayuela ML, Pelegrin P, Surprenant A, Roger S (2011) P2X(7) receptor activation enhances SK3 channels- and cystein cathepsin-dependent cancer cells invasiveness. Oncogene 30(18):2108–2122
28. Albini A (1998) Tumor and endothelial cell invasion of basement membranes. The matrigel chemoinvasion assay as a tool for dissecting molecular mechanisms. Pathol Oncol Res 4(3):230–241
29. Stevenson RP, Veltman D, Machesky LM (2012) Actin-bundling proteins in cancer progression at a glance. J Cell Sci 125(Pt 5): 1073–1079
30. Esnakula AK, Ricks-Santi L, Kwagyan J, Kanaan YM, DeWitty RL, Wilson LL, Gold B, Frederick WA, Naab TJ (2014) Strong association of fascin expression with triple negative breast cancer and basal-like phenotype in African-American women. J Clin Pathol 67(2):153–160
31. García-Solano J, García-Solano ME, Torres-Moreno D, Carbonell P, Trujillo-Santos J, Pérez-Guillermo M, Conesa-Zamora P (2016) Biomarkers for the identification of precursor polyps of colorectal serrated adenocarcinomas. Cell Oncol (Dordr) 39(3):243–252
32. Ghebeh H, Al-Khaldi S, Olabi S, Al-Dhfyan A, Al-Mohanna F, Barnawi R et al (2014) Fascin is involved in the chemotherapeutic resistance of breast cancer cells predominantly via the PI3K/Akt pathway. Br J Cancer 111(8):1552–1561
33. Kanda Y, Kawaguchi T, Kuramitsu Y, Kitagawa T, Kobayashi T, Takahashi N, Tazawa H, Habelhah H, Hamada J, Kobayashi M, Hirahata M, Onuma K, Osaki M, Nakamura K, Kitagawa T, Hosokawa M, Okada F (2014) Fascin regulates chronic inflammation-related human colon carcinogenesis by inhibiting cell anoikis. Proteomics 14(9):1031–1041
34. Rodríguez-Pinilla SM, Sarrió D, Honrado E, Hardisson D, Calero F, Benitez J, Palacios J (2006) Prognostic significance of basal-like phenotype and fascin expression in node-negative invasive breast carcinomas. Clin Cancer Res 12(5):1533–1539
35. Wang CQ, Tang CH, Chang HT, Li XN, Zhao YM, Su CM, Hu GN, Zhang T, Sun XX, Zeng Y, du Z, Wang Y, Huang BF (2016) Fascin-1 as a novel diagnostic marker of triple-negative breast cancer. Cancer Med 5(8):1983–1988
36. Salo T, Dourado MR, Sundquist E, Apu EH, Alahuhta I, Tuomainen K, Vasara J, Al-Samadi A (2018) Organotypic three-dimensional assays based on human leiomyoma-derived matrices. Philos Trans R Soc Lond Ser B Biol Sci 373(1737):20160482

Affiliations

Silvia Montoro-García[1] · Begoña Alburquerque-González[2] · Ángel Bernabé-García[3] · Manuel Bernabé-García[4] · Priscila Campioni Rodrigues[5,6] · Helena den-Haan[7] · Irene Luque[8] · Francisco José Nicolás[3] · Horacio Pérez-Sánchez[9] · María Luisa Cayuela[4] · Tuula Salo[5,6,10,11] · Pablo Conesa-Zamora[2,12]

1 Cell Culture Lab. Health Faculty, Universidad Católica de Murcia (UCAM), Campus de los Jerónimos, s/n, Guadalupe, 30107 Murcia, Spain

2 Pathology and Histology Department. Heatlh Faculty, Universidad Católica de Murcia (UCAM), Campus de los Jerónimos, s/n, Guadalupe, 30107 Murcia, Spain

3 Molecular Oncology and TGF-ß Lab, Biomedical Research Institute of Murcia (IMIB-Arrixaca), Carretera Madrid-Cartagena. El Palmar, Murcia, Spain

4 Telomerase, Cancer and Aging Group, University Clinical Hospital "Virgen de la Arrixaca", Biomedical Research Institute of Murcia (IMIB-Arrixaca) Murcia, Murcia, Spain

5 Cancer and Translational Medicine Research Unit, Faculty of Medicine, University of Oulu, Aapistie 5A, FI-90220 Oulu, Finland

6 Medical Research Center Oulu, Oulu University Hospital, University of Oulu, Oulu, Finland

7 Eurofins Villapharma Research, Parque Tecnológico de Fuente Álamo. Ctra. El Estrecho-Lobosillo, Km 2,5. Av. Azul E, 30320 Murcia, Spain

8 Department of Physical Chemistry and Institute of Biotechnology, University of Granada, Campus Fuentenueva s/n 18071 Granada, Granada, Spain

[9] Structural Bioinformatics and High Performance Computing (BIO-HPC) Research Group, Universidad Católica de Murcia (UCAM), Guadalupe, Spain

[10] Institute of Oral and Maxillofacial Disease, University of Helsinki, Helsinki, Finland

[11] HUSLAB, Department of Pathology, Helsinki University Hospital, Helsinki, Finland

[12] Clinical Analysis Department, Group of Molecular Pathology and Pharmacogenetics, Biomedical Research Institute from Murcia (IMIB), Hospital Universitario Santa Lucía, c/Mezquita sn, 30202 Cartagena, Spain

Supplementary material

Supplementary material S1. Detailed description of experimental protocols.

Supplementary material S2. Fascin1 gene expression in colorectal cell lines.mRNA expression levels of Fascin1 was quantified in eight colorectal cell lines using a β-actin gene expression for data normalizing.

Supplemental material S3. Colorectal cell line viability assay. The effect of migrastatin and compound G2 concentrations in HCT-116 and DLD-1 cell lines is shown. A-B) 24 hours; C-D) 48 hours; E-F) 72 hours incubation.

Supplementary material S4. Representative images of immunofluorescence assays for actin are shown in HCT-116 cells. A) Control condition; B) 100 µM migrastatin; C) 20 µM compound G2; D) 50 µM PD98059 (Mek inhibitor); E) 10 ng/mL Epidermal Growth Factor (EGF, migration stimulator). For actin staining, cells were fixed and stained with anti-actin antibody (1/1000). Images were captured with a LSM 510 META confocal fluorescence microscope with 63X oil objective. Actin filaments are show in red in these structures. Co-staining with Hoechst-33258 was used to show the cell nuclei. Lamellipodium are more prominent in control and EGF conditions.

Supplementary material S5. Representative images of immunofluorescence assays for fascin1 (green), nucleus (blue) and actin (red) are shown. A) Control condition (DMSO) with siRNA-A transfected HCT-116 cells; B) Control condition (DMSO) with fascin1 silenced HCT-116 cells; C) Fascin1 silenced HCT-116 cells with 10 ng/mL Epidermal Growth Factor (EGF, migration stimulator), D) Fascin1 silenced HCT-116 cells with 50 µM PD98059 (Mek inhibitor). Colorectal carcinoma HCT-116 cells were genetically knocked-down for Fascin1 with short interfering siRNA, control HCT-116 was transfected with siRNA-A (MOCK).Cells were fixed with bouin and co-stained with

anti-Fascin1 antibody (1/250) and Hoechst-33258. For actin staining, cells were fixed with methanol and stained with anti-actin antibody (1/1000). Images were captured with a LSM 510 META confocal fluorescence microscope with 63X oil objective.

Supplementary material S6. Transwell invasion assay in HCT-116 cell line. A) Invasiveness of cells after treatment in control conditions, 100 µM migrastatin and 20 µM compound G2, respectively. Pictures were taken under an inverted phase contrast microscope. The magnification was 200X and scale bars =50 µm. B) Quantification of the invasive cells D.O. by a spectrophotometer at λ=560 nm. C) Number of invasive cells using the Image J software. Data is shown as mean ± SD; compared with the control. **p<0.01.

Supplementary material S7. Inhibition of the migration and invasive capacities by compound G2 in transfected cells. A) Percentage of migration. B) Percentage of invasion. Colorectal carcinoma HCT-116 cells were genetically knocked-down for Fascin1 with short interfering siRNA, MOCK control HCT-116 was transfected with siRNA-A. Colorectal carcinoma DLD-1 cells were genetically overexpressed for Fascin1 with Fascin1-GFP vector, MOCK control DLD-1 was transfected with pGFP N3 control vector. Data are representative of two similar experiments Error bars, mean ± SD of duplicates. * p<0.05, ** p<0.01 compared to MOCK condition; n.s: non-significant.

Supplementary material S8. Myomaorganotypic invasion model in HCT-116 cell line. A) Invasion of the cells within myoma discs after treatment in A) control conditions; B) 100 µM migrastatin; C) 20 compound G2 and D) 10 µM compound G2. Pictures were taken under a phase contrast microscope with 100X magnification and 100 µm scale bars. E) Invasion area and F) Invasion depth of cytokeratin positive cells were

quantified with image J. Data is shown as mean ± SD compared with the control. ** $p<0.01$ *** $p<0.001$.

Supplementary material S9. Viability of treated zebrafish larvae in the E3 medium.A)Non injected larvae.B) Additionally, larvae (>20 per condition) were injected with HCT-116 and treatments were added to the E3 medium. C) Larvae were injected with transfected DLD-1 tumoral cell lines and treated.

Supplementary material S10. Metastasis potential. The number of colonies generated was counted at 6 dpi. A) Individual invading DLD-1 cells. B) Both groups of non-transfected and Fascin1-tranfected DLD-1 cells showed a decrease in the number of larvae with metastasis.

Supplementary material S1. Detailed description of experimental protocols

Actin bundling assay and transmission electron microscopy detection

Transmission electron microscopy was assessed, following previous methodology by Jansen et al. 2011(Jansen et al., 2011). Briefly, purified actin (21 μM) was polymerized according to the protocol from the Actin Binding Protein BiochemKit^{TM} Muscle Actin (Cytoskeleton Inc., Denver, CO, USA) and then, incubated with human recombinant Fascin1 (Hypermol, Bielefeld, Germany) (molar ratio 1:1) for 30 min at room temperature.Fascin1 was previously incubated or not for 2 hours at room temperature with 100 μMmigrastatin and 5, 10 and 20μM compound G2, respectively. The samples were directly adsorbed onto 200 mesh copper grids for 30 sec, blotted to remove excess solution, washed twice with distilled water, and negatively stained with 1% (w/v) uranyl acetate for 30sec, blotted and dried again. The TEM study of actin filaments and Fascin1-actin bundles was performed on a PHILIPS TECNAI 12 transmission electron microscope (Japan) at an accelerating voltage of 80 kV and a magnification up to 135,000X. Images were captured on a coupled device camera (Megaview III). The number of filaments per bundle were counted manually in 20 pictures/condition and statistically analyzed (Kruskal-Wallis test).

RNA extraction and quantitation

Fascin1(NM_003088.3) expression was measured aspreviously described [7]. Briefly, RNA was extracted from cells (200,000) by resuspending into 700 μL of Qiazol (Qiagen, Hilden, Germany) supplemented with 140 μL chloroform. The suspension was centrifugedat 12,000 *g* for 15 min, 4ºC. The aqueous phase containing 350 μL was then

subjected to automatic total RNA extraction using the Qiacube equipment and the miRNeasy Mini Kit, both provided by Qiagen (Hilden, Germany). cDNA was obtained using the Maxima First Strand cDNA Synthesis Kit for RT-qPCR by (Thermo FisherScientific, Waltham, MA, USA) following the manufacturer instructions. Five microlitres of 1:5 diluted cDNA was added to the qPCR reaction containing 12.5 µL 2X QuantiTect SYBR Green PCR Kit (Qiagen, Hilden, Germany) and 300 nM of each primer in a total volume of 25 µL qPCR was performed on a 7500F real time PCR system (Applied Biosystems, Foster City, CA, USA) according to the user instruction manual and following the standard protocol: 50ºC 2 min, 95ºC 10 min, 40 cycles of 95ºC 15 sec, 60ºC 1 min and a melt curve stage consisting in 95ºC 15 sec, 60ºC min, 95ºC 30 sec and 60ºC 30 sec. The relative quantitation of Fascin1 was obtained by the $2^{-\Delta Ct}$ method using β-actin as housekeeping gene. The primers for β-actin (β-actinF: GAGCTACGAGCTGCCTGACG, β-actinR: GTAGTTTCGTGGATGCCACAG) and Fascin1 quantitation (FSCN1 115F: TCCACGCGCCAGGGTATGGAC,FSCN1 116R: ACTTGCCCGTGTGGGTACGG) were provided by Merck (Madrid, Spain).

Transfection assay

The human colorectal carcinoma cells were genetically overexpressed (DLD-1) and knocked-down (HCT-116) for Fascin1. In the case of DLD-1, pGFP-N3 control vector or Fascin1-GFP vector (kindly provided by Dr. Milind Valdya from the Advanced Centre for Treatment Research and Education in Cancer, Maharashtra, India) was used. HCT-116 cells were transfected with Fascin1 short interfering siRNA or control siRNA-A (Santa Cruz Biotechnology, Heidelberg, Germany). The cells were seeded in 6-well plate and grown to 50-70% confluence. Transfections were performed using lipofectamine 2000 (Thermofisher, Waltham, MA, USA) according to the manufacturer's protocols. The cells were then washed with PBS before adding 800 µL

standard medium without antibiotics. The final amount of nucleic acids used for transfection was 1 µg and 0.05µmolesper well for DLD-1 and HCT-116 cells, respectively. The nucleic acids were diluted with OptiMEM I Reduced Serum Medium (Invitrogen, Carlsbad, CA, USA). Equal volume of OptiMEM I medium (100 µL) was used to dilute lipofectamine 2000 and nucleic acids, and then incubated for 5 min at room temperature. Mixture was added drop by drop to the lipofectamine-based liposome dilution and incubated at room temperature for additional 30 min. After incubation, the nucleic acids/liposome complexes were added to the cells and incubated for additional 6 hours. After transfection, the residual nucleic acids/liposome complexes were washed off and the cells were replenished with standard medium and incubated up to 72 hours.

Immunofluorescence

Round coverslips (ThermoFisher, Waltham, MA USA) were seeded in 6-well plate with HCT-116 and spontaneously immortalized human keratinocyte cells (HaCaT)(Boukamp et al., 1988) in standard medium. When cells reached 100% confluence, standard medium was discarded and replaced with standard fresh serum free medium for 24 hours. Artificial wounding was performed by transversally dragging a sterilized razor blade on the central area of the coverslips. Briefly, cancer tumor cells were treated with either 100 µM migrastatin, 20 µM compound G2, 10 ng/mL Epidermal Growth Factor (EGF) or50 µM of MEK inhibitor PD98059 (MEKi) (both from Sigma-Aldrich, St Louis, MO, USA) for 24 hours. Cells were then fixed with Bouin solution (5% Acetic acid, 9% Formaldehyde and 0.9% Picric acid, all from Sigma-Aldrich, St Louis, MO, USA) (for Fascin1 protein staining) or 4% formaldehyde DPBS (PanReac AppliChem, Barcelona, Spain) (for Actin protein staining) 15 min and washed 3 times with DPBS subsequently permeabilized in a 0.3% Triton X-100/DPBS solution, and then incubated

in blocking solution [(0.3% Bovine Serum Albumin (BSA) (Santa Cruz Biotechnology, Heidelberg, Germany), 10% FBS (Thermo Fisher Scientific, Waltham, MA, USA), 0.1% Triton X-100 (Sigma-Aldrich, St Louis, MO, USA) and 5% skimmed milk (Beckton Dickinson, Franklin Lakes, NJ, USA) in DPBS for 30 min. Then, samples were incubated for 1 hour with either anti-Fascin1 antibody (1/250) (55K-2 clone; Santa Cruz Biotechnology, Heidelberg, Germany). Samples were washed 3 times with 0.1% Triton X-100/DPBS and incubated with the appropriate fluorescent-labelled secondary antibodies; for Fascin1 Alexa fluor 488-conjugated anti-mouse IgG (Molecular Probes, Thermo Fisher Scientific, Waltham, MA USA) was used. To reveal actin, samples were incubated with Alexa fluor 594-labelled phalloidin(Molecular Probes, Thermo Fisher Scientific, Waltham, MA USA) and Hoechst 33258 (Fluka, Biochemika, Sigma-Aldrich, St Louis, MO, USA) for 30 min in a wet chamberat room temperature, in order to reveal actin and nuclei, respectively. All preparations were examined with a confocal microscope (LSM 510 META from ZEISS, Jena, Germany) and representative images were taken. Quantification of lamellipodes was performed by counting elements in 10 pictures per sample.

REFERENCES:

Boukamp, P., Petrussevska, R. T., Breitkreutz, D., Hornung, J., Markham, A., & Fusenig, N. E. (1988). Normal keratinization in a spontaneously immortalized aneuploid human keratinocyte cell line. *J Cell Biol, 106*(3), 761-771. doi:10.1083/jcb.106.3.761

Jansen, S., Collins, A., Yang, C., Rebowski, G., Svitkina, T., & Dominguez, R. (2011). Mechanism of actin filament bundling by fascin. *J Biol Chem, 286*(34), 30087-30096. doi:10.1074/jbc.M111.251439

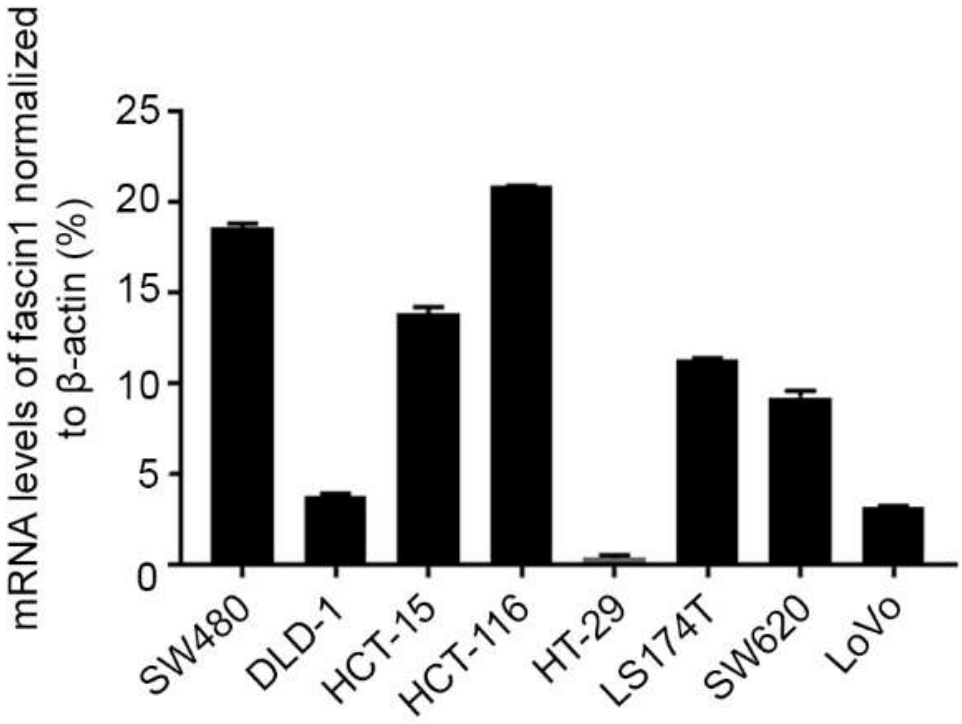

Supplemental material S2

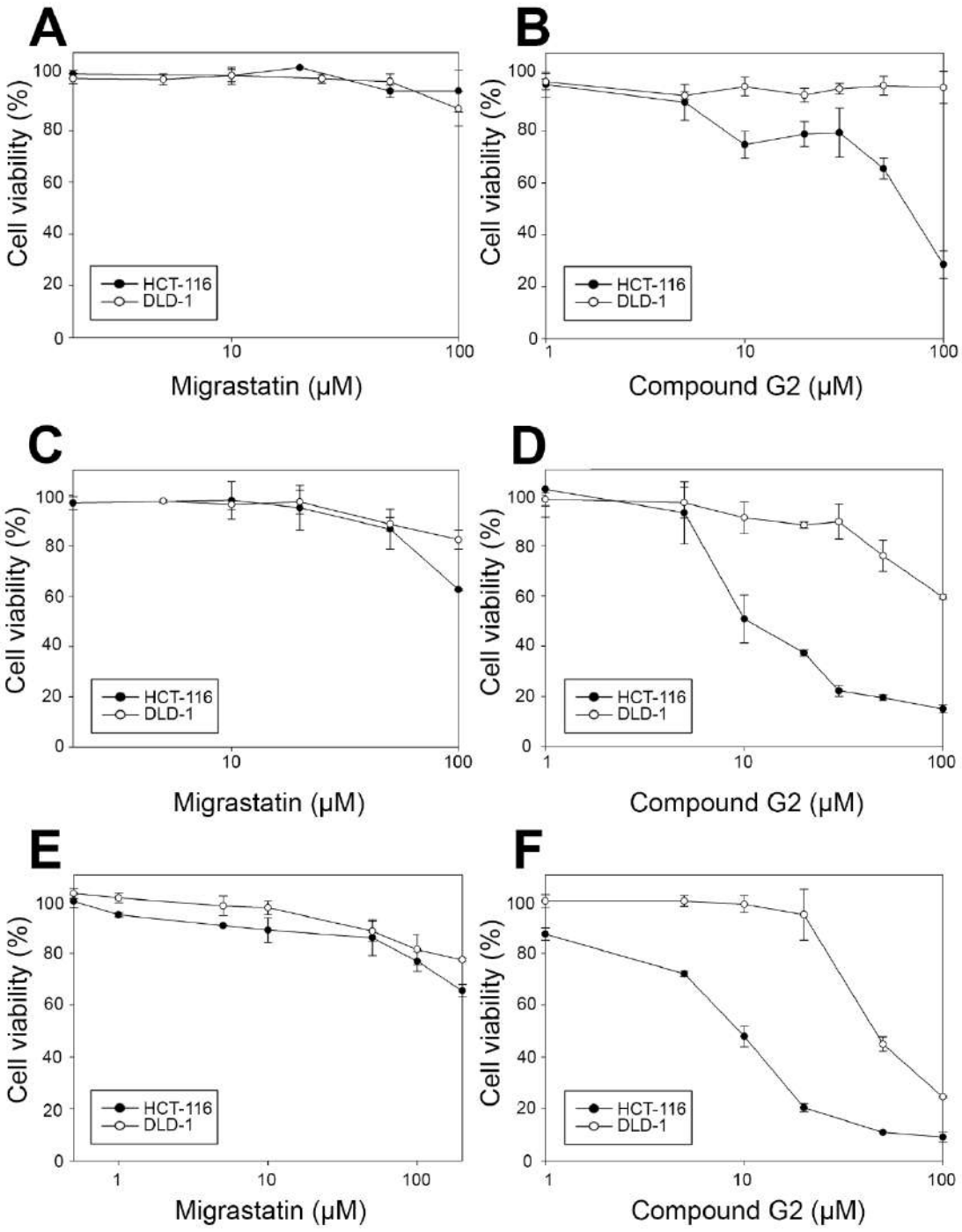

Supplemental material S3

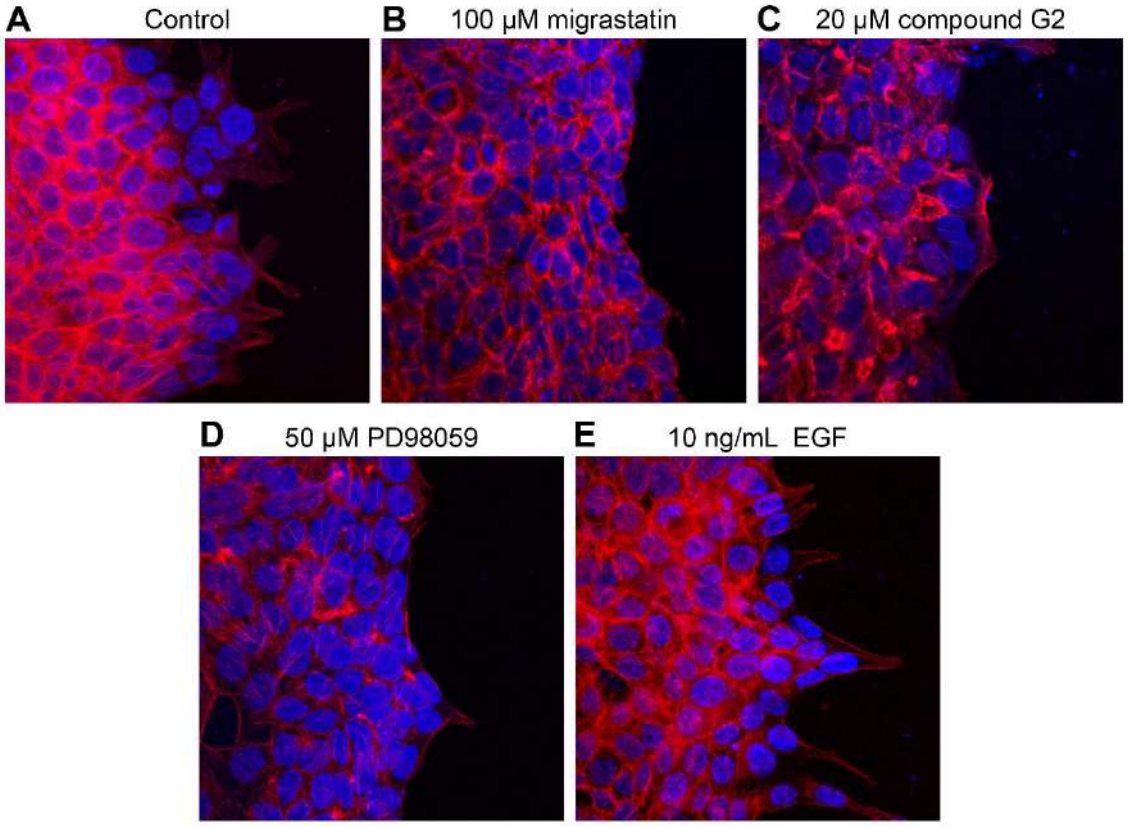

Supplemental S4

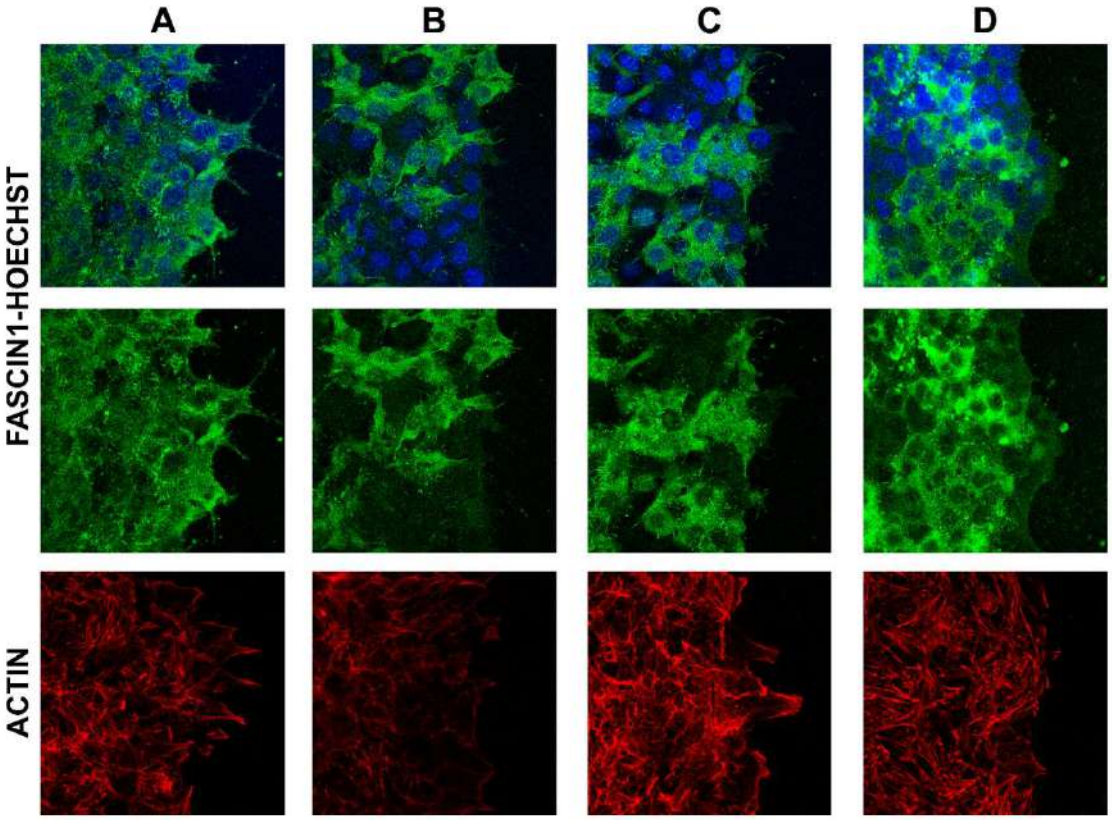

Supplemental S5

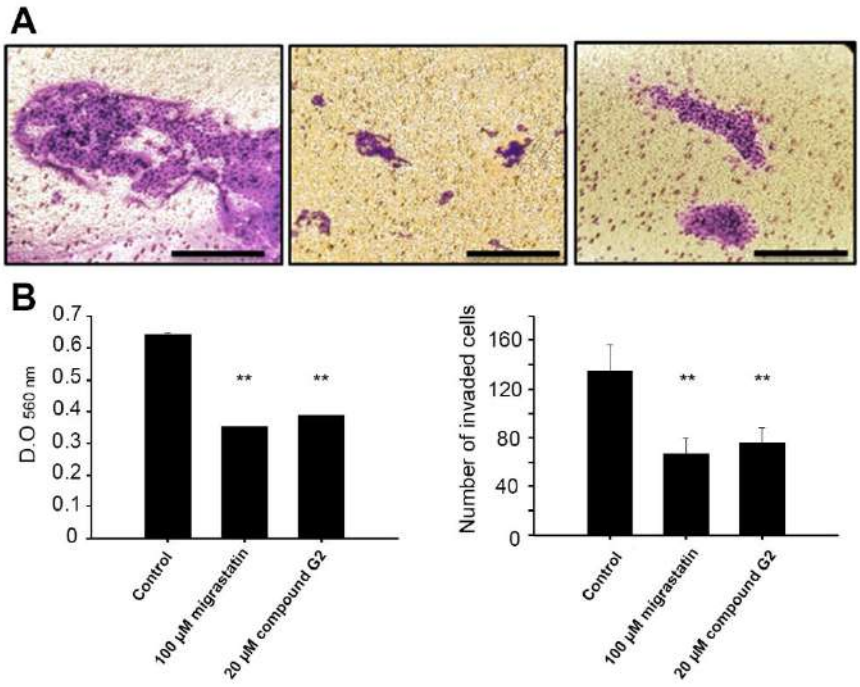

Supplemental S6

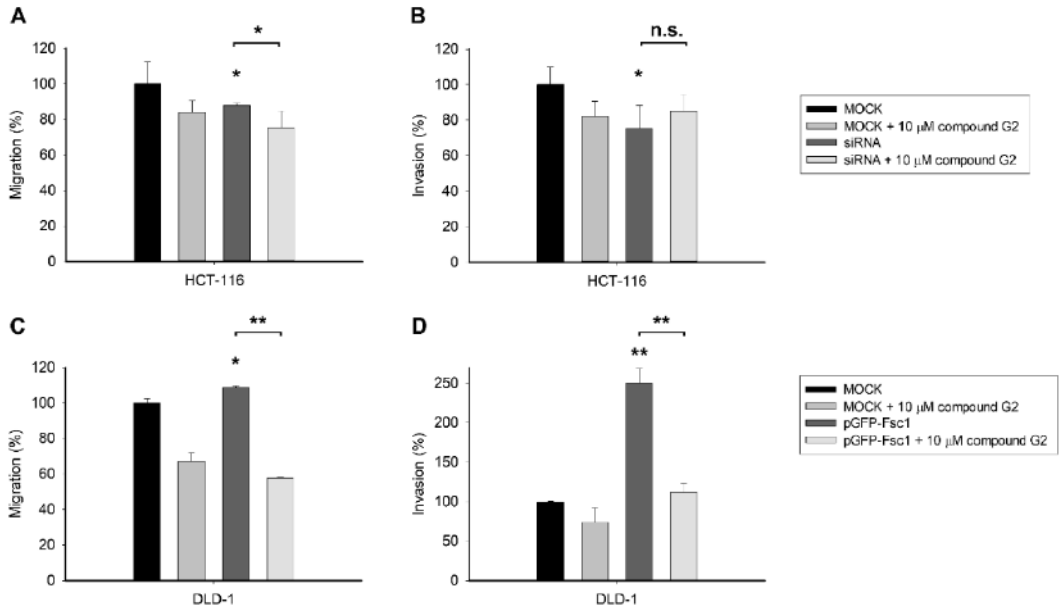

Supplemental S7

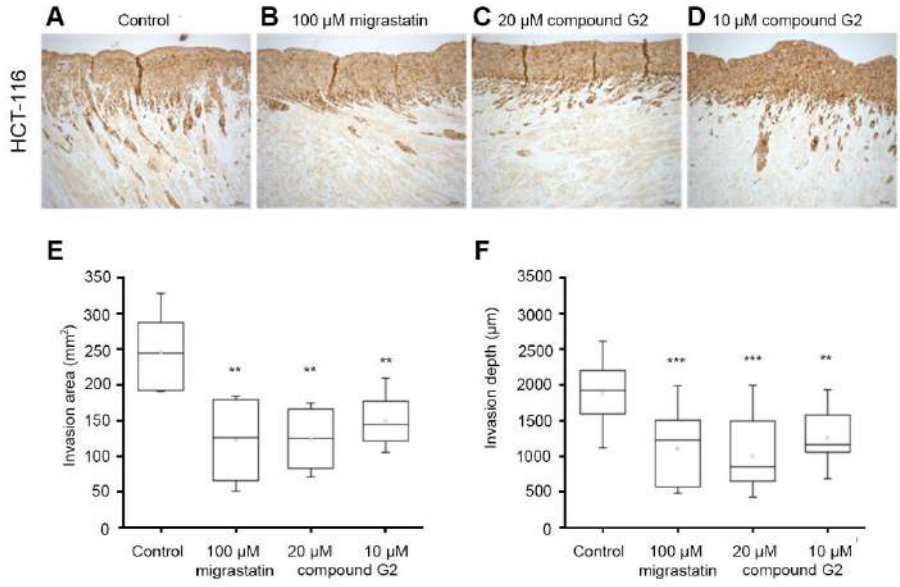

Supplemental S8

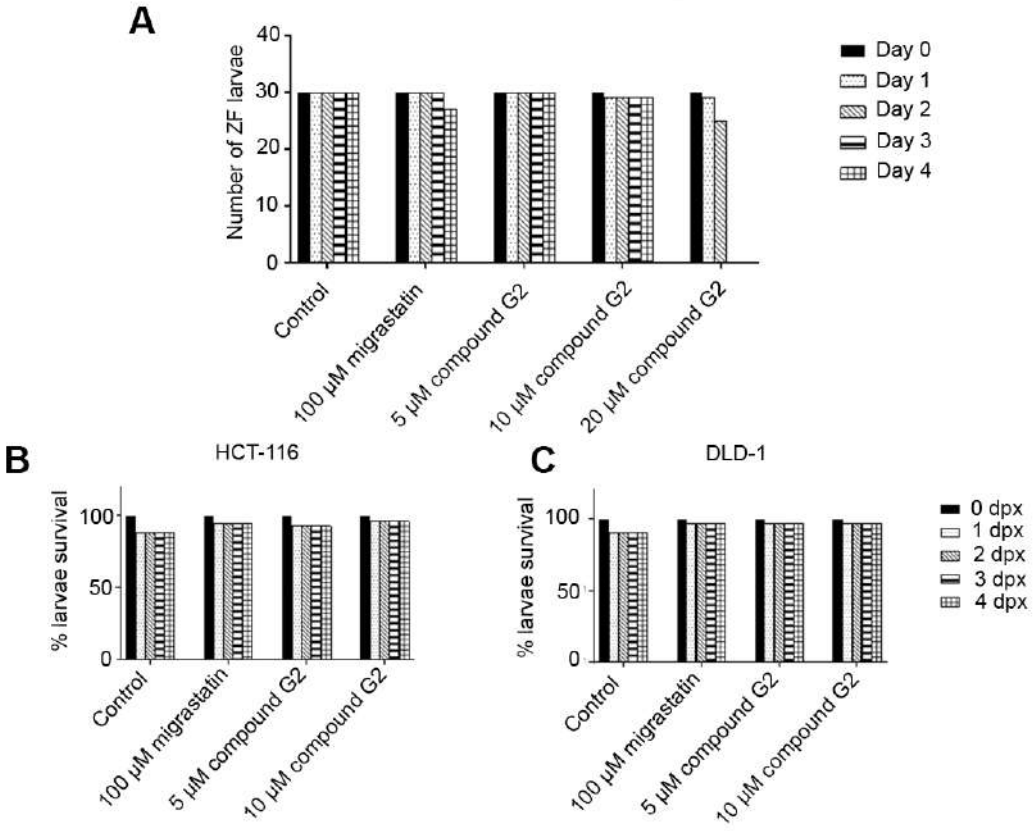

Supplemental S9

Supplemental S8

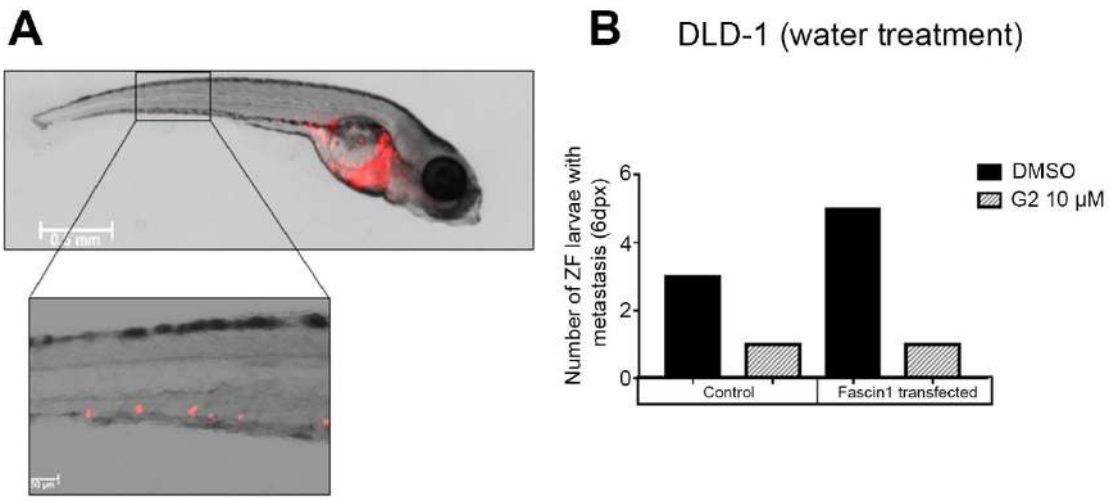

Supplemental S10

ARTÍCULO 3:

Alburquerque-González, B., Bernabé-García, M., Montoro-García, S., Bernabé-García, Á., Rodrigues, P. C., Ruiz Sanz, J., López-Calderón, F. F., Luque, I., Nicolas, F. J., Cayuela, M. L., Salo, T., Pérez-Sánchez, H., & Conesa-Zamora, P. (2020). **New role of the antidepressant imipramine as a Fascin1 inhibitor in colorectal cancer cells.** *Experimental & molecular medicine*, *52*(2), 281–292. https://doi.org/10.1038/s12276-020-0389-x.

Factor de impacto 2020 (JCR): 8.718; Categoría (JCR): MEDICINE RESEARCH & EXPERIMENTAL SCIENCE; Clasificación: 34/295 (Q1); Fecha de publicación:2020.

Alburquerque-González et al. *Experimental & Molecular Medicine*
https://doi.org/10.1038/s12276-020-0389-x

Experimental & Molecular Medicine

ARTICLE Open Access

New role of the antidepressant imipramine as a Fascin1 inhibitor in colorectal cancer cells

Begoña Alburquerque-González[1], Manuel Bernabé-García[2], Silvia Montoro-García[3], Ángel Bernabé-García[4], Priscila Campioni Rodrigues[5,6], Javier Ruiz Sanz[7], Fernando F. López-Calderón[1], Irene Luque[7], Francisco José Nicolas[3], María Luisa Cayuela[4], Tuula Salo[5,6,8,9], Horacio Pérez-Sánchez[10] and Pablo Conesa-Zamora[1,11,12]

Abstract

Serrated adenocarcinoma (SAC) is more invasive, has worse outcomes than conventional colorectal carcinoma (CRC), and is characterized by frequent resistance to anti-epidermal growth factor receptor (EGFR) and overexpression of fascin1, a key protein in actin bundling that plays a causative role in tumor invasion and is overexpressed in different cancer types with poor prognosis. In silico screening of 9591 compounds, including 2037 approved by the Food and Drug Administration (FDA), was performed, and selected compounds were analyzed for their fascin1 binding affinity by differential scanning fluorescence. The results were compared with migrastatin as a typical fascin1 inhibitor. In silico screening and differential scanning fluorescence yielded the FDA-approved antidepressant imipramine as the most evident potential fascin1 blocker. Biophysical and different in vitro actin-bundling assays confirm this activity. Subsequent assays investigating lamellipodia formation and migration and invasion of colorectal cancer cells in vitro using 3D human tissue demonstrated anti-fascin1 and anti-invasive activities of imipramine. Furthermore, expression profiling suggests the activity of imipramine on the actin cytoskeleton. Moreover, in vivo studies using a zebrafish invasion model showed that imipramine is tolerated, its anti-invasive and antimetastatic activities are dose-dependent, and it is associated with both constitutive and induced fascin1 expression. This is the first study that demonstrates an antitumoral role of imipramine as a fascin1 inhibitor and constitutes a foundation for a molecular targeted therapy for SAC and other fascin1-overexpressing tumors.

Introduction

Tumor metastasis is the leading cause of cancer-related deaths[1]. Cell migration and invasion are fundamental features of metastatic cancer cells and involve actin cytoskeleton rearrangement, leading to the formation of protrusive structures, such as filopodia, lamellipodia, and invadopodia, that contribute to cancer cell motility[2].

Fascin1 is an actin filament (F-actin) bundling protein that plays an important role in the formation of protrusive structures and is poorly expressed or absent in most normal epithelia but upregulated in many human carcinomas, with a crucial role in tumor progression, invasion, and metastasis[3,4]. Numerous studies have implicated fascin1 as a potential therapeutic target and biomarker for aggressive carcinomas[4,5]. Recently, our group identified fascin1 as overexpressed in serrated adenocarcinoma (SAC), a WHO-recognized histological subtype of colorectal carcinoma (CRC), which is characterized by worse prognosis[6] and a more active invasive front as evidenced by a higher occurrence of tumor budding[7], E-cadherin loss, and more frequent KRAS or BRAF mutations compared with conventional CRC[8–10]. Migrastatin and its macroketone analogs have been found to efficiently

Correspondence: Horacio Pérez-Sánchez (hperez@ucam.edu) or Pablo Conesa-Zamora (pablo.conesa@carm.es)
[1]Pathology and Histology Department, Facultad de Ciencias de la Salud, UCAM Universidad Católica San Antonio de Murcia, Campus de los Jerónimos, s/n, 30107 Guadalupe, Murcia, Spain
[2]Research group "Telomerasa, Envejecimiento y Cáncer," CIBERehd, Hospital Clínico Universitario Virgen de la Arrixaca, IMIB-Arrixaca, Murcia, Spain
Full list of author information is available at the end of the article.
These authors contributed equally: Begoña Alburquerque-González, Manuel Bernabé-García

inhibit fascin1, thus decreasing metastatic tumor cell migration, invasion, and further metastasis[1]. However, the complex structure of the macroketone hinders its synthesis, and other anti-fascin1 compounds derived from indazol-furan-carboxamides have been tested[11]. To identify novel molecules targeting fascin1 as potential anti-SAC drugs, we performed an in silico compound library screening and subsequent in vitro and in vivo assays to characterize the anti-fascin1, antimigratory, and anti-invasive potential of the selected compounds.

Materials and methods

In silico screening

In silico screening[12] was applied to propose compounds that might have better fascin1 inhibitory properties than migrastatin. Pharmacophore modeling using LigandScout[13,14] was employed to the core of the structure of migrastatin (MGS_CORE) so that a ligand-based pharmacophore model[15] was derived. This model was screened against a subset of the DrugBank library (version 5.0; of 9591 compounds, including 2037 approved by the American FDA, 96 nutraceuticals, and 6000 experimental) after fine-tuning on a high-performance computing (HPC) cluster of all related necessary programs from the LS suite.

Thermofluor and fluorescence titration

Differential scanning fluorimetry (Thermofluor) and titration assays were performed as described in Supplementary Information S1. Briefly, the thermal denaturation profiles of fascin1 (cat. no. 8411-02, Hypermol, Bielefeld, Germany) were obtained by recording the fluorescence intensity for the FAM, HEX, and T-Red predefined filters. T_m values were measured as the minimum of the first derivative of the thermal unfolding profile. Changes in T_m associated with ligand binding were estimated, taking the average T_m value derived from the free protein internal controls. Drugs were provided by MolPort, Latvia (migrastatin, AnalytiCon Discovery, cat. no. NP-006108, and imipramine, Biotrend Chemicals, BG0219).

F-actin bundling assay

The actin-bundling activity in the presence of drugs was measured by a low-speed centrifugation assay using the Actin Binding Protein Biochem Kit™ Muscle Actin (Cytoskeleton, Inc., cat. no. BK001) and following the manufacturer's manual. Additional information is provided as Supplementary Information S1.

Transmission electron microscopy

Transmission electron microscopy (TEM) was assessed following the methodology of a previous paper[16]. Protocol details are provided as Supplementary Information S1.

Cell culture

A total of eight human colorectal adenocarcinoma cell lines—SW-480 (CLS Cat# 300302/p716_SW-480, RRID: CVCL_0546), DLD-1 (CLS Cat# 300220/p23208_DLD-1, RRID: CVCL_0248), HCT-15 (CLS Cat# 300229/p23303_HCT-15.html, RRID: CVCL_0292), HCT-116 (CLS Cat# 300195/p19841_HCT116.html, RRID: CVCL_0291), HT-29 (NCI-DTP Cat# HT-29, RRID: CVCL_0320), LS174T (CLS Cat# 300392/p720_LS-174T, RRID: CVCL_1384), SW-620 SW620 (NCI-DTP Cat# SW-620, RRID: CVCL_0547) and LoVo (NCI-DTP Cat# LOVO, RRID: CVCL_0399)—were obtained from the American Type Culture Collection (ATCC, Rockville, Maryland). The cell lines were cultivated at 37 °C in high-glucose Dulbecco's modified Eagle's medium (DMEM) containing 10% heat-inactivated fetal bovine serum (FBS), 50 U/mL penicillin, and 50 µg/mL streptomycin (Sigma-Aldrich Chemical Co., USA) in an atmosphere of 5% CO_2 and 95% humidified air. Subculture was performed when 90% confluence was reached. Human cell line identification by short tandem repeat profile testing, according to the American National Standards Institute, has shown an appropriate match for HCT-116 and DLD-1 cell lines.

Quantification PCR for fascin1 mRNA expression

Fascin1 gene expression was measured following the protocol previously described[2]. The relative quantitation was obtained by the 2-ΔCt method using β-actin as the housekeeping gene. The amounts of mRNA are given as the number of copies per million copies of β-actin. Primers for β-actin used for FSCN quantitation are shown in Supplementary Information S1.

Cell viability assay

Exponentially growing cells were plated in triplicate in flat-bottomed 96-well plates (Nunc, Roskilde, Denmark) at 1500 cells/well. On the day after plating, drugs were added in serial dilutions from 500 nm to 300 µM. Control wells contained medium without drug plus 0.1% dimethyl sulfoxide (DMSO) (drug carrier). The plates were incubated for 3 days in a humidified 5% CO_2 incubator and assayed for cell viability. Tetrazolium, dissolved in phosphate-buffered saline, pH 7.2, at 1.9 mg/mL was added to the cells (30 µL/well). Additional information is provided as Supplementary Information S1.

RNA labeling, microarray hybridization, and functional enrichment analysis

To obtain a general overview of enriched functions associated with the treatment of colorectal cancer tumor cells, HCT-116 cells were treated with DMSO or imipramine. Detailed information is included in Supplementary Information S1. Datasets are deposited in the Gene Expression Omnibus database under accession number GSE125169.

Immunofluorescence

For the immunofluorescence assays, round coverslips (Thermo Fisher, Waltham, Massachusetts) were seeded with HCT-116 cells in the presence of 10% FBS. Artificial wounding was performed by transversally dragging a sterilized razor blade on the central area of the coverslips. Briefly, cancer cells were treated with 100 μM migrastatin, 20 μM imipramine, 10 ng/mL epidermal growth factor (EGF), or 50 μM MEK inhibitor PD98059 (MEKi) (both from Sigma-Aldrich, St. Louis, Missouri, USA) for 24 h. Additional information is shown as Supplementary Information S1.

Cell migration assay

Cell migration was executed with SW-480, DLD-1, and HCT-116 cell lines by performing the wound-healing assay in the presence of 10% FBS. Colorectal cancer cells (50,000 cells) were plated in low 35-mm dishes with culture inserts (Ibidi, Martinsried, Germany). After appropriate cell attachment and monolayer formation (approximately 24 h), inserts were then removed with sterile forceps to create a wound field of approximately 500 μm, according to the manufacturer's protocol. Additional information is shown in Supplementary Information S1.

Transwell invasion assay

The invasive capacities of HCT-116 cells were determined using a Cell Biolabs Cytoselect™ 24 Well Cell Invasion Assay Kit (Basement Membrane Colorimetric Format, Cat: CBA-110, Cell Biolabs, CliniScience, Barcelona, Spain) with coated transwell chambers (8 μm pore size) following the instruction manual. Cells were resuspended in serum-free medium and treated under the corresponding conditions (0.1% DMSO, 100 μM migrastatin, and 20 μM imipramine). Additional information is shown in Supplementary Information S1.

Myoma organotypic invasion model

Cancer cell invasion was assessed in the myoma organotypic cultures and performed according to the previously published myoma model protocol[17,18]. Briefly, uterine leiomyoma tissues were obtained from routine surgery after informed consent of the donors. Myoma (8 mm disks) were preincubated with migrastatin (100 μM), imipramine (10 μM and 20 μM), or 0.1% DMSO-DMEM treatments at 4 °C for 48 h and placed into transwell inserts (6.5 mm diameter; Corning Incorporated, Corning, New York), and 700,000 cells were added on top of each myoma disk. The cells were allowed to attach overnight on the myoma disks, transferred onto uncoated nylon disks, and treated with the compounds for 14 days. After fixation, 6-μm sections were cut and stained with cytokeratin AE1/AE3 (M3515, Dako). ImageJ v1.46o was used to measure invasion areas and depths. Each treatment was performed in triplicate. Additional information is shown in Supplementary Information S1.

Transfection assay

The day before transfection, DLD-1 cells were seeded in six-well plates and then cultured overnight. The transfection efficiency of lipofectamine 2000-based liposomes was determined using the GFP reporter gene. The pGFP-N3 control vector (MOCK) and fascin1-GFP vector were kindly provided by Dr. Milind Vaidya from the Advanced Centre for Treatment Research and Education in Cancer (Maharashtra, India). The final amount of DNA plasmids was 1 μg/well. Details regarding this experiment are provided as Supplementary Information S1.

Zebrafish invasion and metastasis assays

The colonization of zebrafish (*Danio rerio*) embryos by human cancer cells was performed as previously described[19]. Trypsinized, washed colorectal cancer cells were stained with fluorescent CM-Dil (Vybrant, Invitrogen), and 50–100 labeled cells were injected into the yolk sac of dechorionated zebrafish embryos. The viability of zebrafish embryos was assessed under 100 μM migrastatin or imipramine (5, 10, and 20 μM) treatments and under the combined effect of compound treatment and tumor cell injection. The evaluation criterion for embryos being colonized by human cancer cells was the presence of more than three cells outside the yolk sac. The metastasis assay was based on previous works by Fior et al.[20], and a metastatic potential assay on zebrafish was performed. Transfected DLD-1-overexpressing fascin1 and native HCT-116 cells were stained and xenografted as already mentioned. From the third day post injection, larvae were fed with ZEBRAFEED by Sparos (<100 μm) and treated with imipramine daily. At day 6 post injection, larvae were examined for monitoring of tumor growth and invasion using a fluorescence microscope. The evaluation for metastasis potential by human cancer cells was the presence of cell colonies (dividing cells) outside the yolk sac. Fishes with fluorescently labeled cells appearing outside the implantation area at 2 h post injection were excluded from further analysis. All the fish were incubated at 35 °C and analyzed with a SteReo Lumar V12 stereomicroscope equipped with an AxioCam MR5 camera (Carl Zeiss). The percentage of invasion and the presence of cell colonies were calculated by the researcher (M.B.-G.) without previous knowledge of the experimental treatment conditions. The experiments were completed in triplicate, obtaining an average value at 4 days post xenograft (invasion assay) and 6 days post xenograft (metastasis assay).

Chemical treatment

The effect of treatments on the zebrafish invasion model was tested in two ways: one treating cancer cells before injection in the larvae, and the other treating the larvae with the drugs once injected with tumor cells. Additional information is shown in Supplementary Information S1.

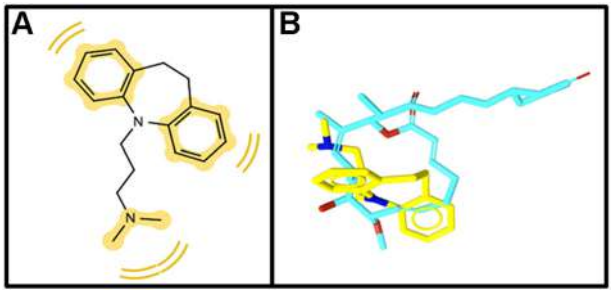

Fig. 1 Results obtained after ligand-based pharmacophore screening with LigandScout. a 2D diagram of matching hydrophobic pharmacophoric features between (yellow spheres) migrastatin and imipramine. **b** 3D alignment of migrastatin (blue skeleton) and imipramine (yellow skeleton).

Statistics

Data are expressed as the mean ± standard deviation (SD). The data were analyzed for significant differences by Student's *t* test for paired and unpaired data after testing for normal distribution of the data. For in vitro experiments, one-way analysis of variance (ANOVA) was performed, followed by a Tukey post hoc test to compare each group. Differences were considered significant at an error probability of $p < 0.05$. SPSS 18.0 software was used for the rest of the statistical analyses (SPSS, Inc., Chicago, Illinois, USA).

Ethics statement

For the myoma organotypic invasion model, uterine leiomyoma tissues were obtained from routine surgery after informed consent of the donors and their use approved by the Ethics Committee of the Oulu University Hospital, Oulu, Finland, in accordance with the ethical standards laid down in the 1964 Declaration of Helsinki and later amendments. The studies on zebrafish were approved by the Bioethical Committee of the University Hospital Virgen de la Arrixaca, Murcia, Spain.

Results

In silico screening identifies imipramine as a plausible ligand for fascin1

In silico screening calculations and careful visual inspection of the results[1,21] detected imipramine as one of the top 31 candidates for posterior experimental validation. The pharmacophore model derived for imipramine is depicted in Fig. 1.

Thermofluor and fluorescence titration experiments validate imipramine binding to fascin1 in vitro

The binding capacity of the distinct compounds to fascin1 was tested using differential scanning fluorimetry. As shown in Supplementary Information S2, at pH 7.4, fascin1 unfolds in a single transition, showing no concentration dependency (panel A) and good tolerance to DMSO (panel B). Average T_m values for unbound fascin1 were obtained for each internal filter (FAM, HEX, and T-Red) as reference for the determination of the changes in T_m upon compound binding ($T_{m,FAM} = 55.6 \pm 0.5$ °C, $T_{m,HEX} = 56.0 \pm 0.0$ °C, $T_{m,Tred} = 56.2 \pm 0.6$ °C, where the error values correspond to the SD for the seven replicas included in each plate as internal controls). The results of the thermal shift assay with the top 31 compounds are summarized in Supplementary Information S1 (Table S1) and shown in Fig. 2a. Some compounds resulted in distorted thermal unfolding profiles from which reliable T_m values could not be extracted, probably due to compound interference with the SYPRO fluorescence signal. Within those that could be analyzed, imipramine resulted in the highest significant increase in T_m of approximately 2 °C, suggesting specific binding to fascin1 (Fig. 2a, arrow). The binding of imipramine to fascin1 was further validated in vitro using fluorescence titration experiments, rendering a dissociation constant of 390 μM (Fig. 2b).

Imipramine significantly decreases the fascin1-induced bundles

In the absence of fascin1, although the bundles of F-actin polymers are present in the pellets, the majority of F-actin was observed in the supernatant fraction. As shown in Fig. 3, purified fascin1 increased the amount of F-actin localized in the pellets. However, upon imipramine addition, the F-actin pellet fraction significantly diminished in favor of the supernatant. Taken together, these results indicate that imipramine partially interferes with fascin1 in bundling F-actin polymers.

Electron microscopy confirms imipramine-driven alteration of actin bundling

Transmission electron microscopy showed that only polymerized F-actin incubated in the presence of fascin1 was able to form filament bundles (9.00 [8.00–9.75]) (Fig. 4). Fascin1 preincubated with 100 μM migrastatin or 10 μM imipramine led to the disorganization of the bundles, resulting in fewer filaments than in control conditions (Kruskal–Wallis test, $p < 0.001$). No significant differences were found between the distinct treatments (Mann–Whitney test, $p = 0.370$).

The expression of fascin1 mRNA varies among different colorectal cell lines

To choose colorectal cell lines with the highest and lowest endogenous fascin1 expression, RT-qPCR was performed on RNA extracted from the eight colorectal cancer cell lines. Supplementary Information S3 illustrates how

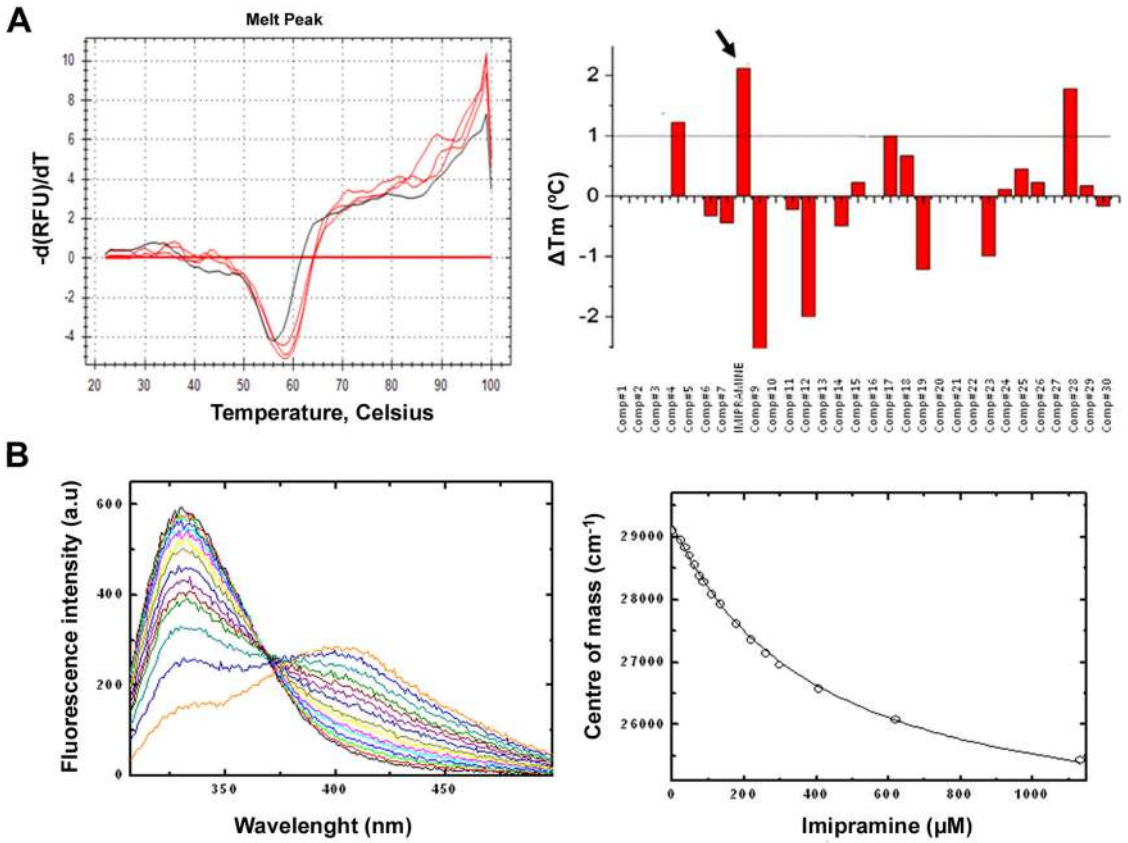

Fig. 2 In vitro validation of imipramine binding to fascin1. a Differential scanning fluorimetry assays. The right panel shows the first derivative of the thermal denaturation profiles of fascin1 in the absence (black) and in the presence of 1 mM imipramine (red in triplicate). The left panel summarizes the changes in T_m induced by the presence of the selected compounds at 1 mM in 10% DMSO. **b** Fluorescence titration. The right panel shows the fluorescence emission spectra of fascin1 in the presence of increasing concentrations of imipramine. The left panel shows the binding isotherm. White circles represent the center of mass of the different spectra, and the continuous lines symbolize the best fit of the data to a one-site binding model.

HCT-116 and SW-480 cells show the highest fascin1 expression, while LoVo, DLD-1, and HT-29 cells show the lowest expression. Given the ease of cell culture and the suitable morphology with prominent cytoplasm for immunofluorescence, migration, and invasion assessment, DLD-1, SW-480, and HCT-116 cell lines were selected for subsequent in vitro assays.

High imipramine concentrations compromise cancer cell viability

Compounds might be toxic to cancer cells, and the effects observed could be a consequence of a general effect of cell functionality and not a specific drug effect. For this purpose, a viability assay on DLD-1, HCT-116, and SW-480 cells was performed to set up the working concentration of the drugs. According to data presented as Supplementary Information S4, HCT-116 was more sensitive than DLD-1 and SW-480, and the working concentrations were set up for subsequent in vitro studies at 10 and 20 μM imipramine and 100 μM migrastatin.

Identification of imipramine-associated enriched functions

To determine which general functions are affected upon imipramine treatment, expression profiling of imipramine-treated HCT-116 colorectal cancer cells from a migration assay was undertaken. Functional enrichment analysis revealed a large number of differentially expressed genes compared with the control treatment (DMSO), among which we selected the top 2000 genes. The Panther Classification System Program was used, and as shown in Supplementary Information S5, 18 Gene Ontology molecular functions were related to these genes. Interestingly, actin binding (GO: 0003779), cytoskeletal protein binding (GO: 0008092), and structural constituent of cytoskeleton (GO: 0005200) were among these 18 functions.

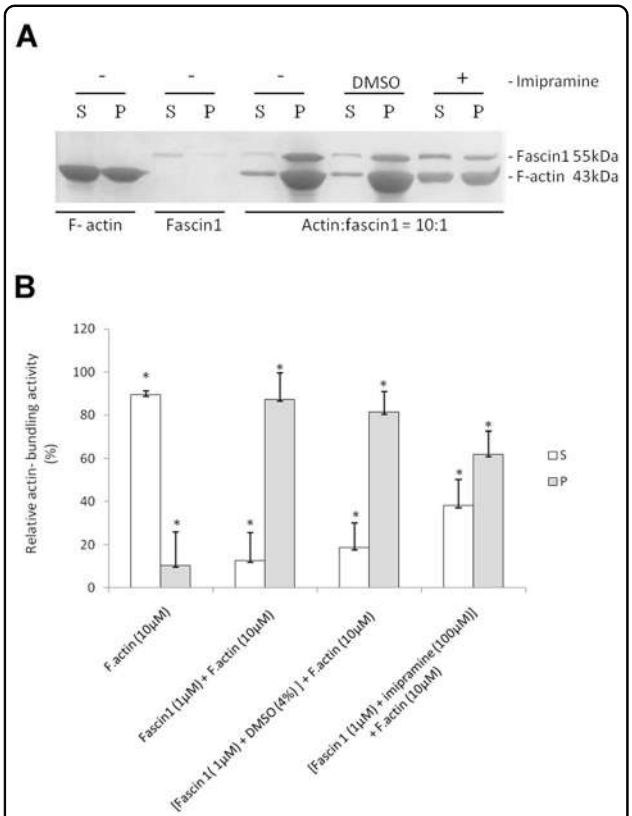

Fig. 3 F-actin bundling activity assay. a Assay of actin-bundling activity with a low-speed cosedimentation assay. Polymerized F-actin (10 μM) was incubated with fascin1 (1 μM) in the presence (+) or absence (−) of imipramine and DMSO (control). **b** Quantification of the F-actin bundling assay from (**a**). The results are the means and SD ($n = 4$, $^*p < 0.01$).

Imipramine affects fascin1 localization and lamellipodium formation

The effect of imipramine on fascin1 localization and actin reorganization, including lamellipodium formation, was assessed by immunofluorescence. Figure 5 shows the fascin1 localization (green) in two cell lines, the cell line expressing higher fascin1 level, HCT-116, and a nontumoral cell line derived from keratinocyte cells, HaCaT, which was used for illustrative purposes because of its ample cytoplasm. A prominent filopodia and lamellipodium formation associated with fascin1 localization was observed in control conditions and EGF-treated cells, whereas these cytoskeleton structures were absent in those cells treated with migrastatin or imipramine to a similar extent to what was observed with the migration inhibitor targeting the MEK pathway (PD98059). The lamellipodia protrusion number was calculated in HCT-116 cells in a quantitative manner under the different conditions, and this number was significantly lower after migrastatin and imipramine treatments (Supplementary Information S2). Taken together, these results identify an effect of imipramine in diminishing invasive actin cytoskeleton structures and fascin1 localization in such structures.

Imipramine diminishes the migration of colorectal cancer cells

To explore whether the observed effect of fascin1 inhibitors on lamellipodium protrusion has a reflexive effect on basal cell migration, migrastatin- and imipramine-treated cells were investigated for their migration activity within the linear growth phase (4−7 h after in vitro scratch). As shown in Supplementary Information S6, imipramine produces a remarkable inhibition of migration in all assayed cell lines ($p < 0.05$). Except for SW-480, the imipramine effect was more pronounced than migrastatin, especially for DLD-1. Table S3 shows the quantitative reduction in migration-associated migrastatin and imipramine treatment in DLD-1, SW-480, and HCT-116 colorectal cancer cell lines (Supplementary Information S1). To correlate fascin1 expression with a quantifiable effect on cell migration, fascin1 expression was then silenced in HCT-116 cells and overexpressed in DLD-1 cells (Supplementary Information S1 and S7). Fascin1-silenced HCT-116 cells led to a slight decrease in migration compared with MOCK HCT-116 cells, while double inhibition (epigenetic and pharmacological) produced a significant decrease in migration. Transfected DLD-1 cells overexpressing fascin1 showed a 15% higher migration activity, which was counteracted in the presence of 10 μM imipramine.

Imipramine inhibits cell invasion through Matrigel

In addition to migration, tumoral cell invasion involves the acquisition of the ability to degrade the extracellular matrix (ECM). For this purpose, a transwell assay was performed on Matrigel, which resembles the ECM composition. As shown in Supplementary Information S8, both migrastatin and imipramine inhibited tumor cell invasion of HCT-116 cells. Similar to the in vitro migration test, the effect of imipramine was slightly more evident than that of migrastatin. Importantly, the addition of imipramine to fascin1 knockdown HCT-116 cells did not decrease invasion further; however, it obviously ameliorated invasion caused by fascin1 overexpression in transfected DLD-1 cells (Supplementary Information S7). This inhibition clearly revealed a fascin1-dependent effect on migration and invasion capacities.

Imipramine diminishes HCT-116 colon cancer cell invasion in human benign leiomyoma tissue in an in vitro 3D model

To determine whether the anti-invasive properties of imipramine could be translated into human tissue of stromal origin, a myoma organotypic model was used to

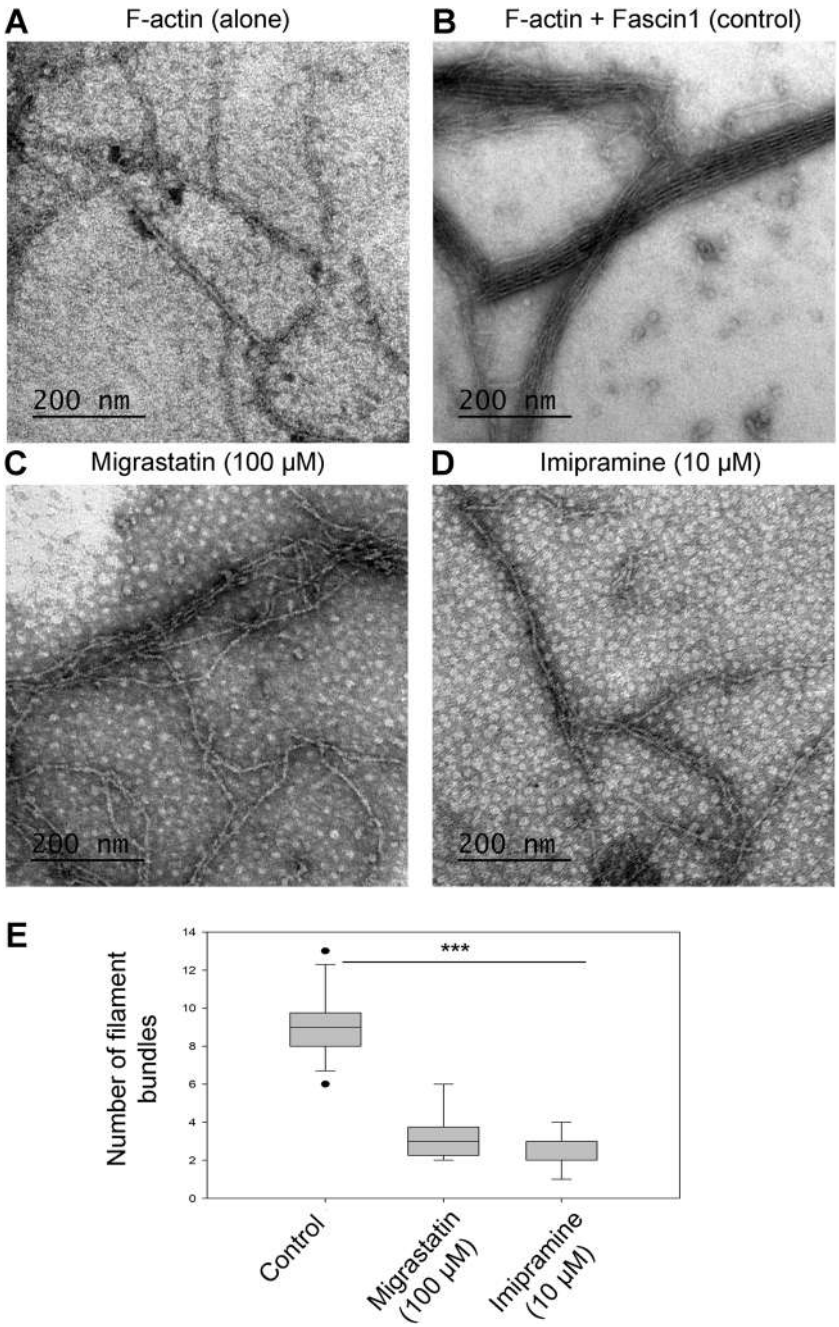

Fig. 4 TEM visualization of actin binding and bundling activities in the presence of fascin1 and inhibitors (negative staining). a Stained polymerized F-actin filaments alone. **b** Under control conditions (DMSO), actin filaments were incorporated into bundles in the presence of untreated fascin1 at a 1:1 ratio. **c** Binding and bundling assays with filamentous F-actin and fascin1 previously incubated with 100 μM migrastatin. **d** Binding and bundling assays with filamentous F-actin and fascin1 previously incubated with 10 μM imipramine. High-magnification images (×93,000) show examples of aberrant morphology in the treated fascin1 conditions (**c**, **d**). **e** Quantitative analysis of the numbers of actin filaments in the presence of the compounds and comparison to control conditions (***$p < 0.001$).

test the invasion of HCT-116 colorectal cancer cells. As shown in Fig. 6, imipramine inhibited both the depth and the area of invasion of HCT-116 cells compared with control conditions and to a comparable extent as migrastatin.

Imipramine inhibits the invasive and metastatic capacity of colorectal tumor cells in an in vivo model

To undercover whether the anti-invasive properties of imipramine could be extrapolated to an animal system, the well-established zebrafish larvae invasion model was

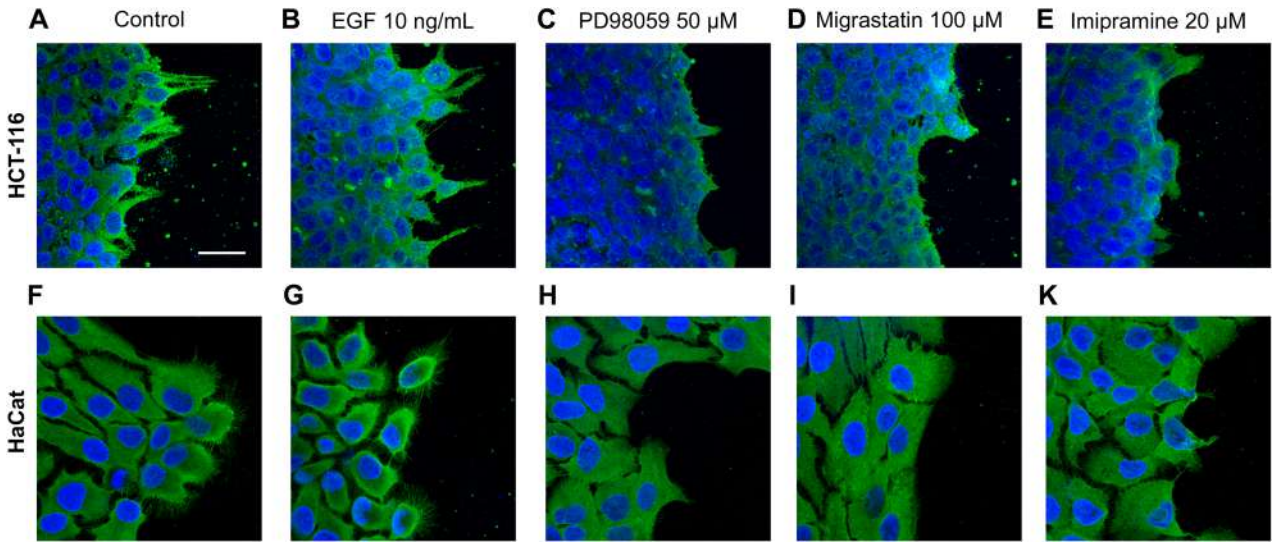

Fig. 5 Cell morphology of HCT-116 and HaCat cells upon inhibition of lamellipodia and filopodia formation. Inset shows the immunofluorescence analysis of the fascin1 marker (green) under control conditions: **a**–**f** control conditions, **b**–**g** 10 ng/mL EGF (migration stimulator), **c**–**h** 50 μM PD98059 (MEK inhibitor), **d**–**i** 100 μM migrastatin, and **e**–**k** 20 μM imipramine. Images were captured using an LSM 510 META confocal fluorescence microscope with a ×63 oil objective. Scale bar 30 μm. Migrastatin and imipramine inhibit lamellipodia protrusion and fascin1 localization in a similar way to the migration MEK inhibitor PD98059 in both cell lines.

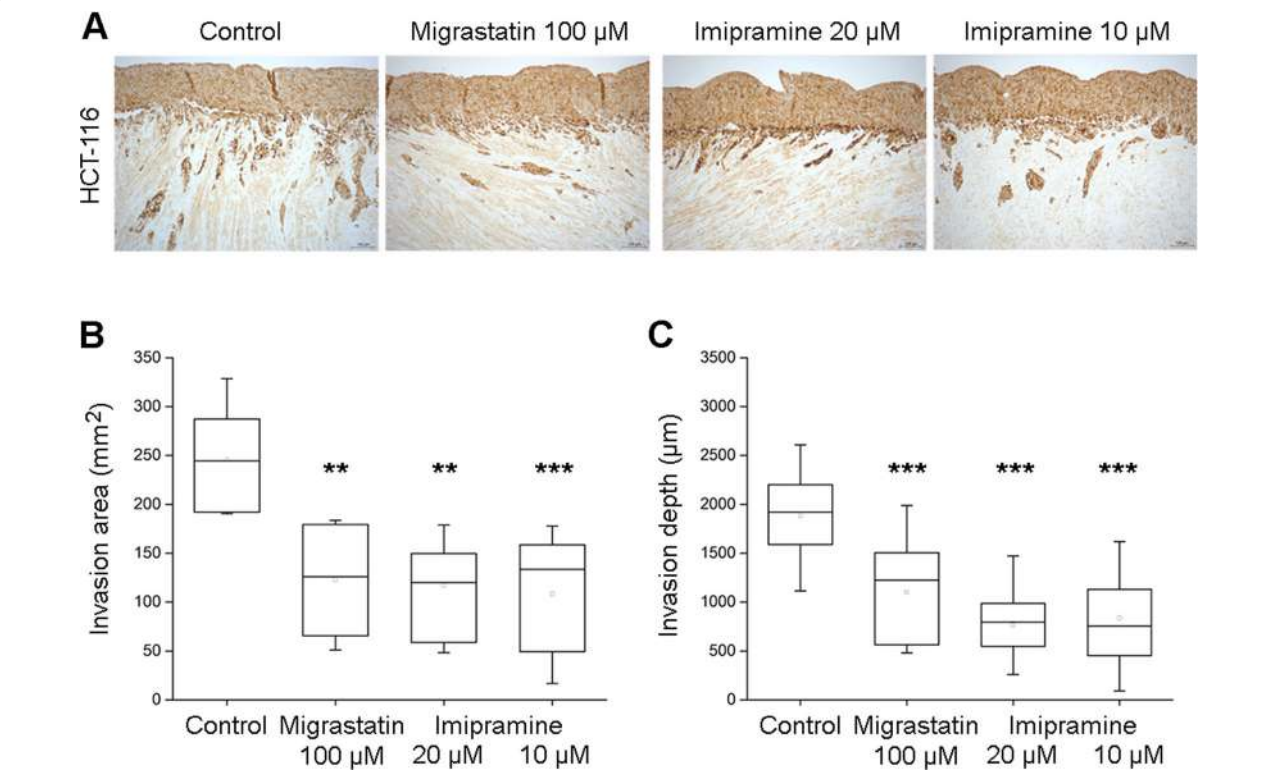

Fig. 6 Myoma organotypic invasion model showing. a The effect of 100 μM migrastatin and imipramine (10 and 20 μM) on the HCT-116 colorectal cell line. Quantifiable effect on the invasion area (**b**) and on the invasion depth (**c**). $^{**}p < 0.001$, $^{***}p < 0.0001$.

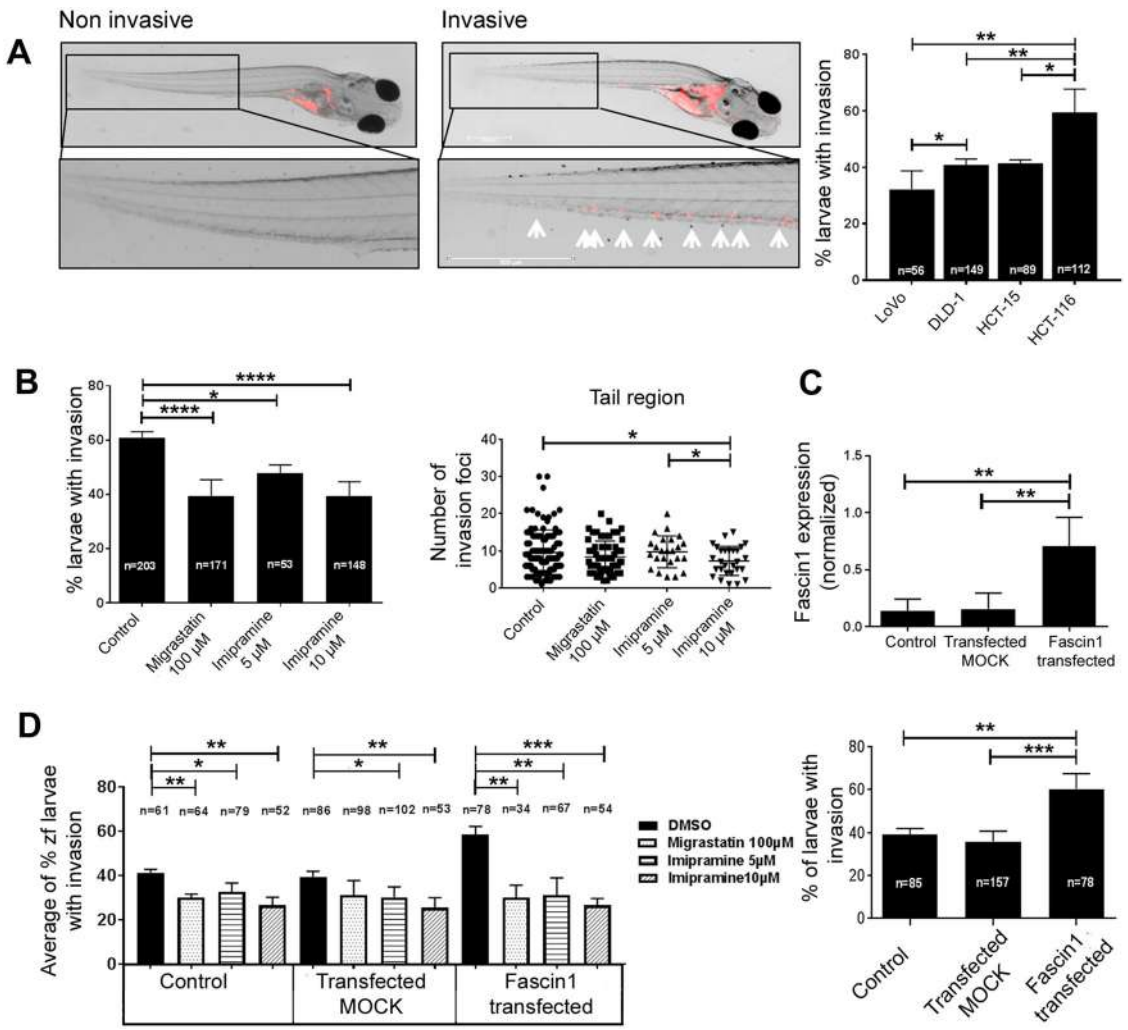

Fig. 7 Zebrafish invasion assays 4 days post xenograft. a The images show the invasive and noninvasive cells in a zebrafish invasion model. The invasiveness of each cell line in this model is shown in the right panel. **b** HCT-116 cancer cells were treated with migrastatin and imipramine and then injected into zebrafish larvae. The effect of imipramine in diminishing the cell invasion percentage and the number of invasive cells is similar to that of migrastatin. **c** Fascin1 mRNA levels in transfected DLD-1 cells and cell invasion associated with transfection (lower panel). **d** Effect of drugs on the average percentage of zebrafish larvae invasion in fascin1-transfected DLD-1 cells. Data are shown as the mean ± SD, compared with the control, $*p = 0.049–0.01$; $**p = 0.001–0.009$; $***p = 0.0001–0.0009$; $****p < 0.0001$.

used, and a xenograft assay was performed (Fig. 7a). The vast majority of larvae were viable when treated at all concentrations; however, the combination of 20 µM imipramine and the injection of naive HCT-116 or transfected DLD-1 resulted in lethality for all larvae after the second day post xenograft (Supplementary Information S9). To check for a dose-dependent effect, 5 and 10 µM concentrations of imipramine were included in the following experiments. The percentage of invasion correlated with fascin1 mRNA expression; HCT-116 had the highest expression, and LoVo and DLD-1 cells had the lowest fascin1 expression and invasion percentage (Fig. 7a). For that reason, HCT-116 was selected as the cell line with the highest constitutive fascin1 expression, and fascin1-transfected DLD-1 cells were selected as the condition to test the effect of induced fascin1 expression. The fascin1-transfected cells increased the level of protein expression and the percentage of zebrafish larvae invasion (Fig. 7c).

Imipramine treatments of larvae exhibited a significantly lower percentage of invasion and a lower number of invasive HCT-116 cells than the control, similar to that observed for migrastatin (Fig. 7b). Similarly, E3 medium treated with imipramine and migrastatin (treatment after cell injection) also diminished fascin1-transfected DLD-1 cell invasion, and this effect was dose-dependent for imipramine (Fig. 7d). The same inhibitory effect was observed when tumor cells were treated prior

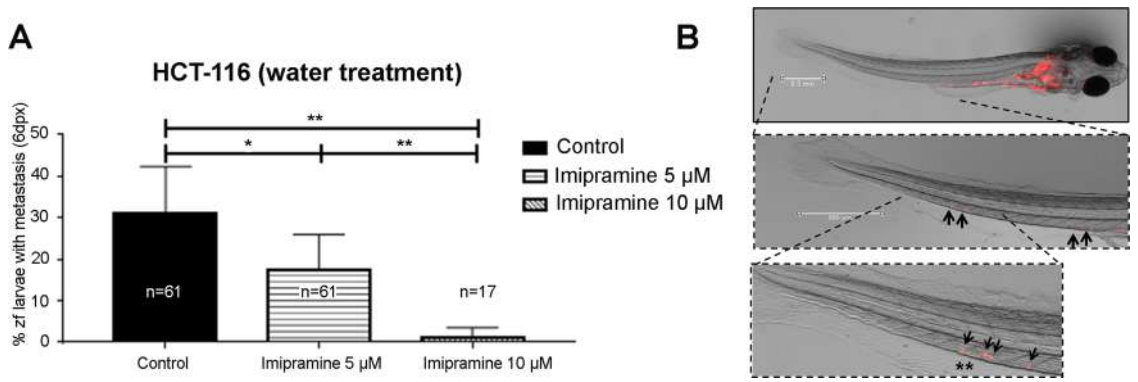

Fig. 8 Antimetastatic potential of imipramine in zebrafish. a At day 6 post injection, larvae were examined to evaluate whether micrometastasis developed by invading native HCT-116 cells. **b** The evaluation criteria were the presence of human cancer cell colonies (arrows) outside the yolk sac. Invading single cells are indicated by asterisks (*). Data are shown as the mean ± SD, compared with the control, *$p = 0.049–0.01$; **$p = 0.001–0.009$.

to injection (Supplementary Information S10). When larvae were fed and kept alive 6 days post xenograft, micrometastasis developed from invading tumor cells. As presented in Fig. 8, HCT-116 colorectal cancer cells were treated with 5 and 10 μM imipramine, causing a significant decrease in the number of larvae with metastasis in a dose-dependent manner. When DLD-1 cells were transfected with the fascin1-GFP vector, a significant increase in larvae with metastasis was observed compared with the pGFP-N3 control vector (MOCK). This metastatic activity diminished when larvae were treated with the lowest imipramine dose with anti-invasive activity (Supplementary Information S11).

Discussion

Our prior study demonstrated, using expression profiling, that fascin1 is overexpressed in SAC compared with CC (88.6% vs. 11.6%)[3]. The high frequency of KRAS or BRAF mutations confers SAC with an important resistance to current anti-epidermal growth factor receptor therapies[9,10]. Similarly, several authors have reported that fascin1 is overexpressed in triple negative/basal phenotype breast carcinoma[22–24]. Given the role of fascin1 in invasion and metastasis, we performed a bioinformatic search for in silico identification of chemical compounds blocking this protein.

We found that imipramine, a tricyclic antidepressant (TCA), gave a high score in the bioinformatics analysis, which was subsequently validated in vitro by Thermofluor, fluorescence titration experiments, and TEM. The application of imipramine in fascin1-overexpressing tumors is patent pending by the authors (no. 18382696.5). A previous study by Jahchan et al.[25] demonstrated the antitumoral effects of imipramine in human small cell lung cancer and other neuroendocrine tumors implanted in mice. In a clinical setting, Sauer and Lang reported unexpected survival associated with imipramine treatment in a patient with metastatic lung cancer[26], and the epidemiological study by Walker et al.[27], which included 31,953 cancer cases from different locations and 61,591 matched controls, concluded that tricyclic antidepressants such as imipramine may have potential for the prevention of both colorectal cancer and glioma in a dose- and time-dependent fashion. The antidepressant effects of TCAs are thought to be due to an overall increase in serotonergic neurotransmission (https://www.drugbank.ca/drugs/DB00458); however, despite the aforementioned evidence, no clear molecular targets have been linked to the antitumoral activity of imipramine. Compelling evidence suggests that imipramine is able to cross the plasma membrane and inhibit intracellular targets. Indeed, CACO-2, a colorectal cancer cell line used to test drug intestinal absorption, was found to be permeable to imipramine (https://www.drugbank.ca/drugs/DB00458).

Furthermore, Kraft et al., by screening 1040 compounds using cultured fascin1-deficient mutant *Drosophila* neurons, whose neurite arbors manifest the "filigree" phenotype, identified imipramine as a fascin1 pathway blocker. Moreover, these authors demonstrated that single substitutions found in other antidepressants (desipramine, trimipramine, and clomipramine) suppress this anti-fascin1 pathway phenotype[28]. Nonetheless, none of these other antidepressants received a significant score in our in silico screening, thus suggesting a direct binding of imipramine to fascin1 and not to other proteins of its pathway. The functional enrichment analysis presented here is also suggestive of an effect of imipramine on the actin cytoskeleton because 3 out of 18 GO molecular functions associated with imipramine treatment are cytoskeleton-related. Despite this evidence, an additional off-target antitumoral effect of imipramine beyond fascin1 is also possible.

The relationship between neural markers and fascin1 overexpression was further confirmed by the fact that neuroblastoma cell lines have the highest fascin1 expression and that Munson et al.[29] demonstrated that

imipramine blue, an imipramine derivative, showed anti-invasion properties against malignant glioma cells in vitro and in vivo. As Kraft et al. pointed out, although the design of the study by Munson et al. was based on the inhibition of NADPH oxidase by imipramine blue, glioma cells treated in vitro showed a dramatic reorganization of their actin cytoskeleton, with marked loss of actin bundle-based protrusions and extensions[28,29], which is consistent with our findings of a direct effect of imipramine causing loss of fascin1 function[28].

Of note, in our study, the HCT-116 colorectal cell line was used for its highest fascin1 expression out of eight CRC cell lines. However, we cannot assure that the primary tumor for this cell line could be an SAC, as this information was not recorded when establishing tumor cell lines, and there is no CRC cell line typified as from SAC origin. Previous articles highlight that cancer cell lines maintain their morphological features and metastatic potential in zebrafish xenografts and further validate the chemosensitive profile of HCT-116 cells in zebrafish and mouse xenografts. The results in mouse xenografts closely matched with zebrafish xenografts[20,30]. It is worth noting that in our study, imipramine did not seem to be toxic to zebrafish at anti-invasive doses.

This study reports, for the first time, an antimigratory and anti-invasive effect of imipramine, an FDA-approved antidepressant oral agent, in colorectal tumor cells possibly due to anti-fascin1 activity, thus paving the way for a new molecular targeted treatment in SAC and other fascin1-overexpressing tumors.

Acknowledgements
We are grateful to Dr. Milind Valdya from the Advanced Centre for Treatment Research and Education in Cancer (Maharashtra, India) for kindly providing us with the vectors used in the transfection assay; to Dr. Steven Almo from Albert Einstein College of Medicine (New York, USA) for kindly providing purified fascin1 protein; to Dr. Antonio Parrado from Genomic Platform, Institute for Biohealth Research from Murcia Region (IMIB), for bioinformatic support; and to Dr. Diego Arcas for revising the English version of the manuscript. This work is supported by the Instituto de Salud Carlos III (Spanish Ministry of Health) and FEDER funds (ref: PI15/00626). B.A.-G. belongs to the "Programa de Doctorado en ciencias de la Salud" from the Catholic University of Murcia (UCAM) and holds a predoctoral grant from UCAM. S.M.-G. was supported by the Fundación Séneca and PCR by the Finnish Cultural and Sigrid Juselius Foundations (2017–2018 and 2018–2019 grants).

Author details
[1]Pathology and Histology Department, Facultad de Ciencias de la Salud, UCAM Universidad Católica San Antonio de Murcia, Campus de los Jerónimos, s/n, 30107 Guadalupe, Murcia, Spain. [2]Research group "Telomerasa, Envejecimiento y Cáncer," CIBERehd, Hospital Clínico Universitario Virgen de la Arrixaca, IMIB-Arrixaca, Murcia, Spain. [3]Cell Culture Lab, Facultad de Ciencias de la Salud, UCAM Universidad Católica San Antonio de Murcia, Campus de los Jerónimos, s/n, Guadalupe, 30107 Murcia, Spain. [4]Research group "Regeneración, oncología molecular y TGF-β", Institute for Biohealth Research from Murcia (IMIB), Hospital Clínico Universitario Virgen de la ArrixacaCarretera Madrid-Cartagena, El Palmar, Spain. [5]Cancer Research and Translational Medicine Research Unit, University of Oulu, Aapistie 5A, FI-90220 Oulu, Finland. [6]Medical Research Center Oulu, Oulu University Hospital, University of Oulu, Oulu, Finland. [7]Department of Physical Chemistry and Institute of Biotechnology, University of Granada, Campus Fuentenueva s/n, 18071 Granada, Spain. [8]Institute of Oral and Maxillofacial Disease, University of Helsinki, Helsinki, Finland. [9]HUSLAB, Department of Pathology, Helsinki University Hospital, Helsinki, Finland. [10]Structural Bioinformatics and High Performance Computing (BIO-HPC) Research Group, Universidad Católica de Murcia (UCAM), Guadalupe, Spain. [11]Clinical Analysis Department, Group of Molecular Pathology and Pharmacogenetics, Institute for Biohealth Research from Murcia (IMIB), Hospital Universitario Santa Lucía, c/Mezquita sn, 30202 Cartagena, Spain. [12]Present address: C/Mezquita s/n CP, 30202 Cartagena, Murcia, Spain

Author contributions
P.C.-Z. and H.P.-S. conceived the presented idea. P.C.-Z., S.M.-G., F.J.N., M.L.C., H. P.-S., and T.S. designed the experiments and supervised the findings of this work. B.A.-G., M.B.-G., S.M.-G., A.B.-G., F.F.L.-C., P.C.R., and J.R.S. performed the experiments. P.C.-Z., B.A.-G., S.M.-G., H.P.-S., and P.C.R. wrote the manuscript. All authors discussed the results and contributed to the final manuscript.

Conflict of interest
The authors declare that they have no conflict of interest.

Publisher's note
Springer Nature remains neutral with regard to jurisdictional claims in published maps and institutional affiliations.

Supplementary information accompanies this paper at https://doi.org/10.1038/s12276-020-0389-x.

Received: 15 July 2019 Revised: 20 December 2019 Accepted: 31 December 2019
Published online: 20 February 2020

References

1. Chen, L., Yang, S., Jakoncic, J., Zhang, J. J. & Huang, X. Y. Migrastatin analogues target fascin to block tumour metastasis. *Nature* **464**, 1062–1066 (2010).
2. Machesky, L. M. & Li, A. Fascin: Invasive filopodia promoting metastasis. *Commun. Integr. Biol.* **3**, 263–270 (2010).
3. Conesa-Zamora, P. et al. Expression profiling shows differential molecular pathways and provides potential new diagnostic biomarkers for colorectal serrated adenocarcinoma. *Int. J. Cancer* **132**, 297–307 (2013).
4. Tan, V. Y., Lewis, S. J., Adams, J. C. & Martin, R. M. Association of Fascin1-1 with mortality, disease progression and metastasis in carcinomas: a systematic review and meta-analysis. *BMC Med.* **11**, 52 (2013).
5. Rodrigues, P. C. et al. Fascin promotes migration and invasion and is a prognostic marker for oral squamous cell carcinoma. *Oncotarget* **8**, 74736–74754 (2017).
6. García-Solano, J. et al. Clinicopathologic study of 85 colorectal serrated adenocarcinomas: further insights into the full recognition of a new subset of colorectal carcinoma. *Hum. Pathol.* **41**, 1359–1368 (2010).
7. García-Solano, J., Conesa-Zamora, P., Trujillo-Santos, J., Mäkinen, M. J. & Pérez-Guillermo, M. Tumour budding and other prognostic pathological features at invasive margins in serrated colorectal adenocarcinoma: a comparative study with conventional carcinoma. *Histopathology* **59**, 1046–1056 (2011).
8. García-Solano, J. et al. Immunohistochemical expression profile of β-catenin, E-cadherin, P-cadherin, laminin-5γ2 chain, and SMAD4 in colorectal serrated adenocarcinoma. *Hum. Pathol.* **43**, 1094–1102 (2012).
9. Stefanius, K. et al. Frequent mutations of KRAS in addition to BRAF in colorectal serrated adenocarcinoma. *Histopathology* **58**, 679–692 (2011).
10. García-Solano, J. et al. Colorectal serrated adenocarcinoma shows a different profile of oncogene mutations, MSI status and DNA repair protein expression compared to conventional and sporadic MSI-H carcinomas. *Int. J. Cancer* **131**, 1790–1799 (2012).
11. Han, S. et al. Improving fascin inhibitors to block tumor cell migration and metastasis. *Mol. Oncol.* **10**, 966–980 (2016).
12. Shoichet, B. K. Virtual screening of chemical libraries. *Nature* **432**, 862–865 (2004).
13. Sanders, M. P. et al. Comparative analysis of pharmacophore screening tools. *J. Chem. Inf. Model.* **52**, 1607–1620 (2012).

14. Wolber, G. & Langer, T. LigandScout: 3-D pharmacophores derived from protein-bound ligands and their use as virtual screening filters. *J. Chem. Inf. Model.* **45**, 160–169 (2005).
15. Geppert, H., Vogt, M. & Bajorath, J. Current trends in ligand-based virtual screening: molecular representations, data mining methods, new application areas, and performance evaluation. *J. Chem. Inf. Model.* **50**, 205–216 (2010).
16. Jansen, S. et al. Mechanism of actin filament bundling by fascin. *J. Biol. Chem.* **286**, 30087–30096 (2011).
17. Salo, T. et al. Organotypic three-dimensional assays based on human leiomyoma-derived matrices. *Philos. Trans. R. Soc. Lond. B Biol. Sci.* **373**, 20160482 (2018). https://doi.org/10.1098/rstb.2016.0482.
18. Åström, P., Heljasvaara, R., Nyberg, P., Al-Samadi, A. & Salo, T. Human tumor tissue-based 3D in vitro invasion assays. *Methods Mol. Biol.* **1731**, 213–221 (2018).
19. Jelassi, B. et al. P2X(7) receptor activation enhances SK3 channels- and cystein cathepsin-dependent cancer cells invasiveness. *Oncogene* **30**, 2108–2122 (2011).
20. Fior, R. et al. Single-cell functional and chemosensitive profiling of combinatorial colorectal therapy in zebrafish xenografts. *Proc. Natl Acad. Sci. USA* **114**, E8234–E8243 (2017).
21. Gaul, C. et al. The migrastatin family: discovery of potent cell migration inhibitors by chemical synthesis. *J. Am. Chem. Soc.* **126**, 11326–11337 (2004).
22. Wang, C. Q. et al. Fascin-1 as a novel diagnostic marker of triple-negative breast cancer. *Cancer Med.* **5**, 1983–1988 (2016).
23. Rodríguez-Pinilla, S. M. et al. Prognostic significance of basal-like phenotype and fascin expression in node-negative invasive breast carcinomas. *Clin. Cancer Res.* **12**, 1533–1539 (2006).
24. Esnakula, A. K. et al. Strong association of fascin expression with triple negative breast cancer and basal-like phenotype in African-American women. *J. Clin. Pathol.* **67**, 153–160 (2014).
25. Jahchan, N. S. et al. A drug repositioning approach identifies tricyclic antidepressants as inhibitors of small cell lung cancer and other neuroendocrine tumors. *Cancer Discov.* **3**, 1364–1377 (2013).
26. Sauer, T. & Lang, U. E. Is imipramine helpful in the treatment of cancer? A case presentation and discussion of possible clinical implications. *Biomed. J. Sci. Tech. Res.* **4**, 4194–4195 (2018).
27. Walker, A. J., Card, T., Bates, T. E. & Muir, K. Tricyclic antidepressants and the incidence of certain cancers: a study using the GPRD. *Br. J. Cancer* **104**, 193–197 (2011).
28. Kraft, R. et al. A cell-based fascin bioassay identifies compounds with potential anti-metastasis or cognition-enhancing functions. *Dis. Model. Mech.* **6**, 217–235 (2013).
29. Munson, J. M. et al. Anti-invasive adjuvant therapy with imipramine blue enhances chemotherapeutic efficacy against glioma. *Sci. Transl. Med.* **4**, 127ra36 (2012).
30. Brown, H. K., Schiavone, K., Tazzyman, S., Heymann, D. & Chico, T. J. Zebrafish xenograft models of cancer and metastasis for drug discovery. *Expert Opin. Drug Discov.* **12**, 379–389 (2017).

Supplementary Information

Supplementary Information S1. Detailed description of the experimental protocols and tables.

Supplementary Information S2. Differential scanning fluorimetry profiles for fascin1 at different protein concentrations (A) and different concentrations of DMSO (B) showing that fascin1 unfolds as a monomeric protein with no effect of the protein concentration on the denaturation profile and with slight sensitivity to DMSO.

Supplementary Information S3. mRNA expression levels of fascin1 in eight colorectal cell lines using β-actin mRNA gene expression for data normalization.

Supplementary Information S4. Colorectal cancer cell line viability assay. The effect of migrastatin (upper panel) and imipramine (lower panel) on the cell viability of DLD-1, HCT-116, and SW-480 colorectal cell lines is shown.

Supplementary Information S5. Panther pie chart of the 18 differentially enriched functions. As indicated, actin binding (GO: 0003779), cytoskeletal protein binding (GO: 0008092), and structural constituent of cytoskeleton (GO: 0005200) were found among these 18 functions.

Supplementary Information S6. Cell migration assay for the three colorectal cancer cell lines after 7 h. (A) HCT-116, (B) DLD-1, (C) SW-480, and (D) migration were calculated with respect to the control conditions for a slope between 4 and 7 h (linear phase). * $p<0.05$, ** $p<0.01$.

Supplementary Information S7. Inhibition of the migration and invasive capacities by imipramine in transfected cells. A) Percentage of migration. B) Percentage of invasion. CRC HCT-116 cells were genetically knocked down for fascin1 with short interfering

siRNA. MOCK control HCT-116 cells were transfected with siRNA-A. CRC DLD-1 cells genetically overexpressed fascin1 with the fascin1-GFP vector. MOCK control DLD-1 cells were transfected with the pGFP-N3 control vector. Data are representative of two similar experiments with error bars, mean ± SD of duplicates. * $p<0.05$, ** $p<0.01$ compared with the MOCK condition; n.s.: nonsignificant.

Supplementary Information S8. Transwell invasion assays were performed to evaluate the HCT-116 cell invasive ability. (A) Invasion after treatment with migrastatin (100 µM) and imipramine (20 µM). Pictures were taken under an inverted phase contrast microscope. The magnification was ×200, and the scale bars =50 µM. (B) Quantification of the invasive cells by DO in a spectrophotometer at λ=560 nm. (C) Number of invasive cells using ImageJ software. Data are presented as the mean ± SD compared with the control.

Supplementary Information S9. Survival curves of the zebrafish larvae when treated with the compounds in E3 medium (A) and when they were injected with HCT-116 or transfected DLD-1 tumor cell lines (B).

Supplementary Information S10. Invasion assay with colorectal tumor cells treated with the drugs prior to injection into the zebrafish larvae. (A) DLD-1, (B) HCT-116, (C) Anti-invasive effect of the drugs on fascin1-transfected DLD-1 cells.

Supplementary Information S11. Effect of imipramine on the development of micrometastasis caused by transfected DLD-1 cells overexpressing fascin1 in zebrafish. (A) The imipramine dose was set as 5 µM, as it was the lowest dose showing anti-invasive properties. (B) Transfection quantitation of fascin1 mRNA expression in transfected DLD-1 cells with the pGFP-N3 control vector (MOCK) and the fascin1-GFP vector.

Supplementary Information S1. Detailed description of experimental protocols and tables.

Thermofluor and fluorescence titration

Thermofluor was performed using a Biorad C1000 Touch Thermal Cycler CFX96 RT-PCR system in a 96-well format. A total of 25 μL reaction mixtures were set up containing 2 μM fascin1 (cat. no. 8411-02, Hypermol, Bielefeld, Germany) in 20 mM Hepes, 150 mM NaCl, 1mM DTT, and 5% sucrose at pH 7.4, in the presence of SYPRO Orange (1,000-fold dilution from the commercial stock [Invitrogen]). The indicated compound, prepared at 10 mM in 100% DMSO, was added to each well to a final concentration of 1 mM and 10% DMSO. Included in the 96-well plates were three replicates per compound, together with six internal controls, containing only free protein in 10% DMSO. The PCR plates were covered and subsequently shaken, centrifuged, incubated for 2 min at 20ºC inside the RT-PCR machine, and heated from 20ºC to 100ºC at a 1ºC/min scan rate. Fascin1 was extensively dialyzed against the appropriate buffer prior to the titration experiment, and its concentration was determined by measuring the absorbance at 280 nm using an extinction coefficient of 67840 $cm^{-1} \cdot M^{-1}$. Fluorescence titration experiments were performed in a Cary Eclipse spectrofluorometer (Varian Inc.). A 15 μM fascin1 solution, kindly provided by Dr. Steven Almo from Albert Einstein College of Medicine (New York, USA), was titrated by adding increasing volumes of concentrated solutions of imipramine. Emission spectra were recorded between 307 and 500 nm at 25ºC in 10% DMSO, 100 mM NaCl, 20 mM Hepes, and pH 7.4, with the excitation wavelength fixed at 280 nm. Binding isotherms were generated and fitted using ORIGIN 7.0 (Microcal Inc.) to a one-site equilibrium binding model, according to the following equation:

$$F = F_f + (F_b - F_f) \cdot \frac{(P_T + L_T + K_d) - \sqrt{(P_T + L_T + K_d)^2 - 4 \cdot P_T \cdot L_T}}{2 \cdot P_T}$$

where Ff and Fb are the fluorescence signal of free and bound fascin1 and PT and LT are the total protein and ligand concentration, respectively, at each addition point.

F-actin bundling assay

Rabbit muscle actin was induced to polymerize to F-actin using 250 µL of general actin buffer, leaving it on ice for 30 min, and adding 25 µL of actin polymerization buffer at room temperature (RT) for 1 h. Test protein, that is, human recombinant fascin1 (Hypermol), was centrifuged (10.000 *g*, 1 h, 4ºC) to obtain the test protein stock, which was diluted at 1 µM and then incubated with imipramine (100 µM) and DMSO (4%) for 30 min at RT. After that, all samples and controls were subsequently incubated with F-actin (10 µM) for another 30 min at RT. F-actin bundling activity was determined performing a low-speed centrifugation after incubation (10.000 *g*, 1 h, RT). Comparable amounts of supernatant and pellet fractions were analyzed by densitometric scanning of Coomassie blue-stained SDS/polyacrylamide gels. The intensities of protein bands in Coomassie-stained gels were measured, and the relative F-acting bundling activity was calculated using ImageJ software.

Transmission electron microscopy

In the control condition, purified actin (21 µM) was polymerized according to the protocol from the Actin Binding Protein Biochem Kit™ Muscle Actin and then incubated with human recombinant fascin1 (molar ratio 1:1) for 30 min at RT. Fascin1 was previously incubated for 2 h with 100 µM migrastatin and 10 µM imipramine. The samples were directly adsorbed onto 200 mesh copper grids for 30 s, blotted to remove excess solution, washed twice with distilled water, and negatively stained with 1%

(w/v) uranyl acetate for 30 s, blotted and dried again. The TEM study of actin filaments and fascin1-actin bundles was performed on a PHILIPS TECNAI 12 transmission electron microscope (Japan) at an accelerating voltage of 80 kV and a magnification up to 135.000 X. Images were captured on a coupled device camera (Megaview III). The numbers of filaments per bundle were counted manually in 25 pictures/condition and statistically analyzed (Kruskal–Wallis test).

Fascin1 mRNA expression assessment by quantitative PCR

RNA was extracted by treating cell line pellets (around 200,000 cells) with 700 µL of Qiazol (Qiagen ref: 1023537) and by adding 140 µL of chloroform and centrifuging at 12,000 *g* for 15 min at 4ºC. The aqueous phase containing 350 µL was then subjected to automatic total RNA extraction using the Qiacube equipment and the miRNeasy Mini Kit (ref: 217004), both provided by Qiagen (Hilden, Germany). cDNA was obtained using the Maxima First Strand cDNA Synthesis Kit by Thermo Fisher (Fisher Scientific, cat. no. K1671, Madrid, Spain) following the manufacturer information. A total of five microliters of 1:5 diluted cDNA was added to the qPCR reaction containing 12.5 µL 2X QuantiTect SYBR Green PCR Kit (ref: 204145) by Qiagen and 300 nm of each primer in a total volume of 25 µL. qPCR was performed on a 7500F real-time PCR system by Applied Biosystems (Foster City, California, USA) following the standard protocol: 50ºC 2 min, 95ºC 10 min, 40 cycles of 95ºC 15 sec, 60ºC 1 min and a melt curve stage consisting of 95ºC 15 sec, 60ºC 1 min, 95ºC 30 sec, and 60ºC 30 sec. The relative quantitation was obtained by the 2-ΔCt method using β-actin as housekeeping gene. The amounts of mRNA are given as number of copies per million of copies of β-actin. Primers of β-actin used for FSCN1 quantitation are shown below:

Primer sequences used for quantitative PCR validation

Gene	Primer name	Sequence (5´-3´)	Fragment size (bp)
FSCN1 (ENSG00000075618)	115F	TCCACGCGCCAGGGTATGGAC	121
	116R	ACTTGCCCGTGTGGGTACGG	
β-ACTIN (ENSG00000075624)	b-a-blgF	GAGCTACGAGCTGCCTGACG	120
	b-a-blgR	GTAGTTTCGTGGATGCCACAG	

Cell viability assay

Exponentially growing cells were plated in triplicate in flat-bottomed, 96-well plates (Nunc, Roskilde, Denmark) at 1,500 cells/well. On the day after, drugs were added in serial dilution from 500 nm to 300 µM of migrastatin and imipramine compounds. Control wells contained medium without drug plus 0.1% DMSO (drug carrier). Plates were incubated at 37ºC for three days in a humidified 5% CO_2 incubator and assayed for cell viability. Tetrazolium dissolved in Dulbecco's phosphate-buffered saline (PBS), pH 7.2, at 1.9 mg/mL was added to the cells (30 µl/well). After incubation at 37°C for 4 h, the medium was aspirated. The formazan crystals were dissolved in 200 µL DMSO for 30 min, and the absorbance was read at 570 nm in a microtiter plate reader. Results were calculated as cell viability (%) = average OD of wells/average OD of control wells.

RNA labeling, microarray hybridization, and function enrichment analysis

To have a general overview of enriched functions associated with the treatment of colorectal cancer tumor cells, HCT-116 cells were treated with DMSO or imipramine. Total RNA was isolated using the miRNeasy Mini Kit (Qiagen, Hilden, Germany) and quantitated on a NanoDrop 2000 (Thermo Fisher Scientific, Waltham, Massachusetts). RNA quality was examined on an Agilent 2100 Bioanalyzer (Agilent Technologies, Palo Alto, California) using the RNA 6000 Nano Kit. All the samples studied had RIN (RNA Integrity Number) =10. RNA samples were labeled using Agilent Two-Color Quick Amp Labelling and RNA Spike-In kits, according to the manufacturers' protocol. Experimental samples were labeled with cyanine 5-CTP and used as tests. The Universal Human Reference RNA (Agilent Technologies) was labeled with cyanine 3-CTP and used as reference. The labeled cRNAs were mixed together and hybridized onto SurePrint G3 Human Gene Expression v3 8x60K Microarrays, targeting 26,083 Entrez Gene RNAs and 30,606 long noncoding RNAs (lncRNAs), using the Agilent Gene Expression Hybridization Kit. Data sets were extracted using the Agilent Feature Extraction software. The normalized expression values were obtained using the function NormalizaWithinArrays with the Lowess method. Probes were collapsed at the gene level using the Avereps function, and the differences between DMSO and imipramine were expressed as log2FC averages. Only one experiment was performed per condition, and thus, no p values were obtained. Enriched functions associated with the gene list were obtained using Gene Ontology category of "molecular function" and Panther Classification System (accessible at http://www.pantherdb.org).

Data sets deposited at the Gene Expression Omnibus (GEO) database under accession number GSE125169 at https://www.ncbi.nlm.nih.gov/geo/query/acc.cgi?acc=GSE125169.

Immunofluorescence

After cells reached 100% confluence, serum-supplemented medium was removed and replaced with fresh serum-free medium for 24 hours. Artificial wounding was performed by transversally dragging a sterilized razor blade on the central area of the coverslips. Coverslips (Thermo Fisher, Waltham, Massachusetts) were then placed in a six-well plate with 2 mL serum-free DMEM and 100 µM migrastatin, 20 µM imipramine, 10 ng/ml EGF, or 50 µM MEK inhibitor PD98059 (MEKi) (both from Sigma-Aldrich, St. Louis, Missouri, USA) for 24 h. Cells were then fixed with Bouin (for fascin1 protein) or 4% formaldehyde (for actin protein) and subsequently permeabilized in a 0.3% Triton X-100/PBS solution and then exposed to blocking buffer for 30 min. Samples were incubated for 1 h with anti-fascin1 antibody (1/250) (55K-2 clone; Santa Cruz Biotechnology, Heidelberg, Germany; Santa Cruz Biotechnology Cat# sc-21743, RRID: AB_627580) or anti-β-actin antibody (1/1000) (Sigma-Aldrich Cat# A5441, RRID: AB_476744, Sigma-Aldrich, St. Louis, Missouri, USA) in a wet chamber. Appropriate fluorescent-labeled primary antibodies were incubated later with Alexa fluor 488-conjugated anti-mouse IgG (from donkey) (1/400) (Molecular Probes Cat# A-21202, RRID: AB_141607) or Alexa fluor 594-labeled phalloidin (1/1000) (Thermo Fisher Scientific Cat# A12381, RRID: AB_2315633) and Hoechst 33258 (Thermo Fisher Scientific Cat# H3569, RRID: AB_2651133) for 30 min at room temperature and darkness. Samples were examined, and representative images were taken with a confocal microscope (LSM 510 META from ZEISS, Jena, Germany).

Transfection assay

To quantify the effect of imipramine upon fascin1-induced and -silenced expression in colorectal cancer cells, transfection assays were performed prior testing the *in vitro*

migration capacities and in the zebrafish invasion model. The human CRC cells were genetically overexpressed (DLD-1) and knocked down (HCT-116) for fascin1. HCT-116 (4 10^5 cells/well) and DLD-1 (9 10^5 cells/well) were seeded in six-well plates and then, cultured overnight, grown to 50%–70% confluence. In the case of DLD-1, pGFPN3 control vector or fascin1-GFP vector (kindly provided by Dr. Milind Valdya from the Advanced Centre for Treatment Research and Education in Cancer, Maharashtra, India) was used. HCT-116 cells were transfected with fascin1, short interfering siRNA or control siRNA-A (Santa Cruz Biotechnology, Heidelberg, Germany). Transfections were conducted using lipofectamine 2000 (Thermo Fisher, Waltham, Massachusetts, USA) according to the manufacturer's protocols. The cells were then washed with PBS before adding 800 µL standard medium without antibiotics. The final amount of nucleic acids used for transfection was 1 µg and 0.05 µmoles per well for DLD-1 and HCT-116 cells, respectively. The nucleic acids were diluted with OptiMEM I Reduced Serum Medium (Invitrogen, Carlsbad, California, USA). Equal volume of OptiMEM I medium (100 µL) was used to dilute lipofectamine 2000 and nucleic acids and then incubated for 5 min at room temperature. Mixture was added drop by drop to the lipofectamine-based liposome dilution and incubated at room temperature for additional 30 min. After incubation, the nucleic acids/liposome complexes were added to the cells and incubated for additional 6 hours. After transfection, the residual nucleic acids/liposome complexes were washed off, and the cells were replenished with standard medium and incubated up to 72 h. Fascin1 mRNA expression was checked with cell lysates by qPCR as described above.

Chemical treatment

HCT-116 and fascin1-transfected DLD-1 cells were treated for 24 h with 0.1% DMSO, 100 µM migrastatin, and 20 µM imipramine. For treatment larvae with drugs, zebrafish

embryos xenografted with HCT-116 and fascin1-transfected DLD-1 cell lines were transferred into 24-well plates and were treated, by bath immersion, with E3 medium (5 mM NaCl, 0.33 mM KCl, 0.33 mM $CaCl_2$, 0.33 mM $MgSO_4$, 0.1% methylene blue [Sigma]) containing 100 μM migrastatin or imipramine at 5 μM or 10 μM diluted in DMSO for 96 h. Fresh drug was added every 24 h. The number of individuals is shown in the graph bars.

End Notes

Patent applications

The following patent related to the findings presented in this manuscript has been submitted: P. Conesa-Zamora, H. Pérez-Sánchez, I. Luque-Fernández, S. Montoro-García, B. Alburquerque-González, P. Campioni-Rodrigues, J. García-Solano, A. Bernabé-García, F. J. Nicolás-Villaescusa, M. Bernabé-García, M. L. Cayuela-Fuentes, J. Ruiz-Sanz, J. C. Martínez-Herrerías, T. Salo, "Imipramine for use as inhibitor of fascin1 overexpression," EP18382696.5 (2018). Patent Pending.

Tables

Table S1. Thermal shift assay results

Compound	**Conc (mM)**	**$T_{m, FAM}$ (ºC)**	**$\Delta T_{m, FAM}$ (ºC)**	**$T_{m, HEX}$ (ºC)**	**$\Delta T_{m, HEX}$ (ºC)**	**$T_{m, TRed}$ (ºC)**	**$\Delta T_{m, TRed}$ (ºC)**
Free fascin1	-	55,7±0,5	-	56,0±0,0	-	56,2±0,6	-
Imipramine	1	58,3±0,6	2,7±1,1	58,0±0,0	2,0±0,0	58,0±0,0	1,8±0,6

Conc (concentration), T_m (melting temperature), ΔT_m (variation of melting temperature)

Table S2. Lamellipodium protrusion number in HCT-116 cells in the different treatment conditions

	Control	**Migrastatin 100 µM**	**Imipramine 20 µM**	**EGF 10 ng/mL**	**PD98059 50 µM**
Lamellipodium number	9 ± 1.5	2 ± 2	0.6 ± 0.8	10.4 ± 1.5	1 ± 1
P value*		**0,0001**	**3,305 E^{-06}**	0,1401	**5,9241E^{-06}**

EGF (epidermal growth factor)

Table S3. Percentage of migration in DLD-1, SW-480, and HCT-116 in control and the different treatment conditions

Cell line	Treatment	Migration percentage	Standard deviation
DLD-1	DMSO 0.1%	100	0
	Imipramine 20 µM	23.21	12.21
	Migrastatin 100 µM	67.91	5.19
SW-480	DMSO 0.1%	100	0
	Imipramine 20 µM	77.52	22.35
	Migrastatin 100 µM	70.34	18.04
HCT-116	DMSO 0.1%	100	0
	Imipramine 20 µM	43.25	6.82
	Migrastatin 100 µM	44.59	6.14

Supplementary Information S2

A

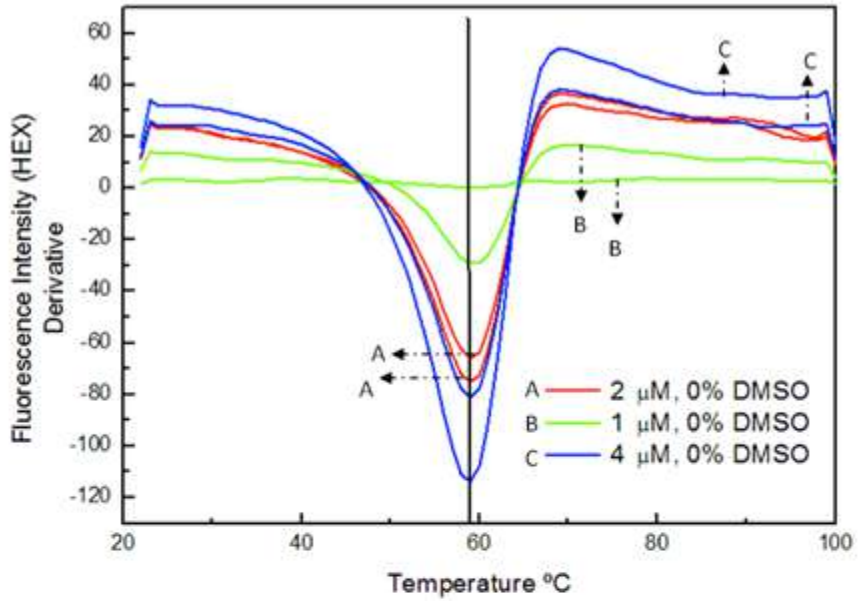

B

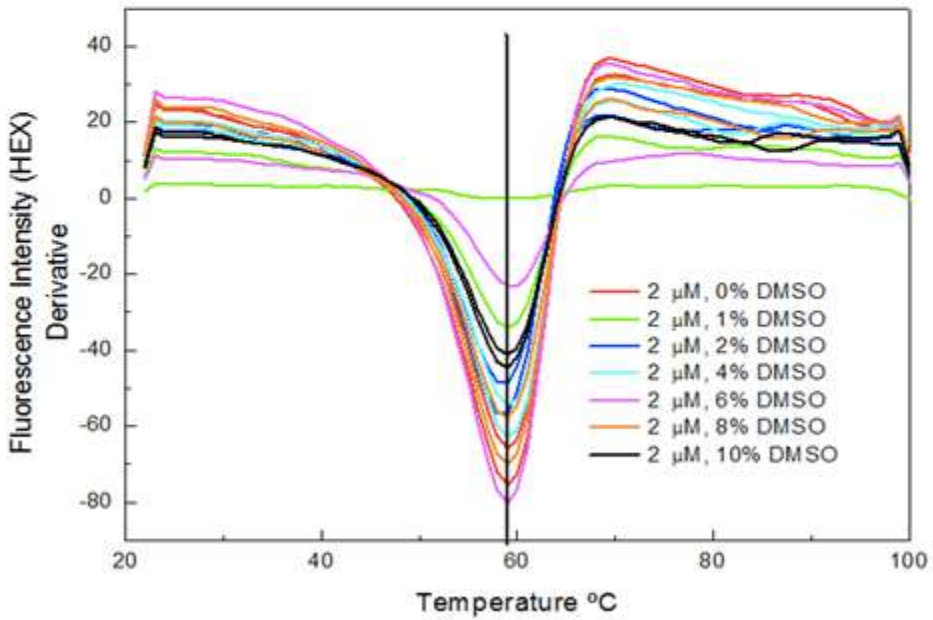

Supplementary Information S3

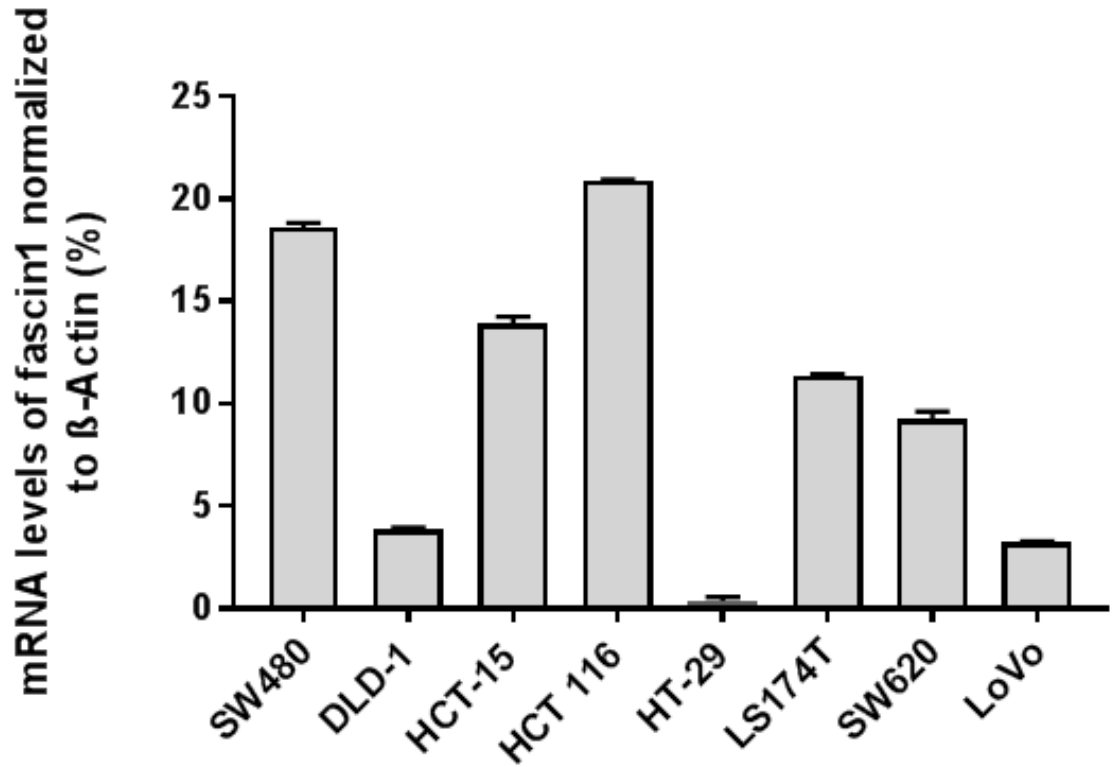

Supplementary Information S4

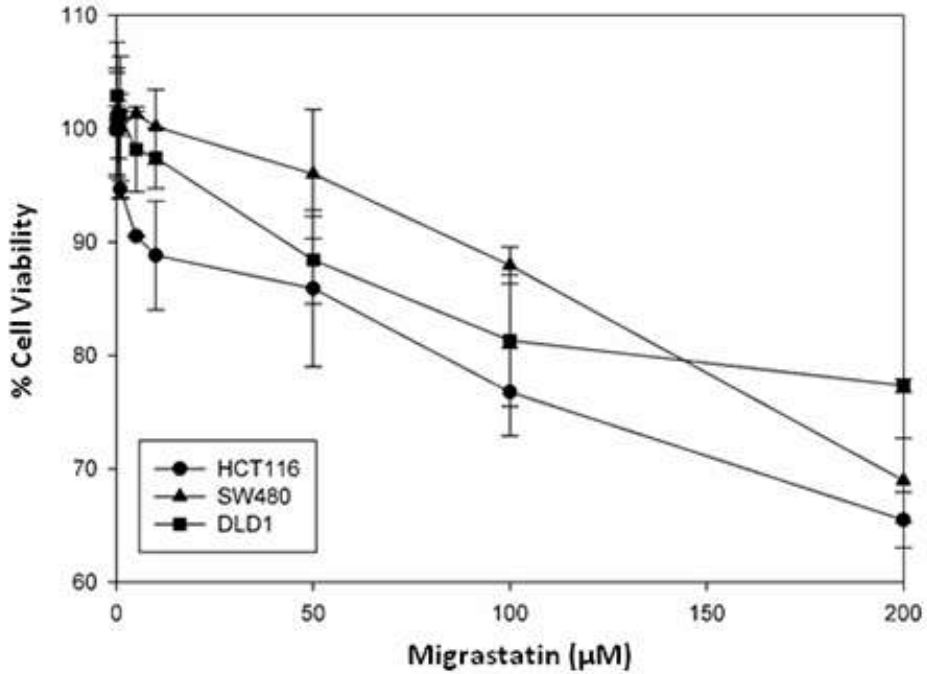

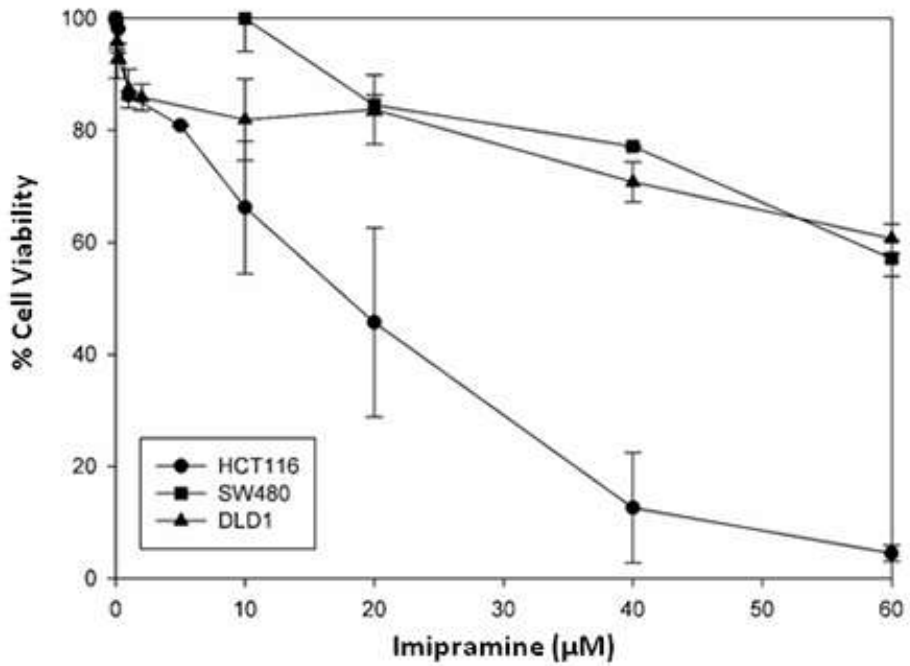

Supplementary Information S5

HOMO SAPIENS (REF)

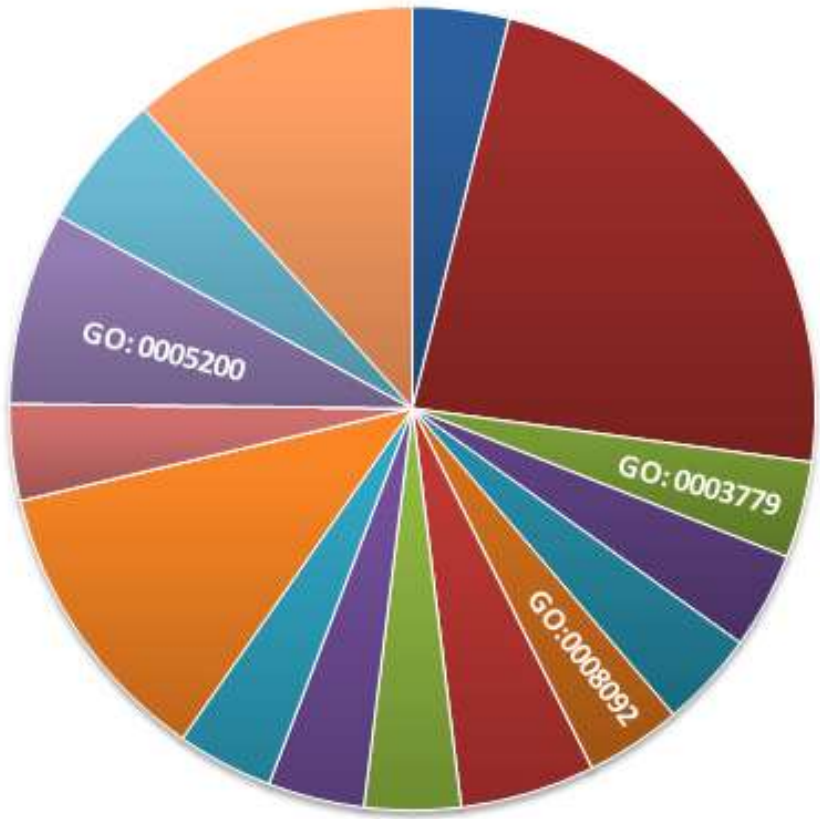

- G-protein coupled receptor activity (GO:0004930)
- RNA polymerase I transcription factor binding transcription factor activity (GO:0001082)
- acting binding (GO:0003779)
- cytokine activity (GO:0005125)
- cytokine receptor binding (GO:0005126)
- cytoskeletal protein binding (GO:0008092)
- interpheron-alpha/beta receptor binding (GO:0005132)
- ligase activity (GO:0016874)
- lipase activity (GO:0016298)
- lyase activity (GO:0016829)
- peptidase inhibitor activity (GO:0030414)
- receptor activity (GO:0004872)
- receptor binding (GO:0005102)
- sequence-specific DNA binding RNA polymerase I transcription factor activity (GO:0001167)
- serine-type endopeptidase inhibitor activity (GO:0004867)
- structural constituent of cytoskeleton (GO:0005200)
- transforming growth factor beta receptor binding (GO:0005160)
- transmembrane transporter activity (GO:0022857)

Supplementary Information S6

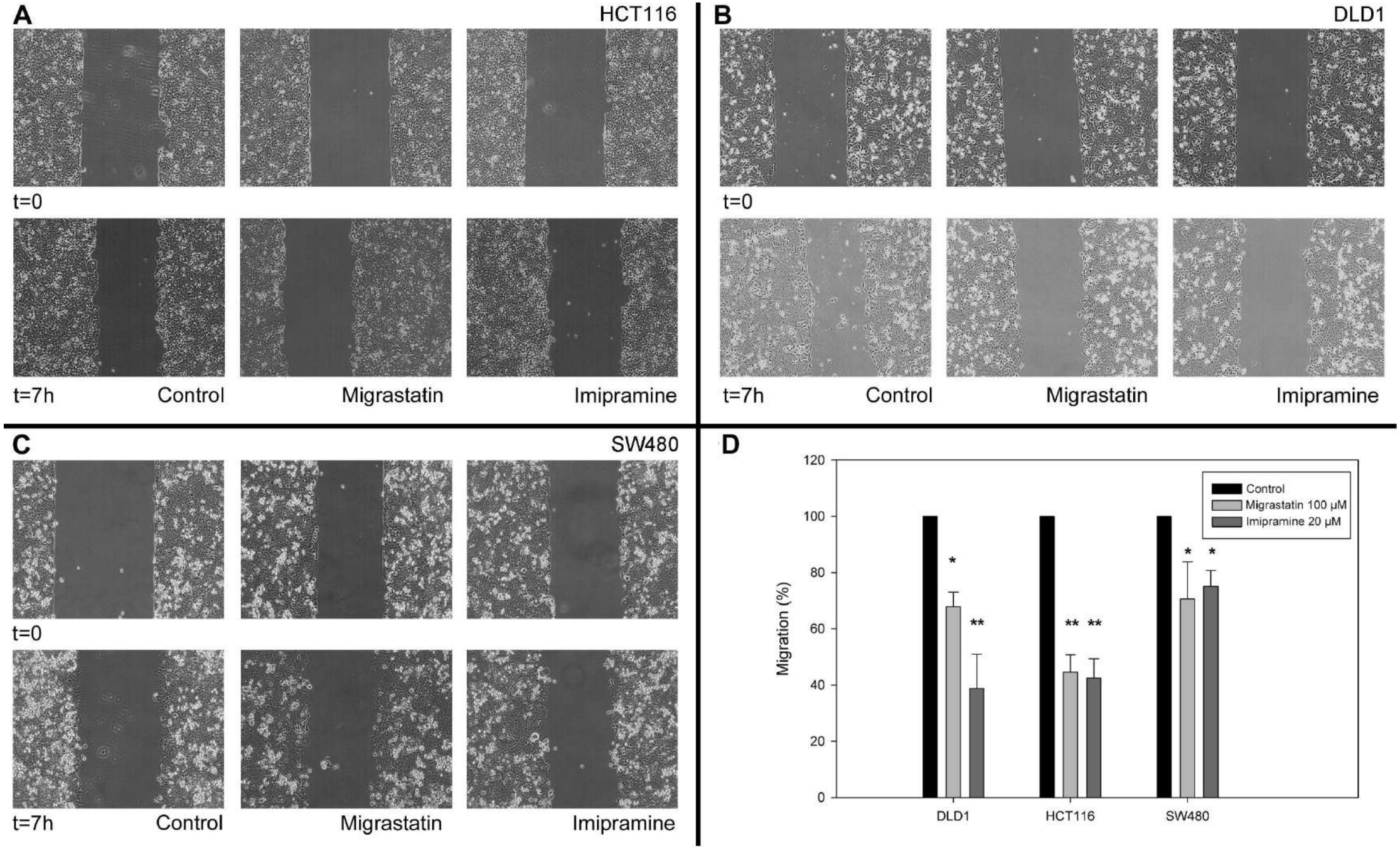

Supplementary Information S7

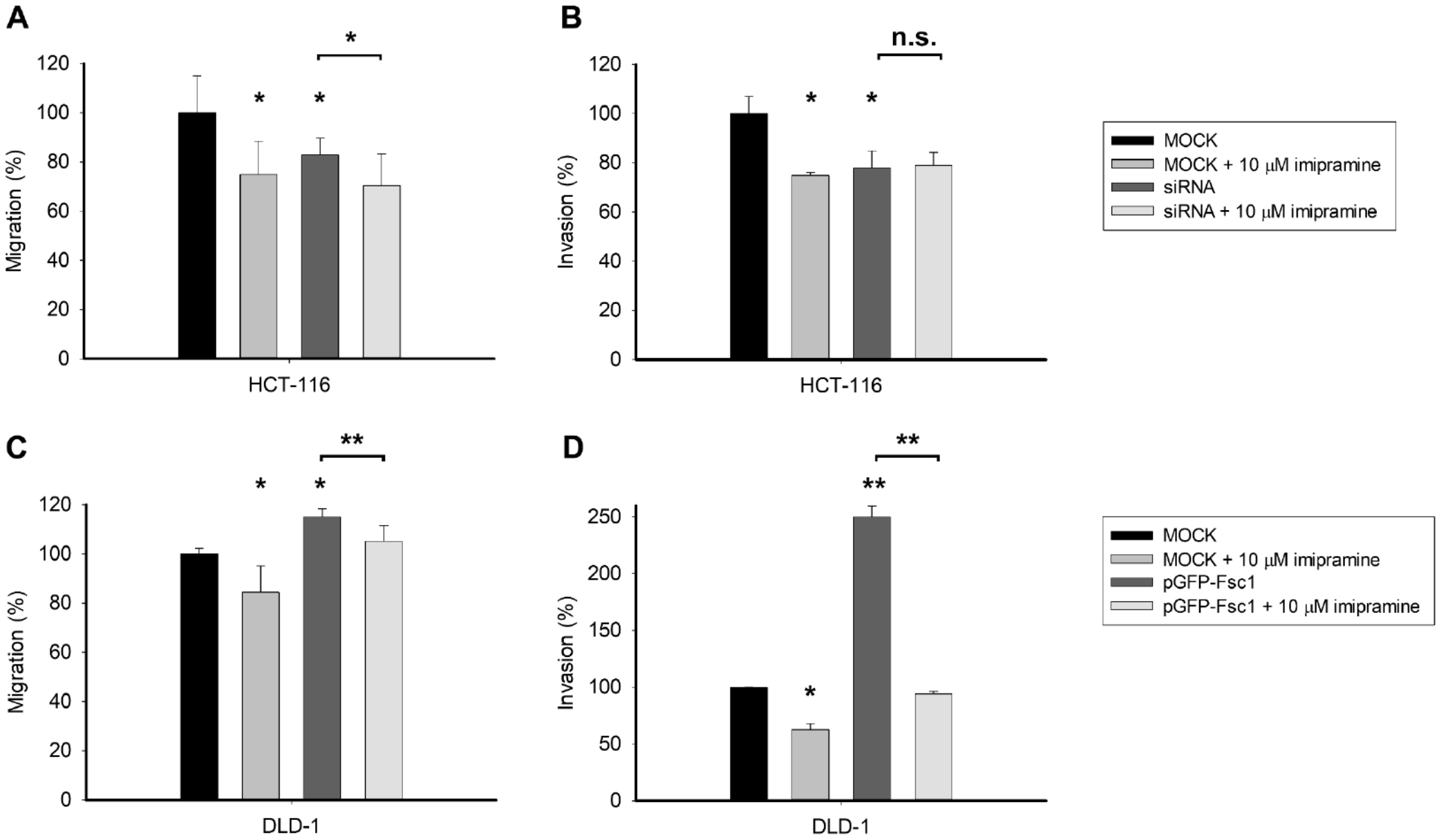

Supplementary Information S8

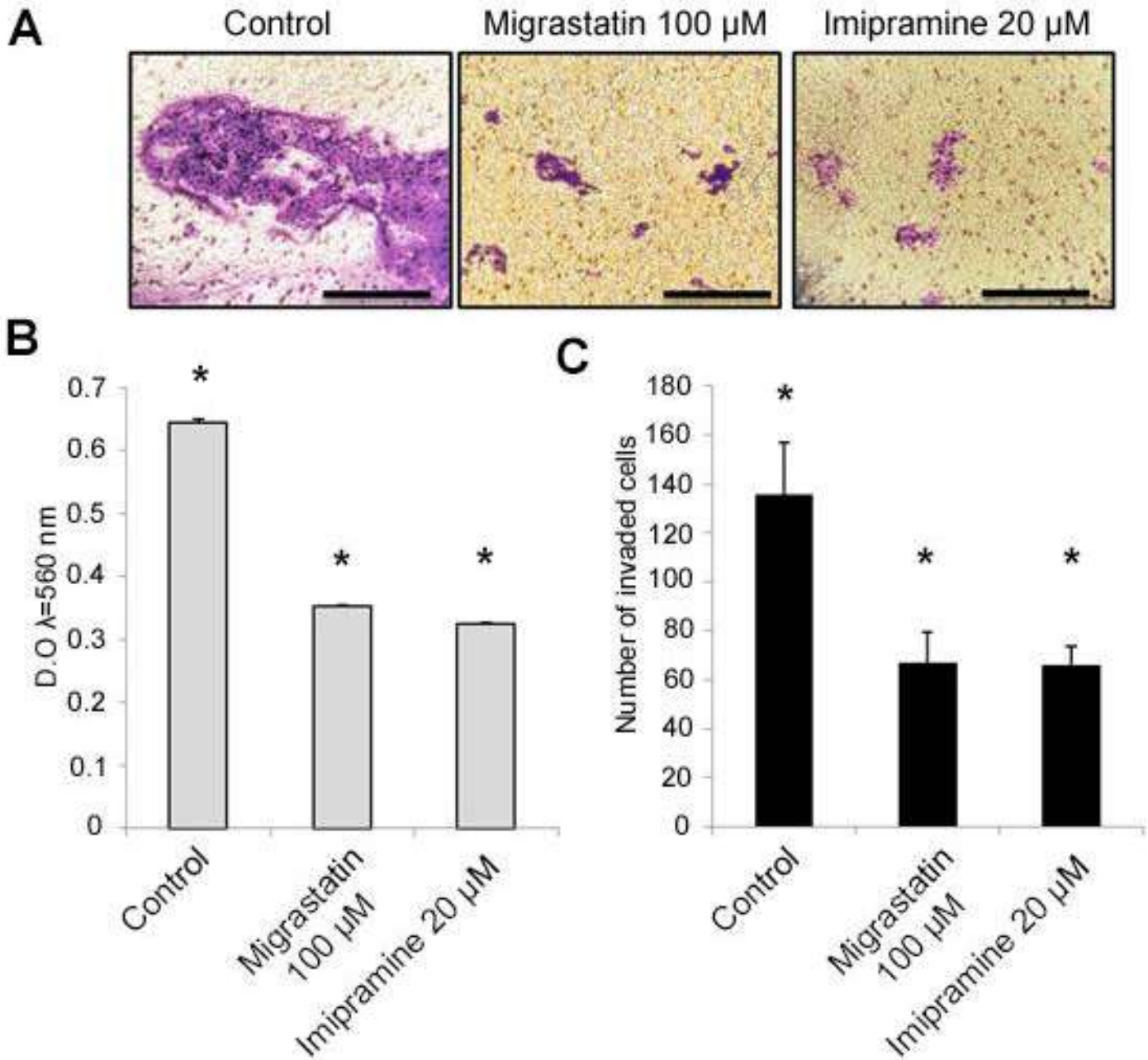

Supplementary Information S9

A

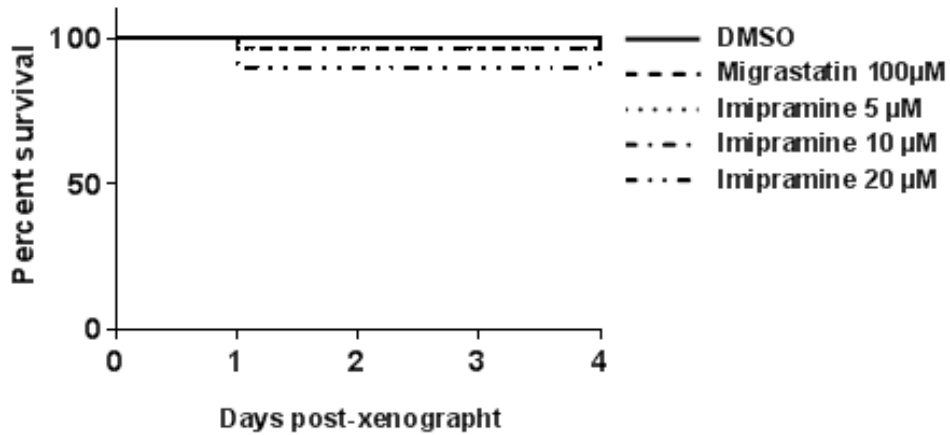

B

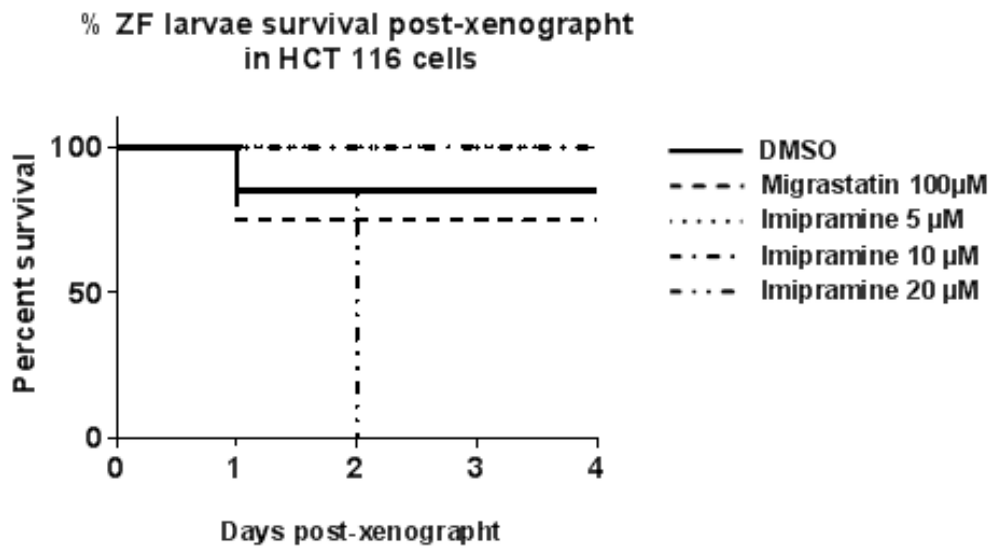

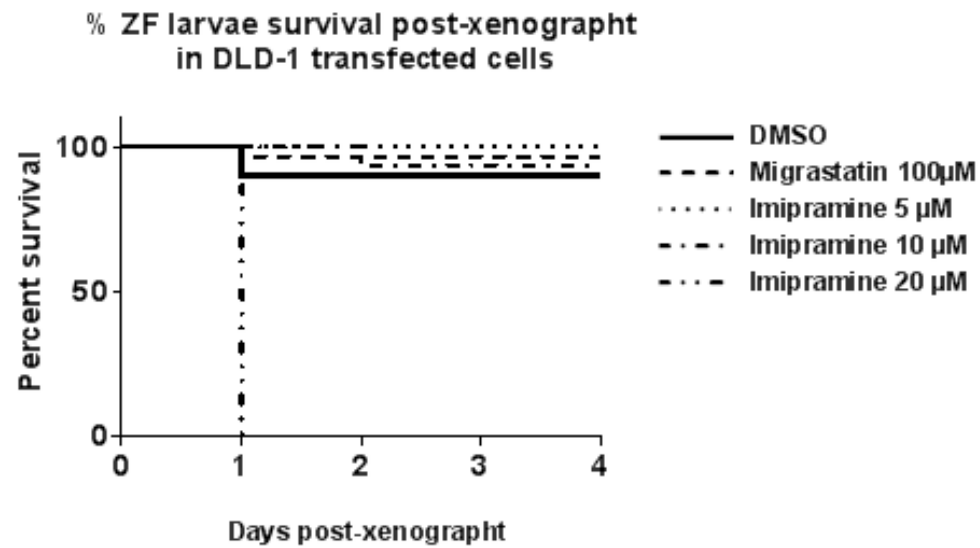

Supplementary Information S10

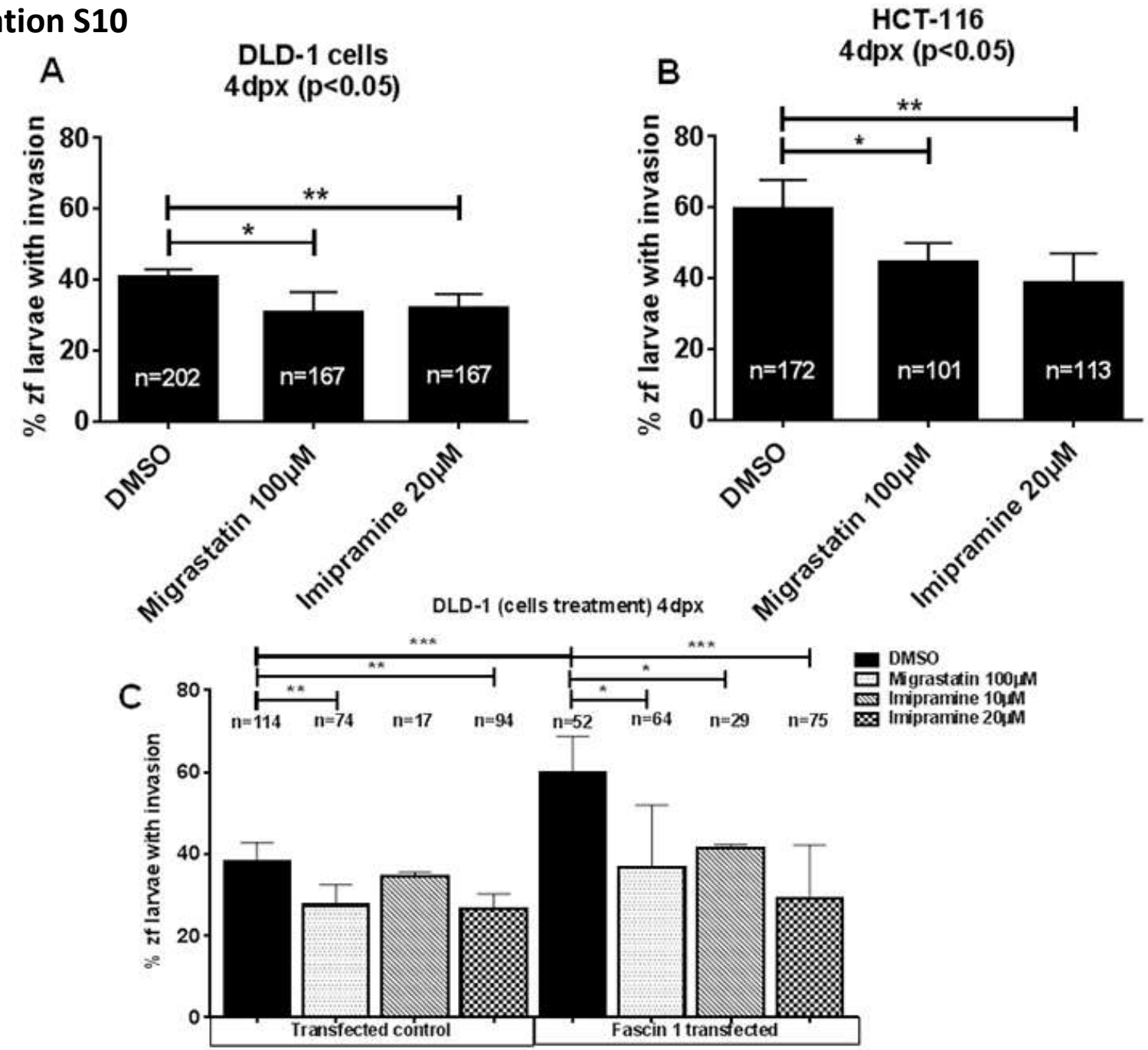

Supplementary Information S11

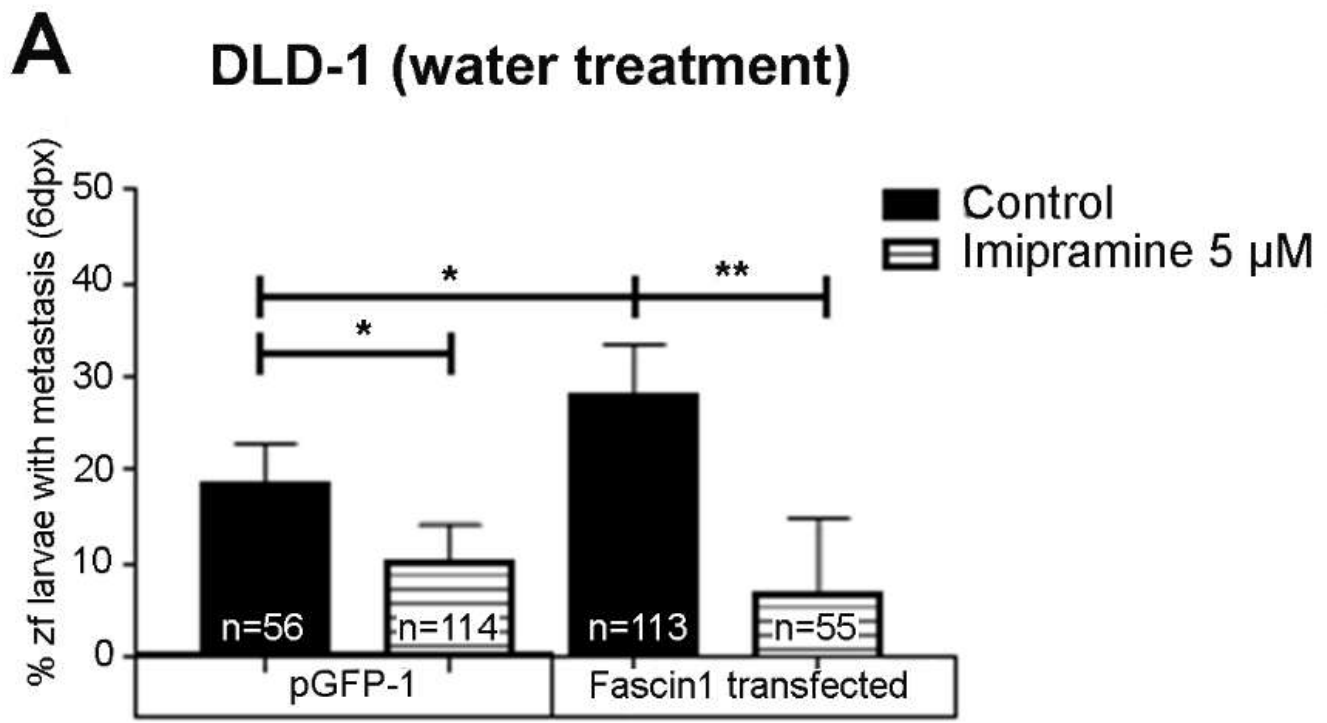

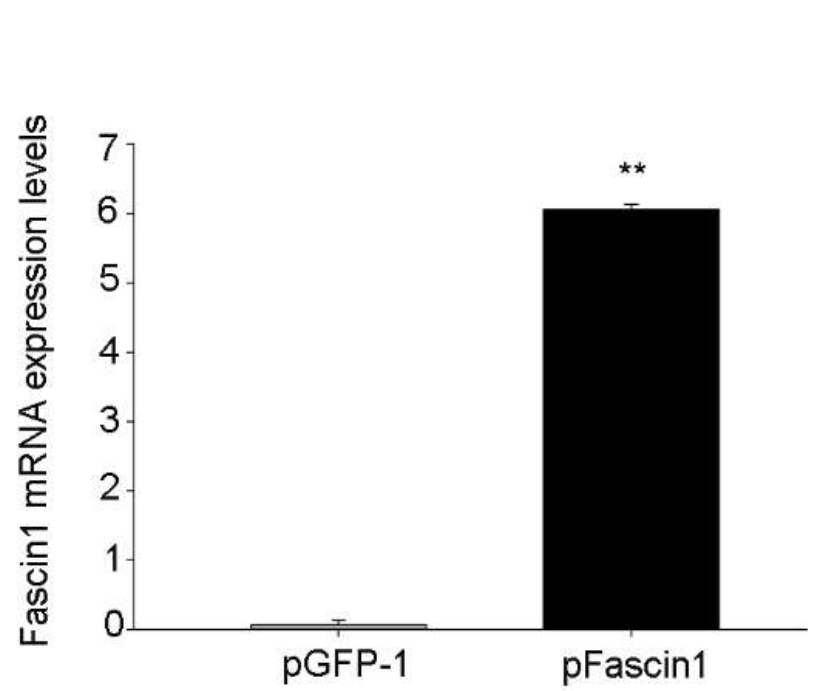

ARTÍCULO 4:

Alburquerque-González, B., Bernabé-García, Á., Bernabé-García, M., Ruiz-Sanz, J., López-Calderón, F. F., Gonnelli, L., Banci, L., Peña-García, J., Luque, I., Nicolás, F. J., Cayuela-Fuentes, M. L., Luchinat, E., Pérez-Sánchez, H., Montoro-García, S., & Conesa-Zamora, P. (2021). **The FDA-Approved Antiviral Raltegravir Inhibits Fascin1-Dependent Invasion of Colorectal Tumor Cells In Vitro and In Vivo**. *Cancers*, *13*(4), 861. https://doi.org/10.3390/cancers13040861.

Factor de impacto 2020 (JCR): 6.639; Categoría (JCR): ONCOLOGY & SCIENCE; Clasificación: 51/242 (Q1); Fecha de publicación: 2020.

cancers

MDPI

Article

The FDA-Approved Antiviral Raltegravir Inhibits Fascin1-Dependent Invasion of Colorectal Tumor Cells In Vitro and In Vivo

Begoña Alburquerque-González [1,†], Ángel Bernabé-García [2,†], Manuel Bernabé-García [3], Javier Ruiz-Sanz [4], Fernando Feliciano López-Calderón [1], Leonardo Gonnelli [5,6], Lucia Banci [5,6], Jorge Peña-García [7], Irene Luque [4], Francisco José Nicolás [2], María Luisa Cayuela-Fuentes [3], Enrico Luchinat [5,8], Horacio Pérez-Sánchez [7], Silvia Montoro-García [9,*] and Pablo Conesa-Zamora [10,*]

1 Department of Pathology and Histology, Campus de los Jerónimos, UCAM Universidad Católica San Antonio de Murcia, s/n, 30107 Murcia, Spain; balburquerque2@ucam.edu (B.A.-G.); fflopez@alu.ucam.edu (F.F.L.-C.)
2 Laboratorio de Regeneración, Oncología Molecular y TGF-ß, Biomedical Research Institute of Murcia (IMIB-Arrixaca), Carretera Madrid-Cartagena, El Palmar, 30120 Murcia, Spain; angel.bernabe@imib.es (Á.B.-G.); franciscoj.nicolas2@carm.es (F.J.N.)
3 Telomerase, Cancer and Aging Group, Biomedical Research Institute of Murcia (IMIB-Arrixaca), 30120 Murcia, Spain; manuel.bernabe@carm.es (M.B.-G.); marial.cayuela@carm.es (M.L.C.-F.)
4 Department of Physical Chemistry, Institute of Biotechnology and Excellence Research Unit of "Chemistry Applied to Biomedicine and the Environment, Spain Campus Fuentenueva s/n, University of Granada, 18071 Granada, Spain; jruizs@ugr.es (J.R.-S.); iluque@ugr.es (I.L.)
5 CERM—Magnetic Resonance Center, Università degli Studi di Firenze, Via Luigi Sacconi 6, 50019 Sesto Fiorentino, Italy; gonnelli@cerm.unifi.it (L.G.); banci@cerm.unifi.it (L.B.); eluchinat@cerm.unifi.it (E.L.)
6 Dipartimento di Chimica, Università degli Studi di Firenze, Via della Lastruccia 3, 50019 Sesto Fiorentino, Italy
7 Structural Bioinformatics and High Performance Computing (BIO-HPC) Research Group, Campus de los Jerónimos, s/n, UCAM Universidad Católica San Antonio de Murcia, Guadalupe, 30107 Murcia, Spain; jpena@ucam.edu (J.P.-G.); hperez@ucam.edu (H.P.-S.)
8 Consorzio per lo Sviluppo dei Sistemi a Grande Interfase—CSGI, Via della Lastruccia 3, 50019 Sesto Fiorentino, Italy
9 Cell Culture Lab, Facultad de Ciencias de la Salud, Campus de los Jerónimos, s/n, UCAM Universidad Católica San Antonio de Murcia, Guadalupe, 30107 Murcia, Spain
10 Laboratory Medicine Department, Group of Molecular Pathology and Pharmacogenetics, Biomedical Research Institute from Murcia (IMIB), Hospital Universitario Santa Lucía, c/Mezquita sn, 30202 Cartagena, Spain
* Correspondence: smontoro@ucam.edu (S.M.-G.); pablo.conesa@carm.es (P.C.-Z.); Tel.: +34-9681-286-02 (Ext. 951615) (P.C.-Z.)
† These authors contributed equally to this paper.

check for updates

Citation: Alburquerque-González, B.; Bernabé-García, Á.; Bernabé-García, M.; Ruiz-Sanz, J.; López-Calderón, F.F.; Gonnelli, L.; Banci, L.; Peña-García, J.; Luque, I.; Nicolás, F.J.; et al. The FDA-Approved Antiviral Raltegravir Inhibits Fascin1-Dependent Invasion of Colorectal Tumor Cells In Vitro and In Vivo. *Cancers* **2021**, *13*, 861. https://doi.org/10.3390/cancers13040861

Academic Editor: Serge Roche

Received: 28 January 2021
Accepted: 15 February 2021
Published: 18 February 2021

Simple Summary: Colorectal cancer (CRC) is the third leading cause of cancer-related deaths worldwide. Serrated adenocarcinoma (SAC) has been recently recognized by the WHO as a histological CRC with bad prognosis. Consistent with previous evidence, our group identified Fascin1 as a protein directly related to the invasiveness of tumor cells, overexpressed and positively correlated with worse survival in various carcinomas, including SAC. Therefore, Fascin1 has emerged as an ideal target for cancer treatment. In the present study, virtual screening has been carried out from a library of 9591 compounds, thus identifying the FDA-approved anti-retroviral raltegravir (RAL) as a potential Fascin1 blocker. In vitro and in vivo results show that RAL exhibits Fascin1-binding activity and Fascin1-dependent anti-invasive and anti-metastatic properties against CRC cells both in vitro and in vivo.

Abstract: Background: Fascin1 is the key actin-bundling protein involved in cancer invasion and metastasis whose expression is associated with bad prognosis in tumor from different origins. Methods: In the present study, virtual screening (VS) was performed for the search of Fascin1 inhibitors and RAL, an FDA-approved inhibitor of human immunodeficiency virus-1 (HIV-1) integrase, was

identified as a potential Fascin1 inhibitor. Biophysical techniques including nuclear magnetic resonance (NMR) and differential scanning fluorimetry (DSF) were carried out in order to confirm RAL as a Fascin1 blocker. The effect of RAL on actin-bundling activity Fascin1 was assessed by transmission electron microscopy (TEM), immunofluorescence, migration, and invasion assays on two human colorectal adenocarcinoma cell lines: HCT-116 and DLD-1. In addition, the anti-metastatic potential of RAL was in vivo evaluated by using the zebrafish animal model. Results: NMR and DSF confirmed in silico predictions and TEM demonstrated the RAL-induced disorganization of the actin structure compared to control conditions. The protrusion of lamellipodia in cancer cell line overexpressing Fascin1 (HCT-116) was abolished in the presence of this drug. By following the addition of RAL, migration of HCT-116 and DLD-1 cell lines was significantly inhibited. Finally, using endogenous and exogenous models of Fascin1 expression, the invasive capacity of colorectal tumor cells was notably impaired in the presence of RAL in vivo assays; without undesirable cytotoxic effects. Conclusion: The current data show the in vitro and in vivo efficacy of the antiretroviral drug RAL in inhibiting human colorectal cancer cells invasion and metastasis in a Fascin1-dependent manner.

Keywords: Fascin1; raltegravir; migrastatin; invasion; migration; zebrafish xenograft; colorectal cancer

1. Introduction

Colorectal cancer (CRC) is the third leading cause of cancer-related deaths worldwide [1]. Serrated adenocarcinoma (SAC) has been recently recognized as a new subtype of CRC [2]. Several drugs are currently being used for the cancer treatment following different mechanisms of action. Therapeutic strategies include drugs targeting specific proteins found altered in cancer cells thus decreasing their growth and survival rate. Hence, during the past few decades, identifying novel chemical compounds that modulate cellular targets has emerged as an exciting approach for the development of selective anticancer treatments. However, given the fact that SAC, compared to conventional colorectal carcinoma, exhibits a higher frequency of *KRAS* or *BRAF* mutations and that most SACs are microsatellite stable [3,4], this CRC subtype is especially resistant to targeted therapy such as anti-EGFR and immune checkpoint inhibitors, respectively. Therefore, there is an urgent need to count with a targeted molecular therapy for treating SAC [5].

Consistent with previous evidence, Fascin1 has been identified as an actin-bundling protein, a key molecule in the invasiveness of tumor cells which is overexpressed and positively correlated with worse survival in various carcinomas, including SAC [6]. Numerous studies have implicated Fascin1 as a biomarker for aggressive carcinomas [6,7]. It is generally believed that Fascin1 plays a mechanical role in driving tumor-cell migration, invasion, and metastasis by facilitating actin-based membrane protrusions such as filopodia and lamellipodia, whereas it is not expressed by normal epithelia [8,9]. Therefore, Fascin1 has emerged as an ideal target for cancer treatment [7,10] and the discovery of Fascin1 blockers deserves further research [11]. Currently, Fascin1 inhibitors such as migrastatin (MGS) and N-(1-(4-(trifluoromethyl) benzyl)-1H-indazol-3-yl) furan-2-carboxamide (G2) analogues such as 4-methyl-N-(1-(4-(trifluoromethyl) benzyl)-1H-indazol-3- yl)isoxazole-5-carboxamide (NP-G2-029) have been tested in vitro and in vivo as they are likely to suppress tumor-cell migration by inhibiting the actin-bundling activity [12–14].

Recent increased knowledge in molecular sciences and bioinformatics is currently contributing to the discovery of new potential drug targets. This has changed the paradigms of anticancer drug discovery toward molecularly targeted therapeutics. Our previous data further illustrates the use of this therapeutic targeted approach [12]. In this study, our group performed virtual screening (VS) for the search of anti-Fascin1 compounds, and found that RAL, an FDA-approved inhibitor of human immunodeficiency virus-1 (HIV-1) integrase, showed Fascin1-binding activity. Additionally, we show that RAL displays important inhibitory effects on lamellipodium formation, migration, and invasion

in different colorectal cancer cell lines. Moreover, RAL treatment resulted in significant reduction of invasion of DLD-1 overexpressing Fascin1 and HCT-116 in zebrafish larvae xenografts. Our results further indicate the use of RAL as a potential treatment for CRC based on in silico molecular drug-target identification.

2. Materials and Methods

2.1. Virtual Screening

Molecular docking-based VS calculations using Autodock Vina [15] were applied to propose FDA compounds repurposed as Fascin1 inhibitors. For such a purpose, the structural model for Fascin1 was extracted from the crystal structure of protein data bank (PDB) with code 6B0T and converted to PDBQT format with MGLTOOLS (http://mgltools.scripps.edu, accessed on 7 January 2021 at 12:30) using default parameters. Ligand cocrystalized with Fascin1 in 6B0T (NP-G2-029) was also converted to PDBQT format. Next, this protein model was screened with Autdock Vina against a subset of the DrugBank library (version 5.0; of 9591 compounds, including 2037 approved by the American FDA, 96 nutraceuticals, and 6000 experimental) and compound NP-G2-029.

2.2. Molecular Dynamics

Molecular dynamics (MD) was applied to selected compound from VS calculations and NP-G2-029 in order to study the dynamics evolution of selected Fascin1-ligand complexes and check stability of the ligands in the binding site. MD simulations were carried out with the GPU version of Desmond included in the Maestro suite 2019.4 (Schrödinger LLC), on a server with a NVIDIA QUADRO PRO 5000. Complexes were solvated in an aqueous environment in a cubic box with a minimal distance of 10 Å between each ligand and the box boundary (for periodic boundary conditions). Afterwards, systems were neutralized in 0.15M NaCl and the OPLS3 force field and the TIP3P-TIP4P water models were employed [16]. Initially, the systems were setup in the NPT ensemble, and pressure was controlled using the Martyna-Tobias-Klein methodology, and the Nose-Hoover thermostat was employed to keep the system near 310K. Production of MD trajectories were extended to 100 nanoseconds (ns) per system. Resulting MD trajectories were analyzed in terms of averaged protein–ligand interactions over time and in terms of the root-mean-square deviation (RMSD) of fluctuations.

2.3. Structural Comparison

The Pocketalign web server (http://proline.physics.iisc.ernet.in/pocketalign/, accessed on 7 January 2021) was used for the alignment of the binding pockets of the structural models for proteins Fascin1 (PDB code 6B0T) and Aldolase A (PDB code 3B8D). After performing the structural alignment of these defined substructures Pocketalign reports information about three-dimensional matching between residue types.

2.4. Compound Purchase-Chemistry

Ralteagravir (RAL) potassium (C20H20FKN6O5; PM 482.51) was purchased from Sigma Aldrich. Migrastatin (MGS) was synthesized by AnalytiCon Discovery (NP-006108) and provided by MolPort (Riga, Latvia).

2.5. Recombinant Fascin1 Expression and Purification

Recombinant Fascin1 for in vitro studies was expressed in BL21-gold (DE3) *E. coli* strain transformed with the pGEX-6P-2A plasmid encoding the full-length human Fascin1 (UniProt Q16658) fused at the N-terminus with glutathione-S-transferase (GST) and the human rhinovirus 3C protease cleavage site. This construct was kindly provided by Dr. S. Windhorst from University Medical Center Hamburg-Eppendorf, Hamburg, Germany). Cells were grown at 37 °C in Terrific Broth (TB) medium previously inoculated with a preculture of transformed cells grown overnight at 28 °C in TB. Protein expression was induced at OD_{600} = 0.8 with 0.5 mM IPTG and carried out for 5 h at 37 °C. The cells were

centrifuged at 4 °C, 5000× g for 15 min, resuspended in binding buffer (20 mM Sodium phosphate buffer, 150 mM NaCl, pH 7.3), and lysed by ultrasonication in ice bath and centrifuged for 40 min at 4 °C, 6000 g. Fascin1 was purified by affinity chromatography. The supernatant was loaded at 2 mL/min in a 5 mL GSTrap FF (Cytiva) column pre-equilibrated with binding buffer, further washed with 10 CV of binding buffer and 10 CV of cleavage buffer (50 mM Tris-HCl, 150 mM NaCl, 1 mM EDTA, 1 mM dithiothreitol, pH 7.5). Proteolytic cleavage was performed on-column by loading a PreScission protease stock solution (Cytiva) diluted 1/25 in cleavage buffer according to the manufacturer protocol and incubating at 4 °C for 4 h. Fascin1 was eluted with 3 CV of cleavage buffer (5 mL/min), concentrated with a centrifugal concentrator (MWCO 30 kDa) at 4000× g, T < 20 °C, and quantified by absorption at 280 nm using a predicted molar extinction coefficient ε_{280} = 68,465 M^{-1} cm^{-1}. A protein yield of ~40 mg/L was estimated.

2.6. Thermofluor and Fluorescence Titration

Differential Scanning Fluorimetry (Thermofluor) assays were performed using a Biorad C1000 Touch Thermal Cycler CFX96 RT-PCR system in a 96-well format. Twenty-five µL reaction mixtures were set up containing 2 µM Fascin1 (Hypermol, Bielefeld, Germany) in 20 mM Hepes, 150 mM NaCl, 1mM DTT, and 5% sucrose at pH 7.4, in the presence of SYPRO Orange (1000-fold dilution from the commercial stock (Invitrogen, Carlsbad, CA, USA). The indicated compounds, prepared at 10 mM in DMSO, were added to each well to a diluted final concentration of 1 mM and 10% DMSO. Three replicates per compound together with six internal controls, containing only free protein in 10% DMSO, were included in the 96-well plates. The PCR plates were covered and subsequently shaken, centrifuged, incubated for 2 min at 20 °C inside the RT-PCR machine, and heated from 20 to 100 °C at a 1 °C/min scan-rate. Fascin1 thermal denaturation profiles were obtained recording the fluorescence intensity for the FAM, HEX, and T-Red predefined filters. The derivative of the fluorescence curve was used to determine the Tm. Changes in Tm associated to ligand binding were estimated taking the average Tm value derived from the free protein internal controls. Fascin1 was extensively dialyzed against the appropriate buffer prior to each titration experiment. Fascin1 concentration was determined by measuring absorbance at 280 nm using an extinction coefficient of 67,840 $cm^{-1} \cdot M^{-1}$.

Fluorescence titration experiments were performed in a Cary Eclipse spectrofluorometer (Varian Inc., Palo Alto, CA, USA). Fascin1 solution at 15 µM (14.7 µM) was titrated with each compound by adding increasing volumes of concentrated solutions. Emission spectra were recorded between 307 and 500 nm at 25 °C in 10% DMSO, 100 mM NaCl, 20 mM Hepes, pH 7.4, with the excitation wavelength fixed at 280 nm. Binding isotherms were generated using the changes in spectral area and fitted using ORIGIN 7.0 (Microcal Inc. Malvern panalytical, Worcerstershire, UK) to a one-site equilibrium binding model, according to the following Equation (1):

$$F = F_f + \left(F_b - F_f\right) \cdot \frac{(P_T + L_T + K_d) - \sqrt{(P_T + L_T + K_d)^2 - 4 \cdot P_T \cdot L_T}}{2 \cdot P_T} \quad (1)$$

where F_f and F_b are the fluorescence signal of free and bound Fascin1 and P_T and L_T are the total protein and ligand concentration, respectively, at each addition point.

2.7. Ligand-Observed NMR

Saturation transfer difference (STD) and WaterLOGSY (WL) NMR experiments were recorded at 298 K with a Bruker Avance NEO 700 MHz (Bruker Corp., Billerica, MA, USA) equipped with a 5 mm cryogenically cooled TCI probe. Stock solutions of each ligand were prepared by dissolving the powder in d_6-DMSO to a final concentration of 50 mM. For the NMR experiments, a protein:ligand ratio of 1:50 was chosen, that is within the working range of both STD and WL experiments. Protein NMR samples contained 10 µM

of Fascin1 and 500 μM of each ligand in NMR buffer (phosphate buffered saline (PBS, Gibco), pH 7.4 + 10% D_2O). Control samples contained 10 μM of each ligand dissolved in NMR buffer. The final DMSO concentration in all NMR samples was 1%. For each sample, a 1D ^1H reference spectrum, a STD and a WL experiment were recorded. STD spectra (stddiffesgp.3 pulse program [17] were acquired with 512 scans with on-resonance irradiation at 0 ppm and off-resonance irradiation at −40 ppm. A train of 40 Gaussian shaped pulses of 50 ms was used, for a total saturation time of 2 s. Final STD spectra were obtained by internal subtraction of the saturated spectrum from the reference spectrum. WL spectra (ephogsygpno.2 pulse program [18] were acquired with 1024 scans with a 7.5 ms selective 180° Gaussian shaped pulse at the water signal frequency and a CLEANEX spinlock time of 30 ms. For both STD and WL, a spectral width of 16 ppm, 2.0 s relaxation delay, 16384 data points for acquisition, and 65536 points for transformation were used. The spectra were processed with the Bruker TOPSPIN software by applying a 1 Hz exponential line broadening.

2.8. Transmission Electron Microscopy Detection

Transmission electron microscopy (TEM) was assessed, following previous methodology by Jansen et al., 2011 [19]. Briefly, purified actin (21 μM) was polymerized according to the protocol from the Actin-Binding Protein Biochem Kit^{TM} Muscle Actin (Cytoskeleton Inc., Denver, CO, USA) and then incubated with human recombinant Fascin1 (Hypermol, Bielefeld, Germany) (molar ratio 1:1) for 30 min at room temperature. Fascin1 was previously incubated for 2 h at room temperature with 0.1% DMSO (control), 100 μM MGS, 10 μM imipramine, 10 μM G2 compound, or 30 μM RAL. The samples were directly adsorbed onto 200 mesh copper grids for 30 sec, blotted to remove excess solution, washed twice with distilled water, and negatively stained with 1% (w/v) uranyl acetate for 30 s, blotted, and dried again. The TEM study of actin filaments and Fascin1-actin bundles was performed on a PHILIPS TECNAI 12 transmission electron microscope (FEI, Osaka, Japan) at an accelerating voltage of 80 kV and a magnification up to 135,000X. Images were captured on a coupled device camera (Megaview III). The numbers of filaments per bundle were counted manually in 20 pictures/condition and statistically analyzed (Mann–Whitney test).

2.9. Cell Culture

Two human colorectal adenocarcinoma cell lines, HCT-116 and DLD-1, and HaCaT (human spontaneously immortalized keratinocyte) [20] cells were obtained from the American Type Culture Collection (ATCC, Rockville, MD, USA). All cell lines were cultivated using standard medium: high-glucose Dulbecco's Modified Eagle's Medium (DMEM) supplemented with 10% heat-inactivated fetal bovine serum (FBS), 50 U/mL penicillin, and 50 μg/mL streptomycin (all from Sigma Aldrich Chemical Co., Darmstadt, Germany), at 37 °C, 5% CO_2, and 95% humidified atmosphere. Subculturing was performed when cells reached 90% confluence. Cell RNA extraction and qPCR for Fascin1 expression quantification was performed as previously described [12]. In vivo assays, the human colorectal carcinoma cells were genetically overexpressed (DLD-1) for Fascin1, as previously reported by our group [13].

2.10. Cell Viability Assay

Exponentially growing cells were plated in flat-bottomed 96-well plates (Nunc, Roskilde, Denmark) in triplicate (1500 cells/well). Cells were treated with a series of concentrations from 5 μM to 100 μM of either MGS or RAL up to 3 days (24, 48 and 72 h) in a 5% CO_2 humidified atmosphere. Control cells were treated with a drug carrier, control (0.1% DMSO). Cells were assayed for viability as follows: In brief, Dulbecco's phosphate-buffered saline (DPBS) supplemented with 1.9 mg/mL tetrazolium (MTT) pH 7.2 was added to the cells (30 μL/well). After incubation at 37 °C for 4 h, the medium was carefully aspirated. The formazan crystals were dissolved in 200 μL DMSO for 30 min, and the absorbance was

read in a microtiter plate reader at 570 nm and 620 nm as reference. Results were calculated as cell viability (%) = average optical density (O.D.) of wells/average O.D. of control wells.

2.11. Cell-Migration Assay

Cell migration was studied using HCT-116 and DLD-1 cell lines by performing a scratch-wound healing assay in standard medium supplemented with 5% FBS. Typically, 50,000 cells were plated in low 35 mm dishes with culture inserts following manufacturer instructions (Ibidi, Martinsried, Germany). After appropriate cell attachment and monolayer formation (around 24 h), inserts were removed with sterile forceps to create a wound field of approximately 500 µm. Detached cells were gently removed with DPBS before the addition of drugs. Confluent cells were incubated in one of the following treatments: control (0.1% DMSO), 100 µM MGS, or 30 µM RAL. Cells were then placed in a cell-culture incubator and they were allowed to migrate. At 0, 4, and 7 h (linear growth phase), 10 fields of the injury area were photographed with an inverted phase contrast microscope using 10× magnification. For each time point, the area uncovered by cells was determined by Image J software (National Institute of Health, Bethesda, MD, USA). Each treatment was performed in triplicate.

The migration speed of the wound closure was given as the percentage of the recovered area at each time point, relative to the initially covered area (t_0). The velocity of wound closure (%/h) was calculated according to the following Equation (2):

$$\textbf{Slope}\left(\%\frac{\boldsymbol{area}}{\mathbf{h}}\right) = \frac{(\%\ \textbf{covered area}\ t_x) - (\%\ \textbf{covered area}\ t_o)}{(t_x - t_o)} \quad (2)$$

Slopes are expressed as percentages relative to control conditions.

2.12. Transwell Invasion Assay

The invasive capacity of HCT-116 and transfected DLD-1 overexpressing Fascin1 was determined using Cytoselect TM 24 Well Cell Invasion Assay (Basement Membrane Colorimetric Format) with Matrigel® coated Transwell chambers (8 µm pore size) (Cell Biolabs Inc., San Diego, CA, USA). In brief, cells (1×10^6) were resuspended in serum free medium with corresponding inhibitors and seeded into the upper chamber. Additionally, 500 µL of standard medium was added to the well. After 24 h of incubation, cells that remained on the upper chamber were scraped away with a cotton swab, and the cells at the bottom side of the filter were eluted and quantified at an absorbance of 560 nm.

2.13. Wounding-Scratch Assay Immunofluorescence

Round coverslips (Thermo Fisher, Waltham, MA, USA) were seeded in 6-well plate with either HCT-116 or HaCaT cells in standard medium. When cells reached 100% confluence, standard medium was replaced by a standard fresh-serum free medium. Then, wounding was performed by transversally dragging a sterilized razor blade on the central area of the coverslips. Just after wounding, cells were treated with either 100 µM MGS, 30 µM RAL, 10 ng/mL Epidermal Growth Factor (EGF), or 50 µM of MEK inhibitor PD98059 (MEKi) (both from Sigma-Aldrich, St Louis, MO, USA), and cells were left for 24 h. Afterwards, a subset of samples were fixed with Bouin solution (5% Acetic acid, 9% Formaldehyde and 0.9% Picric acid, all from Sigma-Aldrich, St Louis, MO, USA) for Fascin1 protein staining. Alternatively, another subset of samples was fixed 15 min with 4% formaldehyde DPBS (PanReac AppliChem, Barcelona, Spain) for actin protein staining. Both types of fixations were DPBS washed three times and subsequently permeabilized for 15 min by using 0.3% Triton X-100/DPBS solution. Then, samples were incubated for 30 min in blocking solution ((0.3% bovine serum albumin (BSA)) (Santa Cruz Biotechnology, Heidelberg, Germany), 10% FBS (Thermo Fisher Scientific, Waltham, MA, USA), 0.1% Triton X-100 (Sigma-Aldrich, St Louis, MO, USA), and 5% skimmed milk (Beckton Dickinson, Franklin Lakes, NJ, USA) in DPBS. Afterwards, samples were incubated for 1 h with anti-Fascin1 antibody (1/250) (55K-2 clone; Santa Cruz Biotechnology, Heidelberg,

Germany). Samples were washed 3 times with 0.1% Triton X-100/DPBS and incubated with the appropriate fluorescent-labelled secondary antibodies; for Fascin1 Alexa fluor 488-conjugated anti-mouse IgG (Molecular Probes, Thermo Fisher Scientific, Waltham, MA, USA) were used. To reveal actin and nuclei, samples were incubated with Alexa fluor 594-labelled phalloidin (Molecular Probes, Thermo Fisher Scientific, Waltham, MA, USA) and Hoechst 33258 (Fluka, Biochemika, Sigma-Aldrich, St Louis, MO, USA) for 30 min at room temperature in a wet chamber. All preparations were examined with a confocal microscope (LSM 510 META from ZEISS, Jena, Germany), and representative images were taken. Quantification of lamellipodia number was performed by counting elements in 20 random pictures per sample at 64× Student´s *t*-test was applied for statistical analysis.

2.14. Zebrafish Invasion and Metastasis Assays

The colonization of zebrafish (*Danio rerio*) embryos by human cancer cells was performed as previously described [21]. Trypsinized, washed colorectal cancer cells were stained with fluorescent CM-Dil (Vybrant, Invitrogen), and 50–100 labeled cells were injected into the yolk sac of dechorionated zebrafish embryos. The viability of zebrafish embryos was assessed under 100 µM MGSor 30 µM RAL treatments and under the combined effect of compound treatment and tumor-cell injection. The evaluation criteria for embryos being colonized by human cancer cells was the presence of more than three cells outside the yolk sac. Metastasis assay was based on previous works by Fior et al., in which a metastatic potential assay on zebrafish was performed [22]. Transfected DLD-1 overexpressing Fascin1 and native HCT-116 cells were stained and xenografted as already mentioned. From the third day post-injection, larvae were fed with ZEBRAFEED by Sparos (<100 µm), and treatments were changed daily. At day six post-injection, larvae were examined for monitoring tumor growth and invasion using a fluorescent microscope. The evaluation for metastasis potential by human cancer cells was the presence of cell colonies (dividing cells) outside the yolk sac. Fish with fluorescently labelled cells appearing outside the implantation area at 2 h post-injection were excluded from further analysis. All the fish were incubated at 35 °C and analyzed with a SteReo Lumar V12 stereomicroscope equipped with an AxioCam MR5 camera (Carl Zeiss). The percentage of invasion and the presence of cell colonies were calculated by the researcher without previous knowledge of the experiment treatment conditions. The experiments were repeated in triplicate, obtaining an average value after four days post-xenograft (invasion assay) and six days post-xenograft (metastasis assay).

All the protocols in the manuscript comply with the recommendation, the approval of which was obtained from the participant institutions and in accordance with the ethical standards laid down in the 1964 Declaration of Helsinki and its later amendments.

2.15. Data Analysis

Data are expressed as mean ± standard deviation (SD). Data were analyzed for statistical differences by the Student's t-test for paired and unpaired data after testing for normal distribution of the data. For in vitro experiments, Mann–Whitney statistical analysis was also performed. Differences were considered significant at an error probability of $p < 0.05$. SPSS 21.0 software that was used for the rest of statistical analyses (SPSS, Inc., Chicago, IL, USA). One-way ANOVA (analysis of variance) with post hoc comparisons based on the Tukey's multiple comparisons test was applied.

3. Results

3.1. Virtual Screening and Molecular Dynamics

After VS calculations were finished, the top 20 compounds were selected in terms of docking score. In this list, NP-G2-029 was detected. Next, and after the visual inspection of resulting docking poses for these compounds, we prioritized ligands that shared the halogenated aromatic ring moiety of NP-G2-029 and the key interactions it establishes with neighboring residues, specifically pi–pi stacking with TRP101 and hydrophobic interactions

with VAL134. We thus selected RAL (DrugBank code DB06817) following these criteria, and then we performed molecular dynamics (MD) for these two protein–ligand complexes. Both complexes yield RMSD fluctuation values less than 4 Å, which implies stability of both ligands in the studied Fascin1-binding site. In Figure 1, we can observe a 2D representation of the averaged protein–ligand interactions over the 100 ns trajectories, while the details can be checked in Appendix A (Figure A1). Both compounds share similar interaction patterns and RAL forms in addition to a dense network of hydrogen bonds with neighboring water molecules, which might be related to an increase of stability if we compare to NP-G2-029.

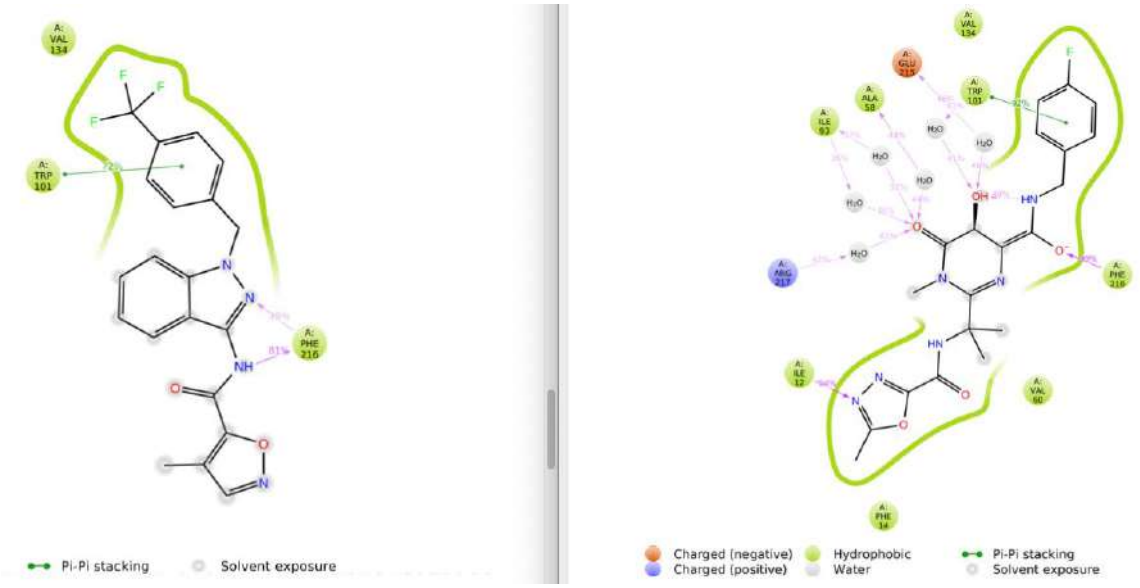

Figure 1. 2D representation of main protein–ligand interactions averaged over 100 ns between Fascin1 and NP-G2-029 (**left**) and raltegravir (RAL) (**right**).

3.2. Differential Scanning Fluorimetry (Thermofluor) Study of Binding to Fascin1

Binding of RAL to Fascin1 was investigated using Thermofluor (differential canning fluorimetry) assays, as described before [12]. The thermal unfolding profile of the protein, alone or in the presence of the putative ligand, was monitored following the fluorescence signal of Sypro Orange, a hydrophobic dye that increases its fluorescence signal upon binding to the hydrophobic patches that become exposed as the protein unfolds. Ligand binding increases the Tm of the unfolding transition in an amount proportional to the ligand-binding affinity.

As shown previously by Alburquerque-González et al. [12], at pH 7.4, Fascin1 unfolds in a single transition showing no concentration dependency and good tolerance to dimethyl sulfoxide (DMSO). RAL at a final concentration of 1 mM in 10% DMSO was tested for binding to 2 μM Fascin1, inducing a modest stabilization of the protein, which was indicative of a weak to moderate interaction with Fascin1. As shown in Figure 2, the binding of RAL to Fascin1 was further validated in vitro using fluorescence titration experiments, which rendered a dissociation constant in the high microMolar range (Kd = 180 ± 10 μM).

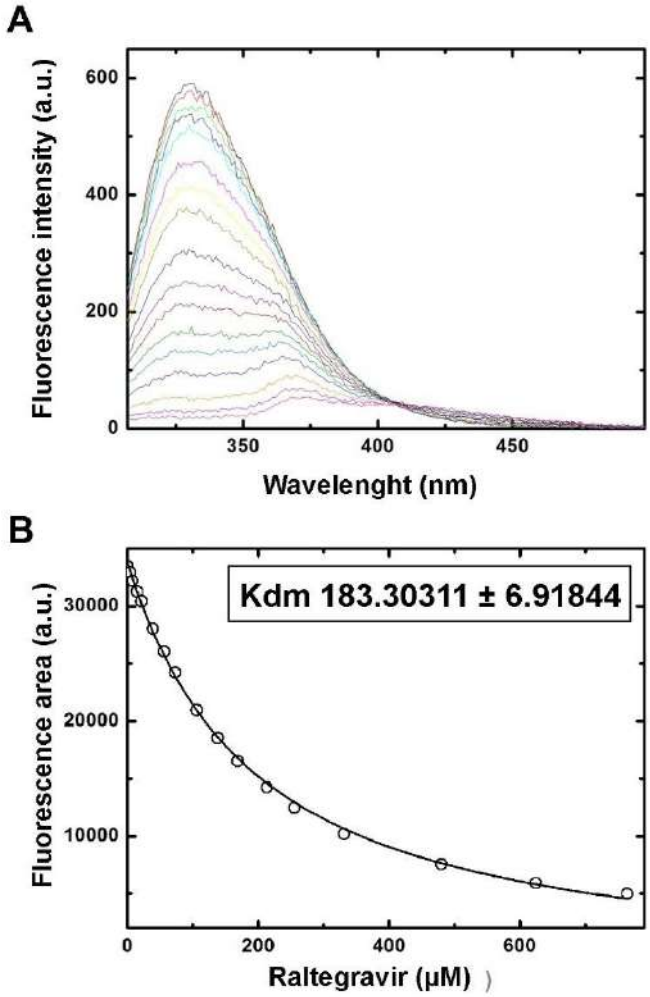

Figure 2. In vitro characterization of raltegravir binding to Fascin1. (**A**) Fluorescence titration experiment of Fascin1 with raltegravir. The fluorescence emission spectra of free Fascin1 are shown as a black line. Colored curves correspond to the emission spectra of Fascin1 in the presence of increasing concentrations of raltegravir, ranging from 4 μM (red) to 760 μM (magenta). Binding of raltegravir induces a progressive decrease in emission intensity and a shift in the intensity maximum. (**B**) Binding isotherm of raltegravir to Fascin1, showing the area the emission peaks in panel A (white circles) as a function of raltegravir concentration. The continuous line corresponds to the best fit of the experimental data to a one-site binding thermodynamic model. 3.3. Ligand-observed NMR confirms RAL–Fascin1 interaction in vitro.

The interaction between RAL and recombinant Fascin1 was further confirmed by ligand-based NMR spectroscopy methods. Specifically, saturation transfer difference (STD) [17] and WaterLOGSY (WL) [18] NMR experiments were employed, which allow the direct assessment of the ligand–protein interaction in solution and are often used in high-throughput screenings thanks to their relatively fast acquisition time. Both experiments showed intensity changes in ligand resonances caused by nuclear Overhauser effect (NOE)-mediated magnetization transfer, as a consequence of the interaction with the target protein. In the STD experiment, two ^{1}H NMR spectra are recorded after on- or off-resonance protein-selective saturation pulse, respectively, and the difference spectrum is then calculated. Ligand–protein interaction is recognized by the presence of positive signals in the difference NMR spectrum, whereas the lack of interaction (e.g., in a control sample in the absence of protein) results in no signals. In the WL experiment, the large bulk water magnetization is partially transferred to the ligand in the protein-bound state, which then rapidly exchanges with the free ligand. A noninteracting compound results

in positive resonances, whereas protein–ligand interactions are characterized by negative signals or by positive signals decreased in intensity with respect to the control sample. The above NMR experiments performed on RAL in the presence of Fascin1 clearly show an interaction (Figure 3). Specifically, positive aromatic signals (see the inset in Figure 3a) were detected in the STD spectrum of the mixture, while being absent in the control spectrum (Figure 3b), and in the WL spectrum, the same signals decreased in intensity compared to the control (Figure 3c). As we can show into the Appendix A, similar effect was observed with the known Fascin1 inhibitors imipramine (Figure A2) and MGS (Figure A3), although the latter gave a less pronounced effect likely due to the absence of aromatic moieties, for which the experiments were optimized. Overall, the NMR data confirm that RAL directly interacts with Fascin1 in solution.

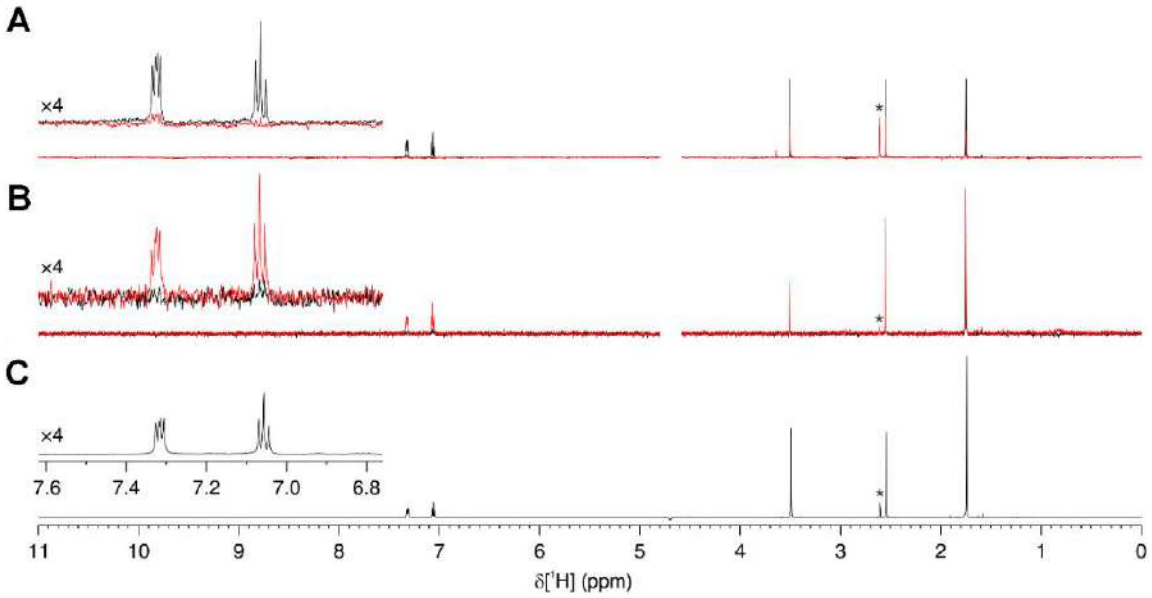

Figure 3. Interaction between raltegravir and Fascin1 observed by ligand-based NMR. (**A**) WaterLOGSY (WL) NMR spectra of 500 μM raltegravir either alone (black) or in the presence of 10 μM Fascin1 (red). The residual ^{1}H signal from d6-DMSO is marked with an asterisk. (**B**) Saturation transfer difference (STD) NMR spectra and (**C**) Reference ^{1}H NMR spectrum of raltegravir. The aromatic signals are shown in the insets on the left of each panel. The residual 1H signal from d6-DMSO is marked with an asterisk.

3.3. RAL Prevents In Vitro Fascin1-Induced F-Actin Bundling

In order to assess the effects of RAL on actin polymerization, we performed an F-actin bundling assay, and the results were observed by transmission electronic microscopy (TEM). As shown in Figure 4, only F-actin incubated in the presence of untreated Fascin1 formed filament bundles. When Fascin1 was pre-incubated with either 100 μM MGS, 10 μM imipramine, 10 μM G2 compound, or 30 μM RAL per separate, a disorganization of the bundles was observed, resulting in fewer filaments than in control conditions (Kruskal–Wallis test, $p < 0.001$). Besides, RAL treatment produced significantly thinner filament bundles than MGS (Mann–Whitney test, $p < 0.05$).

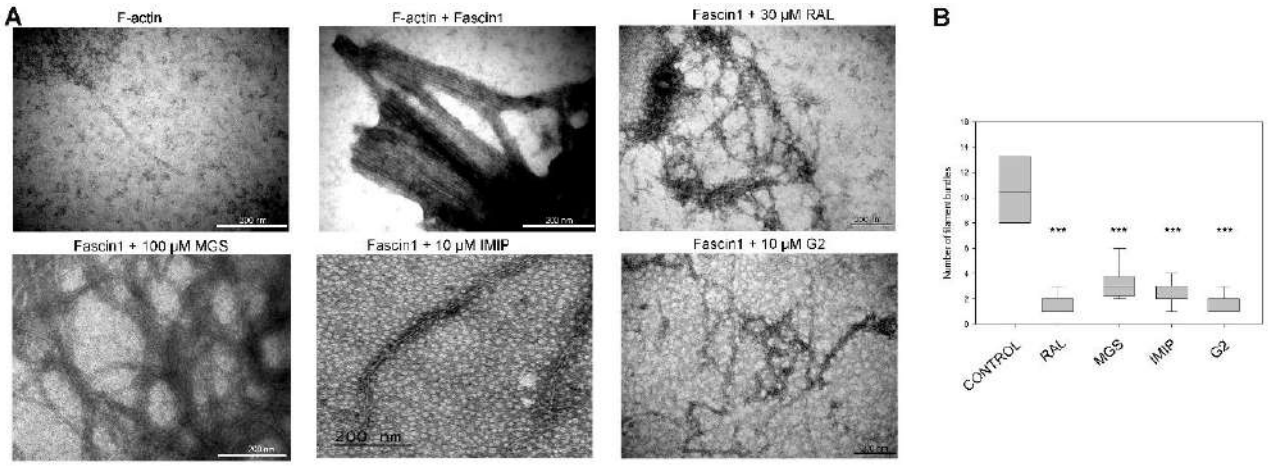

Figure 4. Fascin1 stimulation of actin-bundles formation is prevented by RAL. (**A**) Actin bundle formation in the presence of Fascin1 or Fascin1 with raltegravir (RAL) or different Fascin1-inhibitors: migrastatin (MGS), imipramine (IMIP) and, G2 compound; was visualized by transmission electronic microscopy (TEM). A representative figure is shown. (**B**) Quantitative analysis of the numbers of actin filaments of several pictures acquired by TEM (*** $p < 0.001$).

3.4. RAL Affects Actin Cytoskeleton Formation and Fascin1 Localization at Lamellipodia

As previously reported by our group, HCT-116 and SW480 exhibited the highest Fascin1 expression, whilst LoVo, DLD-1, and HT-29 had the lowest amongst eight colorectal cancer cell lines [13]. In order to perform the in vitro studies with the highest and lowest endogenous Fascin1 expression, we selected DLD-1 (low Fascin1 expression) and HCT-116 (high Fascin1 expression) cell lines for subsequent assays.

To assess the effect of RAL on cell viability, we used DLD-1 and HCT-116 cell lines. RAL was well tolerated up to 30 µM, by the DLD-1 and HCT-116 cell lines (Appendix A, Figure A4). At the experiment, MGS was included as an internal control, confirming the tolerance to 100 µM of both cell lines [13]. Then, the effect of RAL on lamellipodia protrusion at the cell front was assessed performing a wound scratch and observing Fascin1 localization by immunofluorescence of HCT-116 cells. Because the DLD-1 cell line is not suitable for assessing actin-based protrusions [13], HaCaT cells were used instead which showed an intermediate Fascin1 expression between HCT-116 and DLD1 (as observed after consulting Proteinatlas and BioGps databases). In addition, we assessed the reorganization of the cytoskeleton by F-actin staining.

Because lamellipodia were linked to the migratory activity of the tumoral cells, we further tested whether RAL treatment was associated with cell lamellipodium number. Figure 5 shows that prominent lamellipodia formation were observed in control conditions and for epithelial growth factor (EGF) treated cells with significant differences between them. However, these cytoskeleton structures were absent in cells treated with RAL, similarly to what it was observed for both MGS and PD98059, a MEK1 and MEK2 inhibitor. Lamellipodia-protrusion numbers were significantly lowered upon RAL treatment, although MGS had a more powerful diminishing effect (Table 1).

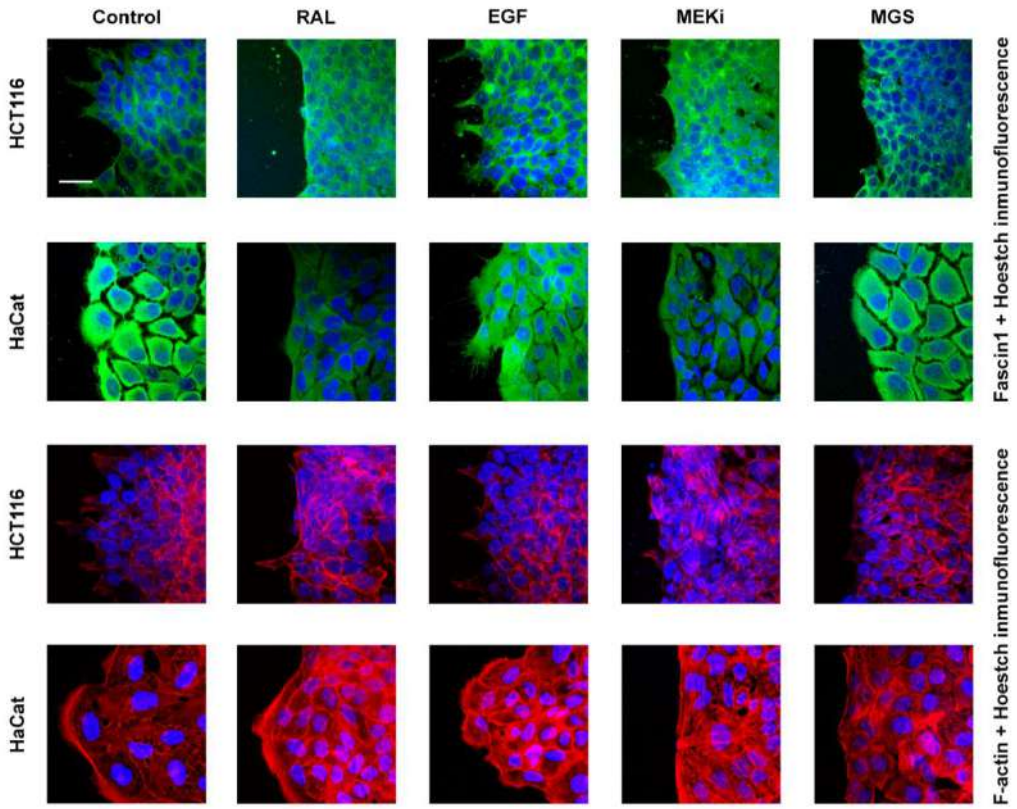

Figure 5. RAL inhibits the formation of lamellipodia and filopodia in HCT-116 and HaCaT cells, respectively. Confocal microscopy images of HCT-116 or HaCaT cells at the migrating edge on a wound scratch assay. Wounded cells were left untreated (control) or treated as indicated in the figure. Fascin1: green; Actin: red; Nuclei: blue; RAL: 30 μM raltegravir; EGF: 10 ng/mL epithelial growth factor; MEKi: 50 μM PD98059; MGS: 100 μM migrastatin; scale barr 23,79 μm.

Table 1. Lamellipodium-protrusion numbers in the different conditions in HCT-116 cells.

	Control	**30 μM RAL**	**10 ng/mL EGF**	**50 μM MEKi**	**100 μM MGS**
Lamellipodium number	8.7 ± 1.73	6.73 ± 1.11	11.58± 2.35	4.14 ± 1.43	4.58 ± 1.39
p value *		3.73×10^{-5}	0.000026	5.76×10^{-10}	3.14×10^{-9}

* T-test compared to control condition. Lamellipodium number was counted in pictures at 64×.

3.5. RAL Diminishes Migration and Inhibits Matrigel Cell Invasion of Colorectal Cancer Cells

With the aim of verifying the properties of Fascin1 inhibitors on actin-based membrane protrusions involved in cell migration, an in vitro wound-healing scratch assay was carried out with cells treated with MGS and RAL. Figure 6 shows that RAL induces a considerable inhibition of HCT-116 DLD-1 cell migration when compared to control conditions ($p < 0.05$).

Tumor cell invasion comprises both the gain of migration capabilities and the faculty to degrade extracellular matrix components such as basement membrane and tumor stoma [23]. Consequently, we carried out a Transwell assay on Matrigel^{R} because it resembles the composition of basement membrane and extracellular matrix. To further verify the inhibitory role of RAL on Fascin1 activity, we used Fascin1 overexpressed DLD-1 cells and tested their invasion properties. Accordingly, 30 μM RAL strongly diminished migration and invasion in Fascin1 overexpressed DLD-1 cells ($p < 0.01$) (Appendix A Figure A5A). As shown in Appendix A Figure A5B, RAL inhibit tumor-cell invasion of HCT-116, such as another tested inhibitor, G2 compound.

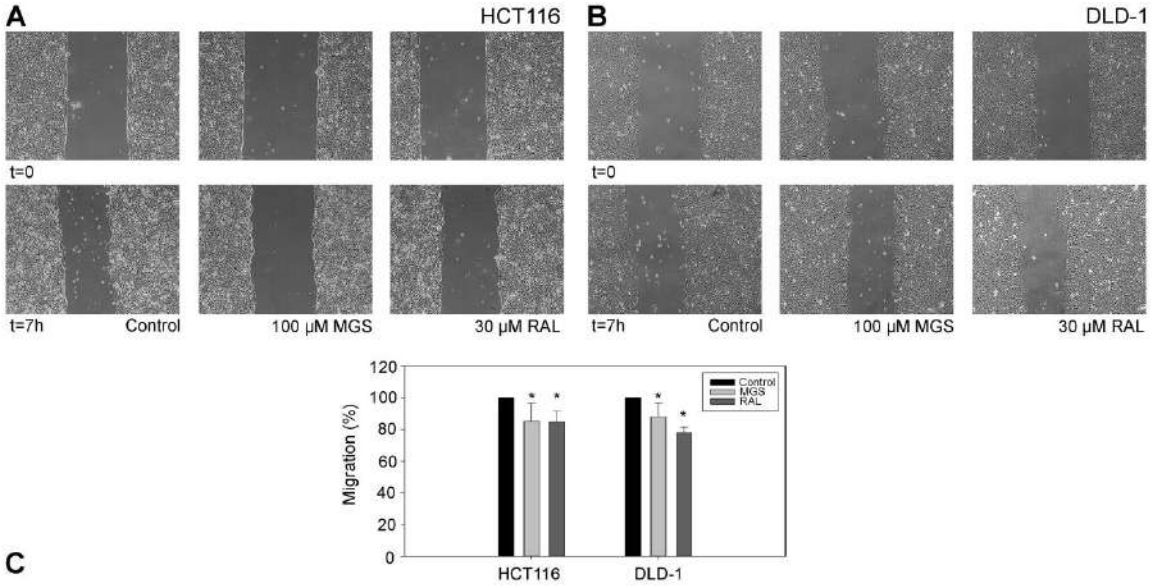

Figure 6. Inhibition of two cell lines by migrastatin (MGS) and RAL. (**A**) HCT-116, (**B**) DLD-1, (**C**) Migration was calculated with respect to the control conditions in lineal phase (* $p < 0.05$).

3.6. RAL Inhibits the Invasive and Metastatic Capacity of Colorectal Tumor Cells in an In Vivo Model

Cancer cell lines in tissue culture are widely utilized in early-stage evaluation of potential cancer targets however, the use of animal models is also crucial. In order to extrapolate the above anti-invasive properties to in vivo experiments, the well-established zebrafish larvae model of invasion as well as a xenograft assay was carried out (Figure 7). Most larvae were viable upon treatment with different RAL concentrations (Appendix A, Figure A6). A correlation between invasion percentage and Fascin1 mRNA expression was observed, where HCT-116 cells showed the highest and LoVo and DLD-1 the lowest expression of Fascin1 as previously reported [12]. Therefore, HCT-116 was chosen as the cell line with the highest constitutive expression of Fascin1, whereas DLD1 transfected with Fascin1 was considered as the condition of induced Fascin1 expression. The transfection efficiency was proven previously. The Fascin1-transfected cells increased the protein expression level more than 20% compared to the control condition [12]. The Fascin1-transfected cells increased the protein expression level and the percentage of the zebrafish larvae invasion (Figure 7C,D). HCT-116 tumor cells injected in larvae treated with RAL exhibited a significantly lower percentage of invasion and lower number of invasion foci than control and similarly to that observed for MGS treatment (Figure 7A,B). Likewise, when Fascin1-transfected DLD-1 cells were injected, RAL and MGS inhibitory effect was increased compared to untreated conditions, thus suggesting a Fascin1-dependent activity of these drugs. The reduction in the percentage of invasion compared to control (DMSO) was higher when DLD-1 cells were transfected with Fascin1 than when DLD-1 cell were transfected with the empty vector for both treatments.

When larvae were fed and kept alive after six days post-xenograft, micro-metastasis developed from invading tumor cells (Figure 8B). As shown in Figure 8A, HCT-116 colorectal cancer cells treated with 30 µM RAL diminished the total number of larvae in which metastasis was observed. DLD-1 cells transfected with Fascin1-GFP plasmid showed a significant increase in metastatic larvae compared to pGFP-N3 control vector (MOCK). The reduction in the percentage of metastasis compared to control (DMSO) was higher when DLD-1 cells were transfected with Fascin1 (64.5%) than when DLD-1 cell were transfected with the empty vector (22.9%) This metastatic activity diminished when larvae was treated with RAL. All these findings suggest a Fascin1-dependent effect of RAL.

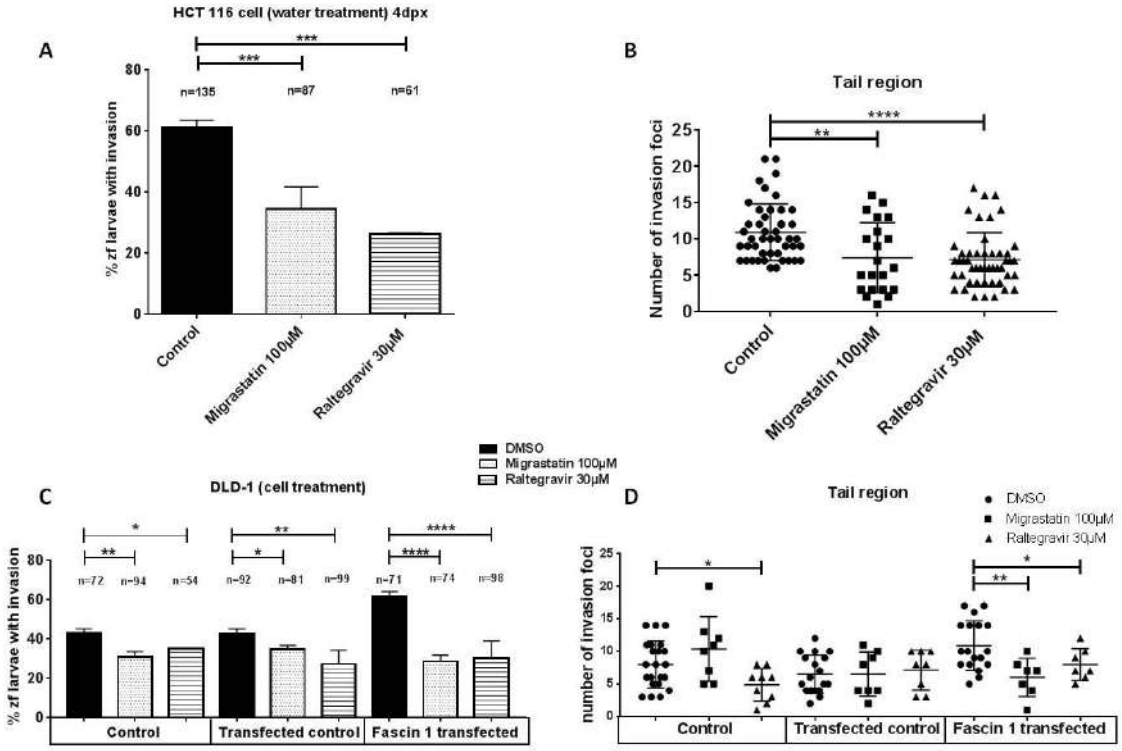

Figure 7. Zebrafish invasion assays 4 days post-xenograft. (**A**) The images show the invasive and non-invasive cells in a zebrafish invasion model. On the right panel, the invasiveness of each cell line is shown. (**B**) HCT-116 cancer cells were injected in zebrafish larvae and then treated with migrastatin and RAL. (**C**) Effects of drugs on the average percentage of zebrafish larvae with invasion in Fascin1-transfected DLD-1 cells. (**D**) Effects of drugs on the number of invasion foci in Fascin1-transfected DLD-1 cells. Data are shown as mean ± SD; compared with the control condition, * p = 0.049–0.01. ** p = 0.001–0.009. *** p = 0.0001–0.0009. **** p < 0.0001.

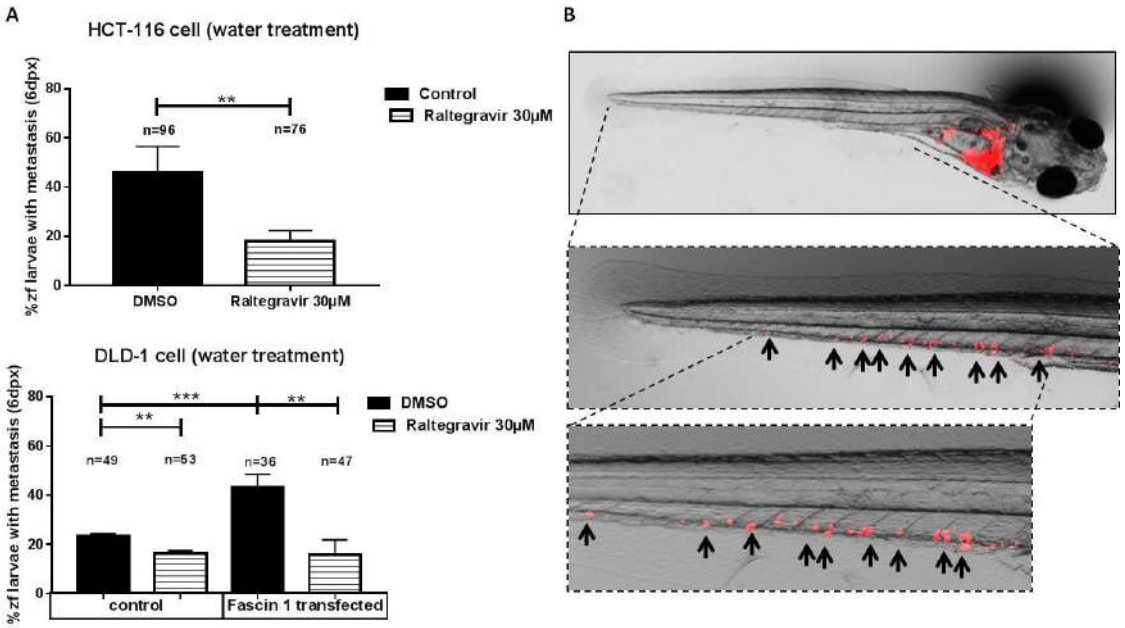

Figure 8. Anti-metastatic potential of RAL in zebrafish. **(A)** At six days post-injection, larvae were examined to evaluate whether micro-metastasis developed by invading native HCT-116 and Fascin1-transfected DLD-1 cells. **(B)** The evaluation criteria were the presence of human cancer-cell colonies (arrows) outside the yolk sac. Data are shown as mean ± SD; compared with the control condition, ** p = 0.001–0.009. *** p = 0.0001–0.0009.

4. Discussion

There is a considerable lapse of time between the discovery of novel potential targets involved in cancer and the development of a successful therapy. The strategy of using existing drugs originally developed for one disease to treat other indications has found success across medical fields. This approach is known as drug repurposing, and it promises faster access of drugs to patients while reducing costs in the long and difficult process of drug development [24]. By using VS for inhibiting pro-invasive and pro-metastatic Fascin1 protein, we identified the VIH antiretroviral, RAL, as a potential drug for treating Fascin1 overexpressing cancers.

The use of antiretrovirals as cancer treatments is not new. Apart from obvious anti-VIH anti-neoplastic effects reported in virus-associated tumors such as Kaposi's sarcoma [25] and Xenotropic murine leukemia-related retrovirus, which has been linked to human prostate cancer and chronic fatigue syndrome [26], several evidences highlight the anti-tumoral properties of anti-retrovirals including RAL. The findings reported in our study do not rule out that RAL could bind other proteins with actin-binding action. In this regard, RAL was found to inhibit γ-actin binding protein, Aldolase A in a xenograft model of lung cancer with no significant toxicity [27]. In fact, by using Pocketalign and the PDB structural information for Aldolase A and Fascin1, it was found that both proteins share a common hydrophobic pocket at the actin-binding site.

Another group of evidence points out the effect of anti-retrovirals in restoring the sensitivity to chemotherapeutic agents. In this line, zidovudine back in 1989 was found to increase sensitivity to cisplatin in resistant human colon cells in vitro [28]. Also, a pilot, serial biopsy study is ongoing in which the potentiation of cisplatin chemotherapy by RAL is being evaluated in patients with head and neck squamous cell carcinoma [29]. Interestingly, another effect of Fascin1, apart from actin cytoskeleton rearrangement, is conferring chemoresistance to tumor cells [30,31]. Cancer drug resistance remains a burden for cancer therapy and patients' outcome, and it often results in more aggressive tumors that tend to metastasize to distant organs. It might be thus envisaged that Fascin1 could represent a novel target to overcome resistance, and our results warrant further research with chemoresistant tumoral cells and RAL.

In addition, actin-bundling activity of Fascin1 has been proven to facilitate release and cell-to-cell transmission of human T-cell leukemia virus type 1 (HTLV1) retrovirus [32] and, more recently, pseudorabies virus (PRV) [33]. Likewise, Epstein–Barr virus (EBV)-encoded oncoprotein (lmp1) via NF-kappaB in lymphocytes induces Fascin1 to increase their invasiveness [34]. In fact, human Fascin1 was firstly cloned and sequenced as a protein over 200-fold induced, by latent Epstein–Barr virus (EBV) infection in B lymphocytes and was absent in non-EBV-infected B- and T-cell lines [35]. Moreover, Fascin1 immuno-histochemical expression was significantly related with EBV-associated gastric and colorectal carcinomas [36,37] and HIV-related lymphoid hyperplasia [38]. Most of these viruses express short miRNAs to regulate their own gene expression or to influence host gene expression and thus contribute to the carcinogenic processes. Fascin1 has been also shown regulated by miRNA-200b, miRNA-539, miRNA-133b, and miRNA-145 [39–42], and thus, a targeted link between viral infection and Fascin1 could also be envisaged. However, the therapeutic effects of antiviral drugs on tumors which overexpress Fascin1 have not been investigated yet.

The aim of this study was to characterize the anti-Fascin1, antimigratory and anti-invasive properties of the anti-retroviral drug, RAL, by using molecular modeling, biophysical and biochemical techniques, immunofluorescence, migration, and invasion assays. In addition, the in vivo effect of RAL was evaluated in metastatic zebrafish model. This study also emphasizes the exciting approaches to decipher novel drugs, sometimes FDA-approved, and their mechanisms of action. Apart from disrupting the role of Fascin1 in tumor-cell invasion and metastasis via inhibiting actin-based membrane protrusions, RAL could also abrogate cancer metastatic colonization by blocking metabolic stress resistance and mitochondrial oxidative phosphorylation (OXPHOS), as Fascin1 has shown to be

involved also in stabilizing mitochondrial actin filaments under metabolic stress, at least in lung cancer [43]. Hence, this is the first description on the in vitro and in vivo antitumoral activity of RAL on colorectal cancer cells, which has been previously predicted by VS calculations, thus guiding the design of improved Fascin1 inhibitors. Our results could contribute to the repurposing of this HIV-1 integrase inhibitor for the treatment of Fascin1-overexpressing tumors.

5. Conclusions

By using VS calculations, we identified, for the first time, RAL as a potential Fascin1 blocker, subsequently being shown by biophysical assays, and also as an inhibitor of cell migration and invasion of human colorectal cancer cells. We also demonstrated the feasibility of docking, molecular-dynamics simulations, and NMR to provide details about the main potential interactions between RAL and Fascin1 key residues and further targeting this mechanism in vitro. Our results also suggest that RAL is likely to reduce the in vivo antimigratory and anti-invasive activity using a zebrafish model with xenograft tumor implants. Importantly, the potential FDA-approved compound used in the present study, which is classified as safe in humans, could be easily repurposed as novel antitumoral drug and used in proof-of-concept clinical trials. Further in vivo studies to evaluate this novel Fascin1-targeted approach are warranted.

6. Patents

Conesa-Zamora P, Alburquerque-González B, Pérez-Sánchez H, Montoro-García S, García-Solano J, Bernabé-García A, Nicolás-Villaescusa FJ, Bernabé-García M, Cayuela-Fuentes ML, Peña-García J, Luque-Fernández I, Ruiz-Sanz J, and Martínez-Herrerías JC. Patent pending no. P202130062.

Author Contributions: P.C.-Z., S.M-G. and H.P.-S. conceived the presented idea. P.C.-Z., S.M.-G., F.J.N., M.L.C.-F. and H.P.-S. designed the experiments and supervised the findings of this work. B.A.-G., H.P.-S., Á.B.-G., S.M.-G., L.G., L.B., M.B.-G., F.F.L.-C., J.P.-G. and J.R.-S. performed the experiments. P.C.-Z., B.A.-G., S.M.-G., H.P.-S., I.L. and E.L. wrote the manuscript. All authors have read and agreed to the published version of the manuscript.

Funding: This research was funded by Instituto de Salud Carlos III (Spanish Ministry of Health) and FEDER funds (references: PI15/00626 and PI18/00144), European Commission´s Corbel Program (PID-3630, and 2334 and 2428); Spanish Ministry of Economy and Competitiveness MINECO (CTQ2017-87974-R), and by the Fundación Séneca del Centro de Coordinación de la Investigación de la Región de Murcia (20988/PI/18 and 20646/JLI/18). B.A.-G. belongs to the "Programa de Doctorado en Ciencias de la Salud, Universidad Católica de Murcia (UCAM)" and holds a grant of the UCAM (FPI05-UCAM/17). F.F.L.-C. was supported by the Junta Provincial Murcia Predoctoral Asociación Española contra el Cáncer (AECC) (REF: PRDMU19002) grant.

Institutional Review Board Statement: The study was conducted according to the guidelines of the Declaration of Helsinki, and approved by the Animal Welfare Ethics Committee of Instituto Murciano de Investigaciones Biosanitarias (IMIB)(REGA code: ES-300303340098).

Informed Consent Statement: Not applicable.

Data Availability Statement: No new data were created or analyzed in this study apart from those presented in the manuscript. Data sharing is not applicable to this article.

Acknowledgments: Supercomputing resources in this work have been supported by the infrastructures of Poznan Supercomputing Center, the e-infrastructure program of the Research Council of Norway, and the supercomputer center of UiT—the Arctic University of Norway, by the Plataforma Andaluza de Bioinformática of the University of Málaga, by the supercomputing infrastructure of the NLHPC (ECM-02, Powered@NLHPC), and by the Extremadura Research Centre for Advanced Technologies (CETA−CIEMAT), funded by the European Regional Development Fund (ERDF). CETA−CIEMAT belongs to CIEMAT and the Government of Spain.

Conflicts of Interest: The authors declare no conflict of interest.

Appendix A

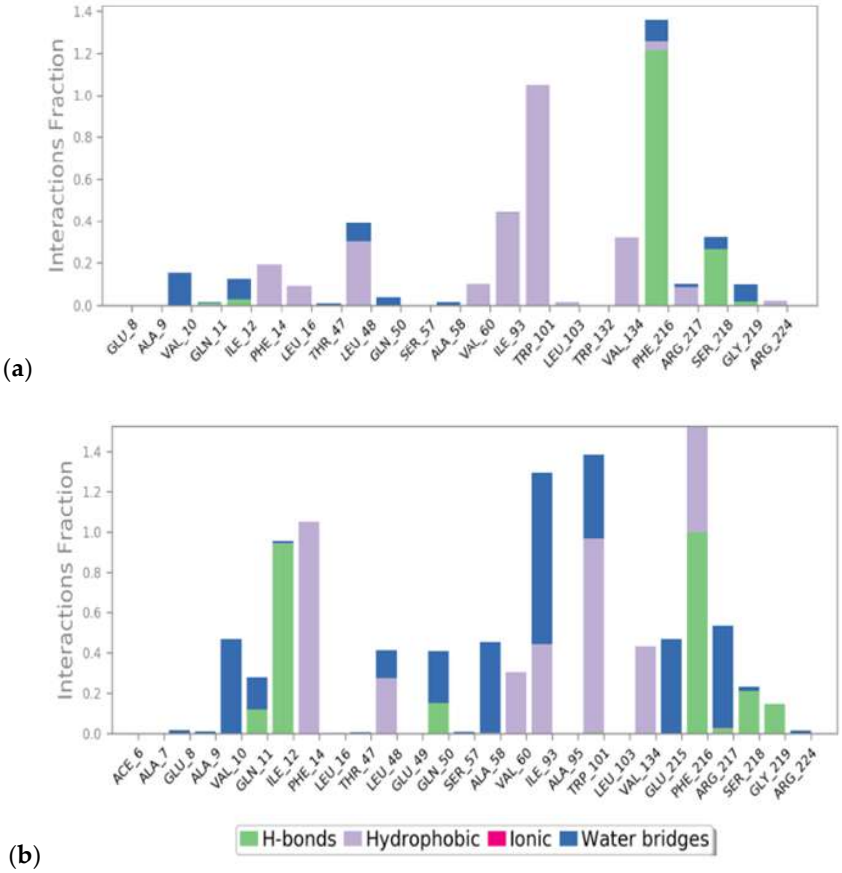

Figure A1. Top interacting residues and interaction types between Fascin1-6b0t_lig (**a**) and Fascin1-RAL (**b**).

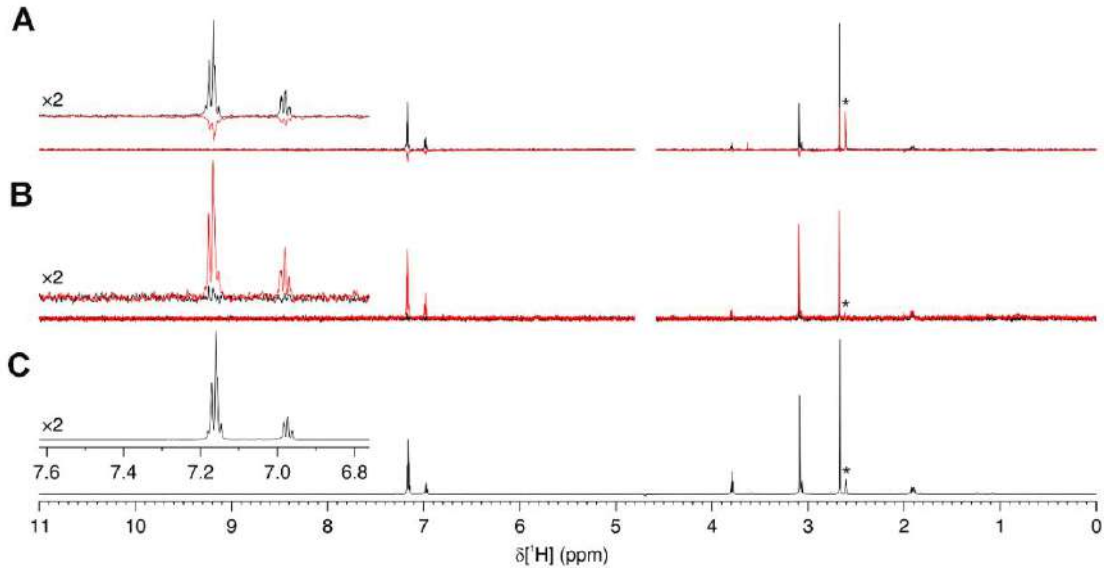

Figure A2. Interaction between imipramine and Fascin1 was observed by ligand-based NMR. (**A**) WL NMR spectra of 500 µM imipramine either alone (black) or in the presence of 10 µM Fascin1 (red); (**B**) STD NMR spectra and (**C**) reference ^{1}H NMR spectrum of imipramine. The residual ^{1}H signal from d6-DMSO is marked with an asterisk. The aromatic signals are shown in the insets on the left of each panel. The residual 1H signal from d6-DMSO is marked with an asterisk.

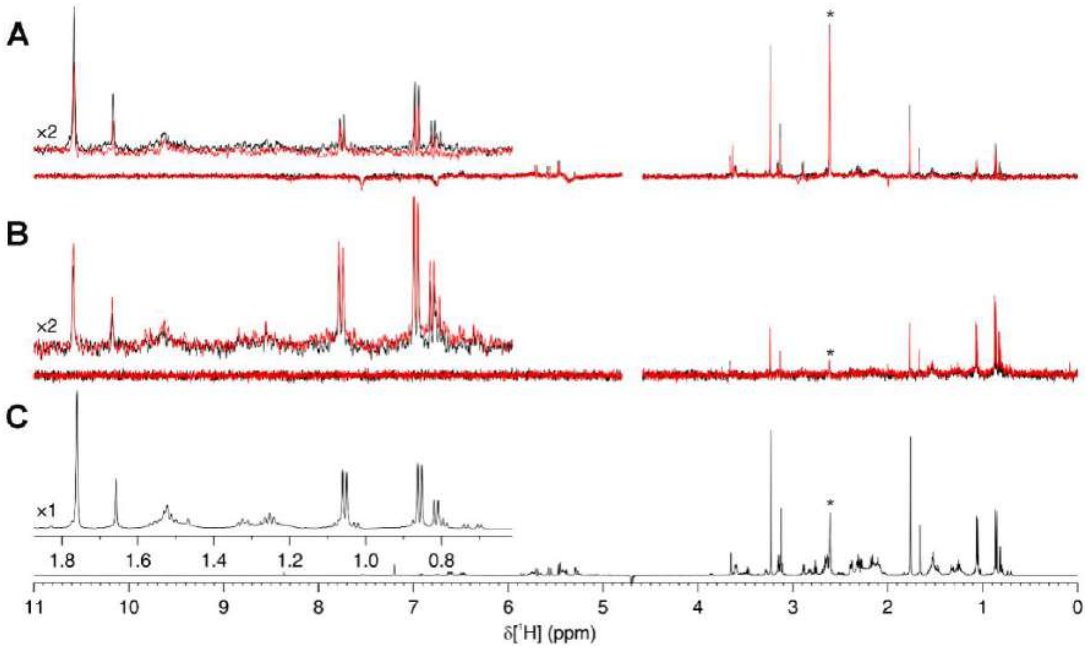

Figure A3. Interaction between migrastatin and Fascin1 was observed by ligand-based NMR. (**A**) WL NMR spectra of 500 μM migrastatin either alone (black) or in the presence of 10 μM Fascin1 (red); (**B**) STD NMR spectra and (**C**) reference ^{1}H NMR spectrum of migrastatin. The residual ^{1}H signal from d6-DMSO is marked with an asterisk. The aliphatic signals most affected from the interaction are shown in the insets on the left of each panel. The residual 1H signal from d6-DMSO is marked with an asterisk.

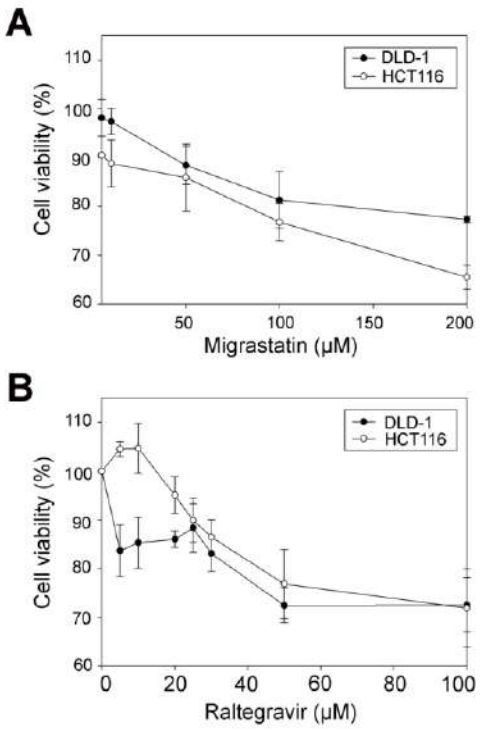

Figure A4. Shows the colorectal cell-line viability assay. The effect of anti-Fascin1 migrastatin (**A**); and RAL (**B**) on the cell viability of DLD-1 and HCT-116 colorectal cell lines is shown.

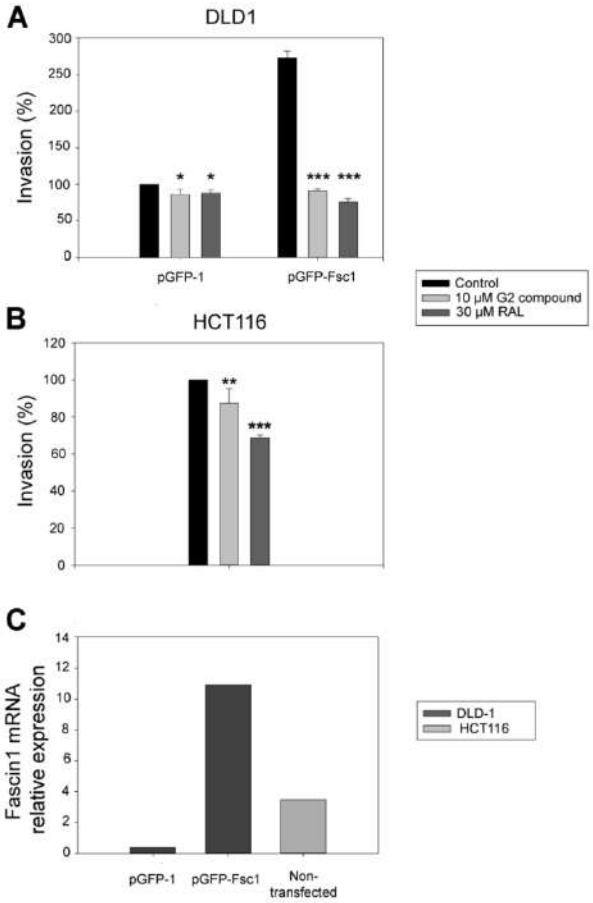

Figure A5. RAL (RAL) and G2 compound inhibition of the cell's invasive ability. (**A**) Percentage of invasion in DLD-1 Fascin1-transfected cells (pGFP vs pGFP-FSC1). (**B**) Percentage of invasion in HCT-116 non-transfected cells. (**C**) Fascin1 mRNA levels expressed in transfected DLD-1 cells. * p = 0.049–0.01. ** p = 0.001–0.009. *** p = 0.0001–0.0009.

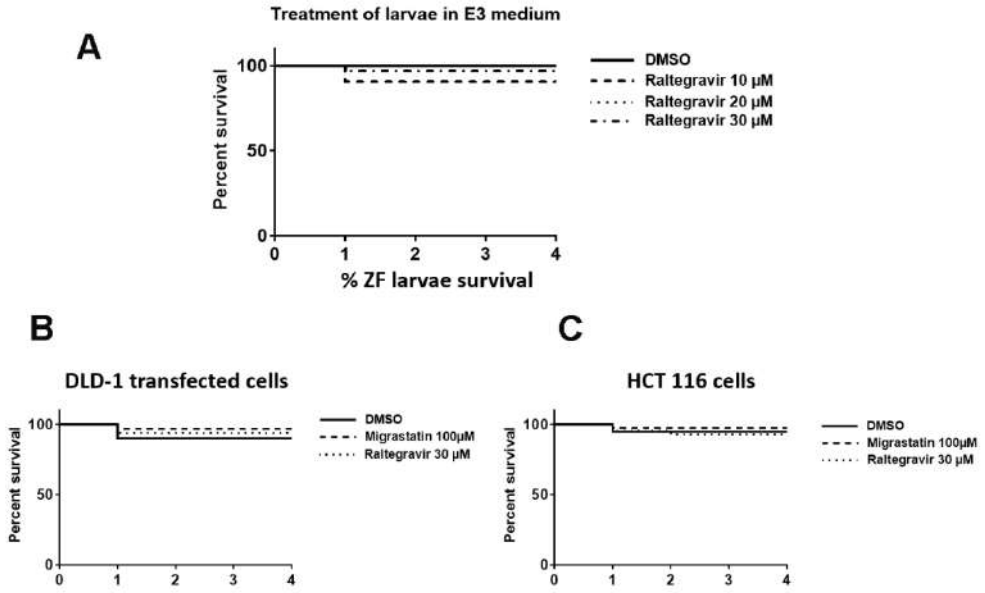

Figure A6. Survival curves of zebrafish larvae when treated with the raltegravir and migrastatin in the E3 medium (**A**) and when additionally, they were injected with (**B**) Fascin1-transfected DLD-1 or (**C**) HCT-116 tumor cell lines.

References

1. Bray, F.; Ferlay, J.; Soerjomataram, I.; Siegel, R.L.; Torre, L.A.; Jemal, A. Global cancer statistics 2018: GLOBOCAN estimates of incidence and mortality worldwide for 36 cancers in 185 countries. *CA Cancer J. Clin.* **2018**, *68*, 394–424. [CrossRef]
2. Conesa-Zamora, P.; García-Solano, J.; Turpin, M.e.C.; Sebastián-León, P.; Torres-Moreno, D.; Estrada, E.; Tuomisto, A.; Wilce, J.; Mäkinen, M.J.; Pérez-Guillermo, M.; et al. Methylome profiling reveals functions and genes which are differentially methylated in serrated compared to conventional colorectal carcinoma. *Clin. Epigenet.* **2015**, *7*, 101. [CrossRef]
3. García-Solano, J.; Conesa-Zamora, P.; Carbonell, P.; Trujillo-Santos, J.; Torres-Moreno, D.; Pagán-Gómez, I.; Rodríguez-Braun, E.; Pérez-Guillermo, M. Colorectal serrated adenocarcinoma shows a different profile of oncogene mutations, MSI status and DNA repair protein expression compared to conventional and sporadic MSI-H carcinomas. *Int. J. Cancer* **2012**, *131*, 1790–1799. [CrossRef]
4. Stefanius, K.; Ylitalo, L.; Tuomisto, A.; Kuivila, R.; Kantola, T.; Sirniö, P.; Karttunen, T.J.; Mäkinen, M.J. Frequent mutations of KRAS in addition to BRAF in colorectal serrated adenocarcinoma. *Histopathology* **2011**, *58*, 679–692. [CrossRef]
5. Alburquerque-González, B.; López-Calderón, F.F.; López-Abellán, M.D.; Esteban-Gil, Á.; García-Solano, J.; Conesa-Zamora, P. Biology and Therapeutic Targets of Colorectal Serrated Adenocarcinoma; Clues for a Histologically Based Treatment against an Aggressive Tumor. *Int. J. Mol. Sci.* **2020**, *21*, 1991. [CrossRef] [PubMed]
6. Tan, V.Y.; Lewis, S.J.; Adams, J.C.; Martin, R.M. Association of fascin-1 with mortality, disease progression and metastasis in carcinomas: A systematic review and meta-analysis. *BMC Med.* **2013**, *11*, 52. [CrossRef]
7. Rodrigues, P.C.; Sawazaki-Calone, I.; de Oliveira, C.E.; Soares Macedo, C.C.; Dourado, M.R.; Cervigne, N.K.; Miguel, M.C.; Ferreira do Carmo, A.; Lambert, D.W.; Graner, E.; et al. Fascin promotes migration and invasion and is a prognostic marker for oral squamous cell carcinoma. *Oncotarget* **2017**, *8*, 74736–74754. [CrossRef] [PubMed]
8. Scott, K.L.; Nogueira, C.; Heffernan, T.P.; van Doorn, R.; Dhakal, S.; Hanna, J.A.; Min, C.; Jaskelioff, M.; Xiao, Y.; Wu, C.J.; et al. Proinvasion metastasis drivers in early-stage melanoma are oncogenes. *Cancer Cell* **2011**, *20*, 92–103. [CrossRef]
9. Lin, S.; Taylor, M.D.; Singh, P.K.; Yang, S. How does fascin promote cancer metastasis? *FEBS J.* **2020**. [CrossRef] [PubMed]
10. Guo, S.; Zou, J.; Wang, G. Advances in the proteomic discovery of novel therapeutic targets in cancer. *Drug Des. Dev.* **2013**, *7*, 1259–1271. [CrossRef] [PubMed]
11. Conesa-Zamora, P.; García-Solano, J.; García-García, F.; Turpin, M.e.C.; Trujillo-Santos, J.; Torres-Moreno, D.; Oviedo-Ramírez, I.; Carbonell-Muñoz, R.; Muñoz-Delgado, E.; Rodriguez-Braun, E.; et al. Expression profiling shows differential molecular pathways and provides potential new diagnostic biomarkers for colorectal serrated adenocarcinoma. *Int. J. Cancer* **2013**, *132*, 297–307. [CrossRef] [PubMed]
12. Alburquerque-González, B.; Bernabé-García, M.; Montoro-García, S.; Bernabé-García, Á.; Rodrigues, P.C.; Ruiz Sanz, J.; López-Calderón, F.F.; Luque, I.; Nicolas, F.J.; Cayuela, M.L.; et al. New role of the antidepressant imipramine as a Fascin1 inhibitor in colorectal cancer cells. *Exp. Mol. Med.* **2020**, *52*, 281–292. [CrossRef] [PubMed]
13. Montoro-García, S.; Alburquerque-González, B.; Bernabé-García, Á.; Bernabé-García, M.; Rodrigues, P.C.; den-Haan, H.; Luque, I.; Nicolás, F.J.; Pérez-Sánchez, H.; Cayuela, M.L.; et al. Novel anti-invasive properties of a Fascin1 inhibitor on colorectal cancer cells. *J. Mol. Med.* **2020**, *98*, 383–394. [CrossRef]
14. Chen, L.; Yang, S.; Jakoncic, J.; Zhang, J.J.; Huang, X.Y. Migrastatin analogues target fascin to block tumour metastasis. *Nature* **2010**, *464*, 1062–1066. [CrossRef] [PubMed]
15. Trott, O.; Olson, A.J. AutoDock Vina: Improving the speed and accuracy of docking with a new scoring function, efficient optimization, and multithreading. *J. Comput. Chem.* **2010**, *31*, 455–461. [CrossRef]
16. Mark, P.; Nilsson, L. Structure and Dynamics of the TIP3P, SPC, and SPC/E Water Models at 298 K. *J. Phys. Chem. A* **2001**, *105*, 9954–9960. [CrossRef]
17. Mayer, M.; Meyer, B. Characterization of Ligand Binding by Saturation Transfer Difference NMR Spectroscopy. *Angew. Chem. Int. Ed. Engl.* **1999**, *38*, 1784–1788. [CrossRef]
18. Dalvit, C.; Fogliatto, G.; Stewart, A.; Veronesi, M.; Stockman, B. WaterLOGSY as a method for primary NMR screening: Practical aspects and range of applicability. *J. Biomol. NMR* **2001**, *21*, 349–359. [CrossRef]
19. Jansen, S.; Collins, A.; Yang, C.; Rebowski, G.; Svitkina, T.; Dominguez, R. Mechanism of actin filament bundling by fascin. *J. Biol. Chem.* **2011**, *286*, 30087–30096. [CrossRef]
20. Boukamp, P.; Petrussevska, R.T.; Breitkreutz, D.; Hornung, J.; Markham, A.; Fusenig, N.E. Normal keratinization in a spontaneously immortalized aneuploid human keratinocyte cell line. *J. Cell Biol.* **1988**, *106*, 761–771. [CrossRef]
21. Jelassi, B.; Chantôme, A.; Alcaraz-Pérez, F.; Baroja-Mazo, A.; Cayuela, M.L.; Pelegrin, P.; Surprenant, A.; Roger, S. P2X(7) receptor activation enhances SK3 channels- and cystein cathepsin-dependent cancer cells invasiveness. *Oncogene* **2011**, *30*, 2108–2122. [CrossRef]
22. Fior, R.; Póvoa, V.; Mendes, R.V.; Carvalho, T.; Gomes, A.; Figueiredo, N.; Ferreira, M.G. Single-cell functional and chemosensitive profiling of combinatorial colorectal therapy in zebrafish xenografts. *Proc. Natl. Acad. Sci. USA* **2017**, *114*, E8234–E8243. [CrossRef]
23. Albini, A. Tumor and endothelial cell invasion of basement membranes. The matrigel chemoinvasion assay as a tool for dissecting molecular mechanisms. *Pathol. Oncol. Res.* **1998**, *4*, 230–241. [CrossRef] [PubMed]
24. Nowak-Sliwinska, P.; Scapozza, L.; Ruiz i Altaba, A. Drug repurposing in oncology: Compounds, pathways, phenotypes and computational approaches for colorectal cancer. *Biochim. Biophys. Acta Rev. Cancer* **2019**, *1871*, 434–454. [CrossRef] [PubMed]

25. Carleo, M.A.; Di Martino, F.; Del Giudice, A.; Gargiulo, M.; Parrella, G.; Rosario, P.; Sangiovanni, V.; Viglietti, R.; Esposito, V.; Chirianni, A. Different impact of anti-retroviral regimen containing protease inhibitors on development of HIV-related Kaposi sarcoma. *Vivo* **2015**, *29*, 133–136.
26. Singh, I.R.; Gorzynski, J.E.; Drobysheva, D.; Bassit, L.; Schinazi, R.F. Raltegravir is a potent inhibitor of XMRV, a virus implicated in prostate cancer and chronic fatigue syndrome. *PLoS ONE* **2010**, *5*, e9948. [CrossRef] [PubMed]
27. Chang, Y.C.; Chiou, J.; Yang, Y.F.; Su, C.Y.; Lin, Y.F.; Yang, C.N.; Lu, P.J.; Huang, M.S.; Yang, C.J.; Hsiao, M. Therapeutic Targeting of Aldolase A Interactions Inhibits Lung Cancer Metastasis and Prolongs Survival. *Cancer Res.* **2019**, *79*, 4754–4766. [CrossRef]
28. Scanlon, K.J.; Kashani-Sabet, M.; Sowers, L.C. Overexpression of DNA replication and repair enzymes in cisplatin-resistant human colon carcinoma HCT8 cells and circumvention by azidothymidine. *Cancer Commun.* **1989**, *1*, 269–275.
29. Oprea, T.I.; Bauman, J.E.; Bologa, C.G.; Buranda, T.; Chigaev, A.; Edwards, B.S.; Jarvik, J.W.; Gresham, H.D.; Haynes, M.K.; Hjelle, B.; et al. Drug Repurposing from an Academic Perspective. *Drug. Discov. Today Strateg.* **2011**, *8*, 61–69. [CrossRef]
30. Zhang, Y.; Lu, Y.; Zhang, C.; Huang, D.; Wu, W.; Shen, J.; Cai, Y.; Chen, W.; Yao, W. FSCN-1 increases doxorubicin resistance in hepatocellular carcinoma through promotion of epithelial-mesenchymal transition. *Int. J. Oncol.* **2018**, *52*, 1455–1464. [CrossRef] [PubMed]
31. Ghebeh, H.; Al-Khaldi, S.; Olabi, S.; Al-Dhfyan, A.; Al-Mohanna, F.; Barnawi, R.; Tulbah, A.; Al-Tweigeri, T.; Ajarim, D.; Al-Alwan, M. Fascin is involved in the chemotherapeutic resistance of breast cancer cells predominantly via the PI3K/Akt pathway. *Br. J. Cancer* **2014**, *111*, 1552–1561. [CrossRef]
32. Mohr, C.F.; Gross, C.; Bros, M.; Reske-Kunz, A.B.; Biesinger, B.; Thoma-Kress, A.K. Regulation of the tumor marker Fascin by the viral oncoprotein Tax of human T-cell leukemia virus type 1 (HTLV-1) depends on promoter activation and on a promoter-independent mechanism. *Virology* **2015**, *485*, 481–491. [CrossRef]
33. Yu, F.L.; Miao, H.; Xia, J.; Jia, F.; Wang, H.; Xu, F.; Guo, L. Proteomics Analysis Identifies IRSp53 and Fascin as Critical for PRV Egress and Direct Cell-Cell Transmission. *Proteomics* **2019**, *19*, e1900009. [CrossRef]
34. Mohr, C.F.; Kalmer, M.; Gross, C.; Mann, M.C.; Sterz, K.R.; Kieser, A.; Fleckenstein, B.; Kress, A.K. The tumor marker Fascin is induced by the Epstein-Barr virus-encoded oncoprotein LMP1 via NF-κB in lymphocytes and contributes to their invasive migration. *Cell Commun. Signal.* **2014**, *12*, 46. [CrossRef]
35. Mosialos, G.; Yamashiro, S.; Baughman, R.W.; Matsudaira, P.; Vara, L.; Matsumura, F.; Kieff, E.; Birkenbach, M. Epstein-Barr virus infection induces expression in B lymphocytes of a novel gene encoding an evolutionarily conserved 55-kilodalton actin-bundling protein. *J. Virol.* **1994**, *68*, 7320–7328. [CrossRef]
36. Gong, L.P.; Chen, J.N.; Xiao, L.; He, Q.; Feng, Z.Y.; Zhang, Z.G.; Liu, J.P.; Wei, H.B.; Shao, C.K. The implication of tumor-infiltrating lymphocytes in Epstein-Barr virus-associated gastric carcinoma. *Hum. Pathol.* **2019**, *85*, 82–91. [CrossRef] [PubMed]
37. Al-Antary, N.; Farghaly, H.; Aboulkassim, T.; Yasmeen, A.; Akil, N.; Al Moustafa, A.E. Epstein-Barr virus and its association with Fascin expression in colorectal cancers in the Syrian population: A tissue microarray study. *Hum. Vaccines Immunother.* **2017**, *13*, 1573–1578. [CrossRef] [PubMed]
38. Said, J.W.; Pinkus, J.L.; Yamashita, J.; Mishalani, S.; Matsumura, F.; Yamashiro, S.; Pinkus, G.S. The role of follicular and interdigitating dendritic cells in HIV-related lymphoid hyperplasia: Localization of fascin. *Mod. Pathol.* **1997**, *10*, 421–427.
39. Xiao, P.; Liu, W.; Zhou, H. miR-200b inhibits migration and invasion in non-small cell lung cancer cells via targeting FSCN1. *Mol. Med. Rep.* **2016**, *14*, 1835–1840. [CrossRef]
40. Yang, X.; Lei, P.; Huang, Y.; Zhang, Z.; Zhang, Y. MicroRNA-133b inhibits the migration and invasion of non small cell lung cancer cells via targeting FSCN1. *Oncol. Lett.* **2016**, *12*, 3619–3625. [CrossRef] [PubMed]
41. Zhang, Y.; Yang, X.; Wu, H.; Zhou, W.; Liu, Z. MicroRNA-145 inhibits migration and invasion via inhibition of fascin 1 protein expression in non-small-cell lung cancer cells. *Mol. Med. Rep.* **2015**, *12*, 6193–6198. [CrossRef] [PubMed]
42. Wang, N.; Zhang, T. Downregulation of MicroRNA-135 Promotes Sensitivity of Non-Small Cell Lung Cancer to Gefitinib by Targeting TRIM16. *Oncol. Res.* **2018**, *26*, 1005–1014. [CrossRef] [PubMed]
43. Lin, S.; Huang, C.; Gunda, V.; Sun, J.; Chellappan, S.P.; Li, Z.; Izumi, V.; Fang, B.; Koomen, J.; Singh, P.K.; et al. Fascin Controls Metastatic Colonization and Mitochondrial Oxidative Phosphorylation by Remodeling Mitochondrial Actin Filaments. *Cell Rep.* **2019**, *28*, 2824–2836.e2828. [CrossRef] [PubMed]

ARTÍCULO 5:

Alburquerque-González, B., Montoro-García, S., Bernabé-García, M., Bernabé-García, A., Campioni-Rodrigues, P., Luque-Fernández, I., Salo, T., Pérez-Sánchez, H., Cayuela-Fuentes, M.L., Luengo-Gil, G., Nicolás-Villaescusa, F.J., Conesa-Zamora, P. (2022). **Monastrol, a kinesin-Eg5 inhibitor, inhibits invasion and metastasis of human colorectal cancer cells by targeting fascin.** *Experimental & Molecular Medicine* (Enviado).

Factor de impacto 2020 (JCR): 8.718; Categoría (JCR): MEDICINE RESEARCH & EXPERIMENTAL SCIENCE; Clasificación: 34/295 (Q1); Fecha de publicación: En revisión.

Detailed Status Information

Manuscript #	EMM2022837
Current Revision #	0
Submission Date	1st Jun 22 05:12:53
Current Stage	Manuscript submitted
Title	Monastrol, a kinesin-Eg5 inhibitor, inhibits invasion and metastasis of human colorectal cancer cells by targeting fascin.
Manuscript Type	Article
Corresponding Author	Dr Pablo Conesa-Zamora (pablo.conesa@carm.es) (Hospital Universitario Santa Lucía)
Authors	Ms Begoña Alburquerque González , Dr Silvia Montoro-García , Dr Ángel Bernabé-García , Dr Manuel Bernabé García , Dr Priscila Campioni Rodrigues , Mr Alejandro Rodríguez Martínez , Dr Irene Luque-Fernández , Dr Tuula Salo , Dr Horacio Pérez-Sánchez , Dr Maria Luisa Cayuela-Fuentes , Dr Ginés Luengo Gil , Dr Francisco José Nicolás-Villaescusa , Dr Alfonso Pérez Garrido
Abstract	Background: The rearrangement of the actin cytoskeleton is a prerequisite for carcinoma cells to develop cellular protrusions, required for migration, invasion, and metastasis. Fascin is the key protein in actin bundling and is expressed in aggressive and invasive carcinomas. Additionally, fascin seems to be involved in tubulin binding and in microtubule rearrangement. Pharmaphoric based in-silico screening was performed to find compounds with better fascin inhibitory properties than migrastatin. We then hypothesize that monastrol has anti-migratory and anti-invasive properties via fascin blocking in colorectal cancer cell lines. Methods: Biophysical (Thermofluor and ligand titration followed by fluorescence spectroscopy), biochemical (actin bundling), and cellular assays (MTT, invasion on human tissue) as well asanimal model studies (zebra fish invasion) were performed to characterize the inhibitory effect of monastrol on fascin activity. Confocal microscopy and immunoprecipitation assays were carried out to test whether monastrol is able to disrupt the fascin-tubulin interaction.Results. The in-silico analysis revealed monastrol as a potentially fascin-binding compound. Biophysical and biochemical assays demonstrated that monastrol binds fascin and interferes with its actin bundlingactivity. Cell culture studies including a 3D human myoma disc model, showed that monastrol inhibits fascin-driven cytoplasmic protrusions as well as invasion. In-silico, confocal microscopy and immunoprecipitation assays demonstrated that monastrol can disrupt the fascin-tubulin interaction. These anti-invasive effects were further confirmed in vivo. Conclusions. This study reports, for the first time, the in vitro and in vivo anti-invasive properties of monastrol on colorectal tumor cells possibly due to a direct inhibition of fascin.
Techniques	Life sciences techniques, Cell/tissue technologies [Flow cytometry]; Life sciences techniques, Cell/tissue technologies [Tissue culture]; Life sciences techniques, Cellular imaging [Electron microscopy]; Life sciences techniques, High throughput screening [High-throughput screening assays]; Life sciences techniques, Experimental organisms [Zebrafish]; Life sciences techniques, Protein techniques [Electrophoresis]; Life sciences techniques, Cellular imaging [Confocal microscopy]; Life sciences techniques, Structural biology [Antibodies];
Subject Terms	Biological sciences/Drug discovery/Biologics Biological sciences/Cancer/Cancer therapy
Research Square author dashboard	I understand that my manuscript and associated personal data will be shared with Research Square for the delivery of the author dashboard.
In Review	Yes, my co-authors and I would like to opt in to *In Review*
Conflict of Interest	There is no conflict of interest
Applicable Funding Source	Ministry of Economy and Competitiveness | Instituto de Salud Carlos III (Institute of Health Carlos III) - PI18/00144 [Conesa-Zamora] Fundación Séneca Jóvenes Líderes JLI 20646/18 [Montoro-García]

Stage	Start Date
Under Review	1st Jun 22 05:12:54
Author Approved Converted Files	1st Jun 22 05:12:53
Preliminary Manuscript Data Submitted	30th May 22 12:21:28

Monastrol, a kinesin-Eg5 inhibitor, inhibits invasion and metastasis of human colorectal cancer cells by targeting fascin.

Begoña Alburquerque-González[1,†], Silvia Montoro-García[1,†], Ángel Bernabé-García[2], Manuel Bernabé-García[3], Priscila CampioniRodrigues[4],Alejandro Rodríguez-Martínez[5],Irene Luque[5], Tuula Salo[6], Alfonso Pérez-Garrido[7,] Horacio Pérez-Sánchez[7], María Luisa Cayuela[3], Ginés Luengo-Gil[8], Francisco José Nicolás[2,#,] and Pablo Conesa-Zamora[1,8,#*]

1 Facultad de Ciencias de la Salud, Universidad Católica de Murcia (UCAM), Guadalupe, Spain; balburquerque2@ucam.edu (B.A.G); smontoro@ucam.edu (S.M.G); pablo.conesa@carm.es (P.C.Z)

2 Regeneración, Oncología Molecular y TGF-ß. IMIB-Arrixaca. Carretera Madrid-Cartagena. 30120 El Palmar, Spain; a.bernabegarcia@gmail.com (A.B.G); franciscoj.nicolas2@carm.es (F.J.N)

3 Researchgroup "Telomerasa, Envejecimiento y Cáncer", CIBERehd, Hospital Clínico Universitario Virgen de la Arrixaca, IMIB-Arrixaca, Murcia, Spain; mbg98181@gmail.com (M.B.G); marial.cayuela@carm.es (M.L.C)

4 Cancer and Traslational Medicine Research Unit, University of Oulu, Aapistie 5A, FI-90220, Oulu, Finland; priscilacampioni@gmail.com

5 Department of Physical Chemistry, Institute of Biotechnology and Excellence Unit in Chemistry Applied to Biomedicine and Environment, School of Sciences, University of Granada, 18071 Granada, Spain; iluque@ugr.es; alrodriguez@ugr.es.

6 Cancer and Traslational Medicine Research Unit, University of Oulu, Aapistie 5A, FI-90220, Oulu, Finland; tuula.salo@oulu.fi; and Medical Research Center, Oulu University Hospital, Oulu, Finland; Department of Oral and Maxillofacial Diseases, University of Helsinki, Haartmaninkatu 8, FI-0014, Helsinki, Finland; tuula.salo@helsinki.fi, and Translational Immunology Research Program (TRIMM), University of Helsinki, Helsinki; Department of Pathology, Helsinki University Hospital, Helsinki, Finland.

7 Structural Bioinformatics and High-Performance Computing (BIO-HPC) Research Group, Universidad Católica de Murcia (UCAM), Guadalupe, Spain; hperez@ucam.edu; aperez@ucam.edu.

8 Pathology and Clinical Analysis Department, Group of Molecular Pathology and Pharmacogenetics, Instituto Murciano de InvestigaciónBiosanitaria (IMIB), Hospital Universitario Santa Lucía, Cartagena, Spain.; ginesluengo@um.es (G.L.G); pablo.conesa@carm.es (P.C.Z)

* Correspondence:pablo.conesa@carm.es (P.C.Z); Tel.: +34-968128600 (ext. 951615).

† These authors have contributed equally to this work.

#These authors have contributed equally to this work and share last authorship.

Abstract

Background: The rearrangement of the actin cytoskeleton is a prerequisite for carcinoma cells to develop cellular protrusions, required for migration, invasion, and metastasis. Fascin is the key protein in actin bundling and is expressed in aggressive and invasive carcinomas. Additionally, fascin seems to be involved in tubulin binding and in microtubule rearrangement. Pharmaphoric based *in-silico* screening was performed to find compounds with better fascin inhibitory properties than migrastatin. We then hypothesize that monastrol has anti-migratory and anti-invasive properties via fascin blocking in colorectal cancer cell lines. *Methods*: Biophysical (Thermofluor and ligand titration followed by fluorescence spectroscopy), biochemical (actin bundling), and cellular assays (MTT, invasion on human tissue) as well asanimal model studies (zebra fish invasion) were performed to characterize the inhibitory effect of monastrol on fascin activity. Confocal microscopy and immunoprecipitation assays were carried out to test whether monastrol is able to disrupt the fascin-tubulin interaction.*Results*. The *in-silico* analysis revealed monastrol as a potentially fascin-binding compound. Biophysical and biochemical assays demonstrated that monastrol binds fascin and interferes with its actin bundlingactivity. Cell culture studies including a 3D human myoma disc model, showed that monastrol inhibits fascin-driven cytoplasmic protrusions as well as invasion. *In-silico,* confocal microscopy and immunoprecipitation assays demonstrated that monastrol can disrupt the fascin-tubulin interaction. These anti-invasive effects were further confirmed *in vivo*. *Conclusions*. This study reports, for the first time, the *in vitro* and *in vivo* anti-invasive properties of monastrol on colorectal tumor cells possibly due to a direct inhibition of fascin.

Keywords: Monastrol; fascin; cytoskeleton rearrangement, colorectal cancer; tubulin; invasion.

Introduction

Remarkable progress has been made in recent years towards the understanding, prevention and treatment of malignant tumors but, unfortunately, metastatic cancer remains a leading cause of disease-related mortality (1). The protein fascin (FSCN1 gene) is an actin-binding protein that plays a role in the organization of actin filament parallel bundles and the formation of microspikes, membrane ruffles, and stress fibers.It is also important for the formation of a diverse set of cell protrusions, such as filopodia, and for cell motility and migration (2-6). In 2013, a meta-analysis reported that fascin is associated with increased risk of metastasis and mortality in several cancer types, including colorectal cancer (7). In the same year, our group identified fascin as an overexpressed protein in serrated adenocarcinoma (SAC) (8), a histological subtype of colorectal carcinoma characterized by very bad prognosis (9) and a more active invasive front evidenced by a higher occurrence of tumor budding, cytoplasmic pseudofragments and infiltrative tumor growth pattern (10).

Given the higher expression of fascin in SAC, its active role promoting an invasive phenotype and its overexpression associated with poorsurvival in a wide variety of cancer types (7), it was then postulated as a target for the search and development of therapeutic compounds with anti- fascin properties (11).

According to this line, migrastatin and its macroketone analogues, considered typical inhibitors of fascin, have been shown to decrease metastatic tumor cell migration, invasion and tumor metastasis (4). Other potential fascin inhibitors have been identified using bioinformatics methods, which are particularly useful in drug discovery, especially when the target protein is defined (12).Monastrol, a small molecule that arrests cells in mitosis by inhibiting Eg5, a member of the Kinesin-5 family (13) already defined as an anticancer drug, was found to bind and inhibit fascin. In the current study,

experimental and *in vivo* approaches are combined to confirm the fascin inhibitory activity of monastrol and its potential as antimetastatic agent.

Materials and Methods

In-silico screening

Pharmaphoric based *in-silico* screening was performed with LigandScout (LS) tofind compounds with better fascin inhibitory properties than migrastatin (14). A pharmacophore model was created from the core of the structure of migrastatin(MGS_CORE) via LS(15). This model was screened against a subset of the DrugBanklibrary (version 5.0; of 9591 compounds, including 2037 approved by the American FDA, 96 nutraceuticals, and 6000 experimental) after fine-tuning on a high-performance computing (HPC) cluster of all related necessary programs from the LS suite (16).

Blind docking

Monastrol structure was obtained from the DrugBank library, identified by DB004331 code as mol2 and pdbqt files. Regarding fascin, the protein structure used for the calculations was extracted from the X-ray crystal structure of the complex of fascin and NP-G2-044 inhibitor (PDB ID: 6B0T)(14). Maestro and Auto Dock Tools preprocessed both structures to prepare structures for blind docking, obtaining mol2 and pdbqt files, respectively.

After obtaining fascin and monastrol structure models, blind docking calculations were carried out via the metascreener tool (https://github.com/bio-hpc/metascreener) to find

out the top interacting poses and the details about their interactions between DB004331 and the fascin protein structure. In this way, two different docking programs were used to perform blind docking: Autodock Vina2 and LeadFinder3. Both methods were executed in a consensus way for fascin model target with monastrol as the query on the computing server (17).

Thermofluor

Differential Scanning Fluorimetry (Thermofluor) assays were performed using a Biorad C1000 Touch Thermal Cycler CFX96 RT-PCR system in a 96-well format. 25 μL of reaction mixtures were set up containing 2 μM fascin (cat. No. 8411-02, Hypermol, Bielefeld, Germany) in 20 mM HEPES, 150 mM NaCl, 1mM DTT and 5% sucrose at pH 7.4, in the presence of SYPRO Orange (1000-fold dilution from the commercial stock (Invitrogen). The indicated compound, prepared at 10 mM in 100% DMSO, was added to each well to a final concentration of 1 mM and 10% dimethyl sulfoxide (DMSO). Three replicates per compound together with six internal controls, containing only free protein in 10% DMSO, were included in the 96-well plates. The PCR plates were covered and subsequently shaken, centrifuged, incubated for 2 min at 20 °C inside the RT-PCR machine and heated from 20 to 100 ºC at a 1ºC/min scan-rate.

The T_m values were measured as the minimum of the first derivative of the thermal unfolding profile. Average Tm values for unbound fascin were obtained for each internal filter (FAM, HEX and T-Red) as reference for the determination of the changes in Tm upon compound binding (T_m, FAM = 55.6 ± 0.5 ºC, T_m, HEX = 56.0 ± 0.0 ºC, T_m, Tred = 56.2 ± 0.6 ºC, where the error values correspond to the standard deviation for the seven replicas included in each plate as internal controls).

Fluorescence titration

Fluorescence titration experiments were performed in a Cary Eclipse spectrofluorometer (Varian Inc.). A 14.7 µM fascin solution was titrated with monastrol by adding increasing volumes of concentrated solutions. Emission spectra were recorded between 307 and 500 nm at 25 °C in 10% DMSO, 100 mM NaCl, 20 mM HEPES, pH 7.4, with the excitation wavelength fixed at 280 nm. Binding isotherms were generated using either the changes in spectral area or in spectral centre of mass (CM), depending whether the change was only in fluorescence intensity or also in the of the maximum emission fluorescence wavelength. The resulting curves were fitted using ORIGIN 7.0 (Microcal Inc.) and a one-site equilibrium binding model, according to the following equation:

$$\mathrm{F} = F_f + \left(F_b - F_f\right) \cdot \frac{\left(P_T + L_T + K_d\right) - \sqrt{\left(P_T + L_T + K_d\right)^2 - 4 \cdot P_T \cdot L_T}}{2 \cdot P_T}$$

Where Ff and Fb are the fluorescence signal (area or CM) of free and bound fascin and PT and LT are the total protein and ligand concentration, respectively, at each addition point.

F-actin bundling assay

Actin-bundling activity was measured by a low–speed centrifugation assay using the Actin Binding Protein Biochem Kit TM Muscle Actin (Cytoskeleton, Inc. Cat. # BK001). Briefly, rabbit muscle actin was induced to polymerize to F-actin using 250 µL of General Actin Buffer, and adding 25 µL of actin polymerization buffer at room temperature (RT) for 1 hour. Fascin (1 µM) protein (Hypermol, Bielefeld, Germany) was incubated with100 µM migrastatin (AnalytiCon Discovery, cat. No. NP-006108)

and 100 µM monastrol (Catalog No. S8439, Selleck.eu)and 4% DMSO for 30 minutes at RT. All samples and controls were subsequently incubated with F-actin (10 µM) for another 30 minutes at RT. F-actin bundling activity was then determined performing a low-speed centrifugation (10.000 *g*, 1h, RT) after samples incubation. Both supernatants and pellets were dissolved in an equivalent volume of SDS sample buffer and loaded into an SDS-PAGE electrophoresis gel. The amount of protein in the different fractions was determined by measuring the intensities of Coomassie-stained proteins using ImageJ v1.52p software (National Institute of Health, Bethesda, MD, USA), from which the relative F-acting bundling activity was calculated.

Transmission Electron Microscopy Detection

Transmission electron microscopy (TEM) was assessed, following as previously described by Jansen et al. 2011 (18-21). Briefly, actin (21 µM) was polymerized according to the protocol from the Actin-Binding Protein BiochemKit™ Muscle Actin (Cytoskeleton Inc., Denver, CO, USA) and then incubated with human recombinant fascin (Hypermol, Bielefeld, Germany) (molar ratio 1:1) for 30 min at room temperature. Fascin was previously incubated for 2 h at RT with 0.1% DMSO (control), 100 µM migrastatin or 100 µM monastrol. The samples were directly adsorbed onto 200 mesh copper grids for 30 sec, blotted to remove excess solution, washed twice with distilled water, and negatively stained with 1% (w/v) uranyl acetate for 30 sec, blotted, and dried again. The TEM study of actin filaments and fascin-actin bundles was performed on a PHILIPS TECNAI 12 transmission electron microscope (FEI, Osaka, Japan) at an accelerating voltage of 80 kV and a magnification up to 135,000X. Images were captured on a coupled device camera (Megaview III). The numbers of filaments

per bundle were counted manually in 20 pictures/condition and statistically analyzed (Mann–Whitney test).

Cell culture

The cell lines were obtained from the American Type Culture Collection (ATCC, Rockville, MD) and cultivated in high glucose Dulbecco's Modified Eagle's Medium (DMEM) containing 10% heat-inactivated fetal bovine serum (FBS), 50 U/ml penicillin and 50 µg/mL streptomycin (Sigma Aldrich Chemical Co., USA) in an atmosphere of 5% CO_2 and 95% humidified air at 37°C. Subculture was performed when 90% confluence was obtained.

Cell viability assay

Exponentially growing cells were plated in triplicate in flat-bottomed 96-well plates (Nunc, Roskilde, Denmark) at 1500 cells/well. The day after, drugs were added in serial dilutions from 0.5 to 300 µM. Control wells contained medium without drug plus 0.1% DMSO. Plates were incubated for 72 h in a humidified 5% CO_2 incubator and assayed for cell viability. Tetrazolium (MTT) dissolved in phosphate-buffered saline (PBS), pH 7.2, at 1.9 mg/mL was added to the cells (30 µL/well). After incubation at 37°C for 4 h, the medium was aspirated. The formazan crystals were dissolved in 200 µL DMSO for 30 min and the absorbance was read at 570 nm in a microtiter plate reader. Results were calculated as: cell viability (%) = average O.D. of wells/average O.D. of control wells.

Immunofluorescence

For immunofluorescence, round coverslips (Thermo Fisher, Waltham, MA USA) were seeded with HCT-116 cell line in the presence of 10% FBS. After cells reached 100% confluence, serum supplemented medium was removed and replaced with fresh serum free medium for 24h. Artificial wounding was performed by transversally dragging a sterilized razor blade on the central area of the coverslips. Coverslips were then placed in 6-well plate with 2 mL serum free DMEM: control condition (0.1% DMSO), 100 µM migrastatin or 100 µM monastrol for 24h. Cells were then fixed with Bouin (for fascin protein) or 4% formaldehyde and subsequently permeabilized in a 0.3% Triton X-100/PBS solution, and then exposed to blocking buffer for 30 min. Samples were incubated for 1 h with anti-fascin antibody (1/250) (55K-2 clone; Santa Cruz Biotechnology, Heidelberg, Germany) in a wet chamber. Appropriate fluorescent-labelled primary antibodies were incubated later with Alexa fluor 488- conjugated anti-mouse IgG (from donkey) (1/400) or Alexa fluor 594-labelled phalloidin, respectively (1/1000) (Molecular Probes, Thermo Fisher Scientific, Waltham, MA USA) and Hoechst 33258 (Fluka, Biochemika, Sigma-Aldrich, St Louis, MO, USA) for 30 min at RTand darkness. Samples were examined and representative images were taken with a confocal microscope (LSM 510 META from ZEISS, Jena, Germany).

In order to test the colocalization of fascin and β-tubulin, an immunofluorescence assay was also performed as previously described (22, 23). The following commercial antibodies were used: mouse anti-β-tubulin (DSHB #E7), anti-fascin antibody ([EP5902] (ab126772)).Images were taken using aConfocal Leica SP8.Co-localization analyses were performed using the JaCoPpluggin co-localization module of the Fiji ImageJ software (24).

Transwell invasion assay

The invasive capacities of HCT-116 cells were determined using Cytoselect TM 24 Well Cell Invasion Assay (Basement Membrane Colorimetric Format) with coated Transwell chambers (8 μm pore size). Briefly, cells were resuspended with serum-free medium and treated with corresponding inhibitors (100 μM migrastatin and 100 μM monastrol). We were seeded 9.5×10^4 cells into the upper chamber, and 500 μL of DMEM containing 10% FBS were added to the lower chamber. After 30 hours of incubation, cells that remained on the upper chamber were scrapped away with a cotton swab, and the cells that migrated to the bottom of the filter were stained with the cell stain solution. The number of invaded cells was reported using an inverted phase contrast microscope and quantified Optical Density (O.D) by a spectrophotometer at λ=560 nm. Likewise, the invasive cells were counted and analyzed using the Image J v1.52p software (National Institute of Health, Bethesda, MD, USA). Each experiment was performed in triplicate.

Myoma organotypic invasion model

To improve the reliability of the experimental model compared to the real tumor microenvironment, cancer cell invasion was assessed in the myoma organotypic cultures and performed according to the previously published myoma model protocol (25, 26) . Briefly, uterine leiomyoma tissues were obtained from routine surgery after informed consent of the donors and their use approved by The Ethics Committee of the Oulu University Hospital. The myoma tissue was sliced into 5 mm and disks were made with an 8-mm biopsy punch (Kai Industries Co., Gifu, Japan). Myoma disks were pre-incubated in control conditions (0.1% DMSO), 100 μMmigrastatin or 100 μM

monastrol, at 4°C for 48 h. The myoma disks were placed into Transwell inserts (diameter 6.5 mm; Corning Incorporated, Corning, NY) and 700,000 cells in 50 μL of media were added on top of each myoma disk. The cells were allowed to attach overnight and the myoma disks were transferred onto uncoated nylon disks resting on curved steel grids in 12-well plates with 1 mL of media plus compounds in each well. The human cells were left to invade the myoma disks for 14 days, while changing the treatment media every 3 days. Subsequently the myoma discs were fixed with 4% neutral buffered formalin at RT for 24 h and processed for histology. Six-μm sections were cut and stained with cytokeratin AE1/AE3 (M3515, Dako). Sections were documented at ×10 magnification, using the Leica DMRB microscope DFC 480 camera with the Leica application suite v3.8 (Leica Microsystems, Wetzlar, Germany). Image J v1.46o software(National Institute of Health, Bethesda, MD, USA) was used to measure invasion areas and depths. Each experimentwas performed in triplicate.

Zebrafish invasion and metastasis assays

The colonization of Zebrafish (*Danio rerio*) embryos by human cancer cells was performed as previously described (27). This was approved by the Bioethical Committee of the University Hospital *Virgen de la Arrixaca* (Murcia, Spain). Briefly, colorectal cancer cells were trypsinized, washed and stained with fluorescent CM-Dil (Vibrant, Invitrogen) as manufacturer described. 50-100 labelled cells were injected into the yolk sac of dechorionated zebrafish embryos. Embryoswere treated in control conditions (0.1% DMSO), 100μM migrastatin or 100 μM monastrol. Fishes with fluorescently labelled cells appearing outside the implantation area at 2 h post-injection were excluded from further analysis. All other fishes were incubated at 35ºC for 48 h and analyzed with a SteReoLumar V12 stereomicroscope equipped with an AxioCam

MR5 camera (Carl Zeiss). The evaluation criteria for embryos being colonized by human cancer cells was the presence of more than 3 cells outside of the yolk sac. A zebrafish colonization index was calculated as being the proportion of embryos being colonized in the wild type and mutant cells divided by the proportion of invaded embryos in the pcDNA transfected cells.

Metastasis assay was based on previous works by Fior et al., in which a metastatic potential assay on zebrafish was performed (28). Native HCT-116 cells were stained and xenografted as already mentioned. From the 3rdday post-injection, larvae were fed with ZEBRAFEED by Sparos (<100 _m), and treatments were changed daily. At 6thday post-injection, larvae wereexamined for monitoring tumor growth and invasion using a fluorescent microscope. The evaluation for metastasis potential by human cancer cells was the presence of cell colonies (dividing cells) outside the yolk sac.

The experiments were repeated in triplicate, obtaining an average value after 4days post-xenograft (invasion assay) and 6 days post-xenograft (metastasis assay). All the protocols in the manuscript comply with the recommendation, the approval of which was obtained from the participant institutions and in accordance with the ethical standards laid down in the 1964 Declaration of Helsinki and its later amendments.The extended treatment of migrastatin in the metastatic assay (beyond the 4th day) was toxic for the larvae and therefore, only monastrol results are presented.

Immunoprecipitation and western blot

For immunoprecipitation, essentially, we follow the protocol as in (29). Briefly, cells were stimulated and total protein extracts were obtained by lysis of harvested cells using lysis buffer: 50 mM HEPES pH 7.2, 150 mMNaCl, 1 mM EDTA, 1.2 mM MgCl2, 1% Triton X-100, 10% Glycerol (all from Sigma-Aldrich, St Louis, MO, USA),

supplemented with 1 mM DTT, 25 mMNaF, 25 mMβ-glycerophosphate, 1:100 phosphatase inhibitors (I and II) and 1:100 protease inhibitors (all from Sigma-Aldrich, St Louis, MO, USA). Cells were treated by 0.1% DMSO and 100µM monastrol. Samples of extract taken prior to IP were processed in parallel with the immunoprecipitates and were considered as inputs.For IP, 500 ng of the control IgG and ß-tubulin antibody was added to 400 µg of protein total extract and incubated for 1 h at 4 °C. Antibodies were purified using A and G protein 4 Fast Flow coupled sepharose (Cytiva, Uppsala, Sweden) previously blocked with BSA 0.2 mg/mL (SantaCruz Biotechnology, Heidelberg, Germany) in lysis buffer. Samples were washed with supplemented lysis buffer and finally resin was resuspended in 60 µl of loading buffer. Then, samples were analyzed by SDS-PAGE followed by western blot (WB) with recombinant 1:2000 anti-fascin antibody (2h, 5% milk) and 1:250 anti-β-tubulins (2h, 1%BSA). Secondary antibodies were anti-rabbit IgG horseradish peroxidase linked F(ab')2 I fragment from donkey (GE Healthcare, GE, Little Chalfont, United Kingdom) and horseradish peroxidase linked rat anti-mouse IgG1 (Beckton Dickinson, Franklin Lakes, NJ, USA). WBs were revealed using horseradish peroxidase substrate (ECL; GE Healthcare, GE, Little Chalfont, United Kingdom). Images were obtained with a Chemidoc XRS® (Bio-Rad, Hercules, CA, USA).

Data analysis

Data are expressed as mean ± standard deviation (SD). Data were analyzed for statistical differences by the Student's t-test for paired and unpaired data after testing for normal distribution of the data. For *in vitro* experiments, Kruskal-Wallis (KW) test was performed for comparisons between groups. Differences were considered significant at

an error probability of $P < 0.05$. SPSS 18.0 software was used for the rest of statistical analyses (SPSS, Inc, Chicago, Illinois, USA).

Results

In-silico screening

After*in-silico*screening calculations and careful visual inspection of the obtained results, monastrol was selected as one of the top 31 candidates for posterior experimental validation. The pharmacophore model derived for migrastatin is depicted in Figure 1A.A 3D aligment of monastrol with migrastatin is shown (Figure 1B).

When Blind Docking calculations were finished, a consensus of the results ofAutoDock Vina and LeadFinderDocking calculations were carried out. Thus, we obtained the best-scored DB004331 clustered poses of the ligand among two techniques results, sorted by binding energy score and the interactions of these poses with fascin residues via PLIP 4. Finally, we obtained the protein-ligand complex snapshot with the PyMOL program 5. We have indicated the actin-binding sites, microtubules binding sites, and those clustered poses with interactions in these sites.First, the clustered poses in the two known actin sites 1,6 are found in the top positions of the calculations. In AutodockVina blind docking results (Figure 2A), poses 2 (Score: -6.11 kJ/mol) and 3 (Score: -5.72 kJ/mol) correspond with the known actin-binding sites. In the case of the Lead Finder method (Figure 2B), the first and second clustered poses also interact with the two indicated actin-binding sites with scores of -8.51 kJ/mol and -7.30 kJ/mol, respectively. Both calculations have found interactions between monastrol and the key

residue Leu40 for the actin-binding site 1 and the key residues Phe216 for the actin-binding site 2.

In addition, in results obtained by both methods, we can observe interactions between monastrol and residues that are part of the tubulin-binding site sequence. The results of Autodock Vina (Supplemental FigureS1A) showed hydrogen bond interactions in Lys244 and Ala245 residues in the clustered pose 17 (Score: -4.48 kJ/mol). On the other hand, we have found a clustered pose in rank 13 (Score: -6.11 kJ/mol) in Lead Finder calculations (Supplemental Figure S1B), where we can observe hydrophobic interactions with Lys244, and hydrogen bonds formation with Lys244, Ala245 and Lys247. Finally, after performing the consensus analysis, the generated poses with ranks 1 and 2 correspond with actin-binding sites 1 and 2, respectively, showing interactions between monastrol and Leu40 in the actin-binding site 1 (Supplemental Figure S2), and between residues Phe216 and Gln11 in the actin-binding site 2. Regarding the tubulin-binding site, three poses with interactions with some of its sequence residues can be observed (Supplemental Figure S2) in ranks 13, 25 and 31, respectively, with monastrol interactions with the following residues: Ala242, Lys 244, Ala245 and Lys247, all of them belonging the amino acid sequences that describe tubulin binding site.

Thermofluor and fluorescence titration

The direct interaction between the compounds selected by virtual screening with fascin was examined *in vitro* using a differential fluorescence screening (Thermofluor) assay, as described before (18, 19).The results of the Thermal Shift assay are summarized in Table 1. Some compounds resulted in distorted thermal unfolding profiles from which

reliable T_m values could not be extracted, probably due to compound interference with the Sypro fluorescence signal. Other induced a clear shift on the T_m to higher values, indicative of a binding-induced stabilization of the protein.Within those that could be analyzed, imipramine and monastrol (Figure 3), consistently resulted in a significant increase in T_m, of about 2 ˚C, suggesting specific binding to fascin.

Binding of monastrol to fascin was validated *in vitro* using fluorescence titration experiments, rendering a dissociation constant in the high microMolar range (K_D = 183 μM).

Monastrol significantly decreases the fascin-induced actin bundles.

In the low speed centrifugation assay, the pellets contain bundles of F-actin polymers (30). Purified fascin increased the amount of F-actin in the pellets (Figure 4A). However, in the presence of 100 μM migrastatin and 100 μM monastrol, the fascin-induced bundling of F-actin polymers decreased significantly (both $p<0.01$) and remained in the supernatant (Figure 3B). In addition, negative contrast in TEM allowed the visualization of actin fibers formed in the presence of fascin and to comparethe effects of inhibitors. In control conditions, actin-fascin consisted of a highly dense packed actin bundle (Figure 5B). When fascin was pre-incubated with either 100 μM migrastatin or monastrol per separate, a disorganization of the bundles was observed, resulting in fewer filaments than in control (Kruskal–Wallis test, $p<0.001$) (Figure 5C-E, respectively). No statistical difference was found between the two inhibitors for any of the two *in vitro* approaches.

Monastrol compromises colorectal cell lines proliferation but not viability

According to data presented in Figure S3, the working concentration of monastrol was set up at 100 µM for subsequent *in vitro* studies.

Monastrol affects actin rearrengement at the lamellipodium

The effect of monastrol on the reorganization of the actin cytoskeleton, which includes the protrusion of the lamellipodium at the cell front, and filopodia formation was assessed by immunofluorescence (Figure 6). A prominent filopodia lamellipodium formation was observed in control conditions whereas these cytoskeleton structures were absent in those cells treated withboth inhibitors (Figure 6). Assays with HaCaT cells in the presence of monastrol as well as with Epidermal growth factor (EGF) and migration inhibitor targeting Mek pathway (PD98059) were also performed in parallel,as in previous studies (data not shown) (18-20). Lamellipodia protrusion number was calculated in the different conditions, being significantly lower after inhibitor treatments (Table S1).

Monastrol inhibits cell invasion of colorectal cancer cells

Tumor cell invasion not only involves the acquisition of migration properties but also the ability to degrade the extracellular matrix (ECM)(31). For that reason, we performed a Transwell assay on Matrigel which resembles the ECM basement membrane composition. As shown in Figure 7, monastrol, similarly to migrastatin, inhibited tumor cell invasion of HCT-116 cells (all $p<0.01$) (19).

As already shown in our previous studies, an interesting *in vitro* model for assay the anti-invasive properties of potential inhibitors is the human uterus myoma tissue derived myoma disc model (32). Figure 8 shows that 100 µM monastrol is an effective inhibitor

in this model in a dose-dependent manner, which was comparable to migrastatin (all $p<0.001$).

Monastrol reduces invasion and metastasis in zebrafish larvae model

Consistent with our previous studies (18, 19), the *in vivo* anti-invasive potential of monastrol was tested by using the well-established zebra fish larvae xenograft invasion model. As shown in Figure 9A, a significant inhibition of DLD-1 and HCT-116 cell invasion was observed in larvae growth in the presence of both, 100 µM migrastatin or 100 µM monastrol when compared to control conditions (all$p<0.05$).DLD-1 cells presented a lower invasion compared to HCT-116 cells (Figure 9A). Due to the higher efficacy of inhibitors in HCT-116 cells, a metastasis model (up to 6^{th}day post-injection) was performed with these cancer cells (Figure 10C). Thus, monastrol was found to inhibit the formation of metastatic foci of HCT-116 cells in the same zebra fish model ($p<0.0001$, Figure 9D)

Monastrol disrupts Fascin-tubulin interaction

Since monastrol has been described as an inhibitor of the Eg5 a member of the kinesin-5 family (33), an immunoprecipitation (IP) assay was carried out to test whether β-tubulin-fascin interaction could be affected in the presence of this compound.Monastrol treatment for 24 h decreased fascin/β-tubulin interaction (Figure 10).Moreover, a co-localization study using immunofluorescence for both proteins in HCT116.cells produced a reduction of the colocalization of both proteins in the presence of monastrol 100 µM. The calculation of Pearson correlation coefficient shows a significantly decrease of the colocalization of both proteins in the presence of 100 µM monastrol when compared to control conditions (0.1% DMSO) (Figure 11).

Discussion

Metastasis is the cause of over ninety percent of cancer deaths. This process involves complex actin cytoskeleton rearrangements enabling the tumor cells gain migratory and invasive properties through the development of cytoplasmic protruding structures such as lamellipodia and invadopodia (34). Fascin plays a critical role in the formation of such structures due to its capacity to bundle actin filaments. In fact, fascin expression is associated with cancers with high metastatic potential and bad prognosis (35). However, the actin bundling activity is just one of the fascin contributions to tumor development and promotion as other non-canonical fascin functions are being discovered including chemoresistance, immune evasion, metabolic reprogramming, and tubulin cytoskeleton rearrangement (36-42). These findings, along with the virtually absent expression of fascin in normal epithelia and its overexpression in aggressive cancers such as SAC and triple negative breast cancer (TNBC), which have no molecular targeted therapy available, makes the discovery of fascin inhibitors a crucial task.

With this aim we performed pharmacophoric based *in-silico* screening, which yielded monastrol, an allosteric mitotic kinesin Eg5 inhibitor involved in microtubule (MT) rearrangement, as a potential fascin blocker. The result was not surprising because of two facts; first Villari et al. in 2015 demonstrated the effect of fascin on MT dynamics reporting the fascin aminoacids 234 to 250 involved in direct MT binding and that this effect is essential for focal adhesion assembly of breast cancer cells (41). Second, as pointed by Riahi et al. in 2019(43), monastrol has structural similarity to nifedipine which, in a previous fascin bioassay using *Drosophila* neurons (44) proved to be a fascin inhibitor. In accordance, monastrol and migrastatin core structures were placed in a common spatial position required for actin binding activity. First, regarding the actin-binding site 1, the residue with more interactions close to the actin-binding site case was

Leu40 (14), appearing in both docking algorithms and showing a hydrophobic union. Other critical residues like Ser39 and Lys43 were found in at least one of the docking techniques. Besides, we got interactions associated with the known in literature in actin-binding site 2 like Phe216 and Gln11 (6). Such ligand protein interactions were further also in relation with the fascin thermal denaturation profiles in the presence of monastrol, which showed a T_m shift, with a similar magnitude of the previously reported fascin inhibitor imipramine (19).

Monastrol is a racemate comprising equimolar amounts of R- and S-monastrol and novel cell-permeable low molecular weight molecule which rolesas an antineoplastic agent, a urease inhibitor, an antileishmanial and antimitotic agent (13). Although many reports have been devoted to elucidating the mechanism of action of monastrol as a mitotic inhibitor in the cell cycle, few examples concerning anticancer activity have been reported (45). In this context, the aim of this study was to evaluate the proprietary compound monastrol as an anti-fascin inhibitor in colorectal cancer cell lines and to compare its effects with those of migrastatin, a typical fascin inhibitor as a control, in *in vitro* and *in vivo* assays.

It is important to highlight that monastrol, despite being suggested as a potential fascin inhibitor (43), has never being characterized for its anti-fascin properties. Subsequently, actin bundling assays confirmed that binding of monastrol, as well as of migrastatin, disrupting the capacity of fascin to form actin bundles which was further validated by TEM.In order to choose colorectal cell lines with highest and lowest endogenous fascin expression, a previous work by our group (19) performed RT-qPCR on RNA extracted from eight cell lines thus selecting DLD-1 and HCT-116 as cell lines with low and high fascin expression, respectively. In this cell culture setting, we observed that monastrol decreased fascin-driven cellular protrusions in colorectal cancer cells. The inability of

fascin to create lamellipodia caused by monastrol translated into a decreased cell invasion in a similar way to the fascin inhibitor control, migrastatin. This finding was further corroborated in a 3D human organotypic model mimicking the tumor microenvironment where monastrol decreased the depth and area of invasion of HCT-116 colorectal cancer cells showing a dose-dependent effect and in a similar way than migrastatin.

In the *in vivo* model, we observed that monastrol induced a decrease in the invasion and the formation of metastatic foci of colorectal cancer cell. Indeed, the drug effect was more pronounced in HCT-116 than for DLD-1, which might be related to the fascin levels in both cell lines.Further studies in other animal models will be needed to demonstrate the efficacy of monastrol as an anti-migratory and anti-invasive agent.

Since a recent study reported that fascin binds to tubulin (42), and other points out that monastrol is considered as an inhibitor of MT dynamics (13), we performed Blind Docking calculations across the whole fascin protein surface (see Figure S2) confirming that monastrol might interact in both, the Fascin actin-binding sites 1 and 2 and in the fascin-tubulinbinding site. These interaction areas agree with previously reported interactions sites based on mutagenesis information (41). To further complement the *in-silico* calculations, we tested *in vitro* whether monastrol could disrupt the fascin-tubulin binding by IP and confocal immunofluorescence. Within this system, fascin binding to tubulin was conditioned by the presence of monastrol. In the absence of the inhibitor, recovery of tubulin and fascin was higher in the pellet. Interestingly, the Pearson correlation coefficient also revealed a colocalization of both proteins in the lamellipodium structures although the coefficient was decreased in the presence of monastrol. Altogether, our *in vitro* results indicate that fascin interaction with tubulin is impaired by the presence of monastrol. However, whether anti-tumoral effect of

monastrol on fascin is via interactions with actin and/or tubulin requires further studies which are out of focus of this work.

Our finding suggest that monastrol is an interesting drug to test in other preclinical studies and could be interesting in clinical trials to prevent metastatic processes in patients with primary colorectal cancer positive for fascin expression. Likewise, this effect could be beneficial against other fascin-overexpressing tumors such as TNBC.These results may also have an impact on the fascin function of chemoresistance, as monastrol treatment could revert this phenomenon and have a synergistic effect with chemotherapeutic agents targeting MT such as taxanes or vinca alkaloids.

Conclusions

This study reports, for the first time, the anti-migratory and anti-invasive properties of monastrol on colorectal tumor cells possibly due, but not restricted, to a direct inhibition of fascin. Besides, our data demonstrate that monastrol interacts outside the actin binding site which should be explored further. These results imply a clinical potential of the use of monastrol as a promising therapy for invasive and metastatic cancers.

References

1. Kohno T, Ninomiya T, Kikuchi S, Konno T, Kojima T. Staurosporine induces formation of two types of extra-long cell protrusions: actin-based filaments and microtubule-based shafts. Mol Pharmacol. 2015;87(5):815-24.
2. Conacci-Sorrell M, Ngouenet C, Anderson S, Brabletz T, Eisenman RN. Stress-induced cleavage of Myc promotes cancer cell survival. Genes Dev. 2014;28(7):689-707.
3. Kim SH, Choe JY, Jeon Y, Huh J, Jung HR, Choi YD, et al. Frequent expression of follicular dendritic cell markers in Hodgkin lymphoma and anaplastic large cell lymphoma. J Clin Pathol. 2013;66(7):589-96.
4. Chen L, Yang S, Jakoncic J, Zhang JJ, Huang XY. Migrastatin analogues target fascin to block tumour metastasis. Nature. 2010;464(7291):1062-6.
5. Kotzor N, Lechmann M, Zinser E, Steinkasserer A. The soluble form of CD83 dramatically changes the cytoskeleton of dendritic cells. Immunobiology. 2004;209(1-2):129-40.
6. Yang S, Huang FK, Huang J, Chen S, Jakoncic J, Leo-Macias A, et al. Molecular mechanism of fascin function in filopodial formation. J Biol Chem. 2013;288(1):274-84.
7. Tan VY, Lewis SJ, Adams JC, Martin RM. Association of fascin-1 with mortality, disease progression and metastasis in carcinomas: a systematic review and meta-analysis. BMC Med. 2013;11:52.
8. Conesa-Zamora P, Garcia-Solano J, Garcia-Garcia F, Turpin Mdel C, Trujillo-Santos J, Torres-Moreno D, et al. Expression profiling shows differential molecular pathways and provides potential new diagnostic biomarkers for colorectal serrated adenocarcinoma. Int J Cancer. 2013;132(2):297-307.
9. Garcia-Solano J, Perez-Guillermo M, Conesa-Zamora P, Acosta-Ortega J, Trujillo-Santos J, Cerezuela-Fuentes P, et al. Clinicopathologic study of 85 colorectal serrated adenocarcinomas: further insights into the full recognition of a new subset of colorectal carcinoma. Hum Pathol. 2010;41(10):1359-68.
10. Garcia-Solano J, Conesa-Zamora P, Trujillo-Santos J, Makinen MJ, Perez-Guillermo M. Tumour budding and other prognostic pathological features at invasive margins in serrated colorectal adenocarcinoma: a comparative study with conventional carcinoma. Histopathology. 2011;59(6):1046-56.
11. Liu H, Zhang Y, Li L, Cao J, Guo Y, Wu Y, et al. Fascin actin-bundling protein 1 in human cancer: promising biomarker or therapeutic target? Mol Ther Oncolytics. 2021;20:240-64.
12. Xia X. Bioinformatics and Drug Discovery. Curr Top Med Chem. 2017;17(15):1709-26.
13. Cochran JC, Gatial JE, 3rd, Kapoor TM, Gilbert SP. Monastrol inhibition of the mitotic kinesin Eg5. J Biol Chem. 2005;280(13):12658-67.
14. Huang J, Dey R, Wang Y, Jakoncic J, Kurinov I, Huang XY. Structural Insights into the Induced-fit Inhibition of Fascin by a Small-Molecule Inhibitor. J Mol Biol. 2018;430(9):1324-35.
15. Geppert H, Vogt M, Bajorath J. Current trends in ligand-based virtual screening: molecular representations, data mining methods, new application areas, and performance evaluation. J Chem Inf Model. 2010;50(2):205-16.
16. Wolber G, Langer T. LigandScout: 3-D pharmacophores derived from protein-bound ligands and their use as virtual screening filters. J Chem Inf Model. 2005;45(1):160-9.
17. Trott O, Olson AJ. AutoDock Vina: improving the speed and accuracy of docking with a new scoring function, efficient optimization, and multithreading. J Comput Chem. 2010;31(2):455-61.
18. Alburquerque-Gonzalez B, Bernabe-Garcia A, Bernabe-Garcia M, Ruiz-Sanz J, Lopez-Calderon FF, Gonnelli L, et al. The FDA-Approved Antiviral Raltegravir Inhibits Fascin1-Dependent Invasion of Colorectal Tumor Cells In Vitro and In Vivo. Cancers (Basel). 2021;13(4).

19. Alburquerque-Gonzalez B, Bernabe-Garcia M, Montoro-Garcia S, Bernabe-Garcia A, Rodrigues PC, Ruiz Sanz J, et al. New role of the antidepressant imipramine as a Fascin1 inhibitor in colorectal cancer cells. Exp Mol Med. 2020;52(2):281-92.
20. Montoro-Garcia S, Alburquerque-Gonzalez B, Bernabe-Garcia A, Bernabe-Garcia M, Rodrigues PC, den-Haan H, et al. Novel anti-invasive properties of a Fascin1 inhibitor on colorectal cancer cells. J Mol Med (Berl). 2020;98(3):383-94.
21. Jansen S, Collins A, Yang C, Rebowski G, Svitkina T, Dominguez R. Mechanism of actin filament bundling by fascin. J Biol Chem. 2011;286(34):30087-96.
22. Martinez-Mora C, Mrowiec A, Garcia-Vizcaino EM, Alcaraz A, Cenis JL, Nicolas FJ. Fibroin and sericin from Bombyx mori silk stimulate cell migration through upregulation and phosphorylation of c-Jun. PLoS One. 2012;7(7):e42271.
23. Alcaraz A, Mrowiec A, Insausti CL, Bernabe-Garcia A, Garcia-Vizcaino EM, Lopez-Martinez MC, et al. Amniotic Membrane Modifies the Genetic Program Induced by TGFss, Stimulating Keratinocyte Proliferation and Migration in Chronic Wounds. PLoS One. 2015;10(8):e0135324.
24. Schindelin J, Arganda-Carreras I, Frise E, Kaynig V, Longair M, Pietzsch T, et al. Fiji: an open-source platform for biological-image analysis. Nat Methods. 2012;9(7):676-82.
25. Salo T, Dourado MR, Sundquist E, Apu EH, Alahuhta I, Tuomainen K, et al. Organotypic three-dimensional assays based on human leiomyoma-derived matrices. Philos Trans R Soc Lond B Biol Sci. 2018;373(1737).
26. Astrom P, Heljasvaara R, Nyberg P, Al-Samadi A, Salo T. Human Tumor Tissue-Based 3D In Vitro Invasion Assays. Methods Mol Biol. 2018;1731:213-21.
27. Jelassi B, Chantome A, Alcaraz-Perez F, Baroja-Mazo A, Cayuela ML, Pelegrin P, et al. P2X(7) receptor activation enhances SK3 channels- and cystein cathepsin-dependent cancer cells invasiveness. Oncogene. 2011;30(18):2108-22.
28. Fior R, Povoa V, Mendes RV, Carvalho T, Gomes A, Figueiredo N, et al. Single-cell functional and chemosensitive profiling of combinatorial colorectal therapy in zebrafish xenografts. Proc Natl Acad Sci U S A. 2017;114(39):E8234-E43.
29. Garcia-Vizcaino EM, Liarte S, Alonso-Romero JL, Nicolas FJ. Sirt1 interaction with active Smad2 modulates transforming growth factor-beta regulated transcription. Cell Commun Signal. 2017;15(1):50.
30. Yamashiro-Matsumura S, Matsumura F. Purification and characterization of an F-actin-bundling 55-kilodalton protein from HeLa cells. J Biol Chem. 1985;260(8):5087-97.
31. Han T, Kang D, Ji D, Wang X, Zhan W, Fu M, et al. How does cancer cell metabolism affect tumor migration and invasion? Cell Adh Migr. 2013;7(5):395-403.
32. Nurmenniemi S, Sinikumpu T, Alahuhta I, Salo S, Sutinen M, Santala M, et al. A novel organotypic model mimics the tumor microenvironment. Am J Pathol. 2009;175(3):1281-91.
33. Mayer TU, Kapoor TM, Haggarty SJ, King RW, Schreiber SL, Mitchison TJ. Small molecule inhibitor of mitotic spindle bipolarity identified in a phenotype-based screen. Science. 1999;286(5441):971-4.
34. Aseervatham J. Cytoskeletal Remodeling in Cancer. Biology (Basel). 2020;9(11).
35. Min KW, Chae SW, Kim DH, Do SI, Kim K, Lee HJ, et al. Fascin expression predicts an aggressive clinical course in patients with advanced breast cancer. Oncol Lett. 2015;10(1):121-30.
36. Lamb MC, Tootle TL. Fascin in Cell Migration: More Than an Actin Bundling Protein. Biology (Basel). 2020;9(11).
37. Wang Y, Song M, Liu M, Zhang G, Zhang X, Li MO, et al. Fascin inhibitor increases intratumoral dendritic cell activation and anti-cancer immunity. Cell Rep. 2021;35(1):108948.
38. Wu Y, Zhou Y, Gao H, Wang Y, Cheng Q, Jian S, et al. LYAR Promotes Colorectal Cancer Progression by Upregulating FSCN1 Expression and Fatty Acid Metabolism. Oxid Med Cell Longev. 2021;2021:9979707.

39. Lin S, Li Y, Wang D, Huang C, Marino D, Bollt O, et al. Fascin promotes lung cancer growth and metastasis by enhancing glycolysis and PFKFB3 expression. Cancer Lett. 2021;518:230-42.
40. Ghebeh H, Al-Khaldi S, Olabi S, Al-Dhfyan A, Al-Mohanna F, Barnawi R, et al. Fascin is involved in the chemotherapeutic resistance of breast cancer cells predominantly via the PI3K/Akt pathway. Br J Cancer. 2014;111(8):1552-61.
41. Villari G, Jayo A, Zanet J, Fitch B, Serrels B, Frame M, et al. A direct interaction between fascin and microtubules contributes to adhesion dynamics and cell migration. J Cell Sci. 2015;128(24):4601-14.
42. Heinz LS, Muhs S, Schiewek J, Grub S, Nalaskowski M, Lin YN, et al. Strong fascin expression promotes metastasis independent of its F-actin bundling activity. Oncotarget. 2017;8(66):110077-91.
43. Riahi N, Kefayat A, Ghasemi A, Asgarshamsi M, Panjehpoor M, Fassihi A. Design, Synthesis and Molecular Docking Studies of Some Tetrahydropyrimidine Derivatives as Possible Fascin Inhibitors. Chem Biodivers. 2019;16(2):e1800339.
44. Kraft R, Kahn A, Medina-Franco JL, Orlowski ML, Baynes C, Lopez-Vallejo F, et al. A cell-based fascin bioassay identifies compounds with potential anti-metastasis or cognition-enhancing functions. Dis Model Mech. 2013;6(1):217-35.
45. Russowsky D, Canto RF, Sanches SA, D'Oca MG, de Fatima A, Pilli RA, et al. Synthesis and differential antiproliferative activity of Biginelli compounds against cancer cell lines: Monastrol, oxo-monastrol and oxygenated analogues. Bioorg Chem. 2006;34(4):173-82.

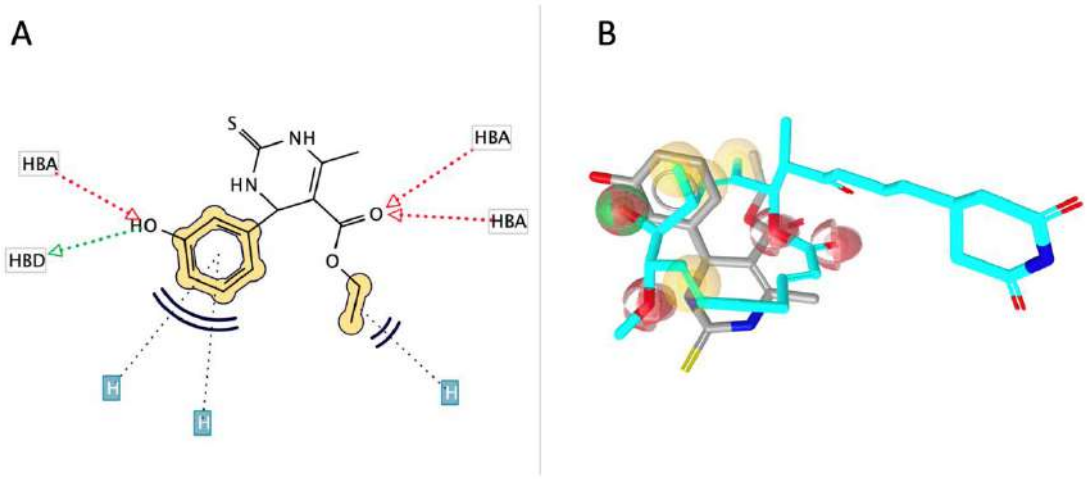

Figure 1. Results obtained after pharmacophoric screening with LigandScout. (A) 2D diagram of matching pharmacophoric features between monastrol and migrastatin pharmacophoric model. (B) 3D alignment of migrastatin (blue skeleton) and monastrol (grey skeleton). Yellow color denotes hydrophobic interactions, red color hydrogen bond acceptors and green color hydrogen bond donors.

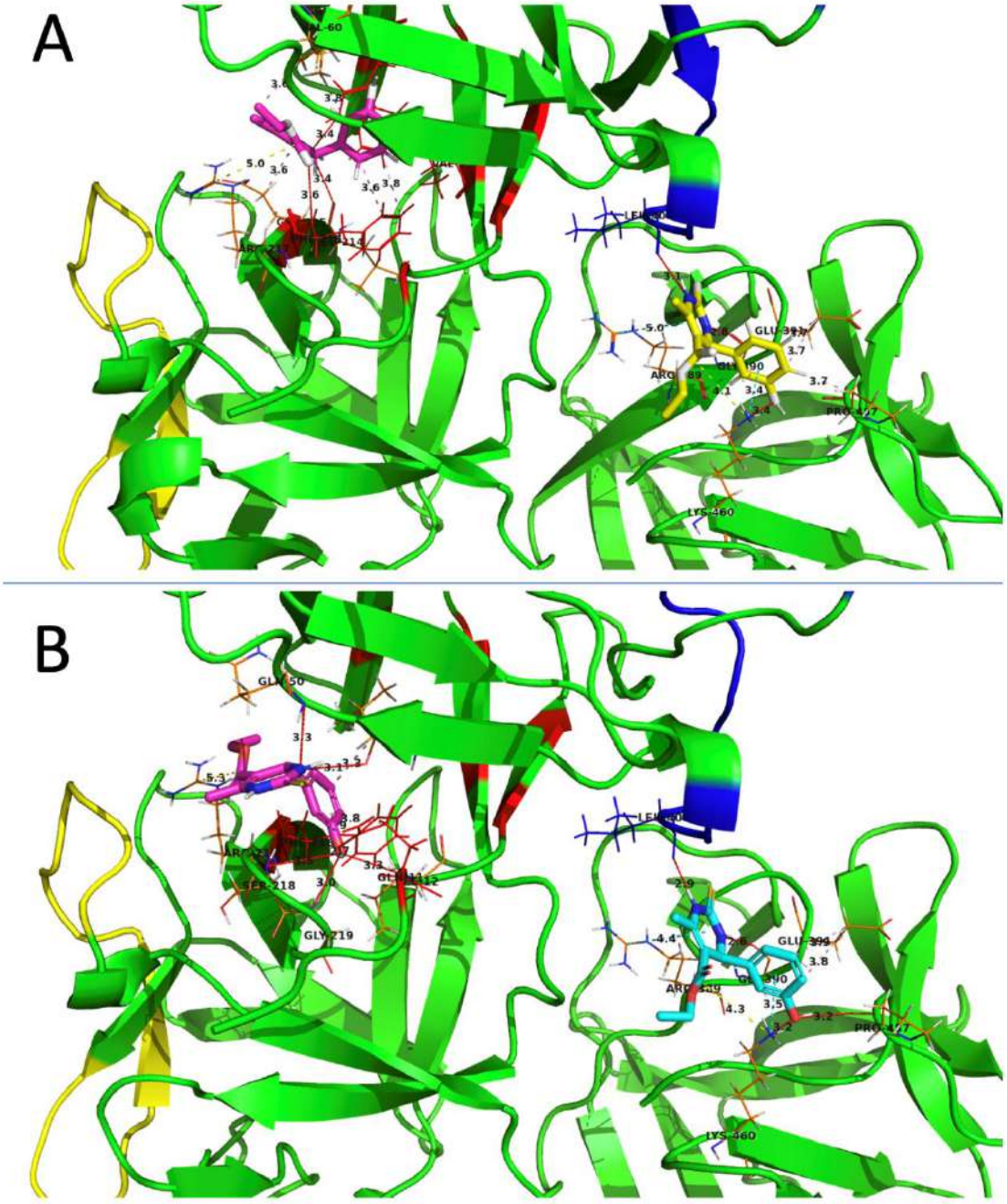

Figure 2. Interactions between monastrol compound and fascin actin-binding site 1 (blue) and 2 (red).(A) Interactions obtained from Autodock Vina calculations.(B) Interactions obtained from Lead Finder calculations. Red dashed lines indicate a hydrogen bond interaction, and dashed pink lines indicate hydrophobic interactions.

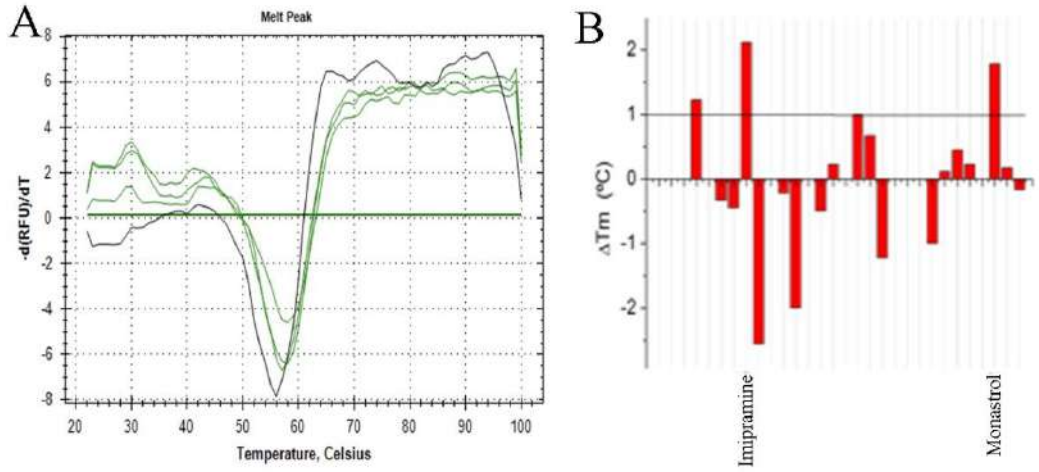

Figure 3.A) First derivative of the differential scanning fluorometry profile for fascin (black line) and fascin in the presence of monastrol 100 µM (fascin concentration 2 µM, 10% DMSO). B) Changes in the denaturation temperature, established as the minimum in the first derivative of the thermal denaturation profile, induced by the presence of different compounds.

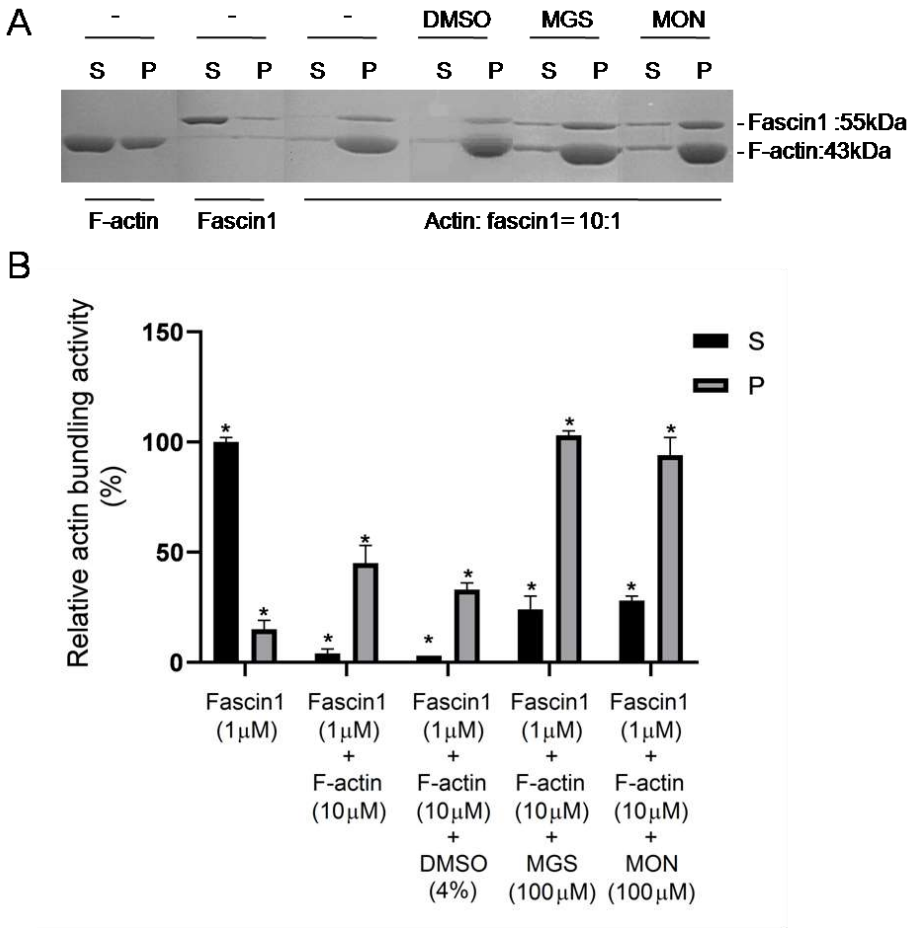

Figure 4.Monastrol interferes with the formation of actin bundles in an actin-bundling assay. (A) Assay of actin-bundling activity with a low-speed co-sedimentation assay, showing a composition of different gels. (B) Quantification of the F-actin bundling assay. The results are the means and SD (n=3;*p<0.01, Kruskal-Wallis test). DMSO: Dimethyl sulfoxide (control); MGS: migrastatin; MON: monastrol, P: pellet; S: supernatant.

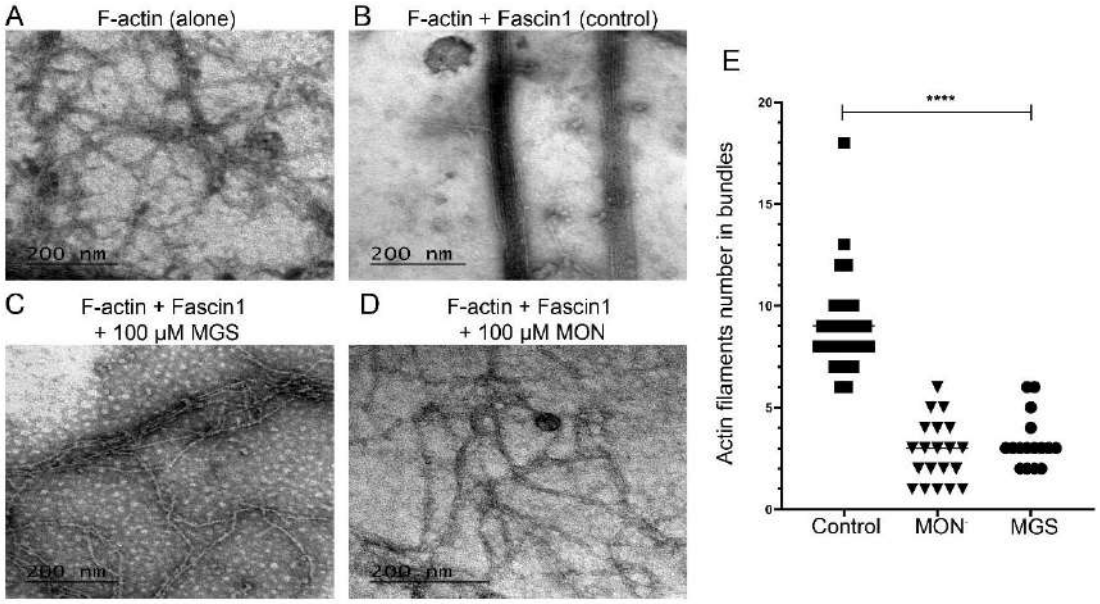

Figure 5.Monastrol interferes with the formation of actin bundles as evidenced by TEM. (A) Actin bundle formation alone, (B) Actin bundle formation in the presence of fascin (C) MGS: migrastatin, (D) MON: monastrol. (E) Quantitative analysis of the numbers of actin filaments of several pictures acquired by TEM (n=3, *** $p < 0.001$, Mann-Whitney U test).

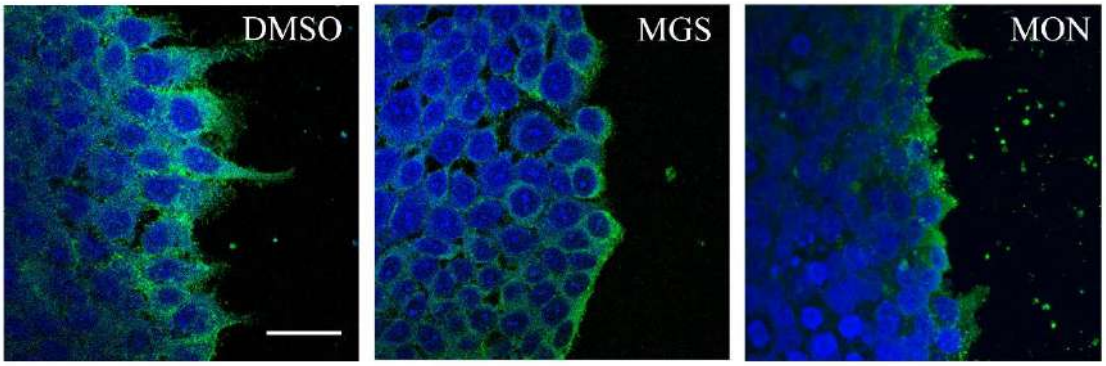

Figure 6.Monastrol interferes with cytoplasmatic protrusions at the migrating edge on a wound scratch assay of HCT-116 cells. Wounded cells were treated with either DMSO (control), MGS: migrastatin100μM, or MON: monastrol100 μM. Fascin was revealed in green and nuclei in blue. Scale barr 24μm.

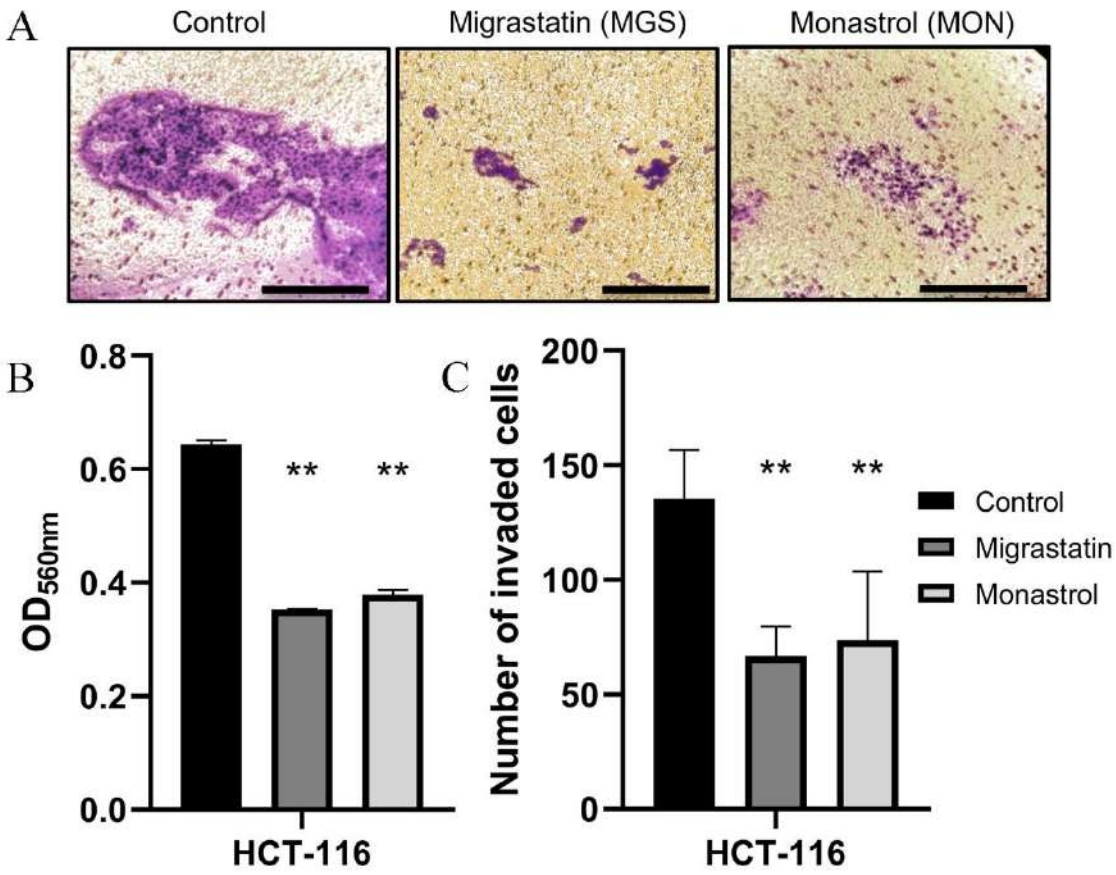

Figure 7. Transwell invasion assay in the presence of fascin inhibitors. (A) Representative images of the invasion assay in HCT-116 cells. The magnification was ×200 and scale bars =50 μm. Statistical analyses are shown in (B) Comparisons of the Optical Density ($DO\lambda=_{560nm}$). (C) Comparisons of the invasive cell counts. MSG: 100 μM migrastatin; MON: 100 μM monastrol.Pictures of representative experiments are shown and the means ± SD are illustrated in the graphs (n = 3; **: $p<0.01$, Kruskal-Wallis test).

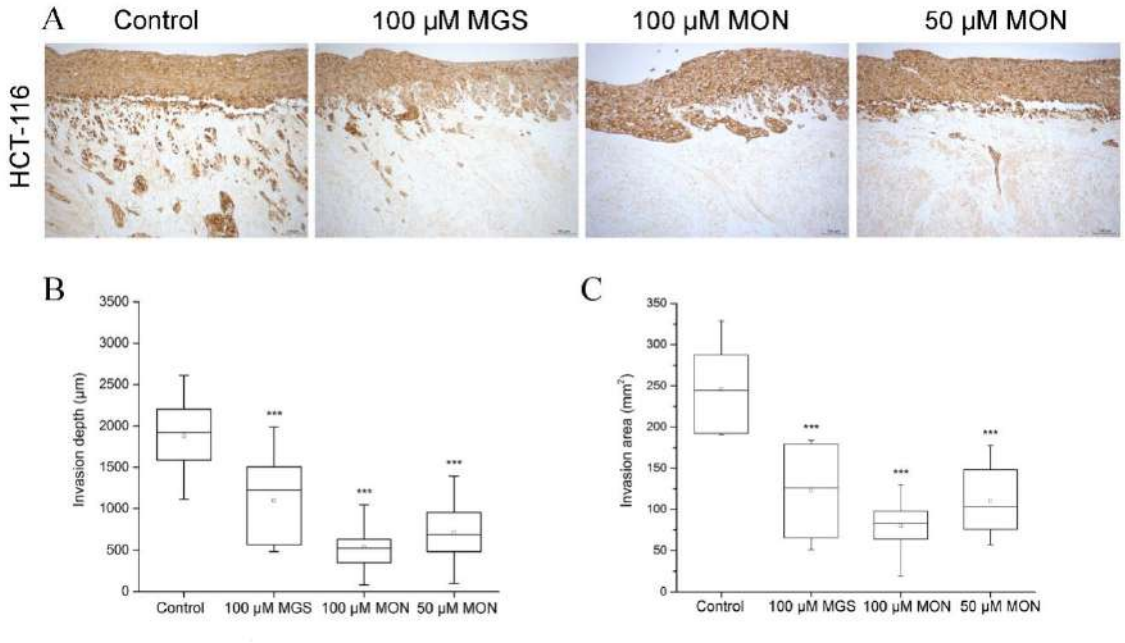

Figure 8.Monastrol prevents invasion of HCT-116 cells in an organotypic myoma invasion model.(A) Immunohistochemical staining demonstrating the effect of 50 and 100 monastrol (MON) and 100 µM migrastatin (MGS) on invasion, compared to control in HCT-116 colorectal cancer cells. Box-plots showing quantification of (B) Depth and (C) Area of invasion of HCT-116 cells. The means ± SD are illustrated in the graphs (n = 3; ***: $p<0.001$, Kruskal-Wallis test).

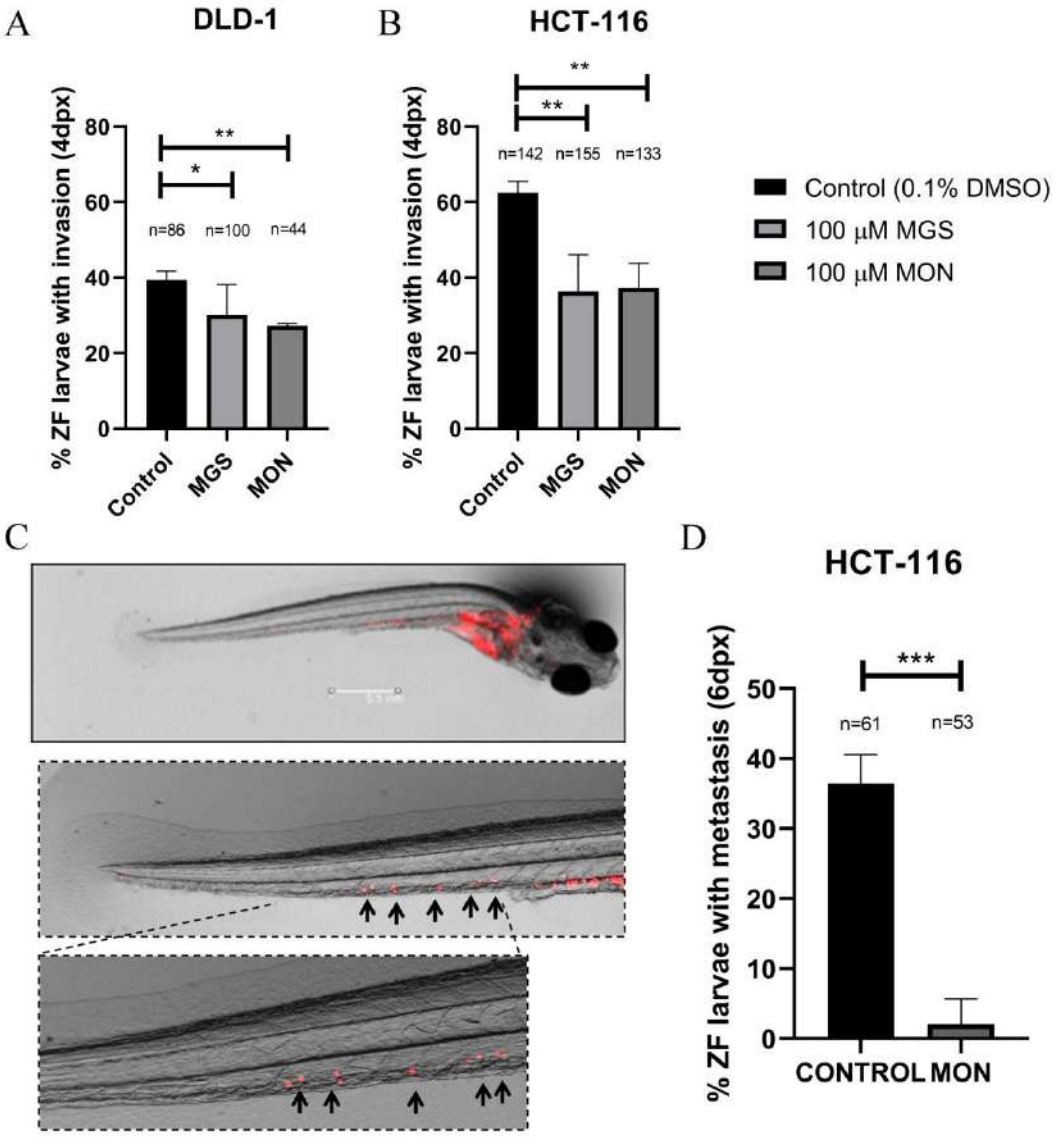

Figure 9.**Anti-invasive and anti-metastatic potential of monastrol in a zebrafish xenotransplantation model.** At four days post-xenographt, the invasive cells (A) DLD-1 and (B) HCT-116 were counted in the presence of 100 µM migrastatin and 100 µM monastrol. (C) At six days post-injection, larvae were examined to evaluate the micro-metastasis developed by invading native HCT-116 cells. D) HCT-116 cells growth outside the yolk sacin the presence of 100 µM monastrol.MGS: migrastatin; MON: monastrol. Data are shown as mean ± SD; compared with the control condition, * $p<0.05$, 0.01** $p = 0.001–0.009$, *** $p = 0.0001–0.0009$.

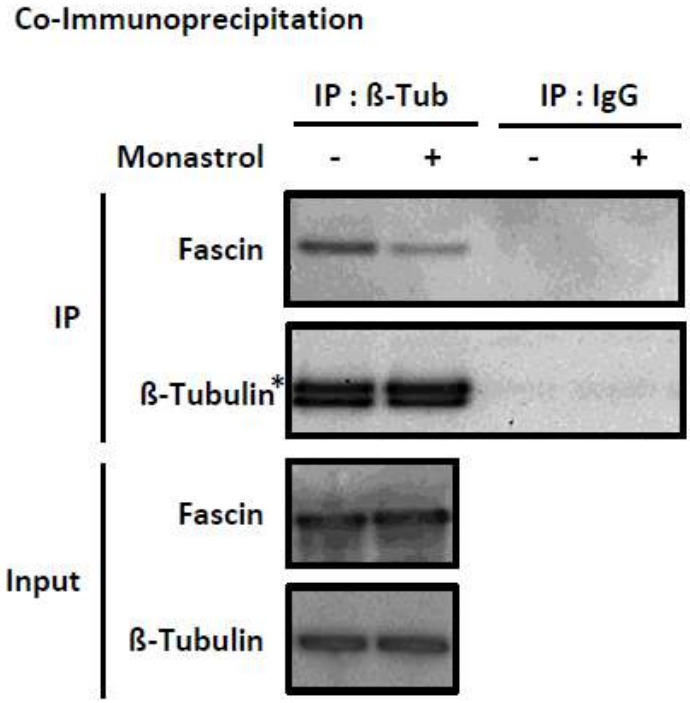

Figure 10.Monastrol interferes with fascin and ß-Tubulin interaction. Cells were treated with DMSO (control) and monastrol for 24h. β-tubulin was purified byimmunoprecipitation. Fascin and β-tubulin were detected by Western Blot.IP: immunoprecipitation.β-Tub: β-Tubulin.The upper band (*) is the cross reaction of secondary antibody to IgG.

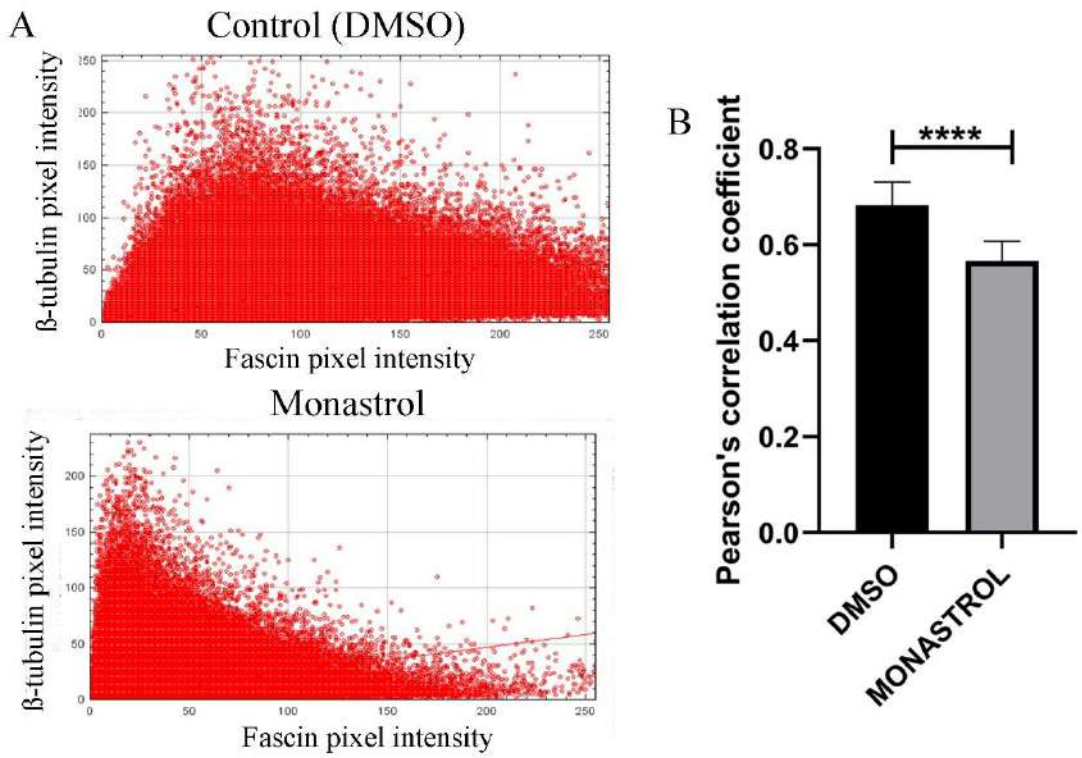

Figure 11. Fascin and ß-tubulin co-localization is partially affected by monastrol in HCT-116 cells. Scatterplot of ß-tubulin and fascin intensities of HCT-116 cells pre-treated with (A) DMSO or monastrol. (B) Pearson's correlation coefficients of images of fascin and ß-tubulin HCT-116 cells (****p<0.0001).

Table 1. Thermal shift assay results.

Compound	Conc. (µM)	T_m,FAM (ºC)	ΔT_m,FAM (ºC)	T_m,HEX (ºC)	ΔT_m,HEX (ºC)	T_m,TRed (ºC)	ΔT_m,TRed (ºC)
Free fascin	-	55.7±0.5	-	56.0±0,0	-	56.2±0.6	-
Monastrol	100	57.7±0,6	2.0±1.1	57.7±0.6	1.7±0.6	58.0±0.0	1.8±0.6

SUPPLEMENTAL MATERIALS

Multiparametric analysis of cell proliferation and viability

The MTT cell assay measures the metabolic activity as an indicator ofcell proliferation and viability. Since monastrol was described to block mitosis, the quantification of cell growth was performed by this approach. Indeed, cell proliferation was highly reduced in the presence of monastrol (Figure S3A), better than with migrastatin(1-3).

Flow cytometric analysis

In order to confirm that monastrol compromises proliferation but not viability, identification of apoptosis by the flow cytometry (FCM) assay of Annexin V (AnV) propidium iodide (PI) double staining was assessed at 100 µM of monastrol (Figure S1B) in a BD LSR Fortessa (BD Biosciences). For that purpose, $1x10^6$HCT-116 cells/mL were stained with fluorescein isothiocyanate (FITC)-conjugated AnVand PI (556547, Annexin V-FITC apoptosis detection kit, BD Pharmingen; BD Biosciences) in a volume of 100 µL on ice for 15 min in the dark and later, 400 µl AnVbinding buffer was added to the cells. The mixture was then analysed in a BD LSR Fortessa flow cytometer and the percentage of apoptosis of 20,000 cells was determined. The data were analyzed using BD CellQuest™ Pro software (version 6.1.1;BD Biosciences) and the percentage viable cells without apoptosis or/and necrosis were calculated.

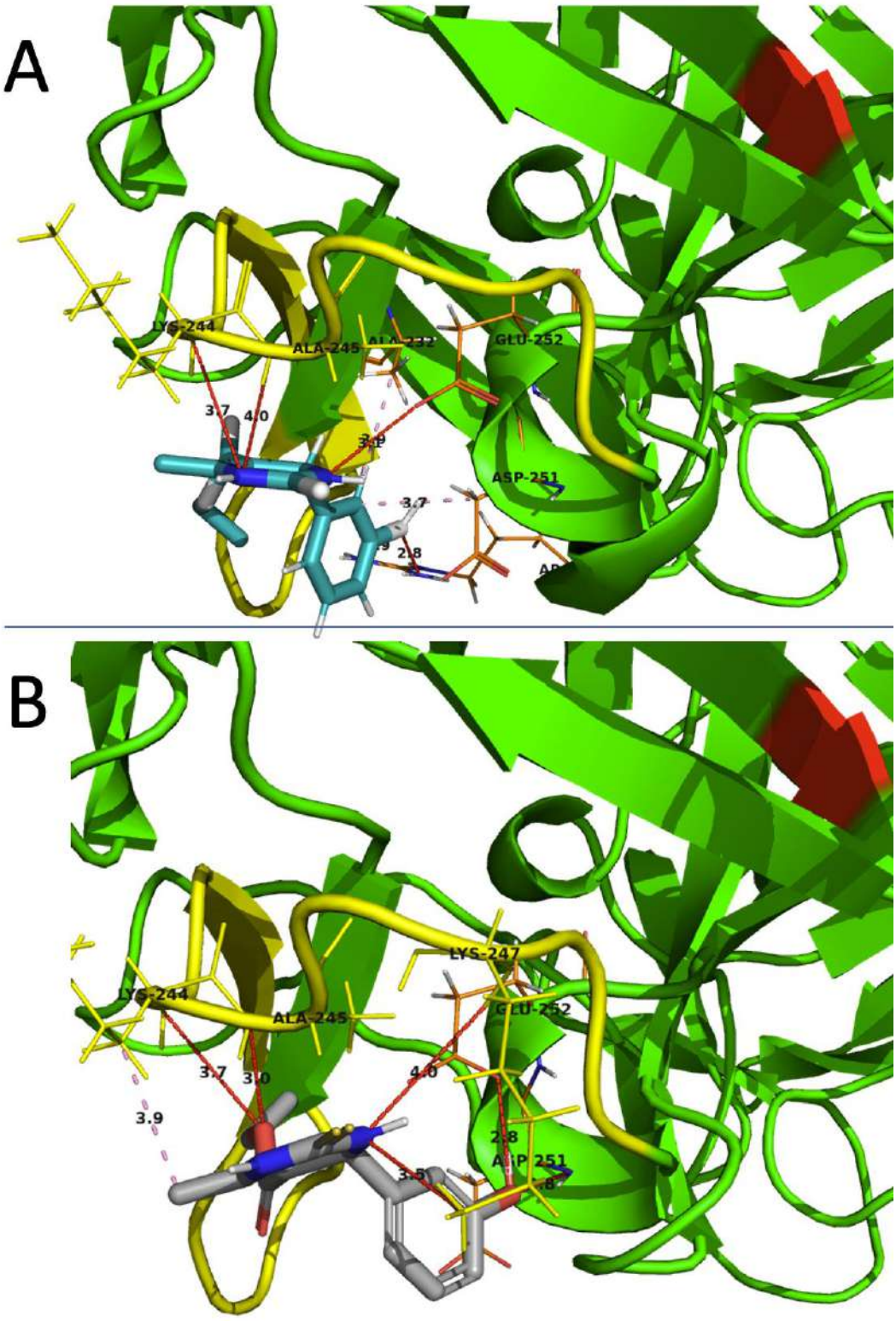

Figure S1. Interactions between monastrol compound and tubulin-binding site residues (yellow).(A) Interactions obtained from Autodock Vina calculations.(B) Interactions obtained from Lead Finder calculations. Red lines indicate a hydrogen bond interaction, and pink lines indicate hydrophobic interactions.

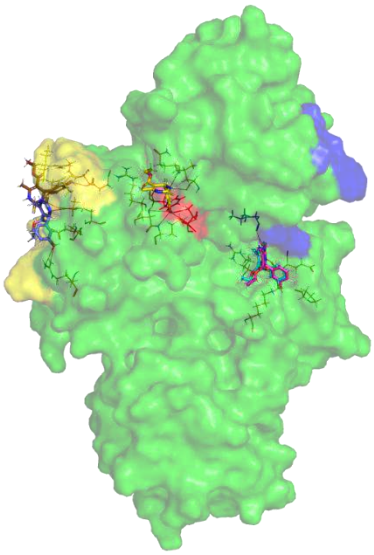

Figure S2. Clustered poses found in the fascin binding sites via consensus analysis results. Blue and red areas show actin-binding sites previously described, while the yellow area shows the β-tubulin binding site

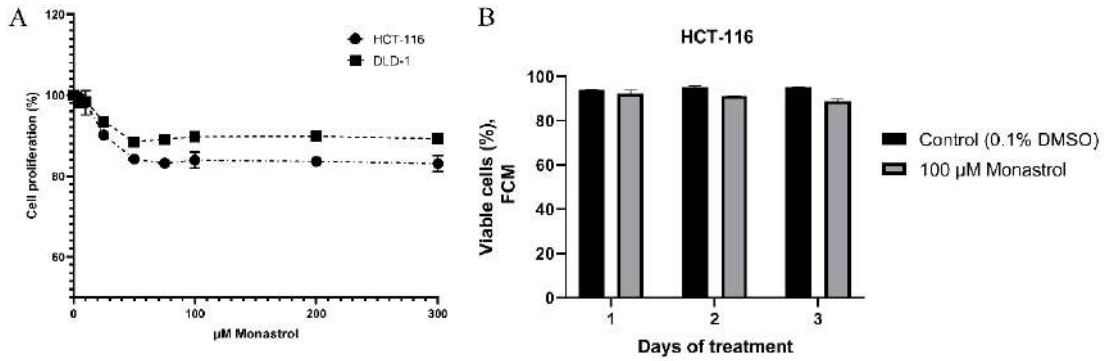

Figure S3. **HCT-116 cell proliferation and viability.** (A) Cell proliferation (MTT assay) in two different colorectal cancer cell lines after treatment with monastrol. (B) Cell Viability (FCM) in HCT-116 cell line after up to 3 days of 100 μM monastrol treatment.

Table S1. Lamellipodium protrusion numbers in the different conditions in HCT-116 cells.

	Control	10 ng/mL EGF	50 μM PD98	100 μM monastrol	100 μM migrastatin
Lamellipodium number	9.0 ±1,58	10,4 ±1,51	1.0 ± 1.0*	4,4 ±1,94*	2.0 ± 2.0*
P value		0,14017782	$5{,}9241E^{-06}$	0,00172362	0,0001386

Lamellipodium number was counted in pictures at 64X.
Kruskal-Wallis test compared to control condition.

1. Alburquerque-Gonzalez B, Bernabe-Garcia M, Montoro-Garcia S, Bernabe-Garcia A, Rodrigues PC, Ruiz Sanz J, et al. New role of the antidepressant imipramine as a Fascin1 inhibitor in colorectal cancer cells. Exp Mol Med. 2020;52(2):281-92.
2. Alburquerque-Gonzalez B, Bernabe-Garcia A, Bernabe-Garcia M, Ruiz-Sanz J, Lopez-Calderon FF, Gonnelli L, et al. The FDA-Approved Antiviral Raltegravir Inhibits Fascin1-Dependent Invasion of Colorectal Tumor Cells In Vitro and In Vivo. Cancers (Basel). 2021;13(4).
3. Montoro-Garcia S, Alburquerque-Gonzalez B, Bernabe-Garcia A, Bernabe-Garcia M, Rodrigues PC, den-Haan H, et al. Novel anti-invasive properties of a Fascin1 inhibitor on colorectal cancer cells. J Mol Med (Berl). 2020;98(3):383-94.

ARTÍCULO 6:

Alburquerque-González B, Montoro-García S, García-Bernal D, Bernabé-García M, Rodriguez-Arcas Mª J, Albaladejo- González A, Luengo-Gil G, García-Solano J, Cabezas-Herrera J, Conesa-Zamora P. **Testing the Potential Therapy with the fascin inhibitors Tofranil® and Issentress® in colorectal cancer mice models.** (En preparación).

TESTING THE POTENTIAL THERAPY OF THE FASCIN INHIBITORS TOFRANIL® AND ISSENTRESS® IN A COLORECTAL CANCER XENOGRAFT MICE MODEL.

Alburquerque-González B[ϯ], Montoro-García S[2ϯ], García-Bernal D[3], Bernabé-García M[4], Rodriguez-Arcas Mª J[5], Albaladejo-González A[6], Luengo-Gil G[6,7], García-Solano[6] J, Cabezas-Herrera J[8], Conesa-Zamora P*[6, 7].*

[1]Pathology and Histology Department. Facultad de Ciencias de la Salud, UCAM Universidad Católica San Antonio de Murcia, Spain.

[2]Cell Culture Lab, Facultad de Ciencias de la Salud, UCAM Universidad Católica San Antonio de Murcia, Spain.

[3]Biomedical Research Institute of Murcia-Arrixaca, Cellular Therapy and Hematopoietic Transplant Unit IMIB-Arrixaca, University of Murcia, Murcia, Spain.

[4] Animalario SPF, IMIB, Murcia,Spain.

[5]Directora técnica en Farmacia Arcas, Cartagena.

[6] Group of Molecular Pathology and Pharmacogenetics, IMIB, Hospital Universitario Santa Lucía, Cartagena,Spain.

[7]Clinical Analysis Department, Hospital Universitario Santa Lucía, Cartagena,Spain

[8]Molecular Therapy and Biomarkers Research Group, Clinical Analysis Service, HCUVA-IMIB, Murcia

[ϯ]Authors contributed equally to this work

**Corresponding authors.*

ABSTRACT

Preclinical animal models have proven to be an important tool for unraveling the biological complexity of the metastatic cascade and they are critical for testing promising therapies. Previously, our group has identified *in vitro* and in a zebrafish invasion model a new role for the antidepressant imipramine through Fascin-1 (fascin) inhibition in colorectal cancer cell lines. Similarly, we showed that raltegravir, an inhibitor of human immunodeficiency virus-1 (HIV-1) integrase reduced the migration and invasion through fascin inhibition in human colorectal cancer cell lines with*in vitro* approaches and in a zebrafish model. Thereby, we now propose that both drugs may be clinically applicable to treat human colorectal carcinoma cells in a valid primary

tumour model. The current study shows the effect of Tofranil® (imipramine) and Issentress® (raltegravir) on tumour growth using a primary tumour model of immunosuppressed miceinduced by xenograft of human HCT-116 bioluminescent cells in order to explore the therapeutics potentials of these drugs.

Keywords: Colorectal Cancer, Tofranil®, Issentress®, Mice Models.

1. INTRODUCTION

Colorectal cancer (CRC) is the third most common cancer worldwide(1).Serrated adenocarcinoma (SAC) is a recently recognized CRC subtype accounting for 7.5-8.7% of CRCs. Fascin, which is associated with tumour cell invasion, emerged as a potential biomarker of SAC(2).Commonly, CRC has been treated with classical chemotherapeutic agents such as 5-fluorouracil and several new targeted drugs such as humanized monoclonal antibody against EGFR (cetuximab) or anti-VEGFR (3).However, SAC shows resistance for these therapies (4). Therefore, drug repurposing could be a rational option for finding new ways of treating SAC(5).Formerly, our group repurposed antiretroviral raltegravir (6) and the antidepressant imipramine (7)as a fascin inhibitors in CRC cell lines using invasion and metastasis zebrafish model.A major advantage of this approach is that extensive clinical data of both drugs are available because of their *Food and drug Administration* (FDA) approved statement. Therefore, the ultimate benefit of repositioning is to take the patients in a drug clinical trial. For that purpose, it is essential to carry out preclinical animal models before.These models have proven to be an important tool for testing promising therapies.Numerous mouse models of CRC have been developed, providing insights into pathogenesis mechanisms, tools for discovery, validation of novel therapeutic targets, and a predictive platform in which to test new chemoprevention strategies(8).

On one hand, Tricyclic antidepressants (TCAs) are efficacious in the treatment of many anxiety disorders (9).Moreover, Walker *et al.* suggested that TCAs may had potential for prevention of both,CRC and glioma (10). On the other hand, the use of antivirals as a cancer treatment is not new. Apart from obvious anti-VIH, anti-neoplastic effects reported in virus-associated tumours such as Kaposi's sarcoma and Xenotropic murine leukemia-related retrovirus, which has been linked to human prostate cancer (6).

The known safety of approved drugs minimizes the possibility of failure for adverse effects, making them attractive de-risked compounds for new applications with potentially lower overall development costs and shorter development timelines. Indeed, a large body of evidence shows the beneficial effects against cancer of drugs previously labeled as non-cancer agents (11). With this information we decided to carry out preclinical trials with proven anti-fascin compounds using HCT-116 bioluminescent cells in order to xenograft in athymic nude mice.

2. MATERIALS AND METHODS

2.1 Drugs and Treatment.

Tofranil®50 mg (Imipramine-HCl), a tricyclic antidepressantagent, was obtained from Ferrer S.A (Barcelona, Spain) and Issentress® (Dynamics International, UK). Syrspend® (Tofranil® vehicle) was acquired from SF ALKA FagrónIbérica(Barcelona, España) and it was formulated in Farmacia Arcas (Cartagena, Murcia).The Issentress® vehicle was Lactose (1.3 mg/mL) (Sigma Aldrich).Tofranil® and Issentress® solution was administrated by *oral gavage* at 95 mg/Kg for 15 days for primary tumour model and Isentress® solution at 120 mg/Kg, twice daily up to 28 days.

2.2 Cell line and Transfection.

HCT-116 cells contain, amongst other, theKRAS p.G13D c.38G>A mutation which we used to follow up the circulating free DNA (cfDNA).

HCT-116 cells (ATCC® CCL-247™) were stably transfected with pGL4.51[luc2/CMV/Neo] vector (Promega) using turbofectin reagent 8.0 (TurboFect™ Transfection Reagent, Thermofisher cat number R0533)protocol for stable transfection. Twenty-four hours post-transfection, cells was harvested (at 1:10 or higher dilution) into fresh growth medium containing selective medium (G418 (1000µg/mL, Sigma Aldrich). A MOCK transfection plate was used in parallel as control.Over the following two months; we selected the clones that emitted more bioluminescence which was measured by IVIS (*In Vivo* Imagining System).

2.3 IVIS

Primary tumours were stablished subcutaneously with cells with luciferase expression.Tumours were analyzed using the IVIS Imaging System (Caliper Life Sciences, Hopkinton, MA, USA).

2.4 Animals.

Male and female athymic nude mice (60%-40%)(5 weeks old; mean body weight, 20 g) were obtained from Charles River (France). Animals were acclimated for 1 week before the xenograftand maintained under specific pathogen-free conditions based on the guidelines established by the Instituto Murciano de Investiación Biosanitaria (IMIB, Murcia) ethical committee.The animal procedure counts with the approval of the ethical committee (REGA code ES300303340098).

2.5 Xenograft Assay

HCT-116 cells (2×10^6 cells/100 μL) were suspended in DMEM High Glucose medium and subcutaneously inoculated with 100 μL matrigel (Inqualab) or 100 μL Geltrex Matrix LDEV-free GF (Thermo Fisher; ref: A1413202) into the left flank of each mouse. When tumours reached 100 mm^3volume, mice were divided into two groups: (a) vehicle and treatment group. The sample size was for the Tofranil® assay: vehicle (Syrspend)n = 9 and Tofranil®n = 12. For Issentress assay: vehicle (Lactose) n=14 and Issentress® n=14.Bioluminescence in alive mice was monitored up to twice per week using *In Vivo* Imagining System (IVIS).The general anesthetic used was isofluorane. Tumour volume was measured three times per week by using a caliper. The mice were housed in laminar flow cabinets under specific pathogen-free conditions and killed by cervical dislocation at different time points post-graft. Subcutaneous tumours were dissected and weighed.

2.6 Inmunohistochemistry.

Tumours were resected after the procedure and then were conserved in 4% paraformaldehyde at 4ªC until the inmunohistochemistry assay. Whole tissue sections were evaluated. We then performed the hematoxilin-eosin staining and immunohistochemical evaluation in whole histological sections of fascin and KI67 expression.

2.7 Sample Characteristics and Circulating free DNA (cfDNA) Extraction.

Peripheral blood was collected by intracardiac puncture at the endpoint and transferred into tubes with EDTA-K2 as anticoagulant.The samples were collected using a blood pool (vehicle and treatment pool) in order to have enough amount of plasma for cfDNA assays. After that, samples were centrifugated twice, firstly at 1600*g* and later at 6000*g* during 10 minutes in both cases. Plasma was carefully retrieved (supernatant) for cfDNA analysis while taking care to stay away from the debris pellet. DNA extraction was performed using QIAsymphony DSP Circulating DNA KIT (Qiagen), according to the manufacturer's recommendations.

2.8 Droplet digital PCR (ddPCR) and Analysis.

Experiments were performed in a singleplex utilizing the QX200™ Droplet Digital PCR System platform (Bio-Rad) operating with the digital PCR supermix for probes (No dUTP)(Biorad, USA),according to the manufacturer's instructions. A negative DNA-free water control and wild type sample(8 ng/µl) were also included in each analysis. The target gene *KRAS proto-oncogene, GTPase (*KRAS p.G13D c.38G>A assay) was analyzed in triplicate using 8 ng/replicate of DNA and *KRAS* G13D probe. The plate underwent thermocycling (C1000 Touch Thermal Cycler) following specific amplification conditions, indicated by the manufacturer: 95ºC for 10′ 1 cycle (ramp rate 2°/sec) ,94ºC for 30′′ and 55 cycles at 55ºC for 1′ (ramp rate ramp rate 2°/sec) followed by a final extension step at 98ºC for 10′. Threshold values were set at 7000 for *KRAS*, according to the manufacturer's instructions. Finally the droplets are analyzed by QX200 Droplet Reader.

2.9 Statistics

The statistical significance was analyzed using Mann-Whitney test and linear logarithmic regression for the bioluminescent slopes in GraphPad Prism software. *P* values <0.05 were considered statistically significant.

3. RESULTS

3.1 Tofranil® *in vivo* data

Tofranil®Decreases the Tumour Volume and Weight

The anti-cancer activity of Tofranil® in mice was determined by subcutaneously transplanting HCT-116 bioluminescent cells into athymic nude mice. We previously established our own LD50 curve (n=4) and then the dose doses at 95 mg/kg three times per week was set up with minimal toxicity. Bioluminescence signal appeared shortly after injection. Mice receiving Tofranil® therapy showed lower spontaneous tumour burden as measured by bioluminescence at day 15 (Total flux [p/s] $p<0.1521$) (Figure 1A, 1B). This difference was not significant, mainly due to the high standard deviation, besides we were not able to appreciate slopes changes during monitoring the assay either (Figure 1C).

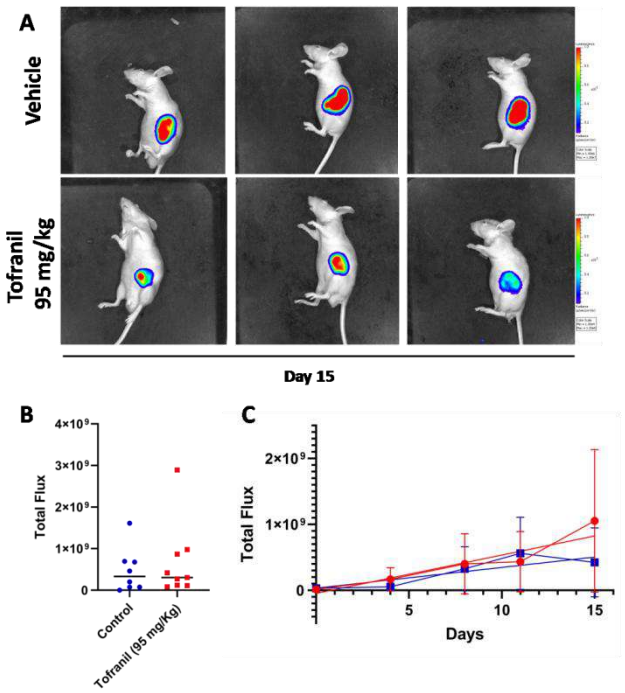

Figure 1.A, *Representative IVIS images from mice xenografted subcutaneously with HCT-116 bioluminescent cells* ***B,*** *Total flux [p/s] of light emission from HCT-116 bioluminescent cells throughout the experiment,* ***Monitoring of Total flux during 15 days.*** *Vehicle group (blue) n= 8, Tofranil group (red) n=9. Data are shown as the mean ± SD, compared with the control, p = 0.523.*

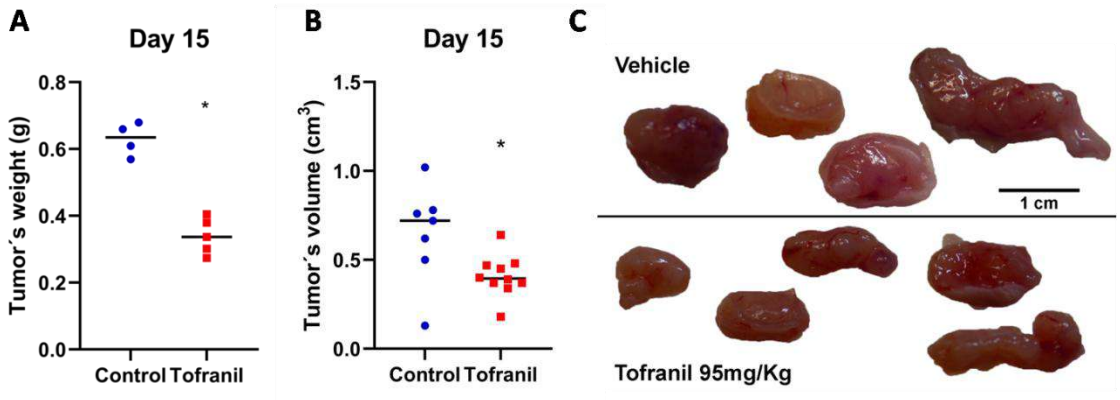

Figure 2.*Tofranil® inhibits tumour weight and growth.* ***A,*** *Tumour weight (g) was recorded after excision on the end-point of the experiment (n vehicle=4, n Tofranil®=5); *p=0, 0159.* ***B,*** *Tumour volume (cm³) (n vehicle=7, n Tofranil®=10). Tumour size was measured three times per week by using a caliper; *p=0, 0235.* ***C****, Tumours at the end-point of the experiment. Vehicle (blue) or Tofranil® 95 mg/kg (red).*

ddPCR Analysis of tumoral DNA.

Hypothetically, due to HCT-116 cells were inoculated to mice, *KRAS* mutation should be higher within non treated plasma mice compared with Tofranil® treatment mice. A total of two blood pool samples vehicle mice and Tofranil® mice were enrolled in this procedure. *KRAS* mutation was determined by ddPCR assay in plasma cfDNA from athymic nude mice xenografted with human HCT-116 bioluminiscent cells. The ratio of mutated copies was calculated as follow describes: number of KRAS mutated copies/ number of wild type (WT) copies. The ratio of mutated KRAS copies did not change after treatment with Tofranil® (Table 1).

Table 1*.Determination of positive copies (Mutated/WT) in mice vehicle and Tofranil®treated.*

Assay 1	**CONTROL**			**Assay 2**	**CONTROL**		
		Nºpositive copies	Ratio 1			Nºpositive copies	Ratio 2
	WT	3971	0,64		WT	496	0,25
	Mutated	2554			Mutated	125	
	TOFRANIL® 95 mg/Kg				**TOFRANIL® 95 mg/Kg**		
	WT	3135	0,93		WT	240	0,33
	Mutated	2913			Mutated	79	

Tofranil® treatment encapsulates mice tumours.

When we reached the endpoint, the tumours were resected and analyzed by immunohistochemistry. We carried out staining with hematoxilin and eosin and immunohistochemistry antibodies for fascin1, cocktail of cytokeratins and the cell proliferation marker Ki67. We did not observe differences between the fascin and the cytokeratin *cocktail*, however, the Ki67 marker helped us to visualize that tumour resected from treated mice were encapsulated, so tumour cells do not present an infiltrative pattern compared to their control as shown in Figure 3 (p=0.008 Mann–Whitney test). Also, we were able to observe micro-metastases in the lung of untreated mice (p=0.008 Mann–Whitney test). (Figure 4).

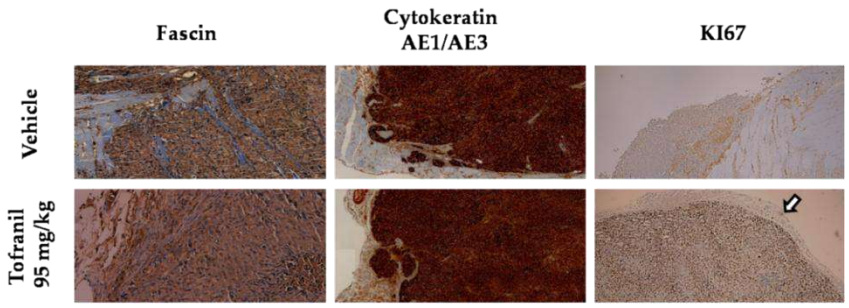

Figure 3. Inmunohistochemistry of resected tumours. *White arrow shows the encapsulated pattern originated by Tofranil® treatment.*

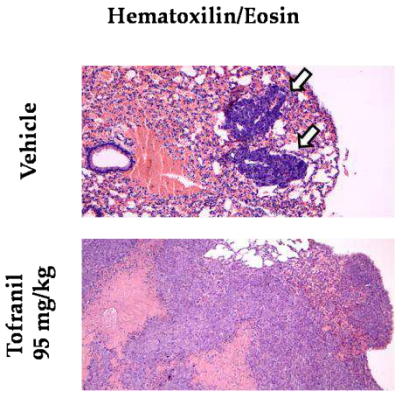

Figure 4.Hematoxilin/eosin staining of lung mice. *White arrow shows the micro-metastases in untreated mice.*

3.2 Issentress® results.

Issentress® has no significant effect against the growth of CRC cells

We administrated Issentress® at 120 mg/kg, twice daily for 28 days in mice xenografted with HCT-116 bioluminescent cells. No significant light emission effects were found between the vehicle (n=10) and the treated group (n=12) during the procedure (Figure 5). At the same manner, when mice were treated with Issentress®, tumour weight (vehicle n=13; Issentress®=13) and tumour volume (vehicle n=12; Issentress® n=13) did not show significant changes (Figure 6).

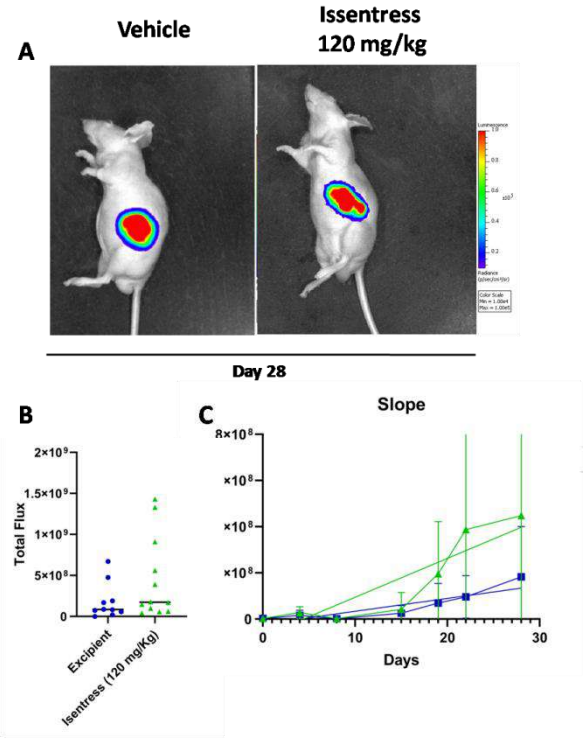

Figure 5.A, *Representative IVIS images from mice xenografted subcutaneously with HCT-116 bioluminiscents cells* ***B,*** *Total flux [p/s] of light emission from HCT-116 bioluminescent cells throughout the experiment at day 28.* ***C,*** *Monitoring of the experiment during28 days. Vehicle group (blue), Issentress® group (green). Data are shown as the mean ± SD, compared with the control, p = 0.1802.*

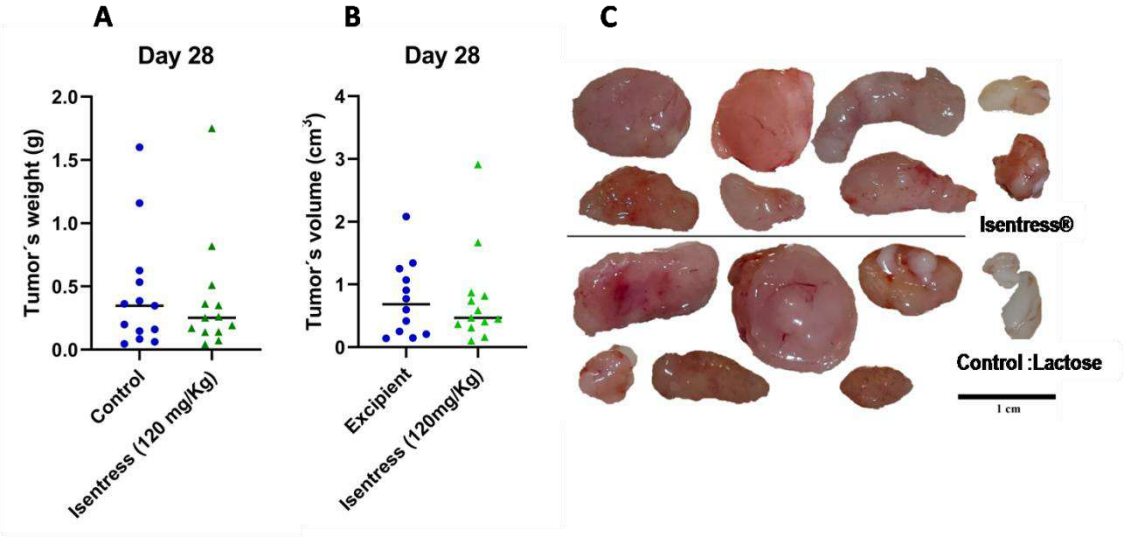

Figure 6.Treatment with Issentress®. A, *Tumour weight (g) was recorded after excision on the end-point of the experiment (n vehicle=13, n Issentress®=13); p=0, 7241.* ***B*** *Tumour volume (cm³) (n vehicle=12, n Issentress®=13). Tumour size was measured three times per week by using a caliper; p=0,7689.* ***C****, Tumours at the end-point of the experiment.*

ddPCR Analysis of tumoral DNA and Inmunohistochemistry.

A total of n=13 vehicle mice and n=13 Tofranil® mice were analyzed. *KRAS* mutation was determined by ddPCR assay in plasma cfDNA. The ratio of mutated KRAS copies improved after treatment with Issentress® as we show in Table 2 but there is no statistical significance, possibly due to the sample assay blood pool size (n=2 assays). Moreover, there are not significant differences in the immunohistochemical fascin expression in the tumour of mice according to the treatment (Figure 7).

***Table 2**.Determination of positive copies (KRAS Mutated/WT) in mice vehicle and Issentress® treated groups.*

Assay 1	**CONTROL**			**Assay 2**	**CONTROL**		
		Nºpositive copies	Ratio 1			Nºpositive copies	Ratio 2
	WT	791	0,174		WT	1429	0,524
	Mutated	134			Mutated	753	
	ISSENTRESS® 120 mg/Kg				**ISSENTRESS® 120 mg/Kg**		
	WT	1403	0.169		WT	1222	0,456
	Mutated	223			Mutated	561	

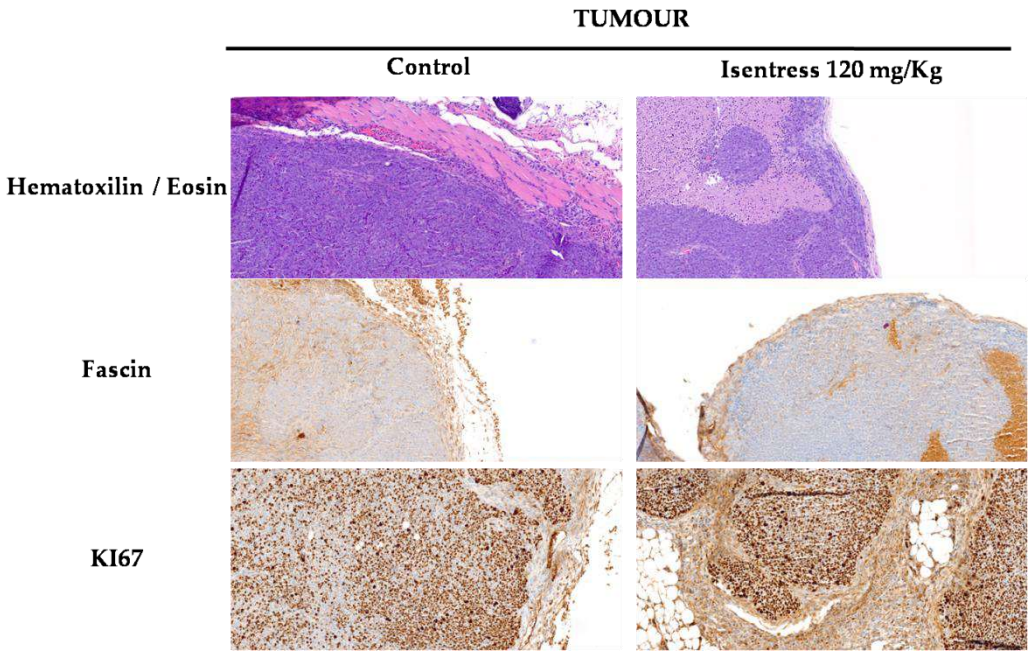

Figure 7. Inmunohistochemistry of resected tumours.

4. DISCUSSION

Our previous studies suggested that imipramine and raltegravir could have a potential use for CRC. For that purpose, we optimized a xenograft mice model and tested Tofranil® and Issentress®. Previously, we have shown that both FDA approved drugs were able to inhibit cell migration and invasion in CRC through fascin protein and it also decreased metastasis in a *zebrafish* model (7).

Interestingly, Jun Jan *et al* reported the fact that Paroxetine, another TCA, showed an anticancer activity in human CRC xenografted in mice (12). For that reason, we envisaged that the mode of action of Tofranil® could be tested with the same approaches. In this line, we accordingly observed that Tofranil® decreased tumour volume and weight in treated mice and it is able to encapsulate tumours.

On the other hand, raltegravir reduced the *in vivo* anti-invasive activity and metastasis in xenografted zebrafish as well (6). Furthermore, owing to the use of antiretrovirals in cancer treatment it is not new (13, 14), we proceeded to test if Issentress® was able to prevent the growth of tumour in mice xenograft with CRC cells. Due to the fact that the bioluminescence of our mice was did not shown significant results after 15 days of Tofranil® treatment, we extended the assay to 28 days. Nonetheless, no significant effects were observed under these specific conditions either .Another fascin inhibitor, the G2 compound, has been shown to inhibit tumour metastasis and also decreases the proliferation of specific subtypes of cancers although CRC was not included in the study (15). Due to the anti-invasive and anti-metastatic properties of Tofranil® and Issentress® previously described (6, 7), it was indeed necessary to use an animal model in with invasive and metastatic cells. Athymic nude mice were accordingly selected because human cells grow limitless, although it may be not the most adequate mice model in a preclinical stage. For these reasons, we are considering modifying our xenografted model by using other strain mice and organoids instead. Such organoids from SAC patients would retain more features of primary tumours. Another option would be to use murine CRC cell lines engrafted into mouse.Finally, Zhang *et al* informed that the combination of paroxetine with fluorouracil together allowed a therapeutic effect against CRC in a mouse model (16). Thus, the coadjuvancy between the chemotherapy treatment (5-fluorouracil, irinotecan or oxaliplatin) and fascin inhibitors could be more effective than alone. Besides, it would not be ethical to only prescribe imipramine nor raltegravir to CRC patients.

REFERENCES

1. Ferlay J, Shin HR, Bray F, Forman D, Mathers C, Parkin DM. Estimates of worldwide burden of cancer in 2008: GLOBOCAN 2008. Int J Cancer. 2010;127(12):2893-917.
2. Conesa-Zamora P, Garcia-Solano J, Garcia-Garcia F, Turpin Mdel C, Trujillo-Santos J, Torres-Moreno D, et al. Expression profiling shows differential molecular pathways and provides potential new diagnostic biomarkers for colorectal serrated adenocarcinoma. Int J Cancer. 2013;132(2):297-307.
3. Benson AB, 3rd, Venook AP, Cederquist L, Chan E, Chen YJ, Cooper HS, et al. Colon Cancer, Version 1.2017, NCCN Clinical Practice Guidelines in Oncology. J Natl Compr Canc Netw. 2017;15(3):370-98.
4. Garcia-Solano J, Conesa-Zamora P, Carbonell P, Trujillo-Santos J, Torres-Moreno DD, Pagan-Gomez I, et al. Colorectal serrated adenocarcinoma shows a different profile of oncogene mutations, MSI status and DNA repair protein expression compared to conventional and sporadic MSI-H carcinomas. Int J Cancer. 2012;131(8):1790-9.
5. Pantziarka P, Bouche G, Meheus L, Sukhatme V, Sukhatme VP, Vikas P. The Repurposing Drugs in Oncology (ReDO) Project. Ecancermedicalscience. 2014;8:442.
6. Alburquerque-Gonzalez B, Bernabe-Garcia A, Bernabe-Garcia M, Ruiz-Sanz J, Lopez-Calderon FF, Gonnelli L, et al. The FDA-Approved Antiviral Raltegravir Inhibits Fascin1-Dependent Invasion of Colorectal Tumor Cells In Vitro and In Vivo. Cancers (Basel). 2021;13(4).
7. Alburquerque-Gonzalez B, Bernabe-Garcia M, Montoro-Garcia S, Bernabe-Garcia A, Rodrigues PC, Ruiz Sanz J, et al. New role of the antidepressant imipramine as a Fascin1 inhibitor in colorectal cancer cells. Exp Mol Med. 2020;52(2):281-92.
8. Burtin F, Mullins CS, Linnebacher M. Mouse models of colorectal cancer: Past, present and future perspectives. World J Gastroenterol. 2020;26(13):1394-426.
9. Zohar J, Westenberg HG. Anxiety disorders: a review of tricyclic antidepressants and selective serotonin reuptake inhibitors. Acta Psychiatr Scand Suppl. 2000;403:39-49.
10. Walker AJ, Card T, Bates TE, Muir K. Tricyclic antidepressants and the incidence of certain cancers: a study using the GPRD. Br J Cancer. 2011;104(1):193-7.
11. Aldea M, Michot JM, Danlos FX, Ribas A, Soria JC. Repurposing of Anticancer Drugs Expands Possibilities for Antiviral and Anti-Inflammatory Discovery in COVID-19. Cancer Discov. 2021;11(6):1336-44.
12. Jang WJ, Jung SK, Vo TTL, Jeong CH. Anticancer activity of paroxetine in human colon cancer cells: Involvement of MET and ERBB3. J Cell Mol Med. 2019;23(2):1106-15.
13. Carleo MA, Di Martino F, Del Giudice A, Gargiulo M, Parrella G, Rosario P, et al. Different impact of anti-retroviral regimen containing protease inhibitors on development of HIV-related Kaposi sarcoma. In Vivo. 2015;29(1):133-6.
14. Singh IR, Gorzynski JE, Drobysheva D, Bassit L, Schinazi RF. Raltegravir is a potent inhibitor of XMRV, a virus implicated in prostate cancer and chronic fatigue syndrome. PLoS One. 2010;5(4):e9948.
15. Wang Y, Zhang JJ, Huang XY. Anti-Metastasis Fascin Inhibitors Decrease the Growth of Specific Subtypes of Cancers. Cancers (Basel). 2020;12(8).
16. Zhang H, Chen M, Liu Y, Dong X, Zhang C, Jiang H, et al. Paroxetine combined with fluorouracil plays a therapeutic role in mouse models of colorectal cancer with depression

through inhibiting IL-22 expression to regulate the MAPK signaling pathway. Exp Ther Med. 2020;20(6):240.

IV –DISCUSIÓN

IV–DISCUSIÓN

Las técnicas computacionales tales como la DM y el VS son métodos ampliamente utilizados para comprender los aspectos moleculares de las proteínas y las interacciones proteína-ligando. De hecho, son técnicas ampliamente utilizadas en el proceso de descubrimiento y desarrollo de nuevos fármacos. La técnica de VS se ha utilizado en la búsqueda de fármacos dirigidos hacia enfermedades emergentes, y también ha demostrado ser una herramienta fundamental en el reposicionamiento de fármacos, lo que supone ofrecer una nueva utilidad clínica a los compuestos (110).

Mediante el uso del VS y de la DM, hemos identificado nuevos compuestos (No aprobados por la FDA (nFDA) y aprobados por la FDA (FDA)) como potenciales inhibidores de la fascina en CCR:

- Un compuesto sintético nFDA: monastrol (MON).
- Dos compuestos FDA: imipramina (IMIP) y raltegravir (RAL).

Estos tres compuestos junto al compuesto G2 (nFDA) han sido testados en líneas de CCR con el objeto de inhibir el efecto pro-invasor y pro-metastásico de la fascina.

1. INHIBIDORES DE LA FASCINA NO APROBADOS POR LA FDA PARA EL CCR.

1.1 COMPUESTO G2

Tanto el compuesto G2 como sus derivados, que fueron identificados por Han *et al*., inhiben la capacidad de la fascina para empaquetar los haces de actina al mismo tiempo que presentan propiedades anti-migratorias y anti-invasivas en células de TNBC, todo ello debido a la unión directa con la fascina (108). Al igual que ocurre con el ACS, El TNBC también presenta un mal pronóstico, sobre-expresa la fascina y no es susceptible de ser tratado mediante terapia molecular dirigida (111). Estas características son comunes con el ACS, por lo que cabría esperar que el compuesto G2 presentara las mismas propiedades en células de CCR y, subsecuentemente, forme parte de futuros tratamientos para el ACS.

Según esta premisa, planteamos diversos ensayos *in vitro* en los que evaluamos el efecto del compuesto G2 sobre la capacidad migratoria, la invasión y la formación de lamelipodios de líneas celulares de CCR (HCT-116 y DLD-1). Observamos que el compuesto G2 disminuyó la capacidad migratoria de las células puesto que es capaz de impedir fuertemente la formación de lamelipodios, incluso a concentraciones más bajas que la MGS. Este efecto fue, además, dosis dependiente. Además, por primera vez, hemos analizado el efecto que tienen tanto MGS como G2 en un modelo de invasión organotípico sobre discos de mioma humanos utilizando líneas celulares de CCR y observando que ambos inhibidores de la fascina disminuyen el área y la profundidad de la invasión de forma significativa.

Además de los efectos *in vitro* no descritos hasta la fecha para el compuesto G2, también hemos demostrado en un modelo de invasión de pez cebra (ZF) (*in vivo*), que el compuesto G2 inhibe la invasión de las líneas celulares de CCR que sobre-expresan la fascina tanto de forma constitutiva como inducida genéticamente de manera análoga. Por todas estas evidencias, nos encontramos en disposición de afirmar que el compuesto G2 puede ser de utilidad para

enfoques terapéuticos cuya diana sean células tumorales invasivas y metastásicas y que sobre-expresen la fascina, como es el caso del ACS.

1.2 MONASTROL

Los análisis *in silico* revelaron al monastrol (MON), (Ethyl-4-(3-hydroxyphenyl)-6-methyl-2-thioxo-1,2,3,4-tetrahydropyrimidine-5-carboxylate) (Figura 10) como un potencial inhibidor de la fascina. El MON es un racemato formado por la mezcla equimolecular de R y S-monastrol.

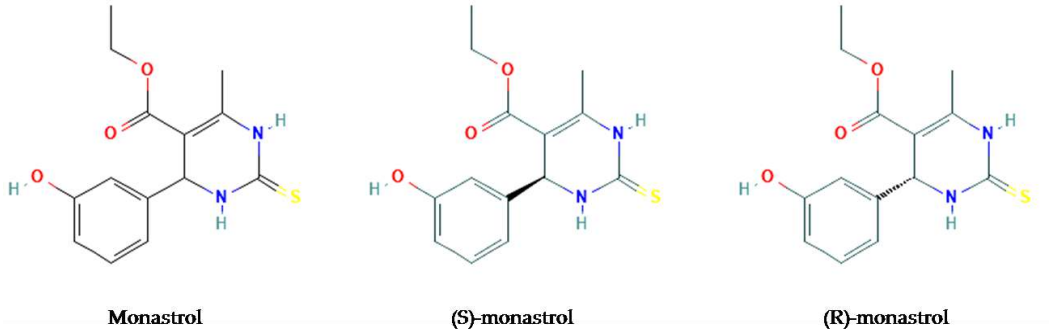

Figura 10. ***Estructura química en 2D del monastrol****. Podemos observar de izquierda a derecha, la estructura del monastrol de la mezcla racémica (S) y (R)- monastrol (112).*

Este compuesto no FDA, presenta diversas acciones biológicas: juega un papel fundamental como agente antineoplásico, como inhibidor de la ureasa, como agente contra la leishmaniosis y antimitótico (Figura 10) (112).

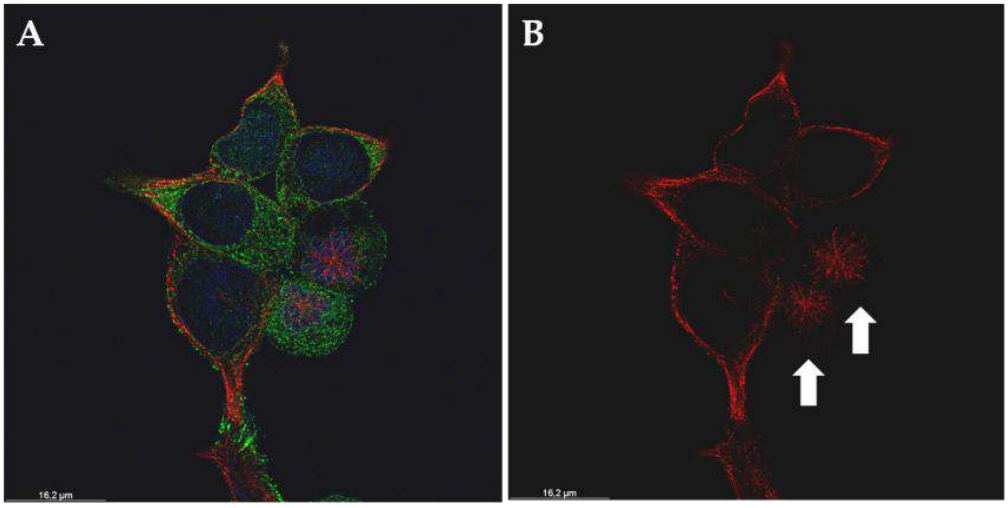

Figura 11. ***Efecto antimitótico del monastrol en líneas celulares de cáncer de colon HCT-116. (A)*** *Imagen obtenida por microscopía confocal donde podemos observar tres canales: azul (tinción nuclear Hoestch), verde (tinción con fascina) y rojo (tinción con β-tubulina).* ***(B)*** *La misma imagen que en A pero con el canal rojo para marcar la presencia de husos acromáticos (flechas blancas) originados por el tratamiento con monastrol. Imagen de elaboración propia.*

Entre sus acciones descritas, el MON es un inhibidor alostérico de la quinesina mitótica Eg5. Los motores homotetraméricos Eg5/KSP son conocidos por su capacidad para deslizar MT antiparalelos durante la formación del huso acromático. De esta forma Eg5 limita la velocidad máxima de desplazamiento de los MT durante la mitosis. Debido a la importancia de la quinesina Eg5 durante la mitosis, se ha convertido en una molécula de partida para el desarrollo de agentes quimioterapéuticos (113).

El hecho de que el MON aparezca como potencial inhibidor de la fascina, tras llevar a cabo los ensayos *in silico*, no es casual puesto que existe evidencia científica muy reciente que avala esta hipótesis. En efecto, se ha descrito que, en esta unión, están implicados los aminoácidos 234-250 de la fascina. Esta unión a los MT es fascina-dependiente y afecta a la formación de adhesiones focales (FAK) y a la velocidad de la migración (114). En este sentido, también se ha determinado que hay una mayor dinámica de los MT a altas concentraciones de la fascina en células MDA-MB-231 y, por consiguiente, un aumento de la metástasis.

Este hecho ocurre independientemente de la unión fascina-actina, aunque sí depende de la concentración de la fascina (69).

El MON tiene una estructura similar a la Nifedipina, una dihidropiridina que inhibe la fascina. Riahi *et al.*, diseñaron un derivado de la tetrahidropirimidina basándose en MON y Nifedipina y comprobaron mediante DM que ambos eran capaces de unirse a la fascina. Es importante resaltar que, el MON, a pesar de ser sugerido como potencial inhibidor de la fascina, nunca había sido caracterizado por sus propiedades anti-fascina (115).

Posteriormente, en esta Tesis hemos comprobado, mediante ensayos de polimerización de haces de actina, que tanto la MGS como el MON interrumpen la capacidad que tiene la fascina de formar haces de actina. Este hecho fue validado por microscopía electrónica de transmisión (MET). Además, el MON reduce las protrusiones citoplasmáticas impulsadas por la fascina en células de cáncer colorrectal. Paralelamente, el MON presenta propiedades anti-invasoras y anti-metastásicas en un modelo *in vivo* de pez cebra.

Puesto que un estudio reciente describió la unión entre la fascina y la tubulina (69) y también se ha descrito que el MON inhibe la dinámica de los MT (116), nos planteamos si el MON era capaz de interactuar en el sitio de unión entre la fascina y la tubulina. Para corroborar esta hipótesis, planteamos los ensayos de inmunoprecipitación e inmunofluorescencia y observamos que la unión de la fascina a la tubulina está condicionada por la presencia del MON. Además, ambas proteínas se descolocalizan parcialmente en presencia del MON.

Estos resultados, también pueden tener impacto en la función de la fascina en la quimioresistencia ya que el tratamiento con el MON podría revertir este fenómeno y tener un efecto sinérgico con agentes quimioterapéuticos dirigidos a los MT, como son los taxanos.

2. INHIBIDORES DE LA FASCINA APROBADOS POR LA FDA PARA EL CCR.

2.1 IMIPRAMINA

La IMIP (3-(10,11-dihidro-5*H*-dibenzo [*b,f*]azepina-5-il)-*N*,*N*-dimetilpropano-1-amina), también llamada melipramina, clorhidrato de imipramina y pamoato de imipramina, es un antidepresivo tricíclico (TCA) que actualmente se usa ampliamente en el tratamiento contra la depresión. Pertenece al grupo de los inhibidores no selectivos de la recaptación de monoaminas. Induce la sedación a través del bloqueo del receptor de histamina1, la hipotensión mediante el bloqueo de los receptores beta-adrenérgicos, y también tiene diversos efectos parasimpaticolíticos. Es utilizada en el tratamiento contra la distimia, depresión bipolar, trastornos por déficit de atención, agorafobia y trastornos de pánico (117). La IMIP es un fármaco aprobado por agencias reguladoras como la FDA y la EMA *(European Medicine Agency*) cuya fórmula comercial recibe el nombre de Tofranil® (118).

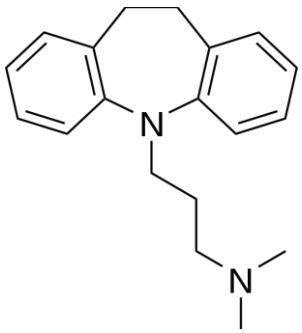

Figura 12. ***Estructura química en 2D de la imipramina***

(119).

A pesar de no relacionar científicamente el consumo de antidepresivos y cáncer, Sauer y Lang informaron de la supervivencia inesperada de un paciente con cáncer de pulmón metastásico asociado al tratamiento con la IMIP (120).

Además, el estudio epidemiológico llevado a cabo por Walker *et al*, que incluía 31.953 casos de cáncer con diferentes localizaciones, concluyó que los antidepresivos tricíclicos, como la IMIP, podían tener un gran potencial contra la prevención de cáncer colorrectal y glioma de manera dosis dependiente (121). Posteriormente, Jahachan *et al.* demostraron el efecto antitumoral de la IMIP en cáncer de pulmón de células pequeñas y otros tumores neuroendocrinos mediante ensayos *in vivo* en ratones. También se observaron efectos de la IMIP sobre la proliferación, migración e invasión en cáncer de próstata metastásico *in vitro* sobre células PC-3 (122). Por último, ha sido demostrado el efecto anti-cancerígeno de la paroxetina (123) y la sertralina (124) (ambos antidepresivos) en modelos *in vivo* de ratones xenotrasplantados con células tumorales de CCR.

La sobre-expresión de la fascina en el ACS y la evidencia *in silico* de la acción de la IMIP sobre la fascina, hicieron plantearnos a cabo ensayos *in vitro* e *in vivo* con el objetivo de confirmar si existía un efecto de la IMIP, a través de la fascina, en el CCR. En coherencia con los resultados obtenidos, hemos demostrado la utilidad de la IMIP como anti-cancerígeno debido a la disminución de las metástasis de manera dosis dependiente en modelos de ZF. Por consiguiente, el siguiente paso en la línea de investigación fue llevar a cabo ensayos en ratones xenotrasplantados con células de CCR que sobre-expresan fascina y tratarlos con IMIP.

2.2 RALTEGRAVIR

El RAL (N-(2-(4-(4-fluorobenzilcarbamoil)-5-hidroxi-1-metil-6-oxo-1,6-dihidropirimidin-2-il)propan-2-il)-5-metil-1,3,4-oxadiazol-2-carboxamida) es un inhibidor de la integrasa, el primero de los antivirales activos contra el virus de la inmunodeficiencia humana (VIH) que se usa en combinación con otros agentes antirretrovirales en el tratamiento contra la infección por VIH, tanto en adultos como en niños. El RAL se presenta en forma comercial como Isentress®, por lo que es un fármaco aprobado por la FDA (125).

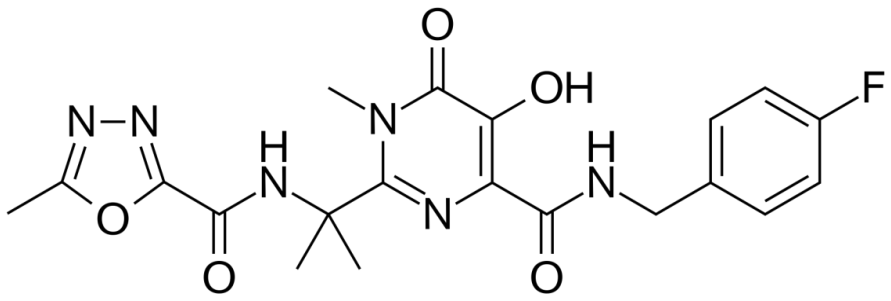

Figura 13. ***Estructura química en 2D del raltegravir*** *(126).*

Al contrario a lo que ocurría como los antidepresivos, el uso de antirretrovirales como tratamiento contra el cáncer no es novedoso. Además del efecto anti-VIH, se ha demostrado que el RAL presenta efectos anti-neoplásicos en relación con tumores asociados a virus, como es el caso del virus del sarcoma de Kaposi (127). También, el RAL es capaz de inhibir un virus xenotrópico relacionado con leucemia murina que está implicado en cáncer de próstata relacionado con la fatiga crónica. De manera interesante, se ha visto que el tratamiento con RAL no se asocia con un aumento del riesgo oncogénico tras estudiar una cohorte de 1470 pacientes pertenecientes a EuroSIDA (128).

Otro grupo de evidencias experimentales señalan el efecto de los antirretrovirales en la restauración de la sensibilidad a los agentes quimioterapéuticos, de tal forma que la zidovudina aumenta la sensibilidad del cisplatino en un modelo *in vitro* de células de cáncer de colon humanas (129).

Recientemente, Chan *et al.* han descubierto que el RAL inhibe la Aldolasa A, una proteína de unión a γ-actina en un modelo *in vivo* de cáncer de pulmón sin toxicidad significativa (130). Según esta evidencia, y siendo la fascina una proteína de unión a F-actina, se podría entrever una relación entre el RAL y la fascina. De hecho, usando *Pocketalign* e información estructural de la base de datos PDB hemos encontrado que ambas proteínas, la Aldolasa A y la fascina, poseen un bolsillo hidrofóbico en común, localizado en el sitio de unión a actina. Además, se ha demostrado la relación entre la fascina y diferentes tipos de virus. La fascina facilita la liberación y trasmisión célula-célula del virus linfotrópico T humano tipo 1 (HTLV1) (131) y del virus de la pseudorabia (PRV) (132). También

se ha encontrado relación entre la fascina y el síndrome gástrico asociado al virus de Epstein-Barr en el CRC (133).

Mediante la herramienta del VS, hemos identificado que el RAL es un potencial inhibidor de la fascina. Posteriormente, esta premisa ha sido corroborada mediante ensayos de Resonancia Magnética Nuclear (RMN), proporcionando detalles sobre los residuos claves que participan en la interacción entre la fascina y el RAL. Además, hemos demostrado que el RAL es capaz de inhibir la actividad anti-migratoria y anti-invasora en modelos *in vitro* e *in vivo*.

El conjunto de las evidencias experimentales anteriores sugiere la relación entre la fascina y el RAL. Además, los datos de esta Tesis también confirman que el RAL es capaz de bloquear la fascina, con posteriores efectos en la invasión y la metástasis de células tumorales, convirtiéndose pues en un potencial inhibidor para el tratamiento de tumores que sobre-expresan fascina.

4. ENSAYOS *IN VIVO* EN RATÓN

Jun Jan *et al.* describieron la actividad anti-cancerígena de la paroxetina, otro TCA, en células de cáncer de colon humano xenoinjertadas en ratones (123). Por esa razón, especulamos que el modo de acción del Tofranil® (IMIP) podría probarse de la misma manera. En esta línea, nuestros resultados muestran que el Tofranil® disminuye el volumen y el peso tumoral en ratones tratados tras sólo 15 días del xenotrasplante, y es capaz de encapsular tumores. Sin embargo, el tratamiento con Issentress® (el cual llevamos hasta 28 días, basándonos los experimentos previos con Tofranil®) no mostró resultados significativos en las mediciones realizadas. Recientemente, se ha descrito que el bloqueo de la fascina no tiene un efecto importante en la proliferación celular. De hecho, Huang *et a*l., describieron que el compuesto G2 inhibía solamente la proliferación celular en algunos tipos de cáncer y en dicho estudio no estaba incluido el CRC (134). Debido a Las propiedades anti-invasoras y anti-metastásicas descritas para el RAL (40, 135), no pudieron confirmarse en el presente modelo murino. Por lo que planteamos que quizás sea necesario modificar el modelo murino a otro en el cual

el tumor tenga la capacidad necesaria de invadir y metastatizar. En nuestros ensayos hemos utilizado ratones atímicos donde las células crecen sin límite y quizás no sea el modelo adecuado en una etapa pre-clínica. Por esta razón, sería conveniente utilizar un modelo de ratón xenotrasplantado con organoides derivados de pacientes diagnosticados de ACS y/o utilizar líneas celulares murinas en ratón. Zhan *et al.* llevaron a cabo un estudio sobre la coadyuvancia de la paroxetina y el 5-fluorouracilo mejorando así la terapia en CRC en un modelo murino (136). Estas evidencias sugieren un nuevo experimento enfocado hacia la coadyuvancia entre los inhibidores de la fascina y la terapia quimioterapéutica (5-fluorouracilo, irinotecán u oxaliplatino). De hecho, este tipo de estudios es más extrapolable a la práctica clínica ya que nunca se tratarían pacientes de ACS sin quimioterapia.

5. REPOSICIONAMIENTO DE FÁRMACOS

La industria farmacéutica es buena conocedora de los elevados tiempos necesarios para el descubrimiento y comercialización de nuevos fármacos. De hecho, para el desarrollo de una terapia exitosa sobre una diana terapéutica recientemente descrita para el cáncer existe un amplio intervalo de tiempo. La idea de utilizar fármacos ya conocidos y aprobados por las agencias reguladoras como la EMA, NHI (*National Institutes of Health*) y la FDA para nuevas indicaciones, recibe el nombre de reposicionamiento de fármacos y ha ganado importancia en muchos campos de la medicina (137). Este enfoque presenta una ventaja importante en comparación con el proceso de descubrimiento de fármacos "*de novo*" al reducir considerablemente los costes del procedimiento así como el tiempo, ya que permite una comercialización más rápida, con el consecuente beneficio directo para los pacientes (138).

Existen diferentes clases de medicamentos que han seguido la estrategia del reposicionamiento:

- Medicamentos que fueron dejados de lado debido a su toxicidad a altas concentraciones cuando se usaban para una indicación determinada pero que no son tóxicos a concentraciones más bajas. Este es el caso de la

Talidomida. Actualmente se utiliza para el tratamiento del mieloma múltiple refractario (excluyendo a mujeres embarazadas).

- Medicamentos que encontraron una utilidad totalmente diferente debido a sus efectos secundarios. Este es el caso de la Viagra. Inicialmente, era un fármaco indicado para el tratamiento de las anginas y finalmente, resultó de utilidad contra la disfunción eréctil (137).

En este contexto, los medicamentos aprobados por la FDA deben ser el punto de partida de la estrategia de reposicionamiento (110). Este hecho se ve reflejado en el descubrimiento de la IMIP y el RAL (fármacos ya aprobados por la FDA y con otras indicaciones previas) como potenciales inhibidores de la fascina en CCR.

Los datos científicos, aquí documentados, apoyarían la posibilidad de reposicionamiento para la IMIP (139). Además, en esta Tesis, aportamos los datos en formato de artículo científico y patente licenciada. Desafortunadamente, se realizan pocos estudios *in vivo* para testar el reposicionamiento de fármacos anti-cancerígenos. De hecho, la insuficiencia de estudios *in vivo* y la falta de ensayos clínicos en humanos son una laguna en el campo del reposicionamiento de fármacos. Sin embargo, las benzodiacepinas (diazepam, midzolam), antidepresivos (IMIP, clomipramina y citalopram), antiepilépticos (ácido valpórico, fenitoína) y antidiabéticos (metformina), sí se han testado y muestran actividad biológica contra determinadas células cancerígenas (140).

Pese a la evidencia científica, no se había demostrado la existencia de dianas moleculares relacionadas con la actividad antitumoral de la IMIP. Tampoco se habían utilizado clínicamente proteínas del citoesqueleto de actina como dianas terapéuticas para el tratamiento del cáncer (85). No obstante, sí que se había observado que la línea celular Caco-2 de cáncer colorrectal, es permeable a la IMIP (141). Otro de los derivados de la IMIP, que sí ha sido recientemente estudiado como inhibidor de la migración en células cancerígenas es la imipramina *blue* (IB). Pese a que los autores no han relacionado el efecto de IB con la fascina, sí que han descrito el efecto anti-migratorio de esta pequeña molécula, bloqueando así la migración en células de glioma. Este efecto se ve incrementado favorablemente cuando se combina DXR (fármaco quimioterapéutico), y aumenta la esperanza de vida en ensayos *in vivo* con ratas (142).

Por otro lado, el RAL, es un fármaco susceptible de reposicionamiento. La bibliografía describe propiedades muy variadas asociadas a este anti-retroviral entre las que podemos destacar propiedades anti-fúngicas (143), además de las predecibles antivirales. Por ejemplo, desde 2020 se ha utilizado contra el virus SARS-Cov-2 (144). Además, existe un estudio piloto que está determinando el efecto del RAL utilizado en tratamiento conjunto, con cisplatino (fármaco quimioterapéutico), en pacientes con carcinoma de células escamosas, de cabeza y cuello (NCT01275183) (145).

Fruto de los resultados obtenidos que mostraron el efecto anti-invasivo y anti-migratorio de la IMIP y del RAL sobre células de CCR, se ha patentado el reposicionamiento de ambos inhibidores para tratar tumores que sobre-expresan la fascina.

- IMIP (número de patente europea 18382696.5 (146)) y licenciado a Ennaid Therapeutics LLC (empresa estadounidense).
- RAL (número de patente P202130062, pendiente de publicación).

6. COMPARATIVA ENTRE LOS DISTINTOS INHIBIDORES DE LA FASCINA EN CCR.

La unión de los inhibidores a la fascina ha sido estudiada mediante la técnica *in vitro* de ThermoFluor. Gracias a esta técnica, hemos podido observar el perfil térmico de la fascina al desplegarse tanto en ausencia como en presencia de los inhibidores. En todos los casos, los inhibidores aumentan la temperatura de *melting* (T_m) de transición del despliegue de la proteína (en torno a un incremento de 2 ºC para la IMIP y el MON). Este aumento de temperatura es proporcional a la capacidad que tiene el ligando (inhibidor) por la proteína (fascina), lo que sugiere que ambos se unen de forma específica a la fascina.

No obstante, no todos los inhibidores tienen la misma afinidad de unión por la fascina. El compuesto G2 se une directamente y posee una constante de disociación (K_d) de 5-20 μM. Este compuesto es uno de los que tiene mayor afinidad por la fascina seguido de RAL, MON e IMIP. No obstante, pese al elevado valor de la K_d de la IMIP (390 μM), hemos observado que la IMIP es el

inhibidor que mejor bloquea la invasión en un modelo *in vitro* 3D de invasión tumoral, siendo incluso más eficaz que la MGS y que el MON, y además es dosis dependiente. Por otro lado, este efecto biológico fue menor para el compuesto G2, pese a su baja constante de disociación. Los motivos por los que ocurren esta discordancia de datos *in vitro* podrían deberse a la menor permeabilidad del G2. Este efecto fue descrito por Tsumura *et al.* que observaron cómo, a pesar de que el fármaco de estudio tenía un valor de K_d elevado, se incrementaba el efecto anti-tumoral del mismo debido a que el fármaco era capaz de penetrar y distribuirse uniformemente por todo el tumor (147).

Como ya se ha comentado previamente, la acción de los inhibidores sobre la reorganización de la actina se relacionada con la formación de lamelipodios. Si comparamos el efecto de cada uno de los inhibidores en la formación de estas estructuras sobre células HCT-116, observamos que hay una disminución más pronunciada al tratar las células con la IMIP. Por lo que evidenciamos que la IMIP es el inhibidor que más afecta a la formación de estas estructuras, siendo de nuevo el compuesto G2 el que obtuvo efectos menores, pero, aun así, significativos. Efectivamente, observamos una disminución de más del 50% en la migración de las líneas celulares cuando fueron tratadas con la IMIP. También disminuyó la migración al tratar con el RAL y el MON pero en menor porcentaje.

Los ensayos de invasión *in vivo* en un modelo de ZF utilizado, revelaron que la IMIP, el RAL y el MON disminuyen el número de focos invasivos de una forma similar a como lo hace la MGS, y que el compuesto G2 también aumentó su actividad inhibitoria de forma dosis dependiente en este modelo. Además, cuando estudiamos el porcentaje de larvas que desarrollan metástasis hay una disminución significativa (más del 50%), cuando las larvas fueron tratadas con la IMIP, el RAL y el MON.

Pese a que los ensayos físico-químicos muestran valores elevados de afinidad del compuesto G2 con la fascina, el resto de inhibidores y más concretamente la IMIP, demostraron una mayor eficacia en ensayos *in vitro* e *in vivo* con células tumorales de cáncer de colon.

A continuación, se muestra una tabla resumen (Tabla 2) donde se comparan las diferentes técnicas empleadas (*in silico*, biofísicas, *in vitro* e *in vivo*) para los diferentes inhibidores de la fascina estudiados. Pese a que la IMIP se planteaba

como el inhibidor con un valor mayor de la K_d es, de entre los tres nuevos inhibidores de fascina estudiados en esta Tesis (IMIP, MON, RAL), el que mejor reduce la inhibición de la metástasis en un modelo *in vivo*.

Tabla 2: Resumen de la efectividad de los inhibidores de la fascina para las diferentes técnicas cuantitativas

HCT-116		**INHIBIDORES DE LA FASCINA**					
Tipo de Técnica	**Medida**	**Control**	**MGS (100 μM)**	**G2 (20 μM)**	**IMIP (10 μM)**	**RAL (30 μM)**	**MON (100 μM)**
Biofísicas	ThermoFluor (ºC)	55.7±0.5 ºC	-	-	58.3±0.6 ºC	-	57.7±0.6 ºC
	Tritiación fluorescente (K_d)	-	-	5-20 μM	390 μM	180 ±10 μM	183 μM
	MET (nº filamentos de actina)	8.8±1.78 ***	3.21±1.31 ***	1.73±0,72 ***	2.41±0.959 ***	3.9±1.74 ***	2.80±1.508 ***
In vitro	Migración (% migración)	100%	44.5±4%	73.9±1%	41.9±2%	84.3±2%	70±2%
	Invasión mioma (% profundidad)	100%	68%	34%	40%	-	24%
	Inmunofluorescencia (nº de lamelipodios)	9±1.58	2±2	5.8±1.09	0.6±0.89	6.73±1.1	4.4±1.95
In vivo	Pez cebra (% de larvas con invasión)	60%	38±2%	31.2±2%	39±2%	29±2%	35±2%
	Pez cebra (% larvas con metástasis)	39.3±3%	-	-	2±3%	18±3%	3±3%

MET: Microscopía electrónica de transmisión; (***P<0,001. Anova, Tukey post hoc test)

V - CONCLUSIONES

V - CONCLUSIONES

1. Por primera vez se ha descrito que el compuesto G2, un inhibidor de la fascina, presenta propiedades anti-migratorias y anti-invasoras en células de cáncer colorrectal, siendo eficaz a concentraciones más bajas que la migrastatina (inhibidor clásico de la fascina).

2. Los resultados experimentales *in vitro* e *in vivo* obtenidos en la presente Tesis, evidencian que la imipramina, un antidepresivo aprobado por la FDA, posee propiedades anti-fascina, y por consiguiente, inhibe la actividad pro-invasora y pro-metastásica en células tumorales de cáncer de colon. Los resultados fueron obtenidos *in vitro* e *in vivo*.

3. Mediante estudios de VS hemos identificado el raltegravir, un antiviral aprobado por la FDA, como inhibidor de la fascina. Así, el tratamiento de células de cáncer colorrectal con este fármaco redujo la migración, invasión y metástasis tanto *in vitro* como *in vivo*.

4. El monastrol bloquea la invasión y la metástasis tumoral en células de cáncer colorrectal, una vez más debido a su unión con la fascina en los sitios de unión a la actina, pero también presenta un efecto sobre el sitio de unión a la β-tubulina.

5. Los resultados obtenidos en el modelo murino sugieren que el Tofranil® disminuye el volumen y el peso tumoral en los ratones tratados y es capaz de encapsular tumores mientras que el efecto del Issentress® no fue significativo.

6. Los datos presentados en esta Tesis destacan el papel fundamental del cribado de fármacos en la investigación traslacional, así como la utilidad del reposicionamiento de fármacos para la práctica clínica diaria.

VI – LIMITACIONES Y FUTURAS LÍNEAS DE INVESTIGACIÓN

VI- LIMITACIONES Y FUTURAS LÍNEAS DE INVESTIGACIÓN

Las líneas de investigación en desarrollo a las que nos lleva de manera natural y lógica esta Tesis Doctoral son tres, y se resumen a continuación:

1. El estudio de la coadyuvancia de los inhibidores con agentes quimioterapéuticos tanto en modelos *in vitro* como *in vivo.*
2. El desarrollo y puesta a punto de ensayos *in vitro* e *in vivo* con organoides de colon obtenidos de pacientes diagnosticados de ACS.
3. La realización de un ensayo clínico en humanos con Tofranil®.

1. ESTUDIO DE LA COADYUVANCIA DE LOS INHIBIDORES CON AGENTES QUIMIOTERAPÉUTICOS.

Puesto que los resultados del modelo murino son preliminares, en futuras líneas de investigación pretendemos evaluar el efecto sinérgico de quimioterapéuticos con los inhibidores de la fascina descritos en esta Tesis Doctoral. Estos experimentos están contemplados y aprobados por el Órgano Habilitado (OH) y se pretenden utilizar docetaxcel, pemborlizumab y PDL-1 como agentes quimioterapéuticos.

2. ENSAYOS *IN VITRO* E *IN VIVO* CON ORGANOIDES DE COLON.

Adaptar e intentar reproducir enfermedades humanas en sistemas *in vitro* es indiscutiblemente una herramienta fundamental en investigación, sin embargo, conlleva una serie de limitaciones. La principal limitación de esta Tesis es que no podemos asegurar que las líneas celulares utilizadas tengan como origen un ACS, puesto que no hay una línea de CCR tipificada como ACS en los registros de líneas tumorales celulares. El establecimiento de un cultivo primario a partir de un ACS sería una posible solución, no obstante, estas líneas no estarían inmortalizadas lo que a su vez sería una limitación añadida.

Estas limitaciones pueden ser superadas gracias a la introducción de cultivos de organoides. Estos cultivos 3D, constituyen un sistema que reproduce fielmente la fisiología, forma, dinámica y composición celular del epitelio intestinal. En comparación con el uso de líneas celulares 2D de cáncer de colon, los organoides de colon permiten recrear el microambiente real del tumor, lo cual es una gran ventaja en investigación traslacional.

Actualmente, estamos estableciendo un banco de organoides de colon derivado de pacientes con ACS con el objetivo de poder testar los inhibidores de la fascina sobre ellos tanto en experimentos *in vitro* como *in vivo* en modelos murinos de CCR. Para ello, contamos con la aprobación del OH Arrixaca-IMIB (código REGA ES300303340098).

3. ENSAYO CLÍNICO CON TOFRANIL

Gracias a los resultados preliminares obtenidos en esta Tesis con modelos animales de ZF y ratón, se planteó el abordaje de un ensayo clínico en humanos que se encuentra actualmente en vías de desarrollo (Ensayo clínico Nº EudraCT 2021-001328-17, (REF MUH/CLIN/EC)), y que se engloba bajo el título:

- "Efectos histológicos y clínicos de la imipramina en el tratamiento de pacientes con tumores que sobre-expresan fascina" Entidad de realización: Instituto Murciano de Investigaciones Biosanitarias (IMIB). Entidad/es financiadora/s: Instituto de Salud Carlos III Tipo de entidad: Organismo Público de Investigación Fecha de inicio-fin: 01/01/2021 - 01/01/2025 Cuantía total: 218.900 €.

Dicho proyecto articula dos fases principales:

- La primera fase investiga los cambios a nivel de tejido tumoral y peritumoral que experimenta el paciente tratado con IMIP sin (CCR) o con neoadyuvancia (recto y el TNBC). Normalmente, los cánceres de colon o de mama, como el ACS y el TNBC se diagnostican mediante el estudio anatomopatológico de una biopsia para ser finalmente operados por cirugía tras un periodo variable. Durante este periodo, se pretende tratar con IMIP (Tofranil®) a los pacientes en cuya biopsia se observe una sobre-expresión de la fascina. Los posibles cambios serán evaluados sobre el tejido extirpado en comparación con el de los pacientes que hayan sido tratados con placebo.
- La segunda fase se realizará si se observan cambios en la primera. En esta fase se investiga el efecto de la IMIP sobre la diseminación, migración e invasión del tumor en una localización metastásica. Entonces se reclutarán nuevos pacientes a los que se les administrará IMIP durante la quimioterapia y serán evaluados a los dos años (tiempo que tardan aproximadamente en desarrollarse las metástasis), en el caso de que se desarrollen. También es realizarán seguimientos en sangre de ADN tumoral mutado para tener un reflejo de la actividad de la enfermedad.

Si los resultados fuesen satisfactorios, se podría extender a un ensayo en fase III con más pacientes e iniciar un ensayo en fase II con pacientes con otros tumores que sobre-expresan la fascina como el carcinoma microcítico de pulmón o el glioma.

VII – REFERENCIAS BIBLIOGRÁFICAS

VII –REFERENCIAS BIBLIOGRÁFICAS

1. Bray F, Ferlay J, Soerjomataram I, Siegel RL, Torre LA, Jemal A. Global cancer statistics 2018: GLOBOCAN estimates of incidence and mortality worldwide for 36 cancers in 185 countries. CA Cancer J Clin. 2018;68(6):394-424.
2. Sung H, Ferlay J, Siegel RL, Laversanne M, Soerjomataram I, Jemal A, et al. Global Cancer Statistics 2020: GLOBOCAN Estimates of Incidence and Mortality Worldwide for 36 Cancers in 185 Countries. CA Cancer J Clin. 2021;71(3):209-49.
3. Lynch HT, de la Chapelle A. Hereditary colorectal cancer. N Engl J Med. 2003;348(10):919-32.
4. Fearon ER, Vogelstein B. A genetic model for colorectal tumorigenesis. Cell. 1990;61(5):759-67.
5. Nguyen LH, Goel A, Chung DC. Pathways of Colorectal Carcinogenesis. Gastroenterology. 2020;158(2):291-302.
6. Snover DC, Jass JR, Fenoglio-Preiser C, Batts KP. Serrated polyps of the large intestine: a morphologic and molecular review of an evolving concept. Am J Clin Pathol. 2005;124(3):380-91.
7. Garcia-Solano J, Turpin-Sevilla MDC, Garcia-Garcia F, Carbonell-Munoz R, Torres-Moreno D, Conesa A, et al. Differences in gene expression profiling and biomarkers between histological colorectal carcinoma subsets from the serrated pathway. Histopathology. 2019;75(4):496-507.
8. Johdi NA, Sukor NF. Colorectal Cancer Immunotherapy: Options and Strategies. Front Immunol. 2020;11:1624.
9. Perincheri S, Hui P. KRAS mutation testing in clinical practice. Expert Rev Mol Diagn. 2015;15(3):375-84.
10. Folprecht G. [Current medicinal treatment of metastasized colorectal carcinoma]. Chirurg. 2010;81(6):507-15.
11. Nagtegaal ID, Odze RD, Klimstra D, Paradis V, Rugge M, Schirmacher P, et al. The 2019 WHO classification of tumours of the digestive system. Histopathology. 2020;76(2):182-8.
12. Makinen MJ. Colorectal serrated adenocarcinoma. Histopathology. 2007;50(1):131-50.
13. Garcia-Solano J, Perez-Guillermo M, Conesa-Zamora P, Acosta-Ortega J, Trujillo-Santos J, Cerezuela-Fuentes P, et al. Clinicopathologic study of 85

.

colorectal serrated adenocarcinomas: further insights into the full recognition of a new subset of colorectal carcinoma. Hum Pathol. 2010;41(10):1359-68.

14. O'Brien MJ, Yang S, Mack C, Xu H, Huang CS, Mulcahy E, et al. Comparison of microsatellite instability, CpG island methylation phenotype, BRAF and KRAS status in serrated polyps and traditional adenomas indicates separate pathways to distinct colorectal carcinoma end points. Am J Surg Pathol. 2006;30(12):1491-501.

15. Alburquerque-Gonzalez B, Lopez-Calderon FF, Lopez-Abellan MD, Esteban-Gil A, Garcia-Solano J, Conesa-Zamora P. Biology and Therapeutic Targets of Colorectal Serrated Adenocarcinoma; Clues for a Histologically Based Treatment against an Aggressive Tumor. Int J Mol Sci. 2020;21(6).

16. Stefanius K, Ylitalo L, Tuomisto A, Kuivila R, Kantola T, Sirnio P, et al. Frequent mutations of KRAS in addition to BRAF in colorectal serrated adenocarcinoma. Histopathology. 2011;58(5):679-92.

17. Garcia-Solano J, Conesa-Zamora P, Carbonell P, Trujillo-Santos J, Torres-Moreno DD, Pagan-Gomez I, et al. Colorectal serrated adenocarcinoma shows a different profile of oncogene mutations, MSI status and DNA repair protein expression compared to conventional and sporadic MSI-H carcinomas. Int J Cancer. 2012;131(8):1790-9.

18. Bettington M, Walker N, Clouston A, Brown I, Leggett B, Whitehall V. The serrated pathway to colorectal carcinoma: current concepts and challenges. Histopathology. 2013;62(3):367-86.

19. Baker AM, Graham TA, Elia G, Wright NA, Rodriguez-Justo M. Characterization of LGR5 stem cells in colorectal adenomas and carcinomas. Sci Rep. 2015;5:8654.

20. Conesa-Zamora P, Garcia-Solano J, Garcia-Garcia F, Turpin Mdel C, Trujillo-Santos J, Torres-Moreno D, et al. Expression profiling shows differential molecular pathways and provides potential new diagnostic biomarkers for colorectal serrated adenocarcinoma. Int J Cancer. 2013;132(2):297-307.

21. Kahi CJ. Screening Relevance of Sessile Serrated Polyps. Clin Endosc. 2019;52(3):235-8.

22. Garcia-Solano J, Conesa-Zamora P, Trujillo-Santos J, Makinen MJ, Perez-Guillermo M. Tumour budding and other prognostic pathological features at invasive margins in serrated colorectal adenocarcinoma: a comparative study with conventional carcinoma. Histopathology. 2011;59(6):1046-56.

23. Conesa-Zamora P, Garcia-Solano J, Turpin Mdel C, Sebastian-Leon P, Torres-Moreno D, Estrada E, et al. Methylome profiling reveals functions and

genes which are differentially methylated in serrated compared to conventional colorectal carcinoma. Clin Epigenetics. 2015;7:101.
24. Davies EJ, Marsh Durban V, Meniel V, Williams GT, Clarke AR. PTEN loss and KRAS activation leads to the formation of serrated adenomas and metastatic carcinoma in the mouse intestine. J Pathol. 2014;233(1):27-38.
25. Nakanishi Y, Diaz-Meco MT, Moscat J. Serrated Colorectal Cancer: The Road Less Travelled? Trends Cancer. 2019;5(11):742-54.
26. Guinney J, Dienstmann R, Wang X, de Reynies A, Schlicker A, Soneson C, et al. The consensus molecular subtypes of colorectal cancer. Nat Med. 2015;21(11):1350-6.
27. Laiho P, Kokko A, Vanharanta S, Salovaara R, Sammalkorpi H, Jarvinen H, et al. Serrated carcinomas form a subclass of colorectal cancer with distinct molecular basis. Oncogene. 2007;26(2):312-20.
28. Tuomisto A, Garcia-Solano J, Sirnio P, Vayrynen J, Perez-Guillermo M, Makinen MJ, et al. HIF-1alpha expression and high microvessel density are characteristic features in serrated colorectal cancer. Virchows Arch. 2016;469(4):395-404.
29. Esteban-Gil A, Perez-Sanz F, Garcia-Solano J, Alburquerque-Gonzalez B, Parreno-Gonzalez MA, Legaz-Garcia MDC, et al. ColPortal, an integrative multiomic platform for analysing epigenetic interactions in colorectal cancer. Sci Data. 2019;6(1):255.
30. Battaglin F, Puccini A, Intini R, Schirripa M, Ferro A, Bergamo F, et al. The role of tumor angiogenesis as a therapeutic target in colorectal cancer. Expert Rev Anticancer Ther. 2018;18(3):251-66.
31. Arai H, Battaglin F, Wang J, Lo JH, Soni S, Zhang W, et al. Molecular insight of regorafenib treatment for colorectal cancer. Cancer Treat Rev. 2019;81:101912.
32. Loupakis F, Cremolini C, Salvatore L, Masi G, Sensi E, Schirripa M, et al. FOLFOXIRI plus bevacizumab as first-line treatment in BRAF mutant metastatic colorectal cancer. Eur J Cancer. 2014;50(1):57-63.
33. Nakanishi Y, Duran A, L'Hermitte A, Shelton PM, Nakanishi N, Reina-Campos M, et al. Simultaneous Loss of Both Atypical Protein Kinase C Genes in the Intestinal Epithelium Drives Serrated Intestinal Cancer by Impairing Immunosurveillance. Immunity. 2018;49(6):1132-47 e7.
34. Pardoll DM. The blockade of immune checkpoints in cancer immunotherapy. Nat Rev Cancer. 2012;12(4):252-64.
35. Postow MA, Callahan MK, Wolchok JD. Immune Checkpoint Blockade in Cancer Therapy. J Clin Oncol. 2015;33(17):1974-82.

.

36. Gatalica Z, Snyder C, Maney T, Ghazalpour A, Holterman DA, Xiao N, et al. Programmed cell death 1 (PD-1) and its ligand (PD-L1) in common cancers and their correlation with molecular cancer type. Cancer Epidemiol Biomarkers Prev. 2014;23(12):2965-70.
37. Llosa NJ, Cruise M, Tam A, Wicks EC, Hechenbleikner EM, Taube JM, et al. The vigorous immune microenvironment of microsatellite instable colon cancer is balanced by multiple counter-inhibitory checkpoints. Cancer Discov. 2015;5(1):43-51.
38. Chen L, Yang S, Jakoncic J, Zhang JJ, Huang XY. Migrastatin analogues target fascin to block tumour metastasis. Nature. 2010;464(7291):1062-6.
39. Montoro-Garcia S, Alburquerque-Gonzalez B, Bernabe-Garcia A, Bernabe-Garcia M, Rodrigues PC, den-Haan H, et al. Novel anti-invasive properties of a Fascin1 inhibitor on colorectal cancer cells. J Mol Med (Berl). 2020;98(3):383-94.
40. Alburquerque-Gonzalez B, Bernabe-Garcia M, Montoro-Garcia S, Bernabe-Garcia A, Rodrigues PC, Ruiz Sanz J, et al. New role of the antidepressant imipramine as a Fascin1 inhibitor in colorectal cancer cells. Exp Mol Med. 2020;52(2):281-92.
41. Natalwala A, Spychal R, Tselepis C. Epithelial-mesenchymal transition mediated tumourigenesis in the gastrointestinal tract. World J Gastroenterol. 2008;14(24):3792-7.
42. Kato Y, Kondo S, Itakura T, Tokunaga M, Hatayama S, Katayama K, et al. SNAIL- and SLUG-induced side population phenotype of HCT116 human colorectal cancer cells and its regulation by BET inhibitors. Biochem Biophys Res Commun. 2020;521(1):152-7.
43. Dongre A, Weinberg RA. New insights into the mechanisms of epithelial-mesenchymal transition and implications for cancer. Nat Rev Mol Cell Biol. 2019;20(2):69-84.
44. Kalluri R, Weinberg RA. The basics of epithelial-mesenchymal transition. J Clin Invest. 2009;119(6):1420-8.
45. Brabletz S, Schmalhofer O, Brabletz T. Gastrointestinal stem cells in development and cancer. J Pathol. 2009;217(2):307-17.
46. Garcia-Solano J, Conesa-Zamora P, Trujillo-Santos J, Torres-Moreno D, Makinen MJ, Perez-Guillermo M. Immunohistochemical expression profile of beta-catenin, E-cadherin, P-cadherin, laminin-5gamma2 chain, and SMAD4 in colorectal serrated adenocarcinoma. Hum Pathol. 2012;43(7):1094-102.
47. Conacci-Sorrell M, Simcha I, Ben-Yedidia T, Blechman J, Savagner P, Ben-Ze'ev A. Autoregulation of E-cadherin expression by cadherin-cadherin

interactions: the roles of beta-catenin signaling, Slug, and MAPK. J Cell Biol. 2003;163(4):847-57.
48. Prall F. Tumour budding in colorectal carcinoma. Histopathology. 2007;50(1):151-62.
49. Fife CM, McCarroll JA, Kavallaris M. Movers and shakers: cell cytoskeleton in cancer metastasis. Br J Pharmacol. 2014;171(24):5507-23.
50. Hall A. Rho family GTPases. Biochem Soc Trans. 2012;40(6):1378-82.
51. Alexander SP, Benson HE, Faccenda E, Pawson AJ, Sharman JL, Spedding M, et al. The Concise Guide to PHARMACOLOGY 2013/14: G protein-coupled receptors. Br J Pharmacol. 2013;170(8):1459-581.
52. Cavallaro U, Christofori G. Cell adhesion and signalling by cadherins and Ig-CAMs in cancer. Nat Rev Cancer. 2004;4(2):118-32.
53. Lin S, Taylor MD, Singh PK, Yang S. How does fascin promote cancer metastasis? FEBS J. 2021;288(5):1434-46.
54. Hashimoto Y, Kim DJ, Adams JC. The roles of fascins in health and disease. J Pathol. 2011;224(3):289-300.
55. Bryan J, Edwards R, Matsudaira P, Otto J, Wulfkuhle J. Fascin, an echinoid actin-bundling protein, is a homolog of the Drosophila singed gene product. Proc Natl Acad Sci U S A. 1993;90(19):9115-9.
56. Edwards RA, Bryan J. Fascins, a family of actin bundling proteins. Cell Motil Cytoskeleton. 1995;32(1):1-9.
57. Yamashiro-Matsumura S, Matsumura F. Purification and characterization of an F-actin-bundling 55-kilodalton protein from HeLa cells. J Biol Chem. 1985;260(8):5087-97.
58. Boer EF, Howell ED, Schilling TF, Jette CA, Stewart RA. Fascin1-dependent Filopodia are required for directional migration of a subset of neural crest cells. PLoS Genet. 2015;11(1):e1004946.
59. Matsumura F, Polz R, Singh S, Matsumura A, Scheller J, Yamashiro S. Investigation of Fascin1, a Marker of Mature Dendritic Cells, Reveals a New Role for IL-6 Signaling in CCR7-Mediated Chemotaxis. J Immunol. 2021;207(3):938-49.
60. Ma Y, Machesky LM. Fascin1 in carcinomas: Its regulation and prognostic value. Int J Cancer. 2015;137(11):2534-44.
61. Liu X, Zhao M, Xie Y, Li P, Wang O, Zhou B, et al. Null Mutation of the Fascin2 Gene by TALEN Leading to Progressive Hearing Loss and Retinal Degeneration in C57BL/6J Mice. G3 (Bethesda). 2018;8(10):3221-30.
62. Tubb B, Mulholland DJ, Vogl W, Lan ZJ, Niederberger C, Cooney A, et al. Testis fascin (FSCN3): a novel paralog of the actin-bundling protein fascin expressed specifically in the elongate spermatid head. Exp Cell Res. 2002;275(1):92-109.

.

63. Jansen S, Collins A, Yang C, Rebowski G, Svitkina T, Dominguez R. Mechanism of actin filament bundling by fascin. J Biol Chem. 2011;286(34):30087-96.
64. Ono S, Yamakita Y, Yamashiro S, Matsudaira PT, Gnarra JR, Obinata T, et al. Identification of an actin binding region and a protein kinase C phosphorylation site on human fascin. J Biol Chem. 1997;272(4):2527-33.
65. Hashimoto Y, Skacel M, Adams JC. Roles of fascin in human carcinoma motility and signaling: prospects for a novel biomarker? Int J Biochem Cell Biol. 2005;37(9):1787-804.
66. Sedeh RS, Fedorov AA, Fedorov EV, Ono S, Matsumura F, Almo SC, et al. Structure, evolutionary conservation, and conformational dynamics of Homo sapiens fascin-1, an F-actin crosslinking protein. J Mol Biol. 2010;400(3):589-604.
67. FSCN-1 fascin actin-bundling protein (updated 29-May-2022).National Library of Medicine (NCBI) Available: https://www.ncbi.nlm.nih.gov/gene/6624#summary.
68. Lamb MC, Tootle TL. Fascin in Cell Migration: More Than an Actin Bundling Protein. Biology (Basel). 2020;9(11).
69. Heinz LS, Muhs S, Schiewek J, Grub S, Nalaskowski M, Lin YN, et al. Strong fascin expression promotes metastasis independent of its F-actin bundling activity. Oncotarget. 2017;8(66):110077-91.
70. Zhang Y, Lu Y, Zhang C, Huang D, Wu W, Zhang Y, et al. FSCN1 increases doxorubicin resistance in hepatocellular carcinoma through promotion of epithelial-mesenchymal transition. Int J Oncol. 2018;52(5):1455-64.
71. Yang S, Huang FK, Huang J, Chen S, Jakoncic J, Leo-Macias A, et al. Molecular mechanism of fascin function in filopodial formation. J Biol Chem. 2013;288(1):274-84.
72. Deinhardt K, Kim T, Spellman DS, Mains RE, Eipper BA, Neubert TA, et al. Neuronal growth cone retraction relies on proneurotrophin receptor signaling through Rac. Sci Signal. 2011;4(202):ra82.
73. Dylan Burnette and Jennifer Lippincott-Schwartz(updated on 9/17/2020 11:57 AM) National Institue of Medical Sciences. Available: https://www.nigms.nih.gov/education/activities-and-multimedia/life-magnified/Pages/7_bottomleft.aspx.
74. Kureishy N, Sapountzi V, Prag S, Anilkumar N, Adams JC. Fascins, and their roles in cell structure and function. Bioessays. 2002;24(4):350-61.
75. Adams JC. Cell-matrix contact structures. Cell Mol Life Sci. 2001;58(3):371-92.

76. Friedl P, Wolf K. Tumour-cell invasion and migration: diversity and escape mechanisms. Nat Rev Cancer. 2003;3(5):362-74.
77. Van Audenhove I, Denert M, Boucherie C, Pieters L, Cornelissen M, Gettemans J. Fascin Rigidity and L-plastin Flexibility Cooperate in Cancer Cell Invadopodia and Filopodia. J Biol Chem. 2016;291(17):9148-60.
78. Lauffenburger DA, Horwitz AF. Cell migration: a physically integrated molecular process. Cell. 1996;84(3):359-69.
79. Mogilner A, Rubinstein B. The physics of filopodial protrusion. Biophys J. 2005;89(2):782-95.
80. Jawhari AU, Buda A, Jenkins M, Shehzad K, Sarraf C, Noda M, et al. Fascin, an actin-bundling protein, modulates colonic epithelial cell invasiveness and differentiation in vitro. Am J Pathol. 2003;162(1):69-80.
81. Lamb MC, Anliker KK, Tootle TL. Fascin regulates protrusions and delamination to mediate invasive, collective cell migration in vivo. Dev Dyn. 2020;249(8):961-82.
82. Vignjevic D, Schoumacher M, Gavert N, Janssen KP, Jih G, Lae M, et al. Fascin, a novel target of beta-catenin-TCF signaling, is expressed at the invasive front of human colon cancer. Cancer Res. 2007;67(14):6844-53.
83. Tan VY, Lewis SJ, Adams JC, Martin RM. Association of fascin-1 with mortality, disease progression and metastasis in carcinomas: a systematic review and meta-analysis. BMC Med. 2013;11:52.
84. Wang CQ, Li Y, Huang BF, Zhao YM, Yuan H, Guo D, et al. EGFR conjunct FSCN1 as a Novel Therapeutic Strategy in Triple-Negative Breast Cancer. Sci Rep. 2017;7(1):15654.
85. Huang FK, Han S, Xing B, Huang J, Liu B, Bordeleau F, et al. Targeted inhibition of fascin function blocks tumour invasion and metastatic colonization. Nat Commun. 2015;6:7465.
86. Omran OM, Al Sheeha M. Cytoskeletal Focal Adhesion Proteins Fascin-1 and Paxillin Are Predictors of Malignant Progression and Poor Prognosis in Human Breast Cancer. J Environ Pathol Toxicol Oncol. 2015;34(3):201-12.
87. Machesky LM, Li A. Fascin: Invasive filopodia promoting metastasis. Commun Integr Biol. 2010;3(3):263-70.
88. Daponte A, Kostopoulou E, Papandreou CN, Daliani DD, Minas M, Koukoulis G, et al. Prognostic significance of fascin expression in advanced poorly differentiated serous ovarian cancer. Anticancer Res. 2008;28(3B):1905-10.
89. Hashimoto Y, Skacel M, Lavery IC, Mukherjee AL, Casey G, Adams JC. Prognostic significance of fascin expression in advanced colorectal cancer: an immunohistochemical study of colorectal adenomas and adenocarcinomas. BMC Cancer. 2006;6:241.

.

90. Alam H, Bhate AV, Gangadaran P, Sawant SS, Salot S, Sehgal L, et al. Fascin overexpression promotes neoplastic progression in oral squamous cell carcinoma. BMC Cancer. 2012;12:32.
91. Jayo A, Parsons M, Adams JC. A novel Rho-dependent pathway that drives interaction of fascin-1 with p-Lin-11/Isl-1/Mec-3 kinase (LIMK) 1/2 to promote fascin-1/actin binding and filopodia stability. BMC Biol. 2012;10:72.
92. Al-Alwan M, Olabi S, Ghebeh H, Barhoush E, Tulbah A, Al-Tweigeri T, et al. Fascin is a key regulator of breast cancer invasion that acts via the modification of metastasis-associated molecules. PLoS One. 2011;6(11):e27339.
93. Schoumacher M, El-Marjou F, Lae M, Kambou N, Louvard D, Robine S, et al. Conditional expression of fascin increases tumor progression in a mouse model of intestinal cancer. Eur J Cell Biol. 2014;93(10-12):388-95.
94. Tao YS, Edwards RA, Tubb B, Wang S, Bryan J, McCrea PD. beta-Catenin associates with the actin-bundling protein fascin in a noncadherin complex. J Cell Biol. 1996;134(5):1271-81.
95. Kaur T, Madgulkar A, Bhalekar M, Asgaonkar K. Molecular Docking in Formulation and Development. Curr Drug Discov Technol. 2019;16(1):30-9.
96. Puertas-Martin S, Banegas-Luna AJ, Paredes-Ramos M, Redondo JL, Ortigosa PM, Brovarets OO, et al. Is high performance computing a requirement for novel drug discovery and how will this impact academic efforts? Expert Opin Drug Discov. 2020;15(9):981-6.
97. Imbernon B, Serrano A, Bueno-Crespo A, Abellan JL, Perez-Sanchez H, Cecilia JM. METADOCK 2: a high-throughput parallel metaheuristic scheme for molecular docking. Bioinformatics. 2021;37(11):1515-20.
98. Perez-Sanchez H, den Haan H, Perez-Garrido A, Pena-Garcia J, Chakraborty S, Erdogan Orhan I, et al. Combined Structure and Ligand-Based Design of Selective Acetylcholinesterase Inhibitors. J Chem Inf Model. 2021;61(1):467-80.
99. Choudhury C, Priyakumar UD, Sastry GN. Dynamics based pharmacophore models for screening potential inhibitors of mycobacterial cyclopropane synthase. J Chem Inf Model. 2015;55(4):848-60.
100. Montalbán MG, Chakraborty S, Peña-García J, Verli H, Villora G, Pérez-Sánchez H, et al. Molecular insight into silk fibroin based delivery vehicle for amphiphilic drugs: Synthesis, characterization and molecular dynamics studies. Journal of Molecular Liquids. 2020;299:112156.
101. Benigni R, Bassan A, Pavan M. In silico models for genotoxicity and drug regulation. Expert Opin Drug Metab Toxicol. 2020;16(8):651-62.

102. Sanchez-Linares I, Perez-Sanchez H, Cecilia JM, Garcia JM. High-Throughput parallel blind Virtual Screening using BINDSURF. BMC Bioinformatics. 2012;13 Suppl 14:S13.
103. Francis S, Croft D, Schuttelkopf AW, Parry C, Pugliese A, Cameron K, et al. Structure-based design, synthesis and biological evaluation of a novel series of isoquinolone and pyrazolo[4,3-c]pyridine inhibitors of fascin 1 as potential anti-metastatic agents. Bioorg Med Chem Lett. 2019;29(8):1023-9.
104. Nakae K, Yoshimoto Y, Ueda M, Sawa T, Takahashi Y, Naganawa H, et al. Migrastatin, a novel 14-membered lactone from Streptomyces sp. MK929-43F1. J Antibiot (Tokyo). 2000;53(10):1228-30.
105. Gaul C, Njardarson JT, Shan D, Dorn DC, Wu KD, Tong WP, et al. The migrastatin family: discovery of potent cell migration inhibitors by chemical synthesis. J Am Chem Soc. 2004;126(36):11326-37.
106. Shan D, Chen L, Njardarson JT, Gaul C, Ma X, Danishefsky SJ, et al. Synthetic analogues of migrastatin that inhibit mammary tumor metastasis in mice. Proc Natl Acad Sci U S A. 2005;102(10):3772-6.
107. Ju J, Rajski SR, Lim SK, Seo JW, Peters NR, Hoffmann FM, et al. Evaluation of new migrastatin and dorrigocin congeners unveils cell migration inhibitors with dramatically improved potency. Bioorg Med Chem Lett. 2008;18(22):5951-4.
108. Han S, Huang J, Liu B, Xing B, Bordeleau F, Reinhart-King CA, et al. Improving fascin inhibitors to block tumor cell migration and metastasis. Mol Oncol. 2016;10(7):966-80.
109. Wahab A, Hyytiainen A, Wahbi W, Tuomainen K, Tervo S, Conesa-Zamora P, et al. The effect of fascin 1 inhibition on head and neck squamous cell carcinoma cells. Eur J Oral Sci. 2021;129(6):e12819.
110. Kandeel M, Al-Nazawi M. Virtual screening and repurposing of FDA approved drugs against COVID-19 main protease. Life Sci. 2020;251:117627.
111. Esnakula AK, Ricks-Santi L, Kwagyan J, Kanaan YM, DeWitty RL, Wilson LL, et al. Strong association of fascin expression with triple negative breast cancer and basal-like phenotype in African-American women. J Clin Pathol. 2014;67(2):153-60.
112. National Center for Biotechnology Information (Retrieved April 12, 2022). PubChem Compound Summary for CID 2987927, Monastrol. Available: https://pubchem.ncbi.nlm.nih.gov/compound/Monastrol.
113. Chen GY, Kang YJ, Gayek AS, Youyen W, Tuzel E, Ohi R, et al. Eg5 Inhibitors Have Contrasting Effects on Microtubule Stability and Metaphase Spindle Integrity. ACS Chem Biol. 2017;12(4):1038-46.

.

114. Villari G, Jayo A, Zanet J, Fitch B, Serrels B, Frame M, et al. A direct interaction between fascin and microtubules contributes to adhesion dynamics and cell migration. J Cell Sci. 2015;128(24):4601-14.
115. Riahi N, Kefayat A, Ghasemi A, Asgarshamsi M, Panjehpoor M, Fassihi A. Design, Synthesis and Molecular Docking Studies of Some Tetrahydropyrimidine Derivatives as Possible Fascin Inhibitors. Chem Biodivers. 2019;16(2):e1800339.
116. Muller C, Gross D, Sarli V, Gartner M, Giannis A, Bernhardt G, et al. Inhibitors of kinesin Eg5: antiproliferative activity of monastrol analogues against human glioblastoma cells. Cancer Chemother Pharmacol. 2007;59(2):157-64.
117. PubChem Compound Summary for CID 3696, Imipramine. . National Center for Biotechnology Information. 2022.
118. Imipramina hidrocloruro (Tofranil) U.S,(sf), Food and Drug Administration.Available: https://www.accessdata.fda.gov/scripts/cder/daf/index.cfm?event=overview.process&ApplNo=087846.
119. Harbin. 2D structure of TCA imipramine (Tofranil),(2019). Available: https://commonswikimediaorg/wiki/File:Imipraminesvg

120. Lang U. Is Imipramine Helpful in the Treatment of Cancer? A Case Presentation and Discussion of Possible Clinical Implications. Biomedical Journal of Scientific & Technical Research. 2018;4.

121. Walker AJ, Card T, Bates TE, Muir K. Tricyclic antidepressants and the incidence of certain cancers: a study using the GPRD. Br J Cancer. 2011;104(1):193-7.
122. Lim EY, Park J, Kim YT, Kim MJ. Imipramine Inhibits Migration and Invasion in Metastatic Castration-Resistant Prostate Cancer PC-3 Cells via AKT-Mediated NF-kappaB Signaling Pathway. Molecules. 2020;25(20).
123. Jang WJ, Jung SK, Vo TTL, Jeong CH. Anticancer activity of paroxetine in human colon cancer cells: Involvement of MET and ERBB3. J Cell Mol Med. 2019;23(2):1106-15.
124. Gil-Ad I, Zolokov A, Lomnitski L, Taler M, Bar M, Luria D, et al. Evaluation of the potential anti-cancer activity of the antidepressant sertraline in human colon cancer cell lines and in colorectal cancer-xenografted mice. Int J Oncol. 2008;33(2):277-86.
125. National Center for Biotechnology Information (Retrieved April 7, 2022). PubChem Compound Summary for CID 54671008, Raltegravir. Available: https://pubchem.ncbi.nlm.nih.gov/compound/Raltegravir.

126. Raltegravir 2D structure (7 February 2014).Available: https://en.wikipedia.org/wiki/Raltegravir#/media/File:Raltegravir_structure.svg.
127. Carleo MA, Di Martino F, Del Giudice A, Gargiulo M, Parrella G, Rosario P, et al. Different impact of anti-retroviral regimen containing protease inhibitors on development of HIV-related Kaposi sarcoma. In Vivo. 2015;29(1):133-6.
128. Cozzi-Lepri A, Zangerle R, Machala L, Zilmer K, Ristola M, Pradier C, et al. Incidence of cancer and overall risk of mortality in individuals treated with raltegravir-based and non-raltegravir-based combination antiretroviral therapy regimens. HIV Med. 2018;19(2):102-17.
129. Scanlon KJ, Kashani-Sabet M, Sowers LC. Overexpression of DNA replication and repair enzymes in cisplatin-resistant human colon carcinoma HCT8 cells and circumvention by azidothymidine. Cancer Commun. 1989;1(4):269-75.
130. Chang YC, Chiou J, Yang YF, Su CY, Lin YF, Yang CN, et al. Therapeutic Targeting of Aldolase A Interactions Inhibits Lung Cancer Metastasis and Prolongs Survival. Cancer Res. 2019;79(18):4754-66.
131. Mohr CF, Gross C, Bros M, Reske-Kunz AB, Biesinger B, Thoma-Kress AK. Regulation of the tumor marker Fascin by the viral oncoprotein Tax of human T-cell leukemia virus type 1 (HTLV-1) depends on promoter activation and on a promoter-independent mechanism. Virology. 2015;485:481-91.
132. Yu FL, Miao H, Xia J, Jia F, Wang H, Xu F, et al. Proteomics Analysis Identifies IRSp53 and Fascin as Critical for PRV Egress and Direct Cell-Cell Transmission. Proteomics. 2019;19(23):e1900009.
133. Gong LP, Chen JN, Xiao L, He Q, Feng ZY, Zhang ZG, et al. The implication of tumor-infiltrating lymphocytes in Epstein-Barr virus-associated gastric carcinoma. Hum Pathol. 2019;85:82-91.
134. Wang Y, Zhang JJ, Huang XY. Anti-Metastasis Fascin Inhibitors Decrease the Growth of Specific Subtypes of Cancers. Cancers (Basel). 2020;12(8).
135. Alburquerque-Gonzalez B, Bernabe-Garcia A, Bernabe-Garcia M, Ruiz-Sanz J, Lopez-Calderon FF, Gonnelli L, et al. The FDA-Approved Antiviral Raltegravir Inhibits Fascin1-Dependent Invasion of Colorectal Tumor Cells In Vitro and In Vivo. Cancers (Basel). 2021;13(4).
136. Zhang H, Chen M, Liu Y, Dong X, Zhang C, Jiang H, et al. Paroxetine combined with fluorouracil plays a therapeutic role in mouse models of colorectal cancer with depression through inhibiting IL-22 expression to regulate the MAPK signaling pathway. Exp Ther Med. 2020;20(6):240.
137. Nowak-Sliwinska P, Scapozza L, Ruiz i Altaba A. Drug repurposing in oncology: Compounds, pathways, phenotypes and computational approaches for colorectal cancer. Biochim Biophys Acta Rev Cancer. 2019;1871(2):434-54.

.

138. Pantziarka P. Scientific advice - is drug repurposing missing a trick? Nat Rev Clin Oncol. 2017;14(8):455-6.
139. Jahchan NS, Dudley JT, Mazur PK, Flores N, Yang D, Palmerton A, et al. A drug repositioning approach identifies tricyclic antidepressants as inhibitors of small cell lung cancer and other neuroendocrine tumors. Cancer Discov. 2013;3(12):1364-77.
140. Kumari P, Dang S. Anti-Cancer Potential of Some Commonly Used Drugs. Curr Pharm Des. 2021;27(45):4530-8.
141. Imipramine. Drugbank (sf). Available: https://go.drugbank.com/drugs/DB00458.
142. Munson JM, Fried L, Rowson SA, Bonner MY, Karumbaiah L, Diaz B, et al. Anti-invasive adjuvant therapy with imipramine blue enhances chemotherapeutic efficacy against glioma. Sci Transl Med. 2012;4(127):127ra36.
143. Capoci IRG, Faria DR, Sakita KM, Rodrigues-Vendramini FAV, Bonfim-Mendonca PS, Becker TCA, et al. Repurposing approach identifies new treatment options for invasive fungal disease. Bioorg Chem. 2019;84:87-97.
144. Indu P, Rameshkumar MR, Arunagirinathan N, Al-Dhabi NA, Valan Arasu M, Ignacimuthu S. Raltegravir, Indinavir, Tipranavir, Dolutegravir, and Etravirine against main protease and RNA-dependent RNA polymerase of SARS-CoV-2: A molecular docking and drug repurposing approach. J Infect Public Health. 2020;13(12):1856-61.
145. Oprea TI, Bauman JE, Bologa CG, Buranda T, Chigaev A, Edwards BS, et al. Drug Repurposing from an Academic Perspective. Drug Discov Today Ther Strateg. 2011;8(3-4):61-9.
146. European Publication Server. EP3628330 (sf). Available: https://data.epo.org/publication-server/document?iDocId=6200014&iFormat=0.
147. Tsumura R, Manabe S, Takashima H, Koga Y, Yasunaga M, Matsumura Y. Influence of the dissociation rate constant on the intra-tumor distribution of antibody-drug conjugate against tissue factor. J Control Release. 2018;284:49-56.

VIII - ANEXOS

VIII: ANEXOS

ANEXO I

APROBACIÓN DEL COMITÉ DE ÉTICA DE LA UCAM PARA LA REALIZACIÓN DE LOS ENSAYOS *IN VIVO*.

UCAM
UNIVERSIDAD CATÓLICA SAN ANTONIO

COMITÉ DE ÉTICA DE LA UCAM

DATOS DEL PROYECTO

Título:	"Diseño y caracterización de inhibidores de fascina para el bloqueo de la invasión y la metástasis en cáncer colorrectal"	
Investigador Principal	**Nombre**	**Correo-e**
Dr.	Pablo Conesa Zamora	pconesa@ucam.edu

INFORME DEL COMITÉ

Fecha	**27/04/2018**	**Código**	**CE041810**

Tipo de Experimentación

Investigación experimental clínica con seres humanos	
Utilización de tejidos humanos procedentes de pacientes, tejidos embrionarios o fetales	
Utilización de tejidos humanos, tejidos embrionarios o fetales procedentes de bancos de muestras o tejidos	X
Investigación observacional con seres humanos, psicológica o comportamental en humanos	
Uso de datos personales, información genética, etc.	
Experimentación animal	X
Utilización de agentes biológicos de riesgo para la salud humana, animal o las plantas	
Uso de organismos modificados genéticamente (OMGs)	

Comentarios Respecto al Tipo de Experimentación
Nada Obsta

Comentarios Respecto a la Metodología de Experimentación
Nada Obsta

UNIVERSIDAD CATÓLICA SAN ANTONIO · COMITE DE ETICA ·

UCAM
UNIVERSIDAD CATÓLICA SAN ANTONIO

COMITÉ DE ÉTICA DE LA UCAM

Sugerencias al Investigador

A la vista de la solicitud de informe adjunto por el Investigador y de las recomendaciones anteriormente expuestas el dictamen del Comité es:

Emitir Informe Favorable	**X**
Emitir Informe Desfavorable	
Emitir Informe Favorable condicionado a Subsanación	
MOTIVACIÓN	
Incrementará conocimientos en su área	

Vº Bº El Presidente,

Fdo.: José Alberto Cánovas Sánchez

El Secretario,

UNIVERSIDAD CATOLICA SAN ANTONIO · COMITE DE ETICA ·

Fdo.: José Alarcón Teruel

ANEXO II

RESOLUCIÓN DE LA CONSEJERÍA DE AGUA, AGRICULTURA, GANADERÍA, PESCA Y MEDIO AMBIENTE DE LA REGIÓN DE MURCIA Y LA APROBACIÓN DEL ÓRGANO ENCARGADO DEL BIENESTAR ANIMAL (OEBA) IMIB-ARRIXACA PARA LA REALIZACIÓN DE ENSAYOS *IN VIVO*.

Tf: 012 / 968362000

PABLO CONESA ZAMORA
DEPARTAMENTO DE ANATOMÍA PATOLÓGICA
HOSPITAL UNIVERSITARIO SANTA LUCÍA DE CARTAGENA

RESOLUCION

Vista la solicitud para la autorización de la realización de un proyecto de investigación con animales presentada con fecha 05/08/2019 y nº registro de entrada por Comunicación Interior nº 256793/2019, por D. Pablo Conesa Zamora, como responsable del mismo.

Vista la subsanación de documentación presentada por registro de entrada CI 283017/2019 con fecha 20/09/2019.

Vista la propuesta del proyecto denominado: “Diseño y caracterización de inhibidores de fascina para el bloqueo de la invasión y la metástasis en cáncer colorrectal”.

Visto el informe favorable del comité ético del establecimiento usuario con código REGA ES300303340098.

Visto el resumen no técnico del proyecto.

Visto el resultado favorable de la evaluación del proyecto por el “Órgano habilitado para la Evaluación de proyectos del Hospital Clínico Universitario Virgen de la Arrixaca-IMIB”.

Visto que en dicha evaluación se clasifica como Tipo II, y no se indica que sea necesario llevar a cabo la evaluación retrospectiva del proyecto.

Visto el Real Decreto 53/2013, de 1 de febrero, por el que se establecen las normas básicas aplicables para la protección de los animales utilizados en experimentación y otros fines científicos, incluyendo la docencia.

Visto el Informe emitido por el Servicio de Producción Animal al respecto.

Considerando la competencia que tiene atribuida la Dirección General de Producción Agrícola, Ganadera y del Medio Marino, sobre la base de lo dispuesto en el Decreto 173/2019 de 6 de septiembre por el que se establecen los órganos directivos de la Consejería de Agua, Agricultura, Ganadería, Pesca y Medio Ambiente, con independencia de otras actuaciones que esta u otra administración puedan emprender, esta Dirección,

RESUELVE

Conceder autorización a D. Pablo Conesa Zamora, para la realización del proyecto solicitado, como responsable y usuario del mismo, asignándole el código de identificación **Nº A13191001**, teniendo esta autorización una validez que se corresponderá con la duración prevista en su memoria, con un máximo de cinco años, siempre y cuando no se produzca una modificación relevante en dicho procedimiento, o una modificación del establecimiento usuario, en cuyo caso sería necesario efectuar una nueva solicitud de autorización a la autoridad competente.

El proyecto se llevará a cabo según memoria y evaluación presentada en el establecimiento usuario con código REGA ES300303340098.

Toda la documentación pertinente del proyecto, incluida la información referida a los protocolos de supervisión y su cumplimentación, tratamientos administrados a los animales durante los procedimientos, informes veterinarios previos a la reutilización de animales (en su caso), bajas imprevistas y fechas y métodos de eutanasia, deberá estar a disposición del personal del “Comité Ético de Experimentación Animal (CEEA) del Hospital Clínico Universitario Virgen de la Arrixaca-IMIB” y de la autoridad competente, desde el inicio del proyecto hasta al menos cinco años después de finalizar el mismo. Así mismo, deberá informar expresamente al

citado Comité con carácter anual y preferiblemente durante el mes de enero, respecto al número de animales sobre los que se haya finalizado su utilización en el año anterior en el contexto de su proyecto, con indicación de la severidad real sufrida por los mismos.

Lo que en cumplimiento del Art. 40 de la Ley 39/2015, de 1 de octubre, del Procedimiento Administrativo Común de las Administraciones Públicas se le NOTIFICA, significándole que contra dicha Resolución cabe Recurso de Alzada ante el Excmo. Sr. Consejero de Agua, Agricultura, Ganadería, Pesca y Medio Ambiente, en el plazo de un mes desde la recepción de la presente notificación, sin perjuicio de poder ejercitar, en su caso, cualquier otro que se estime pertinente.

EL DIRECTOR GENERAL DE PRODUCCIÓN AGRÍCOLA, GANADERA, Y DEL MEDIO MARINO

Fdo. Electrónicamente al margen: Francisco José Espejo García

Órgano Encargado del Bienestar Animal.
Animalario SPF, Libre de Patógenos. Hospital Clínico Universitario Virgen de la Arrixaca
Ctra. Madrid- Cartagena, s/n. 30120 El Palmar, Murcia
Tfno: 968.38.10.97.

A la atención de la Dirección General de Agricultura, Ganadería, Pesca y Acuicultura, Servicio de Sanidad Animal.

Murcia, a 11 de Diciembre de 2019

Investigador Principal	Dr. Pablo Conesa Zamora
Tipo de actividad	Proyecto Nacional
Título del proyecto	Diseño y caracterización de inhibidores de fascina para el bloqueo de la invasión y la metástasis en cáncer colorrectal
Código REGA	ES 300303340098
Informe Ético OEBA	**Favorable**
Registro	111219/1/PI

Le comunico que las instalaciones del Animalario SPF, Libre de Patógenos, con código REGA ES-300303340098 disponen de los medios humanos y materiales para la realización de éste proyecto en peces, garantizando el bienestar de los animales, tal como se recoge en el Real Decreto 53/2013, de 1 de febrero, *por el que se establecen las normas básicas aplicables para la protección de los animales utilizados en experimentación y otros fines científicos, incluyendo la docencia*.

Y para que así conste y a todos los efectos oportunos, lo firmo en Murcia a 11 de Diciembre 2019.

Pablo Pelegrín Vivancos
Pte. Órgano Encargado Bienestar Animal
Animalario SPF. Hospital Clínico Universitario Virgen de la Arrixaca.

ANEXO III

PRODUCCIÓN CIENTÍFICA DERIVADA DE LA TESIS DOCTORAL

1. ARTÍCULOS CIENTÍFICOS

ARTÍCULO 1: Rosa de Alarcón, Alburquerque-González B; et al. 2022. **Pharmacogenetic role of vitamin D-binding protein and vitamin D receptor polymorphisms in the treatment response of dialysis patients with secondary hyperparathyroidism**. Nephrology Dialysis Transplantation. Oxford Academics, En prensa. IF: 5,992.

ARTÍCULO 2: Alburquerque-González B; Bernabé-García A; et al. 2021. The **FDA-approved antiviral raltegravir inhibits fascin1 dependant invasion of colorectal tumor cells *in vitro* and *in vivo*.** Cancers. MDPI. IF: 6,639.

ARTÍCULO 3: Alburquerque-González B; Bernabé-García M; et al. 2020. **New role of antidepressant imipramine as a fascin1 inhibitor in colorectal cancer cells**. Experimental & Molecular Medicine. Nature Springer.IF:5,063.

ARTÍCULO 4: Montoro-García S; Alburquerque-González B; et al. 2020. **Novel anti- invasive properties of a Fascin1 inhibitor on colorectal cancer cells.** Journal of Molecular Medicine. Springer. IF: 4,938.

ARTÍCULO 5: Alburquerque-González B et al. 2020. **Therapeutic targets in colorectal serrated adenocarcinoma: clues for a histological-based treatment against an aggressive tumor**. Int J. Mol Science. IF: 4,183.

ARTÍCULO 6: Esteban-Gil; …; Alburquerque-González B; et al. 2019. **ColPortal, an integrative multiomic platform for analysing epigenetic interactions in colorectal cancer**. Scientific Data. Nature. 6- 1, pp.255. IF:5,929.

ARTÍCULO 7: Kondelova A; Alburquerque-González B; et al. 2019**. miR-181a-2* expression is different amongst carcinomas from the colorectal serrated route.** Mutagenesis. 2019 Nov 30. pii: gez039. doi: 10.1093/mutage/gez039. IF: 2,713.

ARTÍCULO 8: Wasniewski S;…; Alburquerque-González B; et al. 2018. **Low Performance of a Clinical-Genetic Model in the Estimation of Time in Therapeutic Range in Acenocoumarol-Adherent Patients with Nonvalvular Atrial Fibrillation: The Quality of Anticoagulation Challenge**. Biomed Res Int. Hindawi. 8012747. IF:2,583

2. CAPÍTULOS DE LIBRO

1. Alburquerque-González B; López-Abellán MD; Luengo-Gil G; Montoro-García S; Conesa-Zamora P**. Design of personalized neoantigen RNA vaccines against cancer based on Next Generation Sequencing data. Pharmacogenomics.** Methods and Protocols. Springer Nature, 2022. (En prensa).

2. Castillo-Delgado V; Alburquerque-González B; Fernández-Zapata J. **Genética cuantitativa**. Biólogo Interno Residente (BIR). Colegio Oficial de Biólogos de la Región de Murcia (COBRM), 2022.ISBN: 978-84-09-39509-5.

3. Alburquerque-González B; Fernández-Zapata J; Castillo-Delgado V. **Genética de poblaciones**. Biólogo Interno Residente (BIR). Colegio Oficial de Biólogos de la Región de Murcia (COBRM), 2022. (En prensa). ISBN: 978-84-09-39509-5

3. TRABAJOS PRESENTADOS EN CONGRESOS NACIONALES O INTERNACIONALES

Participación en congresos nacionales:

1. Webinar organizado por la Real Academia de Medicina y Cirugía de la Región de Murcia Título del trabajo: Caracterización *in vitro* e *in vivo* del efecto antitumoral de compuestos anti-fascina. **Comunicación oral**. Fecha de celebración: 22/10/2020. **Autor de correspondencia.**

2. Congreso de la Sociedad Española de Oncología Médica (SEOM). Una nueva era de progresos en cadena. **Comunicación Oral**. Adecuando el

tratamiento oncológico a la fragilidad del paciente anciano. Lugar de celebración: Pamplona, Navarra. Fecha de celebración: 22- 25/10/2019.

3. Congreso de la Sociedad Española de Oncología Médica (SEOM). Una nueva era de progresos en cadena. **Póster**. Niveles de FSCN1 en suero en pacientes con cáncer colorrectal, estudio preliminar. Lugar de celebración: Pamplona, Navarra. Fecha de celebración: 22-25/10/2019.

4. XXIX Congreso Nacional de la Sociedad Española de Anatomía Patológica, XXIV Congreso Nacional de la Sociedad Española de Citología y V Congreso Nacional del Sociedad Española de Patología Forense. **Comunicación Oral.** Niveles de fascina1 en suero en pacientes con cáncer colorrectal, estudio preliminar. Lugar de celebración: Granada. Fecha de celebración: 24/05/2019. **Autor de correspondencia.**

5. SEC 2018 - El Congreso de las Enfermedades Cardiovasculares. **Comunicación oral.** Bajo rendimiento de un modelo clínico-genético en la estimación del tiempo en rango terapéutico en pacientes con fibrilación auricular no valvular. Ciudad de celebración: Sevilla, Andalucía, España Fecha de celebración: 25/10/2018 Fecha de finalización: 27/10/2018 Entidad organizadora: Sociedad Española de Cardiología.

Participación en congresos internacionales:

1. Goodbye Flat Biology. Advancing 3D-based models for Cancer Biology and Drug Discovery. **Póster, PREMIO MEJOR PÓSTER**. Antidepressant imipramine is a new fascin1 inhibitor in colorectal cancer cells. Lugar de celebración: Berlín, Alemania. Fecha de celebración: 13/11/2019. **Autor de correspondencia.**

2. 2nd EACR Conference: Defense is the best attack. Inmunooncology Breakthroughs. **Póster.** Study of "inmunocheckpoint" genes expression in histological variants of colorectal carcinoma. Lugar de celebración: Barcelona. Fecha de celebración: 11-13/04/2019.

3. The 6th Leading International Cancer Immunotherapy Conference in Europe / European Journal of Cancer (ITOC6). **Póster.** Study of IDO1 gene

expression in histological variants of colorectal carcinoma. Lugar de celebración: Viena. Fecha de celebración: 11-13/03/2019.

4. MAP 2018 – Molecular Analysis for Personalised Therapy. **Póster.** Título del trabajo: Differences in expression profiling and biomarkers between histological colorectal carcinomas subsets from the serrated pathway.Ciudad de celebración: París, Francia Fecha de celebración: 14/09/2018 Entidad organizadora: Cancer Research UK, ESMO, Unicancer.

5. 25th biennal congress of the European Association for cancer research. **Póster** New anti- migratory and anti-invasive effects of a fascin inhibitor on colorrectal cancer cells Ciudad de celebración: Amsterdam, Holanda Fecha de celebración: 30/06/2018 Fecha de finalización: 03/06/2018. Entidad organizadora: European Association of Cancer Research.

Participación en jornadas

1. VII Jornadas de Investigación y doctorado UCAM 'ODS con Ciencia'. Título del trabajo: "Issentress® decreases tumor size and volume in a primary colorectal cancer mouse model". **Póster**. Ciudad de celebración: Murcia, Fecha de celebración: 25/06/2021. **Autor de correspondencia**

2. VI Jornadas de Investigación y doctorado UCAM. Título del trabajo: Establishment of an Animal Model for Colon Cancer metastasis with human cells. Testing the potential therapy with antidepressant Imipramine. **Comunicación Oral**. Ciudad de celebración: Murcia, Fecha de celebración: 26/06/2020. **Autor de correspondencia**

3. V Jornadas Científicas del IMIB-Arrixaca. Título del trabajo: "Antitumoral effect of antidepressant Tofranil® on primary tumour and metastasis mouse models." **COMUNICACIÓN ORAL PREMIADA**. Ciudad de celebración: Murcia, España. Fecha de celebración: 23/11/2020. **Autor de correspondencia.**

4. IV Jornadas de Investigación del IMIB (Instituto Murciano de Investigación Biosanitaria). **Comunicación Oral.** "A FDA approved integrase inhibitor targets the invasive capacity of colorectal Tumor cells in vitro and in vivo." Lugar de celebración: Murcia. Fecha de celebración: 11/11/2019. **Autor de correspondencia**

5. V Jornadas de Investigación y Doctorado: Ciencias sin Fronteras (UCAM). **Comunicación Oral, PREMIO MEJOR COMUNICACIÓN ORAL DEL PROGRAMA DE DOCTORADO EN CIENCIAS DE LA SALUD.** New role of antidepressant imipramine as a fascin1 inhibitor in colorectal cancer cells. Lugar de celebración: Murcia. Fecha de celebración: 31/05/2019. **Autor de correspondencia.**

6. V Jornadas de Investigación y Doctorado: Ciencias sin Fronteras (UCAM). **Póster.** Niveles de fascina1 en suero en pacientes con cáncer colorrectal, estudio preliminar. Ciudad de celebración: Murcia, Región de Murcia, España Fecha de celebración: 31/05/2019 Entidad organizadora: Universidad Católica San Antonio de Murcia. **Autor de correspondencia.**

7. III JORNADAS IMIB-ARRIXACA. Estudio de expresión de proteínas de "inmunocheckpoints" en los distintos tipos histológicos de cáncer de colon. **Póster.** Ciudad de celebración: Murcia, Fecha de celebración: 19/11/2018. Entidad organizadora: Instituto Murciano de Investigación.

8. III JORNADAS IMIB-ARRIXACA. New role of antidepressant imipramine as a fascin1 inhibitor in colorectal cancer cells. **Comunicación Oral**. Ciudad de celebración: Murcia, Fecha de celebración: 19/11/2018 Entidad organizadora: Instituto Murciano de Investigación Biosanitaria. **Autor de correspondencia.**

9. IV Jornadas de investigación y doctorado Women in Science. Nuevas propiedades anti migratorias y anti-invasivas de un inhibidor de fascina en células de cáncer colorrectal. **Comunicación Oral.** Ciudad de celebración: Murcia, España. Fecha de celebración: 18/05/2018 Entidad organizadora: Universidad Católica San Antonio de Murcia. **Autor de correspondencia.**

10. II Jornadas Científicas del IMIB-Arrixaca. **Póster.** A novel anti-Fascin compound show anit- migratory and anti-invasive properties in colorrectal cancer cell lines Ciudad de celebración: Murcia, Región de Murcia, España Fecha de finalización: 27/11/2017 Entidad organizadora: Instituto Murciano de Investigación Biosanitaria (IMIB). **Autor de correspondencia.**

11. II Jornadas cientificas IMIB-arrixaca. Forkhead box d2 (foxd2) transcription factor regulates immune-related genes in colorectal cancer cell lines. **Póster.** Ciudad de celebración: Murcia, Fecha de celebración: 27/11/2017 Entidad organizadora: Instituto Murciano de Investigaciones Biosanitarias.

4. PATENTES Y PROPIEDAD INTELECTUAL

1. Título propiedad industrial registrada: "**Raltegravir for use as inhibitor of Fascin1 in cancer.**" Inventores/autores/obtentores: Conesa-Zamora P; Alburquerque-González B; Pérez-Sánchez H; Montoro-García S; García-Solano J; Bernabé-García A; Nicolás-Villaescusa FJ; Bernabé-García M; Cayuela-Fuentes ML; Luque-Fernández I; Peña-García J; Ruiz-Sanz J; Martínez-Herrerías JC. Entidad titular de derechos: Universidad Católica San Antonio de Murcia, Universidad de Granada, Fundación para la Formación en Investigación Sanitaria (FFIS) **Nº de solicitud: P202130062** País de inscripción: España Fecha de registro: 28/01/2021 C. Autón./Reg. de explotación: España.

2. Título propiedad industrial registrada: "**Imipramine for use as inhibitor of fascin1 overexpression**" Inventores/autores/obtentores: Conesa-Zamora. P; Pérez-Sánchez. H; Luque-Fernández. I; Montoro-García. S; Alburquerque-González. B; Bernabé-García. A; Bernabé-García. M; Campioni-Rodrigues. P; Ruiz-Sanz. J; Martínez-Herrerías. JC; García-Solano. J; Nicolás-Villaescusa. FJ; Cayuela-Fuentes.ML; Salo.T. **Nº de solicitud: EP18382696.5.** País de inscripción: España, Región de Murcia Fecha de registro: 28/09/2018 Empresas: Fundación para la formación e investigación sanitaria; Universidad Católica San Antonio de Murcia; Universidad de Granada.

5. RECONOCIMIENTOS Y PREMIOS

1. **Premios de Investigación de la Real Academia de Medicina y Cirugía de Murcia (2020).** TEMA SEGUNDO: Premio Doctor Pedro Alonso Carrión. Conado por la Ilma. Sra. Dª María Pilar Cárceles Hernández-Ros Título: "New role of antidepressant imipramine as a fascin-1 inhibitor in

colorectal cancer cells" Autor: Doña Begoña Alburquerque González y colaboradores. Autor de correspondencia.

2. **Premio a la mejor Comunicación Oral (V Jornadas IMIB-Arrixaca 2020).** Título: "Antitumoral effect of antidepressant tofranil® on primary tumour and Metastasis mouse models." Autor: Doña Begoña Alburquerque González y colaboradores. Autor de correspondencia

3. **Premio a la mejor Comunicación Oral (IV Jornadas de Doctorado UCAM 2019).** Título: "New role of antidepressant imipramine as a fascin-1 inhibitor in colorectal cancer cells." Autor: Doña Begoña Alburquerque González y colaboradores. Autor de correspondencia

4. **Premio a mejor póster. Goodbye Flat Biology. Advancing 3D-based models for Cancer Biology and Drug Discovery**. Antidepressant imipramine is a new fascin1 inhibitor in colorectal cancer cells. Lugar de celebración: Berlín, Alemania. Fecha de celebración: 13/11/2019. Autor de correspondencia

6. PARTICIPACIÓN EN PROYECTOS

1. **Aproximación al abordaje farmacológico del adenocarcinoma serrado colorrectal: caracterización funcional de dianas terapéuticas y de sus inhibidores**. Instituto de Salud Carlos III. Pablo Conesa Zamora. (Hospital Universitario Santa Lucía). 01/01/2016-31/12/2018. 86.515 €. PI

2. **Diseño y caracterización de inhibidores de fascina para el bloqueo de invasión y metástasis en cáncer colorrectal**. Instituto de Salud Carlos III. Pablo Conesa Zamora. (Complejo Universitario Hospitalario de Cartagena). 01/01/2019- 31/12/2021. 93.000 €.

3. **Determinación de los mecanismos moleculares y bioquímicos relacionados con la presencia de un cáncer oculto y recidivas tromboembólicas en pacientes con enfermedad tromboembólica venosa**" Nombres investigadores principales (IP, Co-IP,...): Javier Trujillo Santos; Begoña Alburquerque González; Pablo Pérez Cañadas; Silvia Montoro García Fecha de inicio: 30/06/2015 Duración: 3 años Cuantía total: 35.940 €.

4. **Efectos histológicos y clínicos de la imipramina en el tratamiento de pacientes con tumores que sobre expresan fascina1** (REF: ICI20/00044) Entidad de realización: Instituto Murciano de Investigaciones Biosanitarias (IMIB) Entidad/es financiadora/s: Instituto de Salud Carlos III Tipo de entidad: Organismo Público de Investigación Fecha de inicio-fin: 01/01/2021 - 01/01/2025 Cuantía total: 218.900 €.

5. FINANCIACIÓN DE LA DOCTORANDA

1. Contrato predoctoral del plan propio de la Universidad Católica de Murcia. Convocatoria 2017. (marzo 2018-julio 2022).